# Mutagenic, Spectroscopic and Functional Investigations of Pea Cytosolic Ascorbate Peroxidase

Thesis submitted for the degree of

Doctor of Philosophy

at the University of Leicester

by

Daniel Douglas Turner B.Sc. (Hons) Leicester University

Department of Chemistry

Faculty of Science

University of Leicester

November 2000

UMI Number: U551621

UMI

Dissertation Publishing

ProQuest

To Sylvia, Michael, Andrew, Simon and Hazel

# Statement

Unless otherwise acknowledged, the experimental work described in this thesis has been carried out by the author in the Department of Chemistry at the University of Leicester between October 1996 and November 2000. The work has not been submitted, and is not presently being submitted for any other degree at this or any other university.

Signed: _[signature]_                    Date: _[handwritten] 13th March 2001_

Department of Chemistry
University of Leicester
University Road
Leicester
U.K.

LE1 7RH

# Mutagenic, Spectroscopic and Functional Investigations of Pea Cytosolic Ascorbate Peroxidase

## Daniel Douglas Turner

# Abstract

Recombinant pea cytosolic ascorbate peroxidase (wild-type rAPX) has been isolated and characterised using a variety of kinetic and spectroscopic techniques. Mutagenic replacement of single amino acid residues has been performed.

Electrospray mass spectrometry confirmed that the recombinant enzyme expressed without post-translational modification: the measured apoprotein MW (27192.8 ± 0.8 Da) matched that deduced from the primary amino acid sequence (27192.8 Da). Wild-type rAPX was found to be spectroscopically identical to the native enzyme, *i.e. bona fide* enzyme isolated from *Pisum Sativum L.*; the steady- and transient-state kinetic profiles obtained are wholly consistent with that published in the literature.

Investigation of the pH-dependent haem-iron coordination geometry of the ferric resting-state of wild-type rAPX has confirmed the existence of novel six-coordinate low-spin 'acidic form', which was denoted by a peak at 1590 nm in the near-IR MCD spectrum. UV/visible spectra of the 'acidic form' of both H42A and wild-type rAPX were indistinguishable ($\lambda$/nm = 410, 525.5, ~563$^{sh}$ & ~622$^{sh}$), and the consensus of the pH-dependent data supports ligation of the ferric resting-state haem-iron by either an anomalous hydroxide or the distal arginine residue (Arg38) at low pH.

Phenylhydrazine-modification experiments suggest that site-directed replacement of Ala134 with proline does not measurably decrease the extent of haem exposure. Steady- and transient-state kinetics indicate that A134P oxidises ascorbate at a rate comparable (≈85%) to that of wild-type rAPX; a slight increase (≈3-fold) in the rate of phenolic oxidation was noted. These observations are consistent with the purported existence of two distinct substrate-binding sites in ascorbate peroxidase enzymes.

Quick-freeze EPR spectra have resolved a previously undetected tryptophan-based radical in Compound I*, the species that evolves – in the absence of ascorbate – from the initial intermediate (Compound I) formed by the reaction between wild-type rAPX and $H_2O_2$. The protein-based radical is probably not physiologically relevant.

# Contents

## Table of Contents

## Table of Figures

## Table of Tables

# Acknowledgements

# Abbreviations and Units

## Experimental:

CCD – charge coupled device

CD – circular dichroism

EPR – electron paramagnetic resonance

ESI – electrospray ionisation

HQ-dH$_2$O – high-quality deionised water

HPLC – high-performance liquid

    chromatography

IR – infra-red

LB – Luria-Bertani broth

MBP – maltose-binding protein

MCD – magnetic circular dichroism

OTTLE – optically transparent thin layer

electrode

PAGE – polyacrylamide gel electrophoresis

RR – resonance Raman

R$_z$ – reinheitzahl

SCE – saturated calomel electrode

SHE – standard hydrogen electrode

UV – ultra-violet

cDNA – cloned DNA

## Chemicals:

DTT – dithiothreitol

IPTG – isopropyl-β-D-thiogalactoside

PMSF – phenylmethylsulfonyl fluoride

SDS – sodium dodecyl sulphate

## Units/symbols:

ε – absorption coefficient

A – Absorbance

CT – charge transfer

μ – ionic strength

MW – molecular weight

## Enzymes:

APX – ascorbate peroxidase

rAPX – recombinant pea APX

CcP – cytochrome *c* peroxidase

DNase – deoxyribonuclease

HRP – horseradish peroxidase

MnP – manganese peroxidase

LiP – lignin peroxidase

PnP – peanut peroxidase

ARP – *arthromyces ramosus* peroxidase

## Buffers:

MOPS – 3-[N-morpholino]propanesulphonic

    acid

MES – 3-[N-morpholino]ethanesulphonic acid

NaPi/KPi – sodium/potassium phosphate

TAPS – N-tris[hydroxymethyl]methyl-3-

    aminopropanesulphonic acid

pH* – pH uncorrected for deuterium isotope

    effect

*Neutral Amino Acids:*

Ala/A – alanine

Asn/N – asparagine

Cys/C – cysteine

Gln/Q – glutamine

Gly/G – glycine

Ile/I – isoleucine

Leu/L – leucine

Met/M – methionine

Phe/F – phenylalanine

Pro/P – proline

Ser/S – serine

Thr/T – threonine

Trp/W – tryptophan

Tyr/Y – tyrosine

Val/V – valine

*Acidic Amino Acids:*

Asp/D – aspartic acid

Glu/E – glutamic acid

*Basic Amino Acids:*

Arg/R – arginine

His/H – histidine

Lys/K –lysine

# CHAPTER ONE

# INTRODUCTION

# 1 Introduction

In this chapter background information on peroxidases is presented, the relationship between peroxidases and other haem-containing proteins is discussed, and an overview of ascorbate peroxidase enzymes is given. Accordingly, this chapter is organised into the following sections. First, the diverse range of functions exhibited by haemoproteins in general is introduced and properties of different superfamilies are summarised. Second, the plant peroxidase superfamily of enzymes has been classified and representatives from each of the three classes are illustrated. Crystal structures of several plant peroxidases have been resolved, and the information gleaned from the crystallographic data is considered. Third, the peroxidase mechanism and the role(s) of conserved amino acid residues are examined. Fourth, a mini-review of the existing ascorbate peroxidase (APX) research is given and, fifth, particular attention is drawn to the recombinant pea cytosolic enzyme, which is the subject of the research presented in this thesis. Sixth, and finally, the aims of the studies that are reported in the proceeding chapters are briefly summarised.

## 1.1 Haem and haemoproteins

A recent review proposed that haems, *i.e.* iron-porphyrin complexes, might be considered the most versatile of redox centres in biology.[1] A large majority of haemoproteins contain ferriprotoporphyrin IX as the prosthetic group, and this section aims to summarise how the versatility in function of haem-containing proteins is made possible by differences in the structure of the various polypeptides. Whilst the role of the porphyrin itself in influencing haemoprotein function has not gone unnoticed,[2] discussion of the structure and reactivities of

2

other haems present within haemoproteins is not considered in detail here, and for the purposes of this chapter, the discussion will concentrate only on iron protoporphyrin IX.

## 1.1.1 Haem as a prosthetic group

Ferriprotoporphyrin IX, Figure 1-1, is a ubiquitous prosthetic group amongst biological systems and, as such, is capable of supporting a surprisingly diverse range of functions, including oxygen transport, electron transfer, and catalytic chemistry in the peroxidase and monooxygenase enzymes. Ferriprotoporphyrin IX, containing iron(III), is a hemin, whilst ferroprotoporphyrin IX, containing iron(II), is a haem.[1] As the prosthetic group of a protein, the metal-containing porphyrin can exist in several different oxidation states, but provided that the state is clearly specified, the moiety is more simply referred to as haem, regardless of its oxidation state. Indeed, throughout this thesis, haem is mainly used to refer to iron protoporphyrin IX, which is the haem motif found in pea cytosolic ascorbate peroxidase.

Identification of the ways in which protein structure is able to modulate the chemistry of the haem (or any other) prosthetic group is one of the most significant challenges in bio-inorganic chemistry. The acquisition of such fundamental knowledge is of more than academic interest: it is central to developing our understanding of the way enzymes operate and ought to establish a firm foundation upon which the rational design of new enzymes for potential industrial or medical uses can be based. Accordingly, given the diversity in function that is displayed by haemoproteins, an understanding of the mechanisms by which the conformation of the prosthetic group, and the chemical reactivity of the haem-iron, is
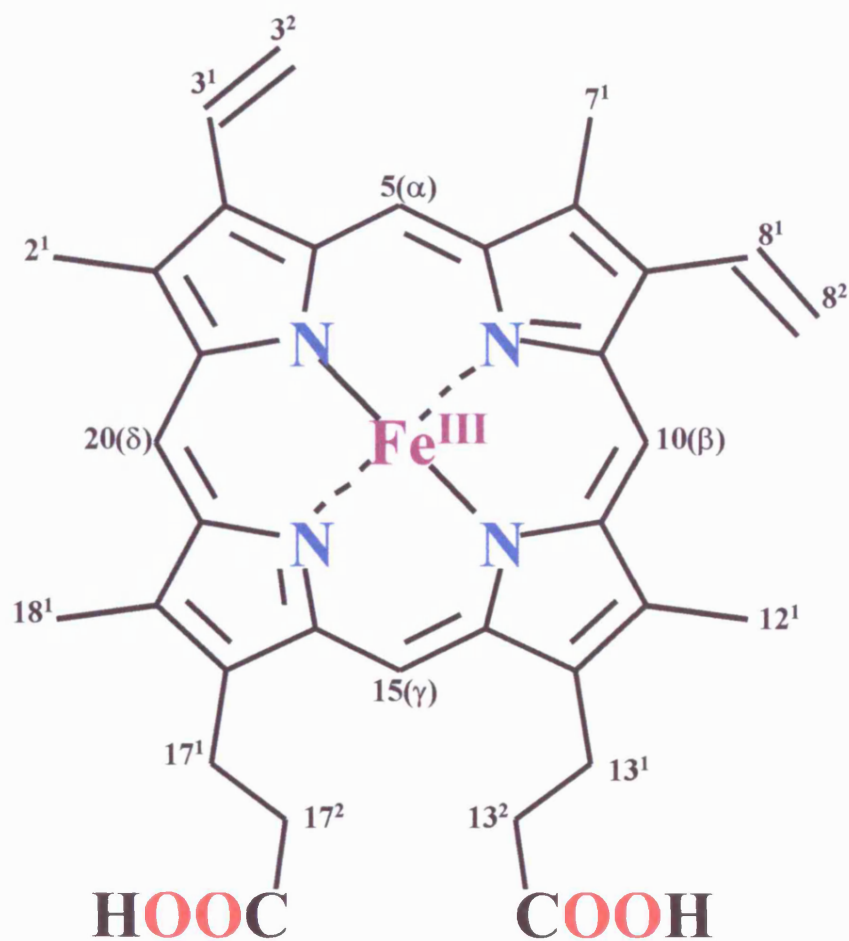
**Figure 1-1 Structure and nomenclature of ferriprotoporphyrin IX.** Proton-bearing carbon atoms are numbered according to the IUB/IUPAC system with Fischer notation in parentheses.

controlled by the polypeptide structure of haemoproteins is of tremendous importance to the advancement of our current ideas on structure-function relationships.

## 1.1.2 Haemoproteins

Haemoproteins comprise a family of metalloproteins that are considerably varied in their physiological functions.[3] The functions that haem-containing proteins are known to perform include: electron transfer reactions, such as those involving cytochrome $c$;[4] oxygen transport and storage, via haemoglobin and myoglobin, respectively;[5] oxygenations of organic substrates as facilitated by cytochrome P450;[6] and hydroperoxide-dependent substrate oxidation by peroxidases.[7,8]

A comparison of the haem-bound iron axial ligand(s) and observed iron redox states of various types of haemoprotein is made in Table 1-1. The redox and coordination chemistry of the haem-iron has a profound role in influencing the function of haemoproteins. Clearly, the haemoproteins involved in simple electron transfer reactions need to avoid substantial reorganisation at the haem-iron and are, consequently, predominantly six-coordinate with the iron in a low-spin state in both oxidation states. In contrast, the availability of a coordination site to bind exogenous ligands is important for haemoproteins that are activated by oxygen or peroxide.

## 1.1.3 Electron transfer

During respiration and photosynthesis, each electron transfer reaction represents a waste of metabolic energy, as the high-energy electron falls further into a potential well. Accordingly,

| | Redox State[a] | | Coordination Geometry[b] | | |
|---|---|---|---|---|---|
| Haemoprotein | Resting | Other | Number | Ligand(s) | Function |
| Cytochrome c | III | II | 6 | His/Met | Electron transfer |
| Myoglobin | II | III | 6 | $H_2O$/His | Oxygen storage |
| Haemoglobin | II | III | 6 | $H_2O$/His | Oxygen transport |
| Cytochrome P450 | III | II & IV | 6[c] | $H_2O$/Cys | Oxygenation of a substrate |
| Cytochrome c peroxidase | III | IV | 5 | His | Ferrocytochrome c oxidation |

Table 1-1 Comparison of haemoprotein function and haem-iron coordination geometry.
[a] Haem-iron oxidation states that are relevant to the normal function of the haemoprotein.
[b] Coordination of the haem-iron in the resting state. [c] The resting-state of P450s are six-coordinate, however, the aqua ligand is sufficiently labile that upon binding of the physiological substrate the axial ligand dissociates and affords a five-coordinate haem-iron that, following reduction to the ferrous state, more readily binds dioxygen.

natural systems must balance the speed of an electron transfer reaction with its energetic efficiency. Whilst, the distance between redox centres during the transfer process itself and the nature of intervening medium, *i.e.* whether the electron travels through bonds or through space, are vital considerations in electron transfer reactions, there are other factors that influence the rate of electron transfer within physiological systems, *e.g.*: the redox potential difference between the electron donor and acceptor, which contributes to the driving force for the reaction, and the reorganisation energy associated with the process, which affects the efficiency of the transfer.

Haems are ideally suited for electron transfer reactions as the extended $\pi$-system of the porphyrin ring delocalises the electron over a wide area, thereby minimising the reordering in the local atomic structure and the surrounding milieu on transfer of an electron. Lower reorganisation energies are associated with rigid hydrophobic systems, so for cytochromes associated with simple electron transfer reactions the haem is usually six-coordinate low-spin and bound within a hydrophobic crevice. The reduction potential of the haem can be modulated over a wide range (>0.7 V) by the surrounding protein.[1] In general, amongst *c*-type cytochromes His/His ligation correlates with a lower reduction potential than His/Met, although there are exceptions to this trend.[1] Site-directed mutagenesis has facilitated quantification of the effect that haem-iron ligation has upon haemoprotein reduction potentials. For example, axial ligand replacement of mitochondrial cytochrome *c* from His/Met to His/His changes the reduction potential by 221 mV, from +260 mV to +41 mV respectively.[9] However, whilst there are a number of other variables that are known to affect the reduction potential – including hydrogen bonding of the proximal ligand,[10] haem

7

orientation,[11] orientation of the haem vinyl groups[12] and orientation of the haem ligands[13] –

experimental strategies aimed at isolating only one of these variables, whilst keeping all other

constant, is difficult and, as such, the exact structural factors controlling reduction potential

are still not clearly defined.

## 1.1.4 Haemoglobin and myoglobin

Globins reversibly bind oxygen, Equation 1-1,

$$\text{Globin}(Fe^{II}, H_2O) + O_2 \overset{K_a}{\rightleftharpoons} \text{Globin}(Fe^{II}, O_2) + H_2O \qquad [1\text{-}1]$$

and the equilibrium requires that the haem-iron be maintained in its ferrous oxidation state

under physiological conditions. The hydrophobic distal haem pocket of globins stabilises the

oxygen-bound complex, and the conserved distal histidine and valine residues ensure that the

binding of other small molecules at the sixth coordination site is highly disfavoured. At

neutral pH, the resting-state haem-iron of haemoglobin and myoglobin is coordinated to a

highly conserved histidine residue and a labile water molecule, which are located on the

proximal and distal protein domains, respectively.

Again, recombinant expression systems and site-directed mutagenesis have greatly

enhanced our understanding of how the structure of globins controls haem coordination

geometry. As such, the active site of myoglobin and the effects of active site amino acid

substitutions have been subjects of intense experimental scrutiny. The details of this work are

beyond the scope of this discussion, but excellent reviews are available.[14,15]

## 1.1.5 Monooxygenase enzymes

Haem-containing monooxygenases,[6] unlike globins, activate molecular oxygen and catalyse the incorporation of an oxygen atom from dioxygen into a substrate molecule.[16,17] Activation of dioxygen requires electrons that are transferred to the enzyme by electron transfer proteins, and the insertion of one of the oxygen atoms into the substrate necessitates that the latter be bound within the vicinity of the former, *i.e.* in the proximity of the haem-iron. The reaction catalysed by these haem-containing enzymes can be generalised as follows, Equation 1-2,

$$XH + O_2 + 2e^- + 2H^+ \rightarrow X(O)H + H_2O \qquad [1\text{-}2]$$
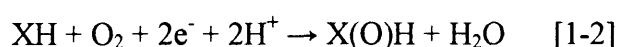
where XH represents substrate. Monooxygenation by P450 enzymes involves four well-characterised and isolable states. First, the six-coordinate ferric resting-state is converted to a five-coordinate high-spin state upon substrate binding, Equation 1-3,

$$P450(Fe^{III}, H_2O) + XH \rightleftharpoons P450(Fe^{III})\cdot XH + H_2O \qquad [1\text{-}3]$$
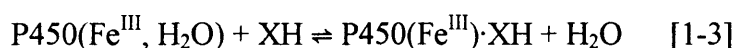
subsequently, the associated change in haem-iron reduction potential (from $-270$ mV to $-170$ mV)[18] favours electron transfer to the P450, which results in the generation of the five-coordinate high-spin deoxyferrous state, Equation 1-4.

$$P450(Fe^{III})\cdot XH + e^- \rightleftharpoons P450(Fe^{II})\cdot XH \qquad [1\text{-}4]$$
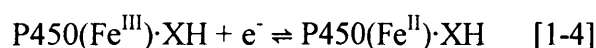
Dioxygen binds to the ferrous enzyme to form the oxyferrous complex, Equation 1-5, the valence structure of which can be considered as either dioxygen bound to a ferrous haem-iron or as the ferric superoxide complex, Equation 1-6.

$$P450(Fe^{II}) \cdot XH + O_2 \rightleftharpoons P450(Fe^{II}, O_2) \cdot XH \qquad [1\text{-}5]$$

$$P450(Fe^{II}, O_2) \cdot XH \rightleftharpoons P450(Fe^{III}, O_2^-) \cdot XH \qquad [1\text{-}6]$$
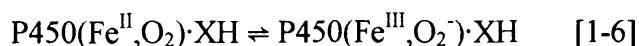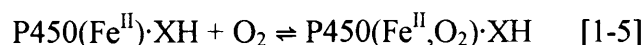
Transfer of a second electron, the rate-limiting step in the catalytic cycle, transiently yields a ferric peroxydianion species, Equation 1-7,

$$P450(Fe^{III}, O_2^-) \cdot XH + e^- \rightleftharpoons P450(Fe^{III}, O_2^{2-}) \cdot XH \qquad [1\text{-}7]$$
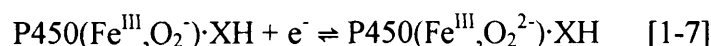
which is protonated by two successive proton transfers. The first yielding a ferric peroxyanion species, Equation 1-8,

$$P450(Fe^{III}, O_2^{2-}) \cdot XH + H^+ \rightleftharpoons P450(Fe^{III}, OOH^-) \cdot XH \qquad [1\text{-}8]$$
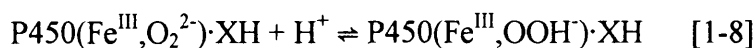
and the second leading to heterolytic O-O bond cleavage, which releases water and generates the 'reactive oxygen' species, Equation 1-9.

$$P450(Fe^{III}, OOH^-) \cdot XH + H^+ \rightleftharpoons P450(Fe^{IV}=O, P^{+\bullet}) \cdot XH + H_2O \qquad [1\text{-}9]$$
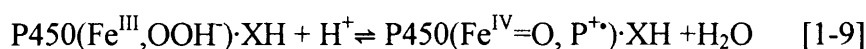
The reactive species, $P450(Fe^{IV}=O, P^{+\bullet})$, is probably an oxyferryl ($Fe^{IV}=O$) porphyrin cation radical intermediate, equivalent to peroxidase enzymes Compound I (section 1.3), and has only very recently been detected.[19,20] Transfer of the oxygen to the substrate, presumably by an oxygen rebound mechanism, yields both the product and regenerates the resting state enzyme, Equation 1-10.

$$P450(Fe^{IV}=O, P^{+\bullet}) \cdot XH \rightleftharpoons X(O)H + P450(Fe^{III}, H_2O) \qquad [1\text{-}10]$$
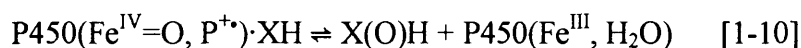
Addition of hydroperoxides to the five-coordinate high-spin substrate-bound P450 complex shunts the reaction to completion, which further highlights the similarity between monooxygenases and peroxidases, where the latter catalyse a wide variety of hydroperoxide-dependent oxidations (section 1.3).

A distinguishing feature of P450s is their ability to reductively cleave the O-O bond of dioxygen, which is capable of oxygen atom insertion into hydrocarbon substrates. The strong electron-releasing character of the P450 proximal cysteinate ligand, also referred to as the push effect, promotes heterolytic O-O bond cleavage. However, the 'push effect' is insufficient, by itself, to promote cleavage of the O-O bond. Hydrogen-bonding networks within the substrate-binding site ensure that the protons required for catalytic turnover are readily available from either the surrounding bulk solvent or an internal solvent pool.

Evidence supporting the influence that the proximal thiolate ligand of P450 enzymes have upon the haem-iron chemistry has come from several sources.[6] Indirect confirmation coming from comparison between the anionic ligand-binding properties of ferric P450 and met-myoglobin, containing iron(III), which revealed that the anionic ligands have a much lower affinity for the monooxygenase, most probably due to the electron-releasing character of the proximal thiolate. The reaction between $H_2O_2$ and wild-type myoglobin results in homolytic O-O bond cleavage; mutagenic replacement of the proximal histidine of myoglobin with cysteine facilitates heterolytic cleavage of peroxide and, subsequently, the axial thiolate ligand present in the myoglobin variant stabilises the oxyferryl haem-iron species formed.[15]

## 1.2 Haem-containing peroxidases

The field of peroxidase chemistry has played an important part in the development of modern enzymology,[8] and the increasing availability of crystallographic data for these enzymes still makes them highly attractive to ongoing research into enzyme structure-function investigations. Furthermore, the availability of recombinant DNA technology means that it is now possible to introduce systematic perturbations to the protein

architecture, and subsequently characterise the new variant proteins using a range of techniques. This section summarises the state of our current knowledge of haem-containing peroxidases, particularly focussing upon the mechanism of catalysis.

## 1.2.1 General properties

Haem peroxidases are a group of haem-containing enzymes that catalyse the $H_2O_2$-dependent oxidation of a wide range of organic and inorganic substrates.[8,21,22] Peroxidases have been isolated from a variety of biological sources, and are known to perform several diverse roles, *e.g.* biosynthesis and defence. The overall equation for the reaction catalysed by a peroxidase is given by Equation 1-11:

$$2S_{red} + H_2O_2 + 2H^+ \rightarrow 2S_{ox} + 2H_2O \qquad [1\text{-}11]$$
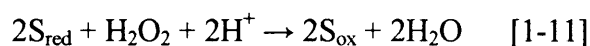
where $S_{red}$ is the reducing substrate and $S_{ox}$ the oxidised product. Consequently, the function of a peroxidase is wholly dependent upon its substrate recognition properties.

The ability of haem peroxidases to react with hydrogen peroxide and form a stable oxidised intermediate, known as Compound I, distinguishes them from other haemoproteins. Peroxidase catalytic turnover proceeds through two detectable oxyferryl ($Fe^{IV}=O$) intermediates, known as Compound I and Compound II:
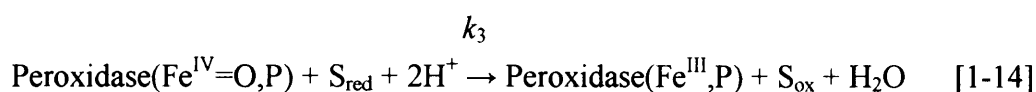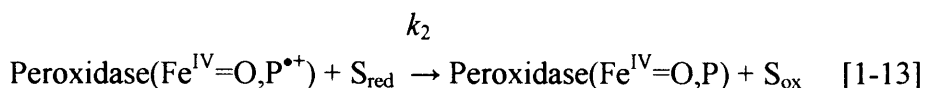
$$\text{Peroxidase}(Fe^{III},P) + H_2O_2 \xrightarrow{k_1} \text{Peroxidase}(Fe^{IV}=O,P^{\bullet+}) + H_2O \qquad [1\text{-}12]$$

$$\text{Peroxidase}(Fe^{IV}=O,P^{\bullet+}) + S_{red} \xrightarrow{k_2} \text{Peroxidase}(Fe^{IV}=O,P) + S_{ox} \qquad [1\text{-}13]$$

$$\text{Peroxidase}(Fe^{IV}=O,P) + S_{red} + 2H^+ \xrightarrow{k_3} \text{Peroxidase}(Fe^{III},P) + S_{ox} + H_2O \qquad [1\text{-}14]$$

where $S_{red}$ & $S_{ox}$ are the reduced and oxidised forms of the substrate, S; $Fe^{III},P$ corresponds to the peroxidase resting-state; $Fe^{IV}=O,P^{\bullet+}$ & $Fe^{IV}=O,P$ Compound I and Compound II, respectively. Moreover, Compound I has been oxidised by two electrons, relative to the resting-state enzyme, and the second oxidising equivalent is stored as either a protein-based radical or a porphyrin $\pi$-cation radical, $P^{\bullet+}$,[21] e.g. cytochrome $c$ peroxidase (CcP) Compound I contains a protein-based radical,[23] whilst horseradish peroxidase (HRP) Compound I has a porphyrin-based radical.[24]

Aside from differing in the location of the second oxidizing equivalent, CcP and HRP belong to different families of peroxidases. On the basis of protein sequence homologies, Welinder proposed a classification of the haem-containing plant peroxidase superfamily that separates the enzymes into three peroxidase families,[25] and the use of this classification has systematically organised our existing peroxidase knowledge.

Yeast cytochrome $c$ peroxidase, chloroplastic and cytosolic ascorbate peroxidases are representatives of class I peroxidases, this plant peroxidase family is of prokaryotic origin and the enzymes that comprise this class have no carbohydrate, no cysteine bridges, no calcium ions, and no signal peptide for secretion. The Trp191 residue of the yeast enzyme appears to be conserved within other class I peroxidases, although a potassium-binding site, not found in CcP, has been identified in the vicinity of the proximal tryptophan residue of ascorbate peroxidase (APX).[26]

Lignin and manganese peroxidases are secreted fungal enzymes and, as such, belong to class II. In addition to the amino terminal signal peptide required for secretion through the endoplasmic reticulum, these fungal peroxidases possess 5% carbohydrate content, two

calcium ions, and four conserved disulphide bridges. The proximal tryptophan, conserved in class I peroxidases, is replaced by phenylalanine or leucine in class II enzymes.

Class III is comprised of classical secretory plant peroxidases that possess two calcium ions, an N-terminal signal peptide for excretion, four conserved disulphides bridges that are in different locations to those of class II peroxidases, and extra helices that play a role in access to the haem edge. Horseradish (perhaps the most well-documented of all peroxidases) and peanut peroxidases are members of the class III peroxidase family. The extent of glycosylation ranges between 0 to 25% and some enzymes have a C-terminal propeptide that may target them for vacuoles.

## 1.2.2 Crystallographic data available for haem peroxidases

In 1980, the first crystal structure for a peroxidase that of yeast cytochrome $c$ peroxidase was published.[27] The crystallisation of this enzyme was greatly facilitated by its lack of glycosylation and propensity to form crystals after extensive dialysis into high-quality deionised water. Over ten years elapsed before a second plant peroxidase crystal structure was published and, because of this, cytochrome $c$ peroxidase became something of a paradigm for the peroxidase enzymes. The use of cloned or synthetic genes has circumvented the problem posed by glycosylation, as peroxidases expressed in $E.$ $coli$ are not glycosylated, resulting in expeditious crystallisation of these enzymes and a subsequent explosion in the availability of recombinant protein crystal structures. Crystal structures have now been published for several peroxidase enzymes: lignin peroxidase,[28] Coprinus cinereus peroxidase,[29] Arthromyces

*ramosus* peroxidase,[30,31] manganese peroxidase,[32] pea cytosolic ascorbate peroxidase,[26] peanut peroxidase,[33] barley peroxidase,[34] and isozyme C of horseradish peroxidase.[35]

In common with many haemoproteins, peroxidase enzyme secondary structures are dominated by α-helices. The gross structural features of all the plant peroxidase families are such that the polypeptide structures can be divided into N- and C-terminal domains, with the haem located in the cavity at the domain interface, *e.g.* the crystal structure of cytochrome *c* peroxidase is shown in Figure 1-2. Peroxidases of classes II and III additionally contain two $Ca^{2+}$-binding sites that are located some distance from the haem-iron (>10 Å) either side of the active-site, one in each of the protein domains. The release of these calcium ions is associated with inactivation of the enzyme,[36,37] and are required, along with exogenous haem, for the correct reconstitution of recombinant HRP,[38] which is initially expressed as apoprotein (*i.e.* without haem).

Crystallographic data for ligand-bound CcP ternary complexes have been published,[39-41] and reveal the conformation of the distal arginine, Arg48 in CcP, is modulated by the electronic charges in the vicinity of the haem-iron. The positively charged amino acid is pushed away (0.6 Å) from the haem-iron upon the binding of nitric oxide, but pulled back towards (2.5 Å) the haem-iron in the presence of fluoride. Also an extended H-bonding network between the distal histidine, a conserved asparagine residue and a peptide-bond carbonyl were identified.

Crystallographic data for substrate-bound peroxidase complexes was, until recently, limited to that of cytochrome *c*-CcP42 and $Mn^{II}$-MnP,[32] which were considered too atypical to be utilised as general structural models for other peroxidase-substrate interactions. A

**Figure 1-2 The crystal structure of yeast cytochrome *c* peroxidase.** Computer-based molecular model of yeast C*c*P based upon the published protein crystal structure coordinates [Finzel, B. C. and Poulos, T. L. (1984) *J. Biol. Chem.*, **259**, 13027-13036 ].

substrate-bound peroxidase complex, between ferulic acid and the cyanide-bound ternary complex of HRP was published during the course of these studies.[43] Unsurprisingly, the substrate-binding sites are different for each enzyme.

## 1.3 Compound I formation and mutagenic studies

The mechanistic aspects of peroxidase catalysis (Figure 1-3) can be viewed as consisting of two distinct stages: first, the generation of the highly oxidising intermediate Compound I, i.e. Equation 1-12; second, two successive single electron transfers from substrate molecules to the oxidised intermediates, i.e. Equation 1-13 & Equation 1-14. Accordingly, the first stage in all peroxidase-catalysed reactions is the formation of Compound I. Amino acid residues that are involved in maintaining the integrity of active-site have been identified and probed using site-directed mutagenesis.

This section begins with a description of the mechanism by which peroxidase enzymes are believed to catalyse the heterolytic cleavage of hydrogen peroxide. Subsequently, the role(s) that key amino acid residues play in the formation of Compound I are discussed in the light of published mutagenic data.

### 1.3.1 Mechanism of compound I formation

Prior to publication of the crystal structure of CcP, it had been established that Compound I of CcP and HRP contain both oxidising equivalents of the peroxide, albeit in the form of different radicals.[8] However, a consensus on the amino acids essential for Compound I formation had not been reached.

17
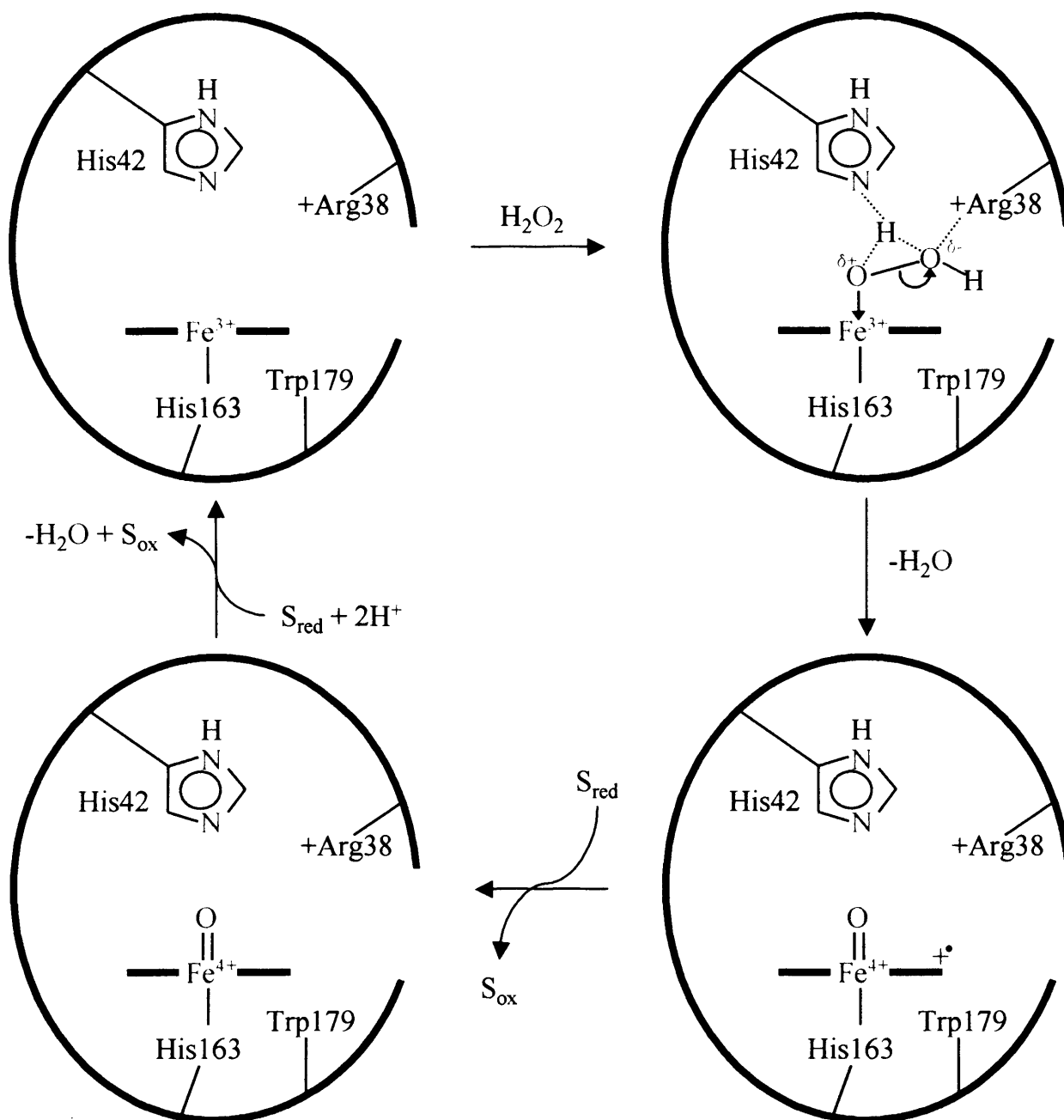
**Figure 1-3 General peroxidase mechanism.** This mechanism is modified from that originally proposed by Finzel and Poulos [Finzel, B. C. & Poulos, T. L. (1984) *J. Biol. Chem.*, **259**, 13027-13036]. The key active-site amino acid residues have been labelled according to the nomenclature used for pea cytosolic ascorbate peroxidase.

The original mechanism proposed for Compound I formation by Poulos and Kraut[44] in 1980 was based upon the crystal structure of yeast cytochrome $c$ peroxidase, and two key features of their original mechanism have stood the test of time – the reader is referred to several recent reviews that have discussed the mechanism of peroxidase catalysis in detail.[7,8,22,45,46] First, the distal histidine residue acts as a proton acceptor from hydrogen peroxide; second, the distal arginine is a charge stabiliser, which facilitates heterolytic cleavage of the O-O bond. The peroxidase active-site residues involved in enzymatic turnover are primarily those illustrated in Figure 1-3.

The distal histidine residue (His42 in Figure 1-3) is believed to perform several roles: first, it acts as a general base removing the α-proton of $H_2O_2$ and facilitating binding of the peroxyanion to the ferric iron; second, it acts as a general acid stabilising the developing negative charge on the β-oxygen during heterolytic O-O bond cleavage through transferral the α-proton. To maintain the resting state general base character of the distal histidine, a strong hydrogen bond is conserved with a distal asparagine which maintains the $N^\varepsilon$ of the distal histidine in a deprotonated form. Heterolytic cleavage of hydrogen peroxide and stabilisation of the resulting oxyferryl species is mainly attributable to the electron 'pull' of the distal arginine and the 'push' of the proximal histidine: the distal arginine residue (Arg38 in Figure 1-3) is believed to favour cleavage of the O-O bond of the peroxide by stabilising developing negative charge on the oxygen closest to it; whilst the proximal histidine residue (His163 in Figure 1-3) is involved in a strong hydrogen bond with the carboxylate functionality of an aspartate residue, which increases its imidazolate character and results in the aforementioned electron 'push' effect.

## 1.3.2 Mutagenic studies

More recently, the development of recombinant expression systems for yeast cytochrome $c$ peroxidase[47] and horseradish peroxidase[38,48] have permitted the role(s) of individual amino acids in peroxidase catalysis to be explored using site-directed mutagenesis. Site-directed replacement of key active-site residues of CcP and HRP has revealed a great deal about the various factors that control peroxidase function. In particular, the residues that comprise the extensive H-bonding network that reaches between the proximal and distal protein domains of peroxidase enzymes has been comprehensively investigated using a combination of mutagenic, kinetic and spectroscopic techniques. The details of these studies are well beyond the scope of this discussion, and the reader is referred to a number of recent review articles that cover these issues in more depth.[7,8,22,45,49] A short summary of the mechanistic implications of various mutations is given below.

Replacement of the distal histidine has a profound effect on the second order rate constant for Compound I formation for both CcP45 and HRP.[50] In contrast, whilst replacement of the distal Arg group in CcP has a rather modest effect,[45] the same mutation in HRP has a 500-fold effect on the rate constant for Compound I formation.[50] Replacement of the proximal aspartate (Asp235) of yeast CcP with asparagine removes a key H-bonding interaction between this residue and the proximal histidine, but only leads to a 5-fold decrease in the rate of Compound I formation, indicating that electron donation to the haem through Asp235 is not influential in peroxide activation.[51]

## 1.4 Ascorbate peroxidases

Ascorbate peroxidase (APX) enzymes have been isolated and characterised from a variety of sources, and a number of genes encoding different isoforms of APX have been identified. Recombinant expression systems now exist for several forms of APX, which enables preparation of wild-type and variant proteins in much higher yields. The aim of this section is to introduce the physiological function of APXs, and concludes with a summary of the general properties of those enzymes for which spectroscopic and kinetic data are available. Biological and physiological aspects of APX enzymes are not dealt with here, but have been comprehensively reviewed elsewhere.[52]

### 1.4.1 Ascorbate peroxidase, ascorbate and monodehydroascorbate radicals

Ascorbate-dependent peroxidase activity was first identified in 1979.[53,54] A sub-family of class I plant peroxidases,[25] ascorbate peroxidases are haem-containing enzymes that catalyse the ascorbate-dependent reduction of hydrogen peroxide in plants and algae, Equation 1-15,

$$2 \text{ ascorbate} + H_2O_2 + 2H^+ \rightarrow 2\text{monodehydroascorbate}^\bullet + 2H_2O \qquad [1\text{-}15]$$
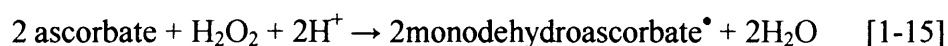
and an ascorbate peroxidase can, therefore, be defined as such if the preferred physiological substrate is L-ascorbic acid, i.e. vitamin C (Figure 1-4). This, in itself, is not a particularly useful definition, since peroxidases are notoriously indiscriminate in their choice of redox partner and, therefore, it is often difficult to identify a clearly perceptible physiological substrate. Accordingly, an alternative is to classify a peroxidase as an APX when the specific activity of the enzyme for ascorbate is higher than that for other substrates. On the whole, this
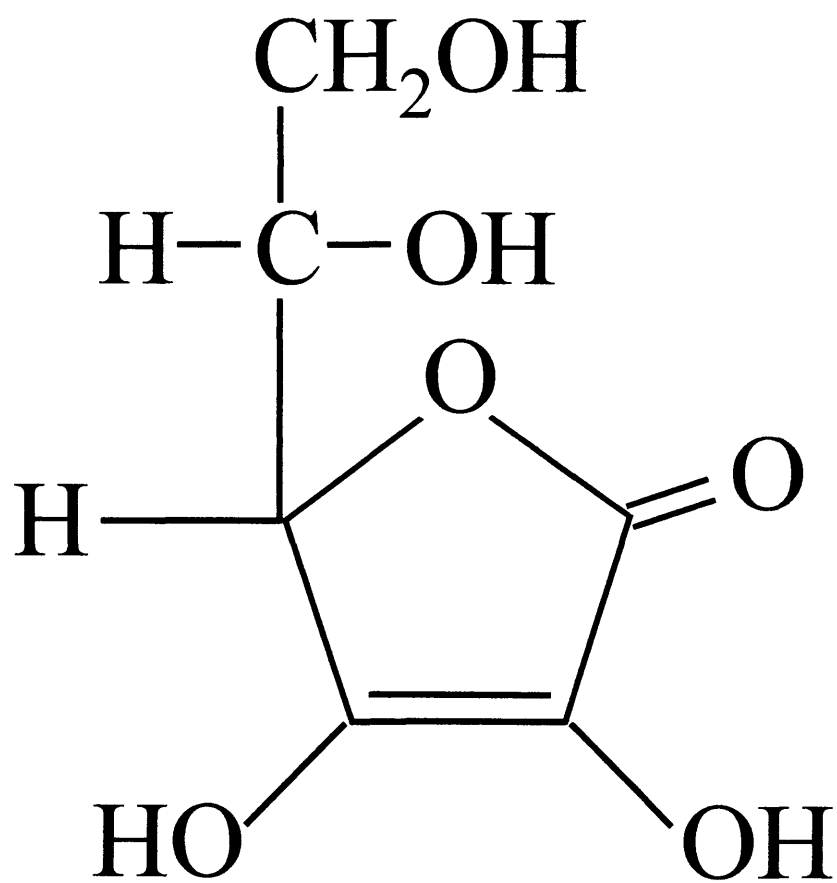
**Figure 1-4 Structure of Vitamin C.** The preferred substrate of ascorbate peroxidase enzymes is L-ascorbic acid, *i.e.* Vitamin C.

has been adopted and has the advantage that it is able to discriminate between authentic APXs and other peroxidases that are, coincidently, able to catalyse oxidation of ascorbate.

Cytosolic and chloroplastic APXs, together with CcP and the gene-duplicated bacterial catalase-peroxidases, comprise class I peroxidases. It is possible, however, that this general classification may need reviewing: recent experiments on tea leaves have identified two APX enzymes that have closer sequence homology to classical class III peroxidases than to class I.[55,56]

The immediate product of the oxidative reaction (Equation 1-15), the monodehydroascorbate radical, is a reactive and unstable species that, in the presence of a suitable reductase system, is reduced back to ascorbate. Monodehydroascorbate reductases have been identified and purified in a few cases.[57-61] In the absence of a suitably efficient reductase system, monodehydroascorbate radicals can readily disproportionate to ascorbate and dehydroascorbate, Equation 1-16.

$$2\text{monodehydroascorbate}^\bullet \rightarrow \text{ascorbate} + \text{dehydroascorbate} \quad [1\text{-}16]$$

### 1.4.2 APX cDNA sequences

Since the publication of the first cDNA sequence for an ascorbate peroxidase,[62] cDNA sequences for a variety of APXs have been published.[63] These include: (a) the soluble cytosolic enzymes from soybean,[64,65] spinach,[66] Arabidopsis,[67] carrot,[63] radish,[68] maize,[69] tobacco,[70] rice,[71] strawberry[72] and bell pepper,[73] (b) the stromal (chloroplastic) enzymes from Arabidopsis,[63,74] spinach[75] and pumpkin,[76] (c) the thylakoid-bound (chloroplastic) enzymes from Arabidopsis,[63,74] spinach[75] and pumpkin[76,77] and (d) the glyoxysomal/peroxisomal

(microbody-bound) enzymes from *Arabidopsis*,[63,74,78] cotton,[79] *M. crystallinum*[63] and spinach.[80]

### 1.4.3 Bacterial expression

Whilst a variety of cloned genes for various APXs are now available, expression of these genes in *E. coli* has been less successful. Recombinant expression systems for APX have, however, been reported in a few cases: the first was for pea cytosolic APX,[81] although this system has subsequently been modified to facilitate variant protein expression.[82] The expression of cytosolic enzymes from soybean[64,83] and spinach[84] have also been reported. Recently, bacterial expression of two chloroplastic (stromal and thylakoid-bound) enzymes[84] and a glyoxysomal enzyme[85] from spinach have been reported.

### 1.4.4 Isolation and characterisation of native APXs

Cytosolic APX enzymes have now been identified and purified from pea,[53,54,86,87] Japanese radish,[88] soybean,[89] wheat,[90,91] potato tubers,[92] maize,[93] komatsuna,[94] tea,[56,95] spinach[84,96] and rice.[57] Chloroplastic enzymes have been isolated and purified from spinach,[84,96,97] pea,[98-101] wheat[102] and tea.[56,95,103,104] Glyoxysomal enzymes have also been identified in cotton,[105] pumpkin[106] and spinach;[80,85] peroxisomal enzymes have been identified in cucumber,[107] pea[98,99] and pumpkin.[106] APXs have also been identified from several algal sources, namely *Galdieria partita*,[108] *Selenastrum capricornutum*,[109] *Chlorella vulgaris*[110] and *Euglena gracilis*,[111,112] in cyanobacteria[113,114] and in insects.[115] An APX enzyme has also been identified in *Trypanosoma cruzi*.[116] Recently, an APX enzyme has been isolated and purified

from bovine eye,[117] raising the intriguing possibility that APX enzymes may have a functional role in mammalian systems.

In many cases, detailed characterisation of these native APXs has been hampered by the poor yields obtained after purification, and only very basic spectroscopic information has been reported together with steady-state catalytic data. For enzymes where more than the bare minimum of functional data are available, a summary of selected physical properties for various cytosolic, chloroplastic, algal and mammalian APXs has been published recently.[118]

## 1.4.5 General properties

The consensus obtained from the existing spectroscopic and kinetic data reveals some general properties associated with APXs. First, the Soret band wavelength maxima of the enzymes, in their ferric resting-state, lie within the range 401-409 nm and are, therefore, broadly consistent with the predominance of high-spin haem-iron. However, the variance observed in the electronic absorption spectra suggests that the proportions of particular spin-states depend upon the source of the APX. Second, values obtained for $K_m$ for ascorbate and $H_2O_2$ fall within comparatively narrow ranges, 55-770 $\mu$M and 3-188 $\mu$M respectively. Third, APXs are capable of catalysing the oxidation of an array of non-physiological reducing-substrates. Indeed, some cytosolic APXs catalyse the oxidation of pyrogallol (1,2,3-trihydroxybenzene) at rates that are faster than that measured for ascorbate.[118]

## 1.4.6 Haem-iron reduction potential

Experimental difficulties associated with direct electrochemistry of peroxidases means that there is very little redox information available for APXs – although some of these deficiencies are now being overcome.[119] Mid-point reduction potentials for the Compound I/Compound II and Compound II/ferric couples are not yet available for APX. However, the mid-point reduction potential for the $Fe(III)/Fe(II)$ redox couple of recombinant soybean APX has been measured by mediated spectroelectrochemistry to be $-159 \pm 2$ mV vs SHE (25.0°C, pH 7.0, $\mu$ = 0.10 M).[120] This is in a similar range as reported values for other peroxidases (all vs SHE): HRP (-261 mV),[121] CcP (-194 mV and -182 mV),[122,123] MnP (-93 mV)[124] and LiP (-130 mV).[124] The observed potential for soybean APX is therefore consistent with the generally accepted mechanism of peroxidase catalysis, i.e. Equations 1-12–1-14, in which stabilization of high iron oxidation states is required. The corresponding potentials for the globins, where stabilization of low oxidation states is required for oxygen binding, are much lower, e.g. for horse heart myoglobin the observed potential vs SHE is +64 mV (pH 6.0).[125]

## 1.5 Pea cytosolic ascorbate peroxidase

Currently, recombinant pea cytosolic ascorbate peroxidase (wild-type rAPX) is the only APX for which a resolved protein crystal structure is available, making this enzyme unique amongst APXs. Wild-type rAPX shares a 33% amino acid sequence homology with yeast CcP but, somewhat unexpectedly, was found to contain a metal-binding site in the vicinity of the class I peroxidase-conserved proximal tryptophan. In addition, whilst the proximal tryptophan of CcP has been identified as the location of the second oxidising equivalent in

CcP Compound I,[126] wild-type rAPX forms a relatively unstable porphyrin π-cation radical even though it contains the same Trp residue.[127] Accordingly, considerable interest has been directed towards identifying structure-function correlations, and differences, that exist between these class I peroxidases.[128-131]

This section is intended to summarise the state-of-the-art studies that have been conducted on wild-type rAPX and its variants. Steady- and transient-state kinetic data are available for the native enzyme,[81,86,132] which facilitates corroboration of the rAPX data. The spectroscopic and kinetic data presented are discussed in relation to the published crystal structure.[26]

## 1.5.1 Crystallographic studies

Native pea cytosolic enzyme was isolated in 1991,[86] and the cDNA sequence was published within the same year.[62] This haem-containing enzyme comprises of 249 amino acid residues and has a calculated relative molecular weight, MW, of ≈28 kDa. A recombinant expression system was reported for the enzyme in 1994[81] and the crystal structure of wild-type rAPX (Figure 1-5) was published in 1995.[26] The high degree of homology between pea cytosolic ascorbate peroxidase and yeast cytochrome c peroxidase certainly provided some of the momentum behind this rapid advancement, but the resolution of the protein crystal structure revealed some unexpected structural differences that have prompted further structure-function studies.

The 33% sequence homology between wild-type rAPX and CcP results in an essentially identical monomeric secondary protein structure. Both class I peroxidases consist of primarily α-helices, which are labelled according to CcP nomenclature (A-B, B', C-F, F', G-J); the
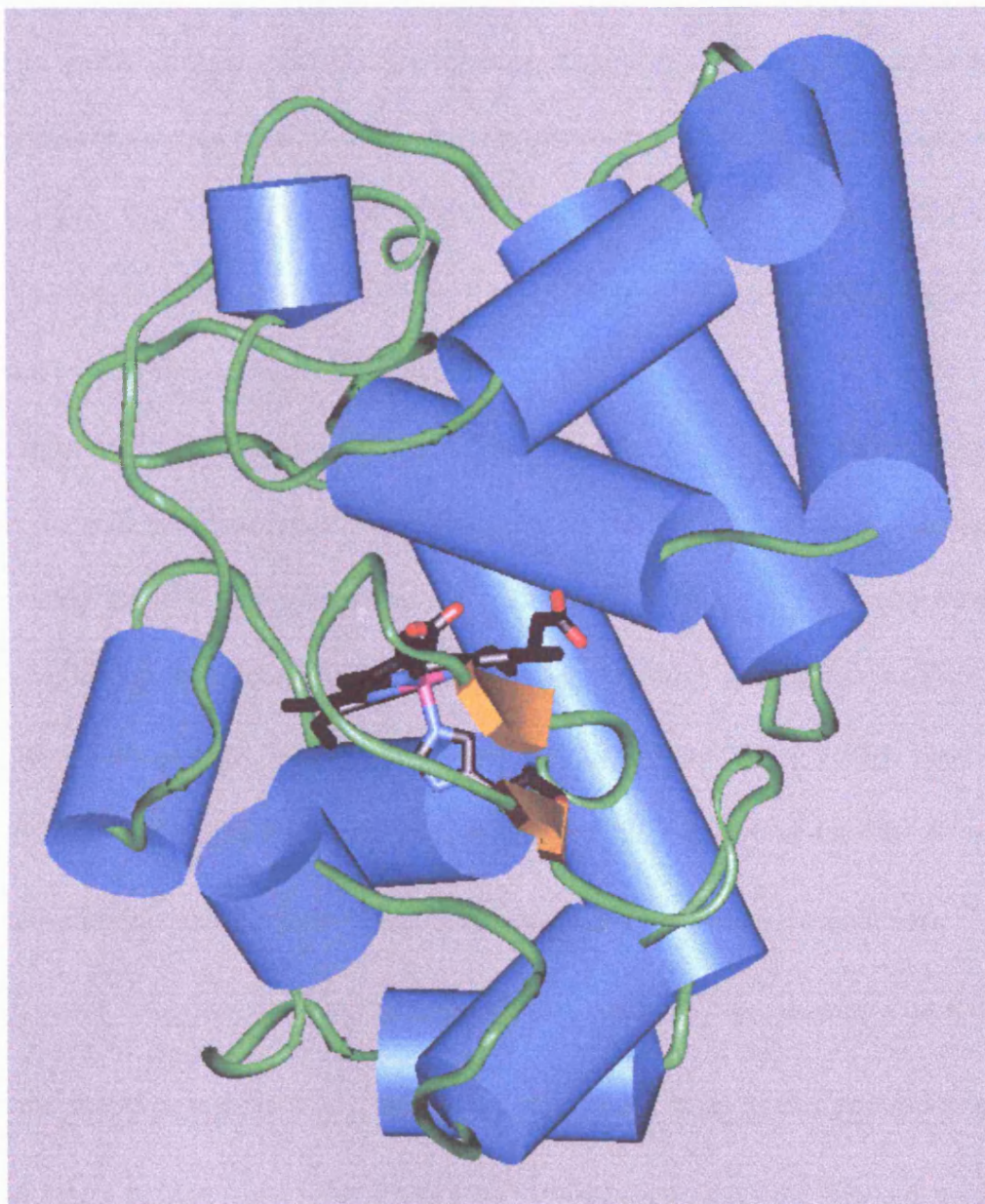
**Figure 1-5 Crystal structure of pea cytosolic ascorbate peroxidase.** Computer-based molecular model of wild-type rAPX based upon the published protein crystal structure coordinates [Patterson, W. R. and Poulos, T. L. (1995) *Biochemistry*, **34**, 4331-4341]. The proximal histidine residue, which ligates to the haem-iron, is indicated in grey and the haem itself in black. The α-helices are shown as blue cylinders and the β-sheet in orange.

truncated C-terminus of rAPX, relative to CcP, does not include the J'-helix of CcP. Wild-type rAPX contains less β-sheet structure than CcP, however, the distal histidine, arginine and tryptophan residues present in the active-sites of both enzymes share identical conformations. The proximal His-Asp-Trp catalytic triad of CcP[123] is retained in wild-type rAPX,[26] although subsequently it has been shown that the proximal tryptophan residue is not important to the enzymatic turnover of APX.[128]

The most striking difference between the protein structures of CcP and wild-type rAPX was the presence of a cation in the vicinity of Trp179 in rAPX,[26] in a location comparable to the proximal $Ca^{2+}$-binding sites identified for class II peroxidases. This tertiary structure feature was wholly unexpected, and unambiguous identification of the cation was not possible from the crystallographic data. However, on the basis of maintaining charge neutrality and metal-ligand bond lengths, the cation was putatively identified as being a potassium ion.

Gel filtration chromatography revealed that the native enzyme is homodimeric,[86] and the protein crystal structure confirmed retention of this quaternary structure in wild-type rAPX. The dimer interface appeared to be mediated by as many as eight electrostatic interactions between Asp, Glu, Arg and Lys residues located on α-helices A, D and J, which results in an axis of two-fold symmetry. Refinement of the crystal structure to 2.2 Å resolution required refinement to a model involving two such homodimers.

The publication of this crystallographic data was essential to all further structure-function studies, and is arguably the single most important contribution to ascorbate peroxidase research.

## 1.5.2 Steady-state kinetics

Whilst the emergence of detailed spectroscopic and kinetic data for APXs in general has been very slow, steady-state kinetic data form a fairly prominent feature of most of the early APX literature.[118] Plots of steady-state oxidation rate against the concentration of hydrogen peroxide, [$H_2O_2$], show a hyperbolic dependence and are consistent with a normal Michaelis-Menten treatment. However, for plots against ascorbate concentration, [L-ascorbic acid], the situation is less clear-cut. In cases where ascorbate concentration-dependence of steady state activity has been examined, the data fall into two categories: (a) APXs for which a normal hyperbolic dependence is observed and (b) APXs for which the steady-state analyses show a non-hyperbolic (sigmoidal) dependence.

A non-hyperbolic dependence has been reported for the cytosolic APXs from soybean[89] and pea.[86,133,134] Since the pea and soybean enzymes are known to exist as homodimers,[26,86,89] whilst the other enzymes are monomeric, it would be tempting to conclude that that source of the sigmoidal kinetics derives from a cooperative (allosteric) interaction between the two subunits. Indeed, arguments of this kind have been previously proposed.[83,134] Recent experiments[134] on recombinant pea cytosolic APX aimed at unravelling these complexities do not, however, support this conclusion. Hence, replacement of Glu112, which forms a salt bridge with Arg24 in the other monomeric half of the homodimer, would be expected to

destabilize the dimer interaction and therefore influence the kinetics. In fact, replacement of

Glu112 with a lysine residue results in a monomeric enzyme below 0.25 μM that, contrary to

expectation, does not exhibit hyperbolic kinetics. Hence, it seems unlikely that the sigmoidal

kinetics derive from a cooperative interaction between the two subunits of the dimer, and the

exact origin of the unusual steady state kinetics remains unclear, although it might arise from

the existence of more than one binding site for the substrate.[135] Indeed, binding

stoichiometries of greater than one have been identified under certain conditions for the

cytochrome $c$-CcP[45] and $Mn^{II}$-MnP[136] interactions, and discrete binding sites for different

substrates have been proposed in LiP137 and CcP.[138] In general, however, the kinetic and

functional competence of these multiple sites is more difficult to establish in an unambiguous

manner and, for pea cytosolic APX, remains unclear.

## 1.5.3 Pre-steady state kinetics

The first information on the mechanism of catalysis in pea cytosolic APX was published in

1996.[132] The kinetic data are consistent with oxidation of the ferric enzyme to the so-called

Compound I intermediate, followed by successive single electron reductions of Compound I

by ascorbate ($S_{red}$), $i.e.$ Equations 1-12–1-14. Rate constants for this mechanism have been

defined ($k_1 = 8.0 \times 10^7$ $M^{-1}s^{-1}$; $k_2 = 8.2 \times 10^7$ $M^{-1}s^{-1}$; $k_3 = 3.8 \times 10^3$ $M^{-1}s^{-1}$)[132] and have been

largely confirmed in the wild-type rAPX enzyme ($k_1 = 9 \times 10^7$ $M^{-1}s^{-1}$ (pH 7.0 20°C);[128] $k_1 =$

$8.3 \times 10^7$ $M^{-1}s^{-1}$ and $k_2 = 3.4 \times 10^7$ $M^{-1}s^{-1}$ (pH 7.0, 20°C)[133]). Pre-steady state kinetic data are

also available for an APX isozyme from tea: rate constants were found to be $k_1 = 8.9 \times 10^6$

$M^{-1}s^{-1}$, $k_2 = 4.5 \times 10^6$ $M^{-1}s^{-1}$ and $k_3 = 3.7 \times 10^4$ $M^{-1}s^{-1}$.[104] Whilst there is a multitude of kinetic

data on the effects of active-site amino acids on the various rate constants for other peroxidases (notably C$c$P and HRP),[8,45,46] there is currently no such information for APX.

## 1.5.4 Electronic structure of Compound I

There is general agreement that the initial product (Compound I) of the reaction of pea cytosolic APX with $H_2O_2$ is a porphyrin $\pi$-cation intermediate (as found in HRP),[24] and not a protein-based radical species as found in C$c$P.[23,126] Evidence for this comes from the similarity of the spectra observed immediately after the addition of $H_2O_2$ to both native pea cytosolic APX132 and tea APX[56,104] to those previously published for HRP.[8] Rapid freeze-quench EPR data for wild-type rAPX[127] are also consistent with the assignment of Compound I as an oxidized porphyrin $\pi$-cation species.

Ascorbate peroxidase Compound I is very unstable and decays, in the absence of substrate, to a stable Compound II-like intermediate. The spectrum of this intermediate is consistent with a ferryl-containing haem.[56,104,132,133] In contrast to Compound I, Compound II of rAPX is stable for up to an hour after preparation.

## 1.6 Aims of this research

In the context of the above discussion, the aims of this work are as follows:

- To characterise in detail the spectroscopic and functional properties of recombinant wild type pea cytosolic ascorbate peroxidase (rAPX) to provide a solid platform upon which the study of site-directed variants of rAPX could be launched.

- To characterise the pH-dependent properties of rAPX and to establish the effect of changes in hydrogen ion concentration on the spectroscopic properties of the molecule.

- To examine the binding of physiological and non-physiological substrates to rAPX, and to assess the effect of amino acid substitutions close to the proposed binding site.

- To investigate the nature of the Compound I intermediate of rAPX under different conditions and to examine whether or not protein radical formation can occur.

## 1.7 References

1 Chapman, S. K., Daff, S. and Munro, A. W. (1997) *Struct. Bond.*, **88**, 40-70

2 Timkovich, R. and Bondoc, L. L. (1990) *Adv. Biophys. Chem.*, **1**, 203-247

3 Ortiz de Montellano, P. R. (1987) *Acc. Chem. Res.*, **20**, 289-294

4 Gray, H. B. and Winkler, J. R. (1996) *Ann. Rev. Biochem.*, **65**, 537-561

5 Antonini, M. and Brunori E. (1971) *Hemoglobin and Myoglobin and their Reactions with Ligands* (Neuberger, A. & Tatum, E. L. eds.), North Holland Publishers, Amsterdam

6 Sono, M., Roach, M. P., Coulter, E. D. and Dawson, J. H. (1996) *Chem. Rev.*, **96**, 2841-2887

7 Bosshard, H. R., Anni, H. and Yonetani, T. (1991) in: *Peroxidases in Chemistry and biology* (Everse, J., Everse, K. E. & Grisham, M. B. eds.), vol. 2, CRC Press, Boca Raton, Florida, pp 51-85

8 Dunford, H. B. (1999) *Heme Peroxidases*, Wiley-VCH, New York, Chichester, Weinheim, Brisbane, Singapore, Toronto

9 Raphael, A. C. and Gray, H. B. (1989) *Proteins Struct. Funct. Genet.*, **6**, 338-340

10 Valentine, J. S., Sheridan, R. P., Allen, L. C. and Kahn, P. C. (1979) *Proc. Natl. Acad. Sci. USA*, **76**, 1009-1013

11 Walker, F. A., Emrick, D., Rivera, J. E., Hanquet, B. J. and Buttlaire, D. H. (1988) *J. Am. Chem. Soc.*, **110**, 6234-6240

12 Reid, L. S., Lim, A. R. and Mauk, A. G. (1986) *J. Am. Chem. Soc.*, **108**, 8917-8201

13 Walker, F. A., Huynh, B. H., Scheidt, W. R. and Osvath, S. R. (1986) *J. Am. Chem. Soc.*, **108**, 5288-5297

14 Sligar, S. G., Olson, J. S. and Phillips, G. N. (1994) *Chem. Rev.*, **94**, 699

15 Raven, E. L. and Mauk, A. G. (2000) *Adv. Inorg. Chem.*, **51**, 1-49

16 Ortiz de Montellano, P. R. (1995) *Cytochrome P450: Structure, Mechanism, and Biochemistry*, Plenum Press, New York, London

17 Lewis, D. F. V. (1996) *Cytochromes P450*, Taylor and Francis, London

18 Sligar, S. G. (1976) *Biochemistry*, **15**, 5399

19 Wilker, J. J., Dmochowski, I. J., Dawson, J. H., Winkler, J. R. and Gray, H. B. (1999) *Angew. Chem. Int. Ed.*, **38**, 90-92

20 Schlichting, I., Berendzen, J., Chu, K., Stock, A. M., Maves, S. A., Benson, D. E., Sweet, R. M., Ringe, D., Petsko, G. A. and Sligar, S. G. (2000) *Science*, **287**, 1615-1622

21 Everse, J., Everse, K. E. and Grisham, M. B. (1991) *Peroxidases in chemistry and biology*, vol. 1 & 2, CRC Press, Boca Raton, Florida

22 English, A. M. and Tsaprailis, G. (1995) *Adv. Inorg. Chem.*, **43**, 79-125

23 Yonetani, T., Schleyer, H. and Ehrenberg, A. (1966) *J. Biol. Chem.*, **241**, 3240

24 Moss, T. H., Ehrenberg, A. and Bearden, A. J. (1969) *Biochemistry*, **8**, 4159-4162

25 Welinder, K. G. (1992) *Curr. Opin. Struct. Biol.*, **2**, 388-393

26 Patterson, W. R. and Poulos, T. L. (1995) *Biochemistry*, **34**, 4331-4341

27 Finzel, B. C. and Poulos, T. L. (1984) *J. Biol. Chem.*, **259**, 13027-13036

28 Poulos, T. L., Edwards, S. L., Wariishi, H. & Gold M. H. (1993) *J. Biol. Chem.*, **268**, 4429-4440

29 Petersen, J. F. W., Kadziola, A. and Larsen, S. (1994) *FEBS Lett.*, **339**, 291-296

30 Kunishima, N., Fukuyama, K., Matsubara, H., Hatanaka, H., Shibano, Y. and Amachi, T. (1994) *J. Mol. Biol.*, **235**, 331-344

31 Kunishima, N., Amada, F., Fukuyama, K., Kawamoto, M., Masunaga, T. and Matsubara, H. (1996) *FEBS Lett.*, **378**, 291-294

32 Sundaramoorthy, M., Kishi, K., Gold, M. H. and Poulos, T. L. (1994) *J. Biol. Chem.*, **269**, 32759-32767

33 Schuller, D. J., Ban, N., van Huystee, R. B., McPherson, A. and Poulos, T. L. (1996) *Structure*, **4**, 311-321

34 Henriksen, A., Welinder, K. G. and Gajhede, M. (1998) *J. Biol. Chem.*, **273**, 2241-2248

35 Gajhede, M., Schuller, D. J., Henricksen, A., Smith, A. T., and Poulos, T. L., (1997) *Nature Struct. Biol.*, **4**, 1032-1038

36 Sutherland, G. R. J., and Aust, S. D. (1996) *Arch. Biochem. Biophys.*, **332**, 128-134

37 Nie, G. and Aust, S. D. (1997) *Biochemistry*, **36**, 5113-5119

38 Smith, A. T., Santama, N., Dacey, S., Edwards, M., Bray, R. C., Thorneley, R. N. F. and Burke, J. F. (1990) *J. Biol. Chem.*, **265**, 13335-13343

39 Edwards, S. L., Poulos, T. L. and Kraut, J. (1984) *J. Biol. Chem.*, **259**, 12984-12988

40 Edwards, S. L., Kraut, J. and Poulos, T. L. (1988) *Biochemistry*, **27**, 8074-8081

41 Edwards, S. L. and Poulos, T. L (1990) *J. Biol. Chem.*, **265**, 2588-2595

42  Pelletier, H. and Kraut, J. (1992) *Science*, **258**, 1748-1755

43  Henriksen, A., Smith, A. T. and Gajhede, M. (1999) *J. Biol. Chem.*, **49**, 35005-35011

44  Poulos, T. L. and Kraut, J., (1980) *J. Biol. Chem.*, **255**, 8199-8205

45  Erman, J. E. (1998) *J. Biochem. Mol. Biol.*, **31**, 307-327

46  Smith, A. T. and Veitch, N. C. (1998) *Curr. Opin. Chem. Biol.*, **2**, 269

47  Erman, J. E., Vitello, L. B., Miller, M. A., Shaw, A., Brown, K. A. and Kraut, J. (1993) *Biochemistry*, **32**, 9798-9806

48  Newmyer, S. L. and Ortiz de Montellano, P. R. (1995) *J. Biol. Chem.*, **270**, 19430-19438

49  Smith, A. T. and Veitch, N. C. (1998) *Curr. Opin. Chem. Biol.*, **2**, 269-278

50  Veitch, N. C. and Smith, A. T. (2000) *Adv. Inorg. Chem.*, **51**, 107-162

51  Vitello, L. B., Erman, J. E., Miller, M. A., Mauro, J. M. and Kraut, J. (1992) *Biochemistry*, **31**, 11524-11535

52  Dalton, D. A., 1991, Ascorbate peroxidase, in: *Peroxidases in Chemistry and Biology*, Vol. 2 (Everse, J., Everse, K. E. and Grisham, M. B., eds.), CRC Press, Boca Raton, pp. 139-154

53  Groden, D. and Beck, E. (1979) *Biochim. Biophys. Acta*, **546**, 426-435

54  Kelly, G. J. and Latzko, E. (1979) *Naturewissenschaften*, **66**, 617-618

55  Kvaratskhelia, M., George, S. J. and Thorneley, R. N. F. (1997) *J. Biol. Chem.*, **272**, 20998-21001

56  Kvaratskhelia, M., Winkel, C. and Thorneley, R. N. F. (1997) *Plant Physiol.*, **114**, 1237-1245

57  Ushimara, T., Maki, Y., Sano, S., Koshiba, K., Asada, K. and Tsuji, H. (1997) *Plant Cell Physiol.*, **38**, 541-549

58  Dalton, D. A., Langeberg, L. and Robbins, M. (1992) *Arch. Biochem. Biophys.*, **292**, 281-286

59  Shigeoka, S., Yasumoto, R., Onishi, T., Nakano, Y. and Kitaoka, S. (1987) *J. Gen. Microbiol.*, **133**, 227-232

60  Borraccino, G., Dipierro, S. and Arrigoni, O. (1986) *Planta*, **167**, 521-526

61  Hossain, M. A. and Asada, K. (1984) *Plant Cell Physiol.*, **25**, 1285-1295

62  Mittler, R. and Zilinskas, B. A. (1991) *FEBS Lett.*, **289**, 257-259

63  Jespersen, H. M., Kjaersgard, I. V. H., Ostergaard, L. and Welinder, K. G. (1997) *Eur. J. Biochem.*, **326**, 305-310

64  Caldwell, C. R., Turano, F. J. and McMahon, M. B. (1998) *Planta*, **204**, 120-126

65 Chatfield, M. and Dalton, D. A. (1993) *Plant Physiol.*, **103**, 661-662

66 Webb, R. P. and Allen, R. D. (1995) *Plant Physiol.*, **108**, 1325

67 Kubo, A., Saji, H., Tanaka, K., Tanaka, K. and Kondo, N. (1992) *Plant Mol. Biol.*, **18**, 691-701

68 Lopez, F., Vansuyt, G., CasseDelbart, F. and Fourcroy, P. (1996) *Physiol. Plant.*, **97**, 13-20

69 van Breusegem, F., Villarroel, R., van Montagu, M. and Inze, D. (1995) *Plant Physiol.*, **107**, 649-650

70 Orvar, B. L. and Ellis, B. E. (1995) *Plant Physiol.*, **108**, 839-840

71 Morita, S., Kaminaka, H., Yokoi, H., Masumara, T. and Tanaka, K. (1997) *Plant Physiol.*, **114**, 102

72 Kim, I. J. and Chung, W. I. (1998) *Plant Science*, **133**, 69-77

73 Schantz, M.-L., Schreiber, H., Guillemaut, P. and Schantz, R. (1995) *FEBS Lett.*, **358**, 149

74 Newman, T., De Bruijin, F. J., Green, P., Keegstra, K., Kende, H., McIntish, L., Ohlrogge, J., Raikhel, N., Somerville, S., Thomashow, M., Retzel, E. and Somerville, C. (1996) *Plant Physiol.*, **106**, 1241-1255

75 Ishikawa, T., Sakai, K., Yoshimura, K., Takeda, T. and Shigeoka, S. (1996) *FEBS Lett.*, **384**, 289-293

76 Mano, S., Yamaguchi, K., Hayashi, M. and Nishimura, M. (1997) *FEBS Lett.*, **413**, 21-26

77 Yamaguchi, K., Hayashi, M. and Nishimura, M. (1996) *Plant Cell Physiol.*, **37**, 405-409

78 Zhang, H., Wang, J., Nickel, U., Allen, R. D. and Goodman, H. M. (1997) *Plant Mol. Biol.*, **34**, 967-971

79 Bunkelmann, J. R. and Trelease, R. N. (1996) *Plant Physiol.*, **110**, 589-598

80 Ishikawa, T., Sakai, K., Takeda, T. and Shigeoka, S. (1995) *FEBS Lett.*, **367**, 28-32

81 Patterson, W. R. and Poulos, T. L. (1994) *J. Biol. Chem.*, **269**, 17020-17024

82 Cheek, J., Mandelman, D., Poulos, T. L. and Dawson, J. H. (1999) *J. Biol. Inorg. Chem.*, **4**, 64-72

83 Dalton, D. A., Diaz del Castillo, L., Kahn, M. L., Joyner, S. L. and Chatfield, J. M. (1996) *Arch. Biochem. Biophys.*, **328**, 1-8

84 Yoshimura, K., Ishikawa, T., Nakumura, Y., Tamoi, M., Takeda, T., Tada, T., Nishimura, K. and Shigeoka, S. (1998) *Arch. Biochem. Biophys.*, **353**, 55-63

85 Ishikawa, T., Yoshimura, K., Sakai, K., Tamoi, M., Takeda, T. and Shigeoka, S. (1998) *Plant Cell Physiol.*, **39**, 23-34

86 Mittler, R. and Zilinskas, B. A. (1991) *Plant Physiol.*, **97**, 962-968

87 Gerbling, K.-P., Kelly, G. J., Fischer, K.-H. and Latzko, E. (1984) *J. Plant Physiol.*, **115**, 59-67

88 Ohya, T., Morimura, Y., Saji, H., Mihara, T. and Ikawa, T. (1997) *Plant Science*, **125**, 137-145

89 Dalton, D. A., Hanus, F. J., Russell, S. A. and Evans, H. J. (1987) *Plant Physiol.*, **83**, 789-794

90 De Gara, L., de Pinton, M. C., Paciolla, C., Cappetti, V. and Arrigoni, O. (1996) in: *Plant Peroxidases: Biochemistry and Physiology* (Obinger, C., Burner, U., Ebermann, R., Penel, C. and Greppin, H., eds.), University of Geneva, pp. 157-162

91 De Gara, L., de Pinto, M. C. and Arrigoni, O. (1997) *Physiol. Plant.* **100**, 894-900

92 Elia, M. R., Borracino, G. and Dipierro, S. (1992) *Plant Science*, **85**, 17-21

93 Koshiba, T. (1993) *Plant Cell Physiol.*, **34**, 713-721

94 Ishikawa, T., Takeda, T. and Shigeoka, S. (1996) *Plant Science*, **120**, 11-18

95 Chen, G.-X. and Asada, K. (1989) *Plant Cell Physiol.*, **30**, 987-998

96 Tanaka, K., Takeuchi, E., Kubo, A., Sakaki, T., Haraguchi, K. and Kawamura, Y. (1991) *Arch. Biochem. Biophys.*, **286**, 371-375

97 Nakano, Y. and Asada, K. (1987) *Plant Cell Physiol.*, **28**, 131-140

98 Jimenez, A., Hernandez, J. A., del Rio, L. A. and Sevilla, F. (1997) *Plant Physiol.*, **114**, 275-284

99 Jimenez, A., Jimenez, J. A., Barcelo, A. R., Sandalio, L. M., del Rio, L. A. and Sevilla, F. (1998) *Physiol. Plant.*, **104**, 687-692

100 Jablonski, P. P. and Anderson, J. W. (1982) *Plant Physiol.*, **69**, 1407-1413

101 Gillham, D. J. and Dodge, A. D. (1986) *Planta*, **167**, 246-251

102 Meneguzzo, S., Sgherri, C. L. M., Navari-Izzo, F. and Izzo, R. (1998) *Physiol. Plant.*, **104**, 735-740

103 Chen, G.-X., Sano, S. and Asada, K. (1992) *Plant Cell Physiol.*, **33**, 109-116

104 Kvaratskhelia, M., Winkel, C., Naldrett, M. T. and Thorneley, R. N. F. (1999) *J. Plant Physiol.*, **154**, 273-282

105 Bunkelmann, J. R. and Trelease, R. N. (1997) *Plant Science*, **122**, 209-216

106  Yamaguchi, K., Hori, H. and Nishimura, M. (1995) *Plant Cell Physiol.*, **36**, 1157-1162

107  Corpas, F. J. and Trelease, R. N. (1998) *J. Plant Physiol.*, **153**, 332-338

108  Sano, S., Ueda, M., Kurano, N., Miyachi, S. and Yokota, A. (1996) in: *Plant Peroxidases: Biochemistry and Physiology* (Obinger, C., Burner, U., Ebermann, R., Penel, C. and Greppin, H., eds.), University of Geneva, pp. 168-172

109  Sauser, K. R., Liu, J. K. and Wong, T.-Y. (1997) *BioMetals*, **10**, 163-168

110  Takeda, T., Yoshimura, K., Ishikawa, T. and Shigeoka, S. (1998) *Biochimie*, **80**, 295-301

111  Ishikawa, T., Takeda, T., Kohno, H. and Shigeoka, S. (1996) *Biochim. Biophys. Acta*, **1290**, 69-75

112  Shigeoka, S., Nakano, Y. and Kitaoka., S. (1980) *Arch. Biochem. Biophys.*, **201**, 121-127

113  Miyake, C., Michihata, F. and Asada, K. (1991) *Plant Cell Physiol.*, **32**, 33-43

114  Tel-Or, E., Huflejt, M. E. and Packer, L. (1986) *Arch. Biochem. Biophys.*, **246**, 396-402

115  Mathews, M. C., Summers, C. B. and Felton, G. W. (1997) *Arch. Insect Biochem. Physiol.*, **34**, 57-68

116  Boveris, A., Sies, H., Martino, E. E., Docampo, R., Turrens, J. F. and Stoppani, A. O. M. (1980) *Biochem. J.*, **188**, 643-648

117  Wada, N., Kinoshita, S., Matsuo, M., Amako, K., Miyake, C. and Asada, K. (1998) *Biochem. Biophys. Res. Comm.*, **242**, 256-261

118  Raven, E. L. (2000) *Subcellular Biochemistry*, **36**, 318-350

119  Armstrong, F. A., Heering, H. A. and Hirst, J. (1997) *Chem. Soc. Rev.*, **26**, 169-179

120  Jones, D. K., Dalton, D. A., Rosell, F. I. and Lloyd Raven, E. (1998) *Arch. Biochem. Biophys.*, **360**, 173-178

121  Tanaka, M., Ishimori, K. and Morishima, I. (1998) *Biochemistry*, **37**, 2629-2638

122  Conroy, C. W., Tyma, P., Daum, P. H. and Erman, J. E. (1978) *Biochim. Biophys. Acta*, **537**, 62-69

123  Goodin, D. B. and McRee, D. E. (1993) *Biochemistry*, **32**, 3313-3324

124  Millis, C. D., Cai, D., Stankovich, M. T. and Tien, M. (1989) *Biochemistry*, **28**, 8484-8489

125  Lim, A. R. (1989) PhD dissertation, University of British Columbia

126  Sivaraja, M., Goodin, D. B., Smith, M. and Hoffman, B. M. (1989) *Science*, **245**, 738-740

127  Patterson, W. R., Poulos, T. L. and Goodin, D. B. (1995) *Biochemistry*, **34**, 4342-4345

128 Pappa, H., Patterson, W. R. and Poulos, T. L. (1996) *J. Biol. Inorg. Chem.*, **1**, 61-66

129 Náray-Szabó, G. (1997) *J. Biol. Inorg. Chem.*, **2**, 135-138

130 Jense, G. M., Buunte, S. W., Warshel, A. and Goodin, D. B. (1998) *J. Phys. Chem.*, **102**, 8221-8228

131 Poulos, T. L., Patterson, W. R. and Sundaramoorthy, M. (1995) *Biochem. Soc. Trans.*, **23**, 228-232

132 Marquez, L. A., Quitoriano, M., Zilinskas, B. A. and Dunford, H. B. (1996) *FEBS Lett.*, **389**, 153-156

133 Mandelman, D., Jamal, J. and Poulos, T. L. (1998) *Biochemistry*, **37**, 17610-17617

134 Mandelman, D., Schwarz, F. P., Li, H. and Poulos, T. L. (1998) *Protein Science*, **7**, 2089-2098

135 Çelik, A., Cullis, P. M. and Lloyd Raven, E. (2000) *Arch. Biochem. Biophys.*, **373**, 175-181

136 Mauk, M. R., Kishi, K., Gold, M. H. and Mauk, A. G. (1998) *Biochemistry*, **37**, 676-677

137 Doyle, W. A., Blodig, W., Veitch, N. C., Piontek, K. and Smith, A. T. (1998) *Biochemistry*, **37**, 15097-15105

138 DePillis, G. D., Sishta, B. P., Mauk, A. G. and Ortiz de Montellano, P. R. (1991) *J. Biol. Chem.*, **266**, 19334- 19341

# CHAPTER TWO

# CHARACTERISATION OF

# RECOMBINANT PEA

# CYTOSOLIC ASCORBATE

# PEROXIDASE

# 2 Characterisation Of Wild-Type Ascorbate Peroxidase

Native wild-type pea cytosolic ascorbate peroxidase has been isolated from macerated young pea shoots by a combination of ammonium sulphate precipitation and affinity column chromatography.[1] Subsequently, an increase in the amount of purified protein, obtainable through a recombinant expression system, yielded more enzyme for characterisation.[2]

The successful sub-cloning of the *Pisum Sativum L.* APX gene into an inducible expression vector has been reported; the recombinant wild-type enzyme was found to be essentially indistinguishable from the native protein. Furthermore, the availability of crystal structure data for the recombinant peroxidase facilitates an appreciation of the structure-function relationship of APX.[3] Kinetic and spectral properties of the native enzyme have defined a series of reference points for subsequent research work on recombinant enzymes.[4]

The basis of research is experimental falsification, which means that scientists develop experiments with a view to disproving any given hypothesis.[5] Strong foundations reinforce the platform from which successful research developments are launched, and support the evolution of working theories. Hence, the starting point for enzyme structure-function relationship studies, particularly research involving variant proteins, is construction of a control model, which is based upon fundamental data.

This chapter will focus upon the characterisation of recombinant wild-type pea cytosolic ascorbate peroxidase enzyme. Initially, the general expression and isolation protocols, described in more detail in Chapter Six, will be overviewed and pertinent observations or deviations from the literature associated with the preparation and handling of the enzyme will be highlighted. The moderate yields, typically 8 mg per litre of rich growth medium, of the purified enzyme facilitated several novel investigative studies. However the primary focus of

the work discussed in this section was the spectroscopic characterisation of the wild-type

rAPX based upon comparisons with the data reported within the literature.

## 2.1 Preparation and isolation

Based upon the New England Biolabs™ amylose resin protocol, the use of a

maltose-binding fusion protein vector facilitates separation of the target recombinant protein

from the other soluble cell lysis products.[2] Inducible expression of the target was achieved by

fermentation of TOPP2 E. Coli transformed with the pMAL-c2 vector encoding for wild-type

APX maltose-binding fusion protein, and fusion enzyme over-expression was confirmed by

SDS PAGE analysis, Figure 2-1.

Resuspended cells were lysed, using hen egg white lysosyme (Sigma) and the cell free

lysate obtained was applied to an amylose affinity column. Haem-based absorptions within

the visible region facilitates direct observation of the binding of the MBP-fusion protein to the

amylose resin, whilst the soluble cell proteins flow through. Elution of the fusion product

results in a single band, ~69 kDa molecular weight, on an SDS-PAGE gel. Occasionally,

traces of authentic MBP (41 kDa MW), which expresses during the natural growth of E. Coli,

were observed.

A room temperature tryptic digest, conducted with a 1:100 w/w ratio of trypsin, was used

to cleave the isolated MBP-fusion protein.[2] Under these conditions, the tryptic digest results

in separation of the MBP and APX proteins without undesirable fragmentation, as observed

by SDS PAGE analysis, Figure 2-2.
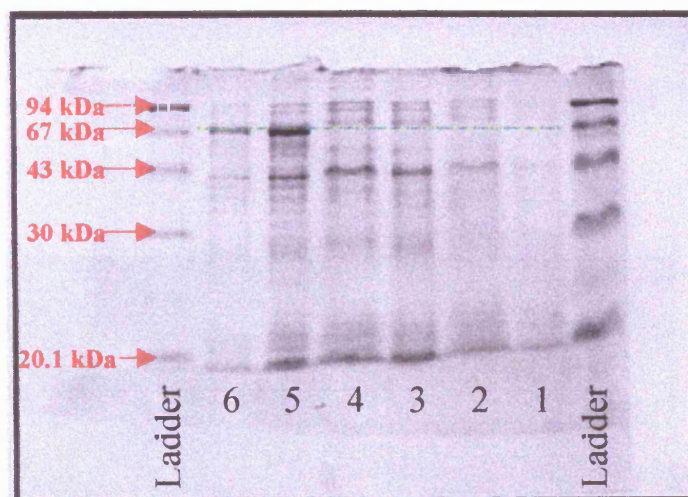
**Figure 2-1 IPTG-induced MBP-rAPX fusion protein over-expression monitored by SDS-PAGE.** Aliquots of Rich LB growth medium, which were removed at various stages during a typical grow-up, were analysed for protein content by SDS-PAGE:

> Lane 1 – 30 minutes growth
> Lane 2 – 1 hour growth
> Lane 3 – 1½ hours growth
> Lane 4 – 2 hours growth
> Lane 5 – 2 hours after IPTG induction (4 hours growth)
> Lane 6 – Harvest six hours after IPTG induction.
> Ladder – Protein MW markers

All samples (10 μl loading volume) were prepared from pelleted *E. Coli* cells that were obtained following centrifugation of aliquots (1 ml) of Rich LB medium. To avoid excessive protein loading, pellets that were used for lanes 1-4 were resuspended in 50 μl SDS sample buffer, whilst the pellets used for lanes 5 and 6 were resuspended in 100 and 200 μl respectively. The green line indicates the position of the over-expressed MBP-rAPX fusion protein band (~69 kDa).

44
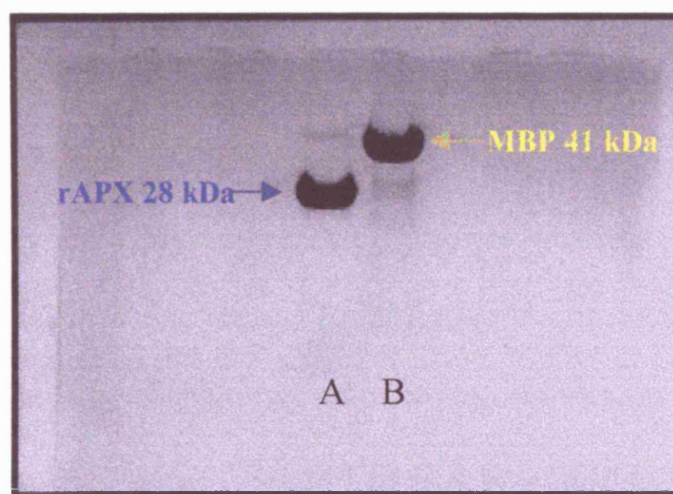
**Figure 2-2 Confirmation of rAPX and MBP separation by SDS-PAGE analysis.**
Samples A & B were obtained following tryptic digest: (A) coloured fractions eluted from
the second amylose resin column; (B) maltose-binding protein eluted from second
amylose column using 10 mM maltose. Both sample lanes were overloaded substantially,
with minimal overspill, so as to ensure that any trace impurities would be discernible.

Hydroxyapatite resin, which Patterson and Poulos reported[2] using at this stage of rAPX

purification, was observed to tightly bind haem, and the resulting decrease in holoenzyme

yields was both undesired and avoidable. Consequently, deviating from the published

procedure, the tryptic digestion mixture was passed over a second amylose resin column,

consistent with the New England Biolabs™ protocol.[6] Damage to MBP is reported to affect

its binding to amylose resin: hence, whilst the majority of the MBP was routinely extricable

by this method, variable success was noted.[7]

Further purification of the holoenzyme was achieved using anion exchange

chromatography, by fractional elution with a linear chloride gradient, and yielded purified

recombinant APX (Figure 2-3). Fractions were collected and pooled in accordance with the

spectroscopic purity index, and were then exhaustively exchanged into doubly deionised

water to remove any remaining salt and buffer content. Protein with $R_Z$ > 1.90 was flash

frozen and stored in liquid nitrogen (the effect of long-term storage and storage conditions

will be commented upon later in this chapter). Enzyme stocks across the $R_Z$ = 1.90-2.27 range

of spectroscopic purities were used routinely with reproducible behaviour.
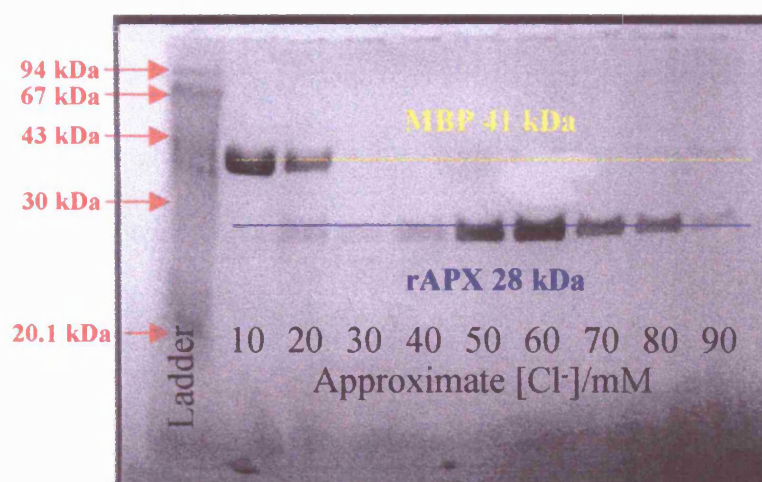
**Figure 2-3 SDS-PAGE analysis of fractions eluted from anion exchange column.** The extent of maltose-binding protein migration is indicated by the yellow line, and the blue line corresponds to rAPX. Elution of MBP can be observed across the 0-150 mM chloride concentration range.

## Results

## 2.2 Mass-spectral analysis

Although, the gene encoding wild-type rAPX sequenced without any undesirable mutations, confirmation of the absence of post-translational modification required examination of the expressed rAPX. Therefore, electrospray ionisation mass spectral analysis was conducted in order to further evaluate the structural integrity of the recombinant wild-type protein.

The charge distribution obtained and the computationally reconstructed singularly charged mass spectrum are shown in Figure 2-4. From the broad distribution of multiply charged species, associated with using this 'soft' ion source, an average molecular mass of 27192.7 ± 0.8 Da was measured. This value was essentially identical to the exact mass of the apo-protein, 27192.77 Da, as calculated from the deduced amino acid sequence (Barbara Zilinskas, personal communication).

### 2.2.1 Evidence supporting a bound potassium ion

The relatively low haem retention by the protein, under the conditions employed, is consistent with a non-covalently bound haem. A somewhat unexpected observation within the wild-type rAPX mass spectrum was that of a significant component, associated with the peptide-derived peak, at +39-40 Da (consistent with the retention of a potassium ion, which is purported to be bound within the proximal domain of the enzyme). However, an exact mass determination of the additional component was prohibited by the overlap of this peak with that of the apo-protein.[8]

48
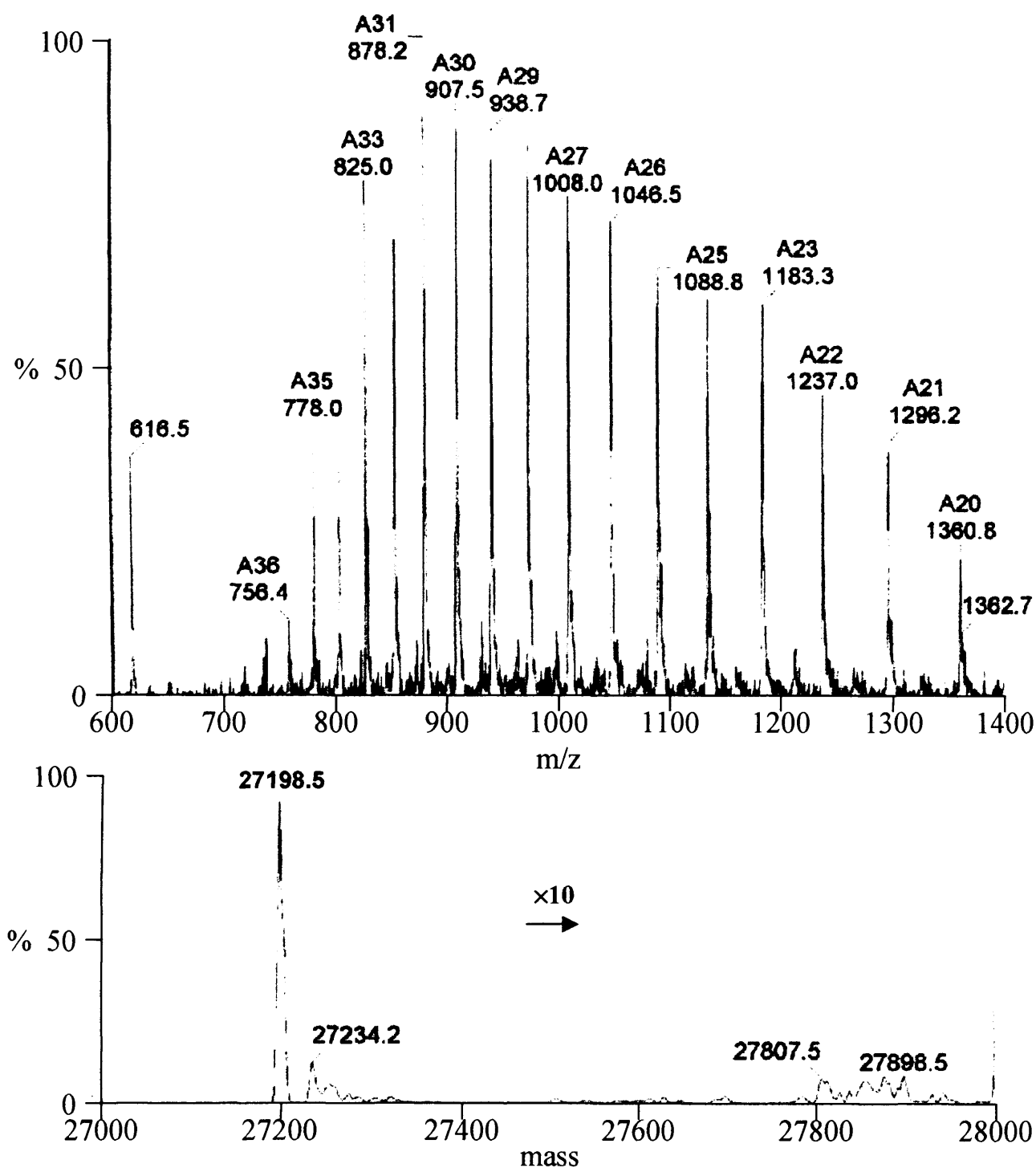
**Figure 2-4 Mass spectral analysis of wild-type rAPX.** Top: a typical electrospray ionisation mass spectrum, which mostly comprises of multiply charged protein species. Bottom: computationally-derived molecular masses, the region 27500-28000 has been amplified by a factor of ten, enhanced resolution was obtained through the application of a maximum entropy algorithm to the transformed electrospray ionisation component data.

## 2.3 Electronic absorption spectroscopy

Five-coordinate high-spin ferric iron, the archetypal haem-containing peroxidase resting state, results in average maximum molar absorptivities of $105 \pm 7$ mM$^{-1}$cm$^{-1}$ whilst the six-coordinate globins consistently display higher average molar absorption values $(177 \pm 9$ mM$^{-1}$cm$^{-1})$.[9] Accordingly, haemoprotein electronic absorption bands are semi-diagnostic of the haem-iron coordination number and spin state.[10]

This section will detail the UV/visible spectroscopic characterisation experiments conducted upon wild-type rAPX, and the comparisons that can be made to published literature. All the rAPX variants, which expressed as holoprotein, were characterised by UV/visible absorption spectroscopy, and the relevant chapters contain summaries of the results obtained from pertinent characterisation experiments.

### 2.3.1 Pyridine haemochromagen assay

Soret band absorption coefficient values for native and recombinant forms of wild-type pea cytosolic APX have been reported as 150 mM$^{-1}$cm$^{-1}$ and 114 mM$^{-1}$cm$^{-1}$, respectively.[4,11] The native enzyme absorption coefficient value is disproportionately high for a haem-containing peroxidase; moreover the value of the recombinant enzyme was reported ~30 % lower than the native. In order to reconcile this apparent discrepancy, the absorption coefficient of ferric rAPX was recalculated using an average of two haem contents measured using the pyridine haemochromagen assay.[12]

An average absorption coefficient value of $\varepsilon_{403} = 88 \pm 2$ mM$^{-1}$cm$^{-1}$ was obtained for the wild-type rAPX; this value has been published and the recombinant wild-type enzyme concentrations reported throughout this thesis have been calculated using this value.[8]

Subsequent independent experiments, aimed at altering the proposed cation binding-site, reported a similar absorption coefficient, $\varepsilon_{405}$ = 91 mM$^{-1}$cm$^{-1}$, for reconstituted histidine-tagged recombinant wild-type pea ascorbate peroxidase.[13] This calculated absorption coefficient for the pea enzyme is comparable to those reported for HRP ($\varepsilon_{403}$ = 91 mM$^{-1}$cm$^{-1}$) and CcP ($\varepsilon_{408}$ = 93 mM$^{-1}$cm$^{-1}$).[14,15] However, a wide range of values exist for the absorption coefficients and 102 mM$^{-1}$cm$^{-1}$ has been reported independently for CcP and HRP.[16,17]

## 2.3.2 Ligand-bound derivatives

In principle, the simplest of all the peroxidase reactions are those involving iron centred ligand binding, Equation 2-1.

$$Fe + X \rightleftarrows Fe\text{-}X \qquad [2\text{-}1]$$
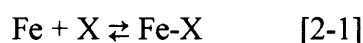
A great deal of structural information can be derived there from.[9] Sufficiently high exogenous ligand concentrations are known to inhibit peroxidase function through competitive binding at the haem iron, and the use of non-oxidative ligands has also provided models for probing the mechanism of $H_2O_2$ binding prior to Compound I formation.[18]

The ferric and ferrous derivatives, along with several ligand-bound ternary complexes, of wild-type rAPX were prepared and the peak positions, and millimolar absorption coefficients, are summarised below (Table 2-1).

The ferric and ferrous spectra, Figure 2-5 & Figure 2-6, respectively, of the various wild-type rAPX complexes are consistent with those reported elsewhere in the literature.[1,2] The spectrum of the ligand-free ferric species is consistent with the predominantly five-coordinate, high-spin iron peroxidase resting state, with a broad Soret maxima positioned at around 400 nm.[3] UV/visible electronic absorption peak positions have been published[13] for

| Derivative | $\delta$ | ($\gamma$) Soret | CT$_2$ | $\beta$ | $\alpha$ | CT$_1$ |
|---|---|---|---|---|---|---|
| Fe$^{III}$ | ~380$^{sh}$ | 403 (88) | 506 (11) | ← ~540$^{sh}$ → | | 636 (3.4) |
| Fe$^{III}$-F | ~365$^{sh}$ | 403 (111) | 494 (10) | ← ~532$^{sh}$ → | | 616 (5.8) |
| Fe$^{III}$-N$_3$ | ~360$^{sh}$ | 412 (106) | ~525 (9.7) | ~543$^{sh}$, 569$^{sh}$ | | 633 (2.9) |
| Fe$^{III}$-CN | ~363$^{sh}$(31) | 419 (104) | - | 540 (12) | 572$^{sh}$ | - |
| Fe$^{II}$ | 378 (42)$^a$ | 434 (98) | - | 556 (13) | 587$^{sh}$ | - |
| Fe$^{II}$-CN | $^b$ | 426 (123) | - | 529 (13) | 559 (18) | - |
| Fe$^{II}$-CO | $^b$ | 419 (161) | - | 539 (13) | 569 (14) | - |

**Table 2-1 UV/visible spectra peak positions (nm) and millimolar absorption coefficients ($mM^{-1}cm^{-1}$) for wild-type rAPX.** Millimolar absorption coefficients for resolved peaks are noted in parentheses, "$^{sh}$" denotes unresolved shoulder. All spectra were obtained at 25.0 °C, pH 7.01 NaPi $\mu$ = 0.10 M. $^a$ Calculated from the spectroelectrochemistry data (Figure 2-10). $^b$ Bands below 390 nm were obscured by the dithionite absorption in this region.
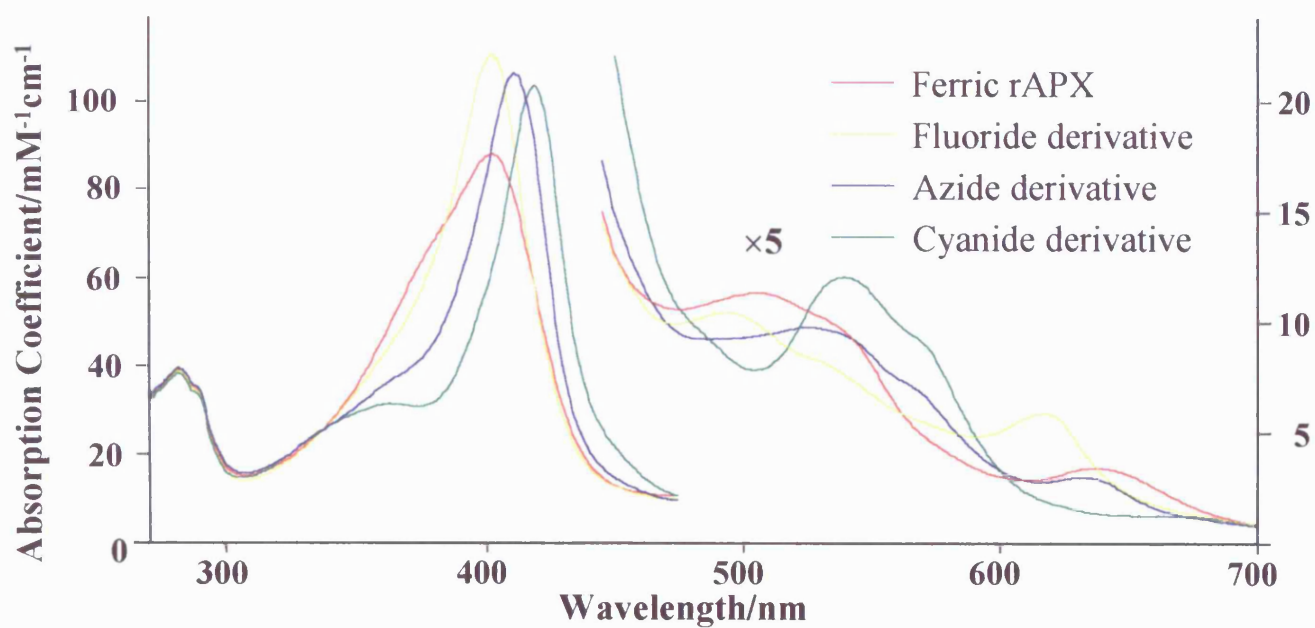
**Figure 2-5 Ferric wild-type rAPX ligand-bound derivative spectra.** Normalisation has been made with respect to the calculated millimolar absorption coefficient; the region 450-700 nm has been multiplied by a factor of five. Sample conditions: ~20 μM wild-type rAPX, 25°C, NaPi pH 7.0, μ = 0.1 M.
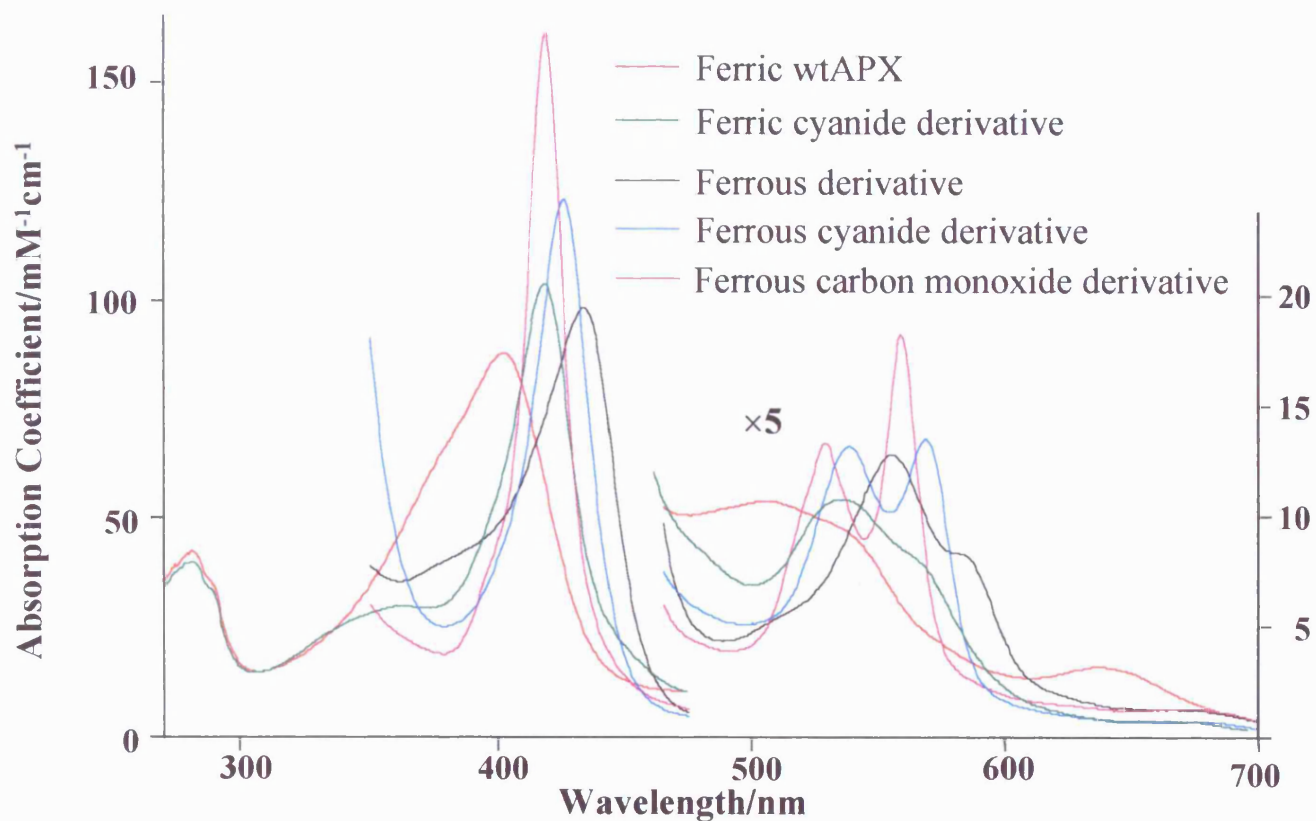
**Figure 2-6 Ferrous wild-type rAPX ligand-bound derivative spectra.** Normalisation has been made with respect to the calculated millimolar absorption coefficient; the region 450-700 nm has been multiplied by a factor of five. Typical sample conditions: ~10 μM wild-type rAPX, 25°C, NaPi pH 7.0, μ = 0.1 M.

the his-tag expressed form of the recombinant wild-type enzyme and a number of ligand-bound derivatives; the data presented here are essentially the same as that of reconstituted apo-protein.

The UV/visible absorption spectra of the fluoride-bound and cyanide-bound ferric ternary complexes are characteristic of the six-coordinate high-spin and low-spin ferric haem, respectively.

### 2.3.3 Temperature-dependency of wild-type rAPX azide-bound spectrum

The relative peak intensities of the ferric azide-bound complex displayed temperature dependent properties that were indicative of a potential high/low spin equilibrium for this species. Therefore, to further substantiate this qualitative observation, a variable temperature experiment was conducted.

An azide-saturated sample of wild-type rAPX, suitable for UV/visible absorption spectroscopy, was prepared and equilibrated to 15°C. Subsequently, the sample temperature was raised stepwise, up to 30°C, and thermally equilibrated spectra were obtained at each temperature, Figure 2-7. Comparison of overlaid spectra, which were obtained throughout the variable temperature experiment, highlighted a temperature-dependency, indicative of a thermal equilibrium. The low-spin features, particularly the α & β absorption bands, diminish in intensity as the temperature is raised across the 15-30°C range (temperatures above 35°C resulted in precipitation). This indicates that azide-bound wild-type rAPX exists as an equilibrium mixture of six-coordinate high and low-spin haem-iron centres, the proportion of which is thermally sensitive.

Further reduction of the sample temperature required the use of an alternative spectrophotometer and was conducted by Dr Emma Raven (Department of Chemistry,
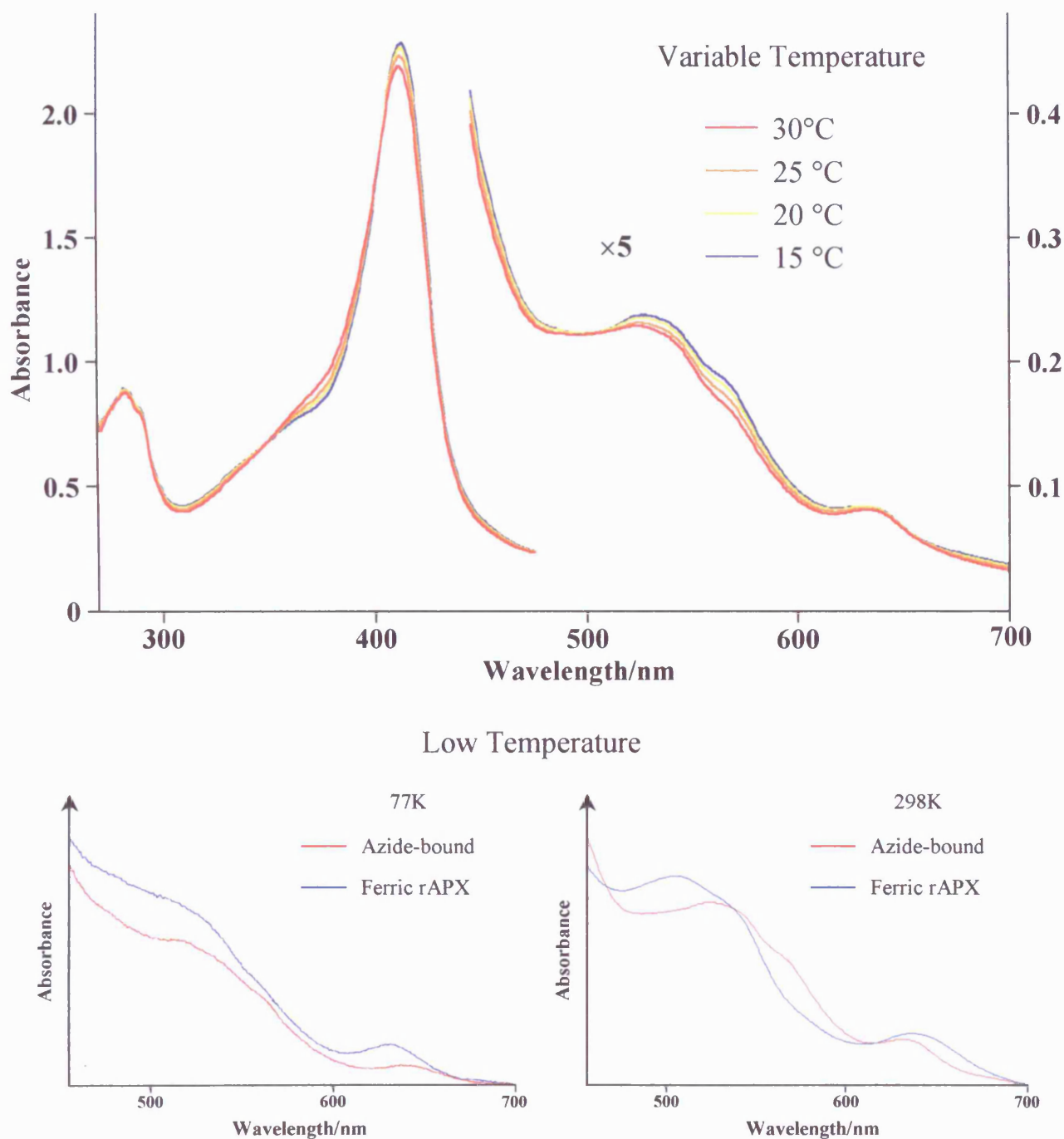
**Figure 2-7 Variable and low temperature UV/visible electronic absorption spectra Wild-type rAPX azide-bound ternary complex.** Variable temperature: spectra of azide-bound wild-type rAPX obtained across the 15-30°C range, the 450-700 nm region has been multiplied by a factor of five, ~20 μM wild-type rAPX, NaPi pH 7.0, μ = 0.1 M. Low temperature: spectra of ferric and azide-bound wild-type rAPX obtained at 77K, and reference spectra acquired at 298K.

56

Leicester University) in the laboratory supervised by Prof. A. G. Mauk (Department of Biochemistry and Molecular Biology, University of British Columbia, Vancouver, Canada). The UV/visible spectra of frozen rAPX, which were obtained at 77K, do not display the isosbestic points observed in solution at 298K, Figure 2-7. Scattering of incident light by ice crystals the magnitude of visible light wavelengths, which would be randomly distributed and orientated in both sample and reference beam, may contribute significantly to the observed difference between the low temperature spectra obtained for ferric and azide-bound wild-type rAPX. Freezing-induced artifacts are observed in the electron paramagnetic resonance spectrum of ferric wild-type rAPX, section 2.6, suggesting that data obtained from frozen solutions may be extraneous. Whilst the low temperature UV/visible spectral features of azide-bound are predominantly six-coordinate low-spin, the retention of the charge-transfer band (~630 nm) is consistent with retention of the high-low spin admixture observed between 15°C and 30°C.

### 2.3.4 Ligand binding studies

The wild-type rAPX equilibrium dissociation values for various exogenous ligands were calculated from spectrophotometric titration data. A typical example of the titration data and a corresponding binding affinity plot are shown in Figure 2-8. The equilibrium dissociation constants measured for the binding of cyanide, fluoride and azide to wild-type rAPX are compiled in Table 2-2.

The binding affinity observed for cyanide decreases as the pH becomes mildly acidic (Table 2-2). However, extraction of a meaningful $pK_a$ for the process was hampered by acid-induced precipitation of the protein.
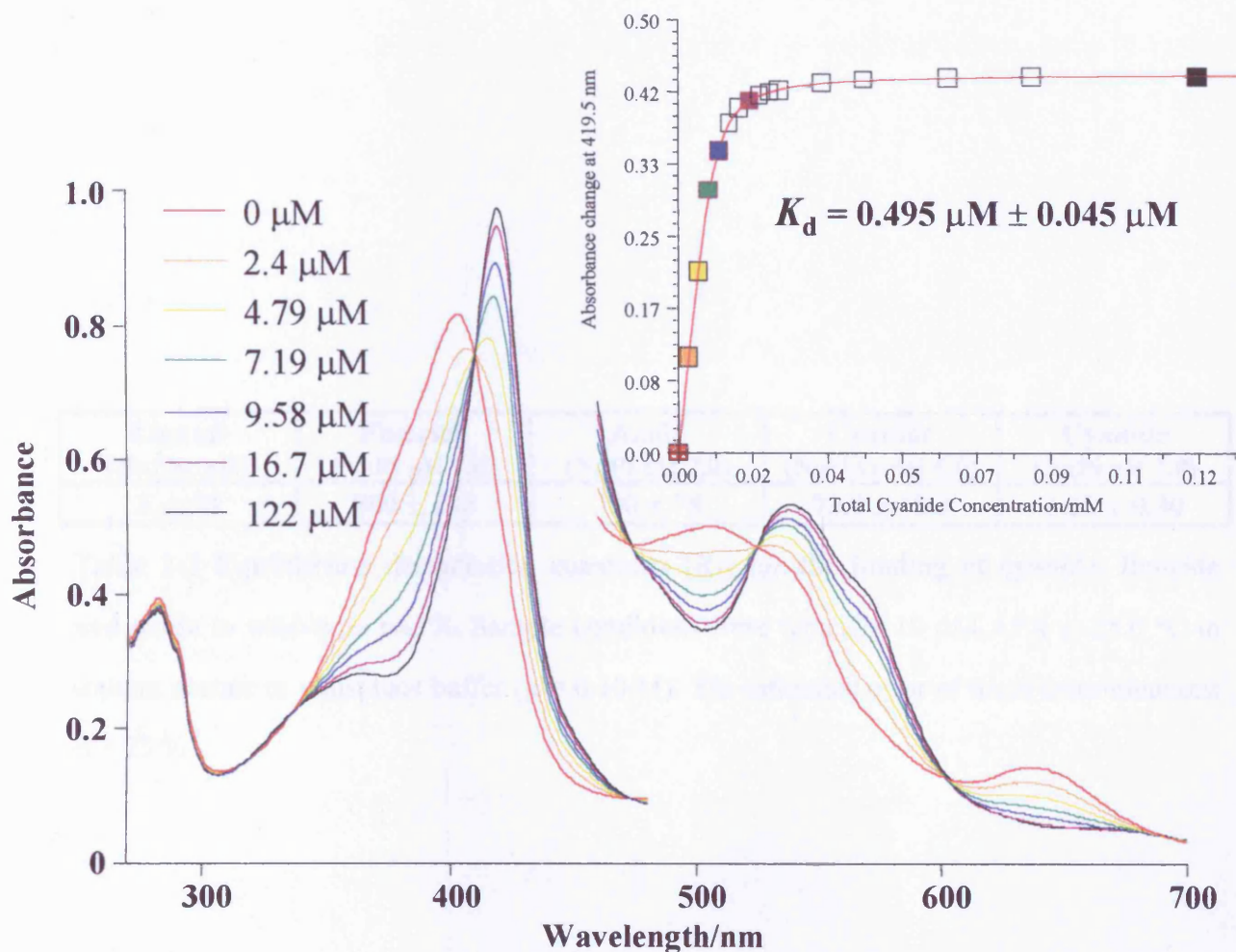
**Figure 2-8 Spectrophotometric titration spectra.** Selection of overlaid UV/visible spectra obtained throughout a titration of ferric wild-type rAPX with potassium cyanide. The calculated fit of the change in the experimentally measured absorbance at 419.5 nm ($\Delta A_{419.5}$) with the increase in total cyanide concentration is included as an inset. Total cyanide concentration is as indicated by the coloured key, which is maintained in the inset as a fill colour for the data points that are selected in the overlaid spectra. Sample conditions: 9.3 µM wild-type rAPX, 25 °C, NaPi pH 7.0, µ = 0.1 M.

| Ligand (Buffer pH) | Fluoride (NaPi pH 7.0) | Azide (NaPi pH 7.0) | Cyanide (NaOAc pH 5.0) | Cyanide (NaPi pH 7.0) |
|---|---|---|---|---|
| $K_d/\mu M$ | $800 \pm 200$ | $300 \pm 75$ | $73.0 \pm 18.3$ | $1.18 \pm 0.30$ |

**Table 2-2 Equilibrium dissociation constants ($K_d$) for the binding of cyanide, fluoride and azide to wild-type rAPX.** Sample conditions were typically 10 $\mu M$ APX at 25.0 °C in sodium acetate or phosphate buffer ($\mu = 0.10$ M). The estimated error of these determinations is $\pm 25$ %.

## 2.4 Steady state L-ascorbic acid activity measurements

Having established that the spectroscopic properties of the recombinant wild-type enzyme were in agreement with those reported previously, both for the native and recombinant wild-type forms of cytosolic pea APX,[1,2] confirmation of the retention of the reported specific activity was sought.

### 2.4.1 Specific activity

Under the standard assay conditions (0.5 mM ascorbate, 0.1 mM $H_2O_2$, pH 7.0 phosphate buffer) the reported activity measured by Patterson and Poulos for native and recombinant wild-type enzyme was 101 ± 3 and 117 units per mg of enzyme respectively.[2] The observation of non-Michaelis-Menton behaviour had been reported for enzymatic turnover with ascorbate; maximum activity was noted to occur at an optimum of pH 7.[1] Accordingly, two distinct experiments were conducted to examine the steady-state behaviour of the isolated wild-type rAPX: a pH-dependent assay of ascorbate oxidation; and the ascorbate concentration-dependence of the steady-state reaction profile.

The plots obtained from the steady-state assay data confirm retention of wild-type rAPX specific activity, Figure 2-9. Optimal pH for the oxidation of ascorbate was found at around pH 7.0, the maximum of a bell-type curve, as reported for the native wild-type enzyme.[1] The non-Michaelis-Menton profile obtained by plotting specific activity against ascorbate concentration is in accordance with the literature. A discussion of a possible rationale behind the deviation from the theoretical model is discussed at the end of this chapter.
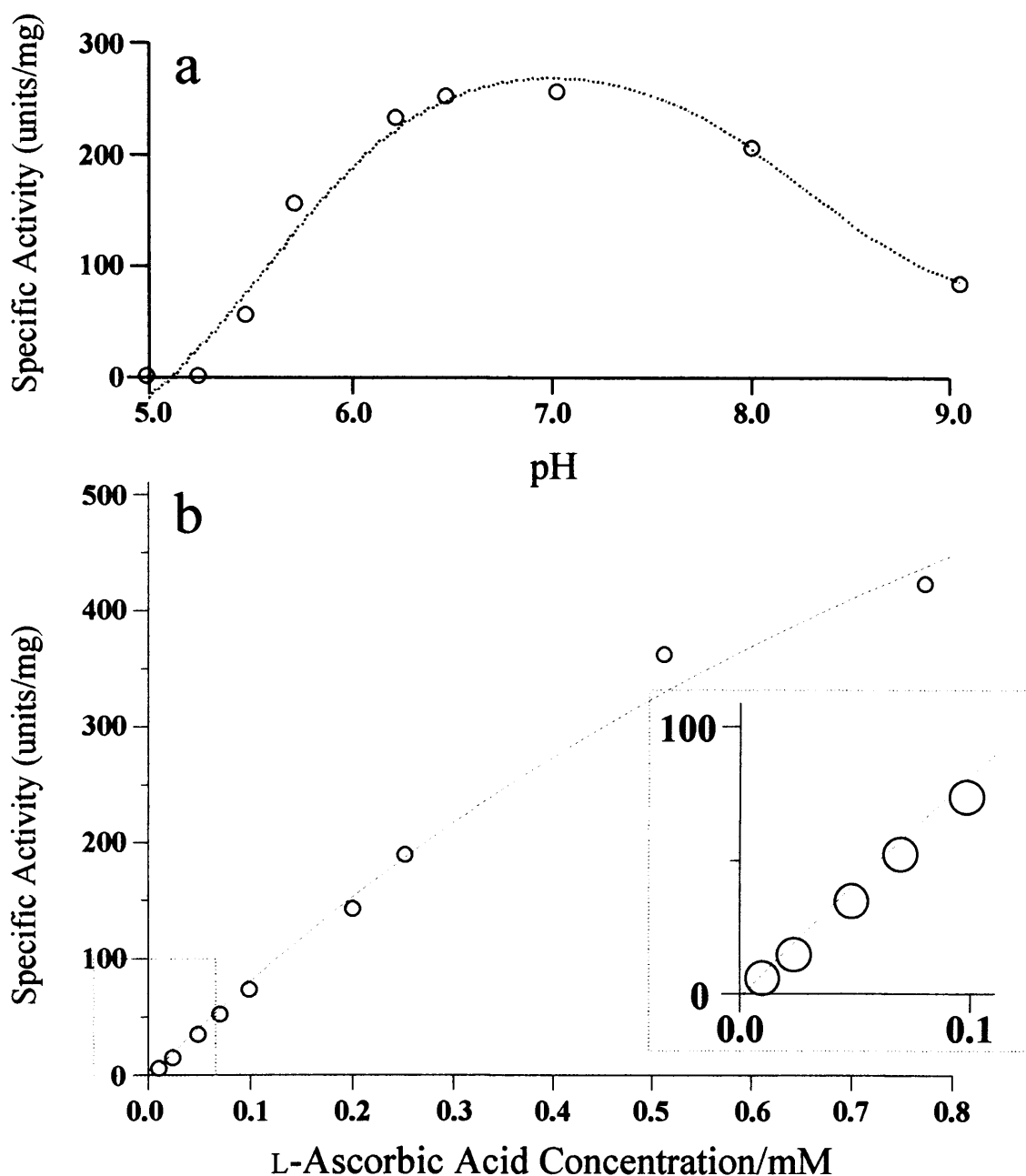
**Figure 2-9 (a&b) Steady state activity measurements.** (a) The pH dependence of ascorbate oxidation by wild-type rAPX, in mixed sulphonic acid buffers, the dashed red line represents a fit to a Henderson-Hasselbach derived double $pK_a$ equation ($pK_1 = 8.2 \pm 0.3$ & $pK_2$ $5.6 \pm 0.2$ ). Assay conditions: 25 nM rAPX , 0.5 mM L-ascorbic acid and 0.1 mM $H_2O_2$ at 25 °C, $\mu$ = 0.95-0.110 M. (b) A plot of specific activity versus L-ascorbic acid concentration, an attempt to fit the steady state data to the Michaelis-Menten equation is denoted by the dashed red line, the inset highlights the sigmoidal deviation from the simple kinetic model. Assay conditions: 25 nM rAPX & 0.1 mM $H_2O_2$ at 25 °C, pH 7.0 NaPi $\mu$ = 0.10 M.

## 2.5 Paramagnetic haem $^1$H-NMR spectrum

Porphyrin proton resonances are shifted in the presence of a paramagnetic centre. The 200 MHz $^1$H-NMR spectrum obtained for wild-type rAPX is consistent with a predominantly high-spin ferric iron. Assignment of the haem-proton resonances would have required reconstitution of APX with a series of haem derivatives; consequently, assessment of the ferric $^1$H-NMR spectrum, Figure 2-10, is made on a purely qualitative basis.[19]

The relatively intense proton resonances in the 60-80 ppm region of the spectrum probably correspond to the haem methyl resonances. The proton resonances found at: +79.5 ppm; +74.4 ppm; +64.2 ppm & +62.6 ppm in the ferric wild-type rAPX spectra correlate with haem methyl resonances that have been reported for native CcP: +80.4 ppm; +70.9 ppm; +67.6 ppm & +58.6 ppm.

## 2.6 Electron paramagnetic resonance spectroscopy

Electron paramagnetic resonance spectroscopy is a powerful technique for studying haem environments, particularly when used in conjunction with magnetic circular dichroism, facilitating an assessment of the number of paramagnetic species present.[20] Comparison of the EPR spectrum of ferric wild-type rAPX with those previously published for the recombinant enzyme would extend confirmation of the isolated enzyme's integrity.

### 2.6.1 Effect of glycerol

Low temperature UV/visible electronic absorption spectrum of ferric wild-type rAPX suggested that the enzyme was relatively insensitive to temperature, Figure 2-7. However, freezing-induced artifacts have been observed in the EPR spectra of other peroxidases.[21,22] At pH 7.0, in the presence of 50 % glycerol, the predominant species is characterised by the
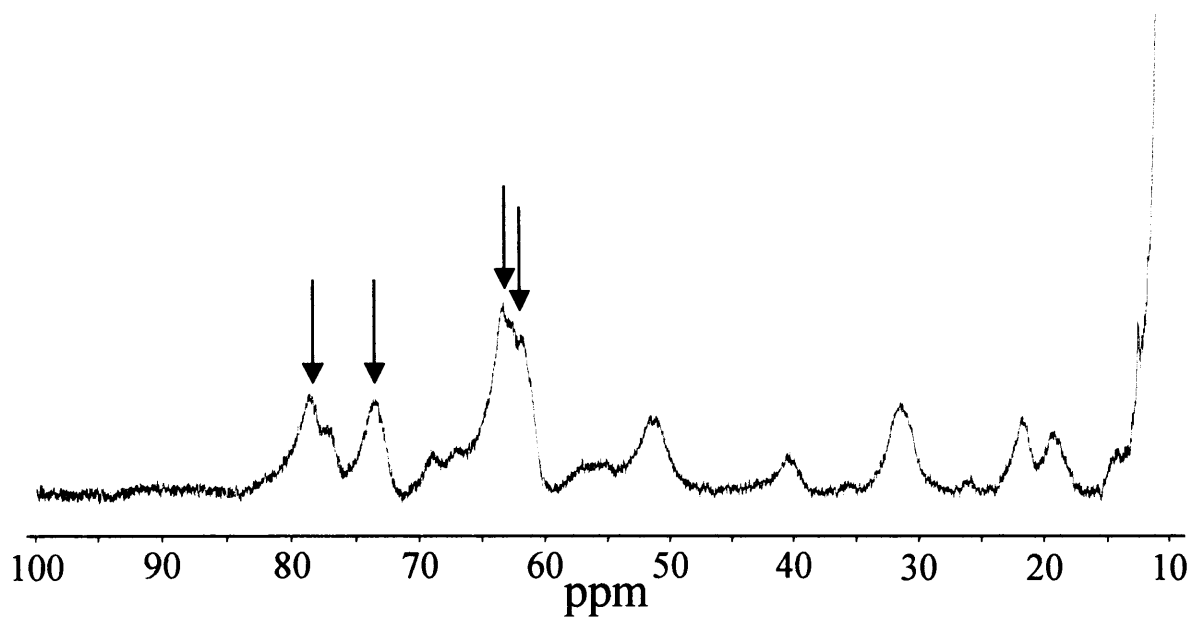
**Figure 2-10 Ferric wild-type rAPX paramagnetic 200 MHz $^1$H-NMR spectrum.** Obtained using 0.4 mM wild-type rAPX dissolved in $D_2O$ containing 50 mM sodium phosphate pH* = 7.0 (uncorrected for the deuterium isotope-effect). The arrows indicate the resonances putatively assigned to the haem methyl groups.

g-values of 6.05, 5.27 and 1.99. However, residual freezing-induced artifacts are evident from the features with g-values of 2.69, 2.23 and 1.79. The spectra obtained at neutral pH in the presence and absence of glycerol, see Figure 2-11, are essentially the same as that previously reported for the recombinant wild-type enzyme.[22]

## 2.7 Spectroelectrochemistry

The ferric-ferrous mid-point potential of wild-type rAPX was determined from thin-layer spectra obtained across an applied potential range of -550 mV to +150 mV vs SHE. These experiments were conducted by Dr Emma Raven (Department of Chemistry, University of Leicester) using apparatus in the laboratory supervised by Prof. A. G. Mauk (University of British Columbia Vancouver, Canada). The electrochemical oxidation of the fully reduced enzyme back to the ferric resting state is shown in Figure 2-12, and the Nernst plot derived from this data is depicted within the insert.

Data from two determinations were then fitted into Nernst plots; the mean average of these determinations was a mid-point reduction potential of -183.1 ± 1.7 mV vs SHE (25.0 °C, pH 6.99, $\mu$ = 0.10 M). The average Nernst slope of the determinations was 73 ± 2 mV, consistent with a single electron process. Previously unreported for wild-type rAPX, the calculated mid-point potential is comparable with that recorded for the ferric-ferrous redox potential of CcP under identical conditions, -194 mV vs SHE.[23]
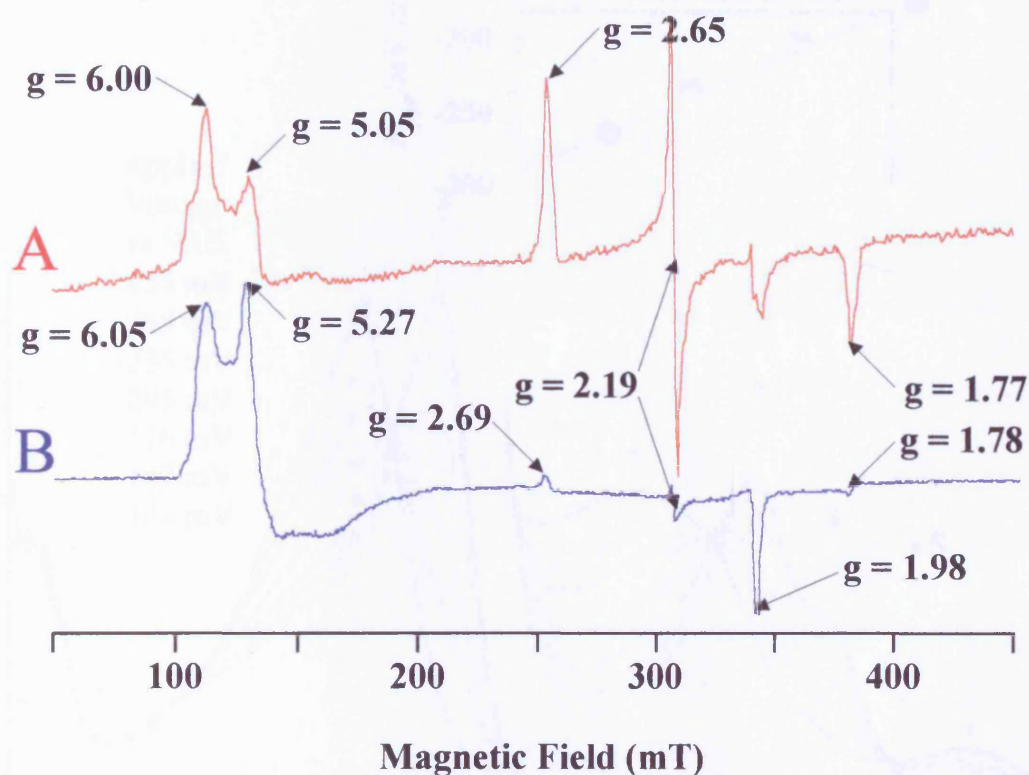
**Figure 2-11 Low temperature electron paramagnetic resonance spectra of ferric wild-type rAPX in the presence and absence of glycerol.** A: 10 K EPR spectrum obtained from a sample of rAPX, which had been prepared for MCD (pH* 8.0 50 mM NaPi, $D_2O$) using the instrument at the University of East Anglia: microwave power 2.01 mW, microwave frequency 9.45 GHz, and modulation amplitude 1 mT. B: 7 K EPR spectrum obtained in the presence of 50% glycerol (pH 7.0 NaPi, $\mu$ = 0.1 M) using the spectrometer at the University of British Columbia: microwave power 1 mW, microwave frequency 9.46 GHz, and modulation amplitude 12.8 G.
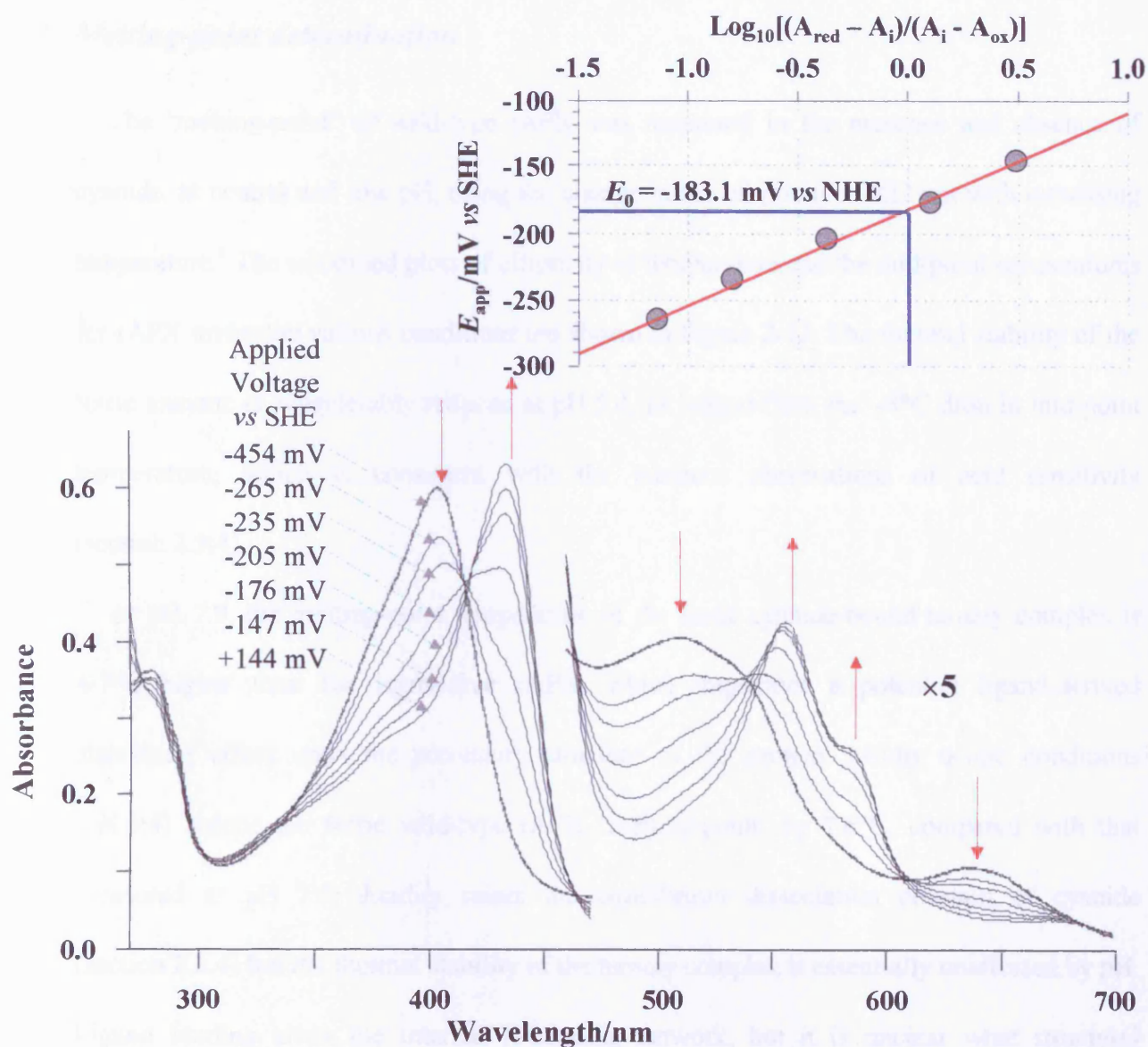
**Figure 2-12 Spectroelectrochemical thin-layer spectra of wild-type rAPX**. Overlaid UV/Visible electronic absorption spectra of wild-type rAPX, which were obtained using an OTTLE, at various applied potentials. The region 450-700 nm has been amplified by a factor of five, red arrows indicate the direction of the spectral changes upon reduction. Sample conditions: 30 μM wild-type rAPX, 25°C, NaPi pH 7.0, μ = 0.1 M. The insert shows the Nernst plot that was derived from the change in absorbance at 436 nm ($\Delta A_{436}$) and the applied potential (i mV).

## 2.8 Melting-point determination

The 'melting-point' of wild-type rAPX was measured in the presence and absence of cyanide, at neutral and low pH, using the change in the ellipticity at 222 nm with increasing temperature.[a] The smoothed plots of ellipticity $vs$ temperature and the mid-point temperatures for rAPX under the various conditions are shown in Figure 2-13. The thermal stability of the ferric enzyme is considerably reduced at pH 5.4, as judged from the ~8°C drop in mid-point temperature, which is consistent with the previous observations of acid sensitivity (section 2.3.4).

At pH 7.0, the melting-point temperature of the ferric cyanide-bound ternary complex is 4.7°C higher than the ligand-free rAPX, which implicates a potential ligand-derived stabilising effect upon the secondary structure of the protein. Mildly acidic conditions (pH 5.4) reduce the ferric wild-type rAPX 'melting-point' by 7.6°C, compared with that measured at pH 7.0. Acidity raises the equilibrium dissociation constant of cyanide (section 2.3.4) but the thermal stability of the ternary complex is essentially unaffected by pH. Ligand binding alters the internal H-bonding network, but it is unclear what structural stabilisation could be gained during ligand binding.

---

[a] The 'melting-point' is defined as the mid-point temperature, $T_m$, at which 50% of the initial α-helical content protein has been removed through thermal denaturation.
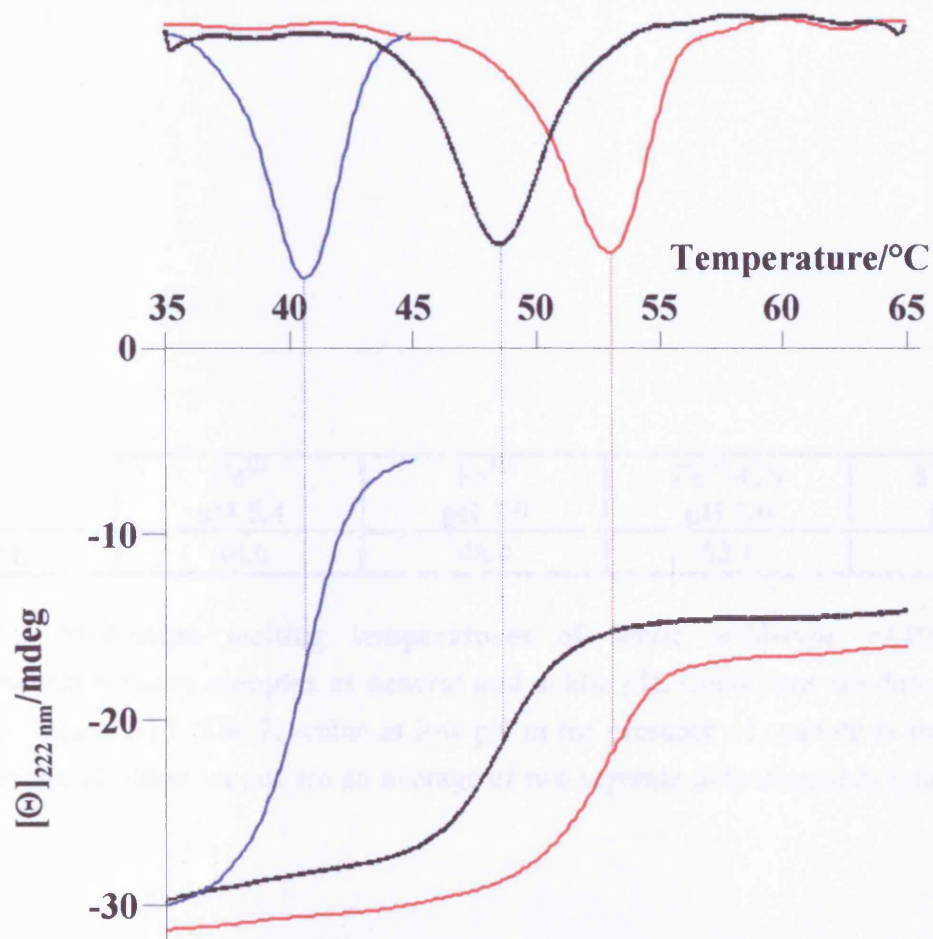
**Figure 2-13 Melting-point temperature determination of wild-type rAPX.** Overlaid plots of the measured ellipticity at 222 nm against temperature for samples of wild-type rAPX under various conditions: – sodium acetate (pH 5.4), – sodium phosphate (pH 7.0), and – cyanide-bound derivative in sodium phosphate (pH 7.0). All plots were recorded using 9.8 µM APX in NaOAc/NaPi buffer (µ = 0.1 M), rate of temperature increase was 50°C/hour. The first derivatives of the temperature-dependent plots, which were used to obtain the mid-point temperatures ($T_m$), are shown at the top of the figure.

| | $Fe^{III}$ pH 5.4 | $Fe^{III}$ pH 7.0 | $Fe^{III}$-CN pH 7.0 | $Fe^{III}$-CN pH 5.4 |
|---|---|---|---|---|
| $T_m/°C$ | 40.6 | 48.4 | 53.1 | 55.4 |

Table 2-3 Mid-point melting temperatures of ferric wild-type rAPX and its cyanide-bound ternary complex at neutral and acidic pH. Conditions are described in the caption to Figure 2-13. The $T_m$-value at low pH in the presence of cyanide is from a single determination; all other values are an average of two separate determinations (standard error ± 1°C).

## 2.9 Discussion

Primarily, the characterisation studies were conducted in order to ensure that the recombinant wild-type displayed essentially the same behaviour as that documented for the native enzyme. Subsequently, detailed spectroscopic characterisation of this newly prepared recombinant ascorbate peroxidase lays extensive foundations: supporting future ascorbate peroxidase research, and to act as a reference point for the variant data. The aim of this section is to summarise the results described earlier within the chapter, discussing the implications of observed behaviour, elaborating upon key-features that will be explored further in subsequent chapters.

Isolation of recombinant pea cytosolic ascorbate peroxidase in moderate yields, typically 8 mg per litre of rich LB medium, facilitated detailed characterisations of the by a number of spectroscopic techniques. Procedures similar to that described by Patterson and Poulos[2] were followed, Chapter 6. The minor deviations from the published protocol had no discernable effect upon expression of the recombinant protein, section 2.1.

Whilst the rAPX-encoding gene sequenced without mutation, the integrity of the recombinant enzyme expressed by the gene was confirmed by obtaining a mass spectrum of the wild-type recombinant enzyme. There was no evidence to support either post-translational modification of the protein or peroxidase-derived tryptic cleavage products. Observation of a significant shoulder at +39-40 Da is consistent with the retention of a structural potassium ion, as implicated in the published crystal structure of the recombinant wild-type enzyme.[3]

Exhaustive exchanges and dialysis against deionised water failed to remove all the potassium from the enzyme. Qualitative assessment of the extent of potassium ion retention, based upon the lack of a significant holoenzyme (haem-containing) peak, provides supporting

evidence for an apparent structural role for the metal-binding site. Site-directed mutagenesis has been reported to facilitate replacement of the rAPX proximal metal binding-site with a CcP-like H-bonding region.[13] The absence of the structural potassium is reported to result in behaviour similar to that reported for thermally inactivated lignin peroxidase, which results in the expulsion of structural calcium ions, with the enzyme displaying spectroscopic properties indicative of a six-coordinate low-spin ferric haem centre.[24]

The Soret band molar absorption coefficient of the wild-type recombinant enzyme was calculated from the haem content of a sample of rAPX, which was assayed by the pyridine haemochromagen method.[12] The calculated millimolar absorption coefficient ($\varepsilon_{403}$ = 88 mM$^{-1}$cm$^{-1}$) is consistent with those of other haem-containing peroxidases, which display resting states that are predominantly five-coordinate high-spin iron(III).[9] A millimolar absorbtivity of 32.0 mM$^{-1}$cm$^{-1}$ at 557 nm was used to quantify the bipyridyl-derivative of ferrous haem produced during the haemochromagen assay, and maximising the reproducible formation of this relatively unstable species requires great care.

Variations in the proportion of six-coordinate species, high- and/or low-spin states, and the conformation of the prosthetic haem group, in particular the degree of vinyl side-chain conjugation, result in spectral shifts that limit the value of ferric resting-state electronic absorption spectral data. Peroxidase resting-states may be comprised of poorly defined spin-admixtures, which may exist in equilibrium. Thus, the ability to manipulate the haem, through reduction and/or the binding of exogenous ligands, facilitates comparison of spectral data obtained from different peroxidases by constraining the haem-iron to defined states. Compiled within Table 2-4 are data extracted from ferric and ferrous peroxidase UV/visible derivative spectra.

| | Pea Cytosolic Ascorbate Peroxidase | | | | | |
|---|---|---|---|---|---|---|
| Derivative | Wild-type rAPX | Native APX | his-tag rAPX | Soybean rAPX | Native CcP | Native HRP |
| $Fe^{III}$ | 403, 506, 540, 636 | 403 | 405, 508, 532, 637 | 407, 511, 633 | 408, 505, 535, 645 | 403, 498, 640 |
| $Fe^{III}$-F | 403, 493, 532, 616 | - | 403, 488, 528, 616 | 416 | 407, 490, 570, 617 | 404, 488, 530, 560, 612 |
| $Fe^{III}$-N$_3$ | 412, 525, 543, 569, 633 | - | 412, 529, 560, 621 | 413, 523 | 535, 570, 635 | 416, 495, 534, 565, 635 |
| $Fe^{III}$-CN | 419, 540, 572 | - | 419, 539, 564 | 419, 539 | 424, 540, 570 | 422, 439, 580 |
| $Fe^{II}$ | 434, 556, 587 | 435, 550, 585 | 432, 555, 584 | 421, 554 | 438, 530, 561, 625 | 440, 510, 557, 580 |
| $Fe^{II}$-CN | 426, 529, 559 | 425, 530, 560 | - | - | - | 432, 536, 566 |
| $Fe^{II}$-CO | 419, 538, 569 | - | 418, 538, 568 | 419, 539, 569 | 423, 542, 570 | 423, 542, 572 |

**Table 2-4 Peroxidase UV/visible electronic absorption spectral data.** The reported wavelength maxima/nm for various ferric and ferrous derivatives of several peroxidases. References from which data has been cited: wild-type rAPX;[8] native pea cytosolic APX;[1] histidine-tagged rAPX;[13] soybean rAPX;[25] native CcP and HRP.[26]

Wild-type rAPX samples, which could potentially contain a variable mixture of five and six coordinate high- and low-spin haem, were routinely spectroscopically analysed to ensure that no discernible peak shifts were evident. The behaviour of the ferric resting-state enzyme and the ferrous cyanide-bound ternary complexes of the recombinant wild-type were essentially identical to that reported for the native wild-type enzyme, which supports retention of the native enzyme haem conformation.[1] Slight differences in the UV/visible absorption spectra, obtained for a series of similarly isolated wild-type rAPX samples, were due to variations in the proportion of ferric haem species present.[b]

The azide-bound ternary complex of wild-type rAPX displayed a significant temperature-dependent UV/visible absorption spectrum, Figure 2-7. Within a relatively narrow range, centred about ambient room-temperature, the azide-bound derivative of ferric rAPX displayed changes indicative of a high/low spin equilibrium. The sharpening of the Soret band and concomitant reduction of the associated 380 nm shoulder, along with enhancement of the $\alpha$ and $\beta$ absorption bands, supports an increase in the proportion of low-spin iron with temperature reduction. However, retention of the high-spin charge-transfer band (633 nm) at 77 K suggests that the equilibrium is not dominated by either spin state. UV/visible spectra obtained at 77 K suggests that the resting-state haem-environment is somewhat perturbed upon freezing in the absence of a glassing-agent, which obscures the value of the data obtained.

The equilibrium ligand-binding constants for wild-type rAPX provide evidence to support an accessible haem-iron. Peroxidases are known to preferentially bind exogenous ligands,

---

[b] UV/visible absorption spectroscopy is too insensitive to detect subtle differences in the proportion of ferric species present, and therefore samples that displayed dramatic spectral shifts (>0.5 nm) were discarded.

such as fluoride, azide and cyanide, along with an associated proton.[27] The uncharged conjugate acid form of an anionic ligand is evidently a better analogue of electroneutral hydrogen peroxide, which rAPX utilises as an oxidant, than the bare anion. Acting as a general base, the distal histidine removes the proton from the conjugate acid, allowing the anionic form of the ligand to complex the iron centre, indicated by the equilibrium between a & d in Figure 2-14. Uptake of a proton upon ligand-binding is consistent with the initial stages of the catalytic mechanism: $H_2O_2$ diffuses into the distal haem cavity, whereupon the distal histidine removes a proton; concomitant with the rapid heterolytic cleavage of the transient peroxyanion, the proton is relocated to the developing hydroxyl (Chapter 1, Figure 1-3). During ligand-binding the proton may only be retransferred to the anionic ligand, which results in a rapid ligand-binding equilibrium, and is therefore retained within the distal pocket.

At pH 5.0 the cyanide-binding affinity of wild-type rAPX is ~1.4 % of that observed at neutral pH; this increase in the equilibrium dissociation constant correlates well with the titration of an internal protein residue ($pK_a \approx 5$), which is indicated by the equilibrium between a & b in Figure 2-14. Under mildly acidic conditions the general-base character of the distal histidine will be partially quenched, which accordingly suppresses the ability of the residue to dissociate the proton from hydrocyanic acid, represented by the equilibrium between c & d in Figure 2-14. The result is a drop in the ligand-binding affinity.

The pH-dependent data obtained for wild-type rAPX equilibrium cyanide-binding is consistent with the behaviour reported for cytochrome $c$ peroxidase, which implicated a two-$pK_a$ process, involving the distal histidine residue of CcP and the acid-base equilibrium of cyanide.[28] However, wild-type rAPX is stable within too narrow a pH range (pH 5.0-8.0) to facilitate such a comprehensive analysis of the ligand-binding pH-dependent profile.
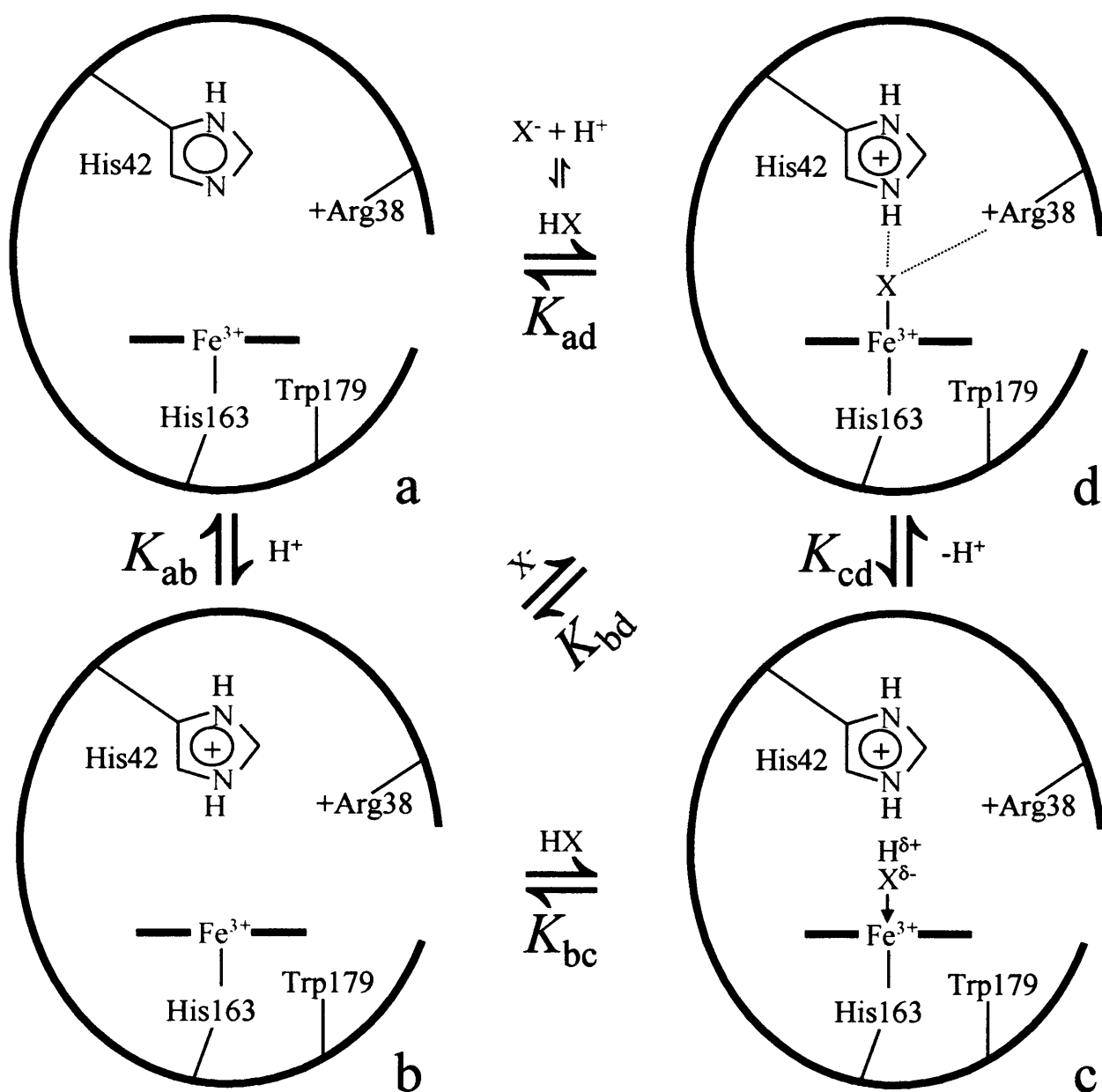
**Figure 2-14 Ferric wild-type rAPX ligand-binding equilibria.** Under mildly acidic conditions a number of potential equilibria exist, which involve protonated and unprotonated forms of the ligand and enzyme. Several species of rAPX that are involved in the pH-dependent equilibria include: (a) the ferric resting state of rAPX; (b) an acidic form of rAPX, which is characterised by protonation of the distal histidine; (c) a weakly coordinated complex involving HX, the electroneutral conjugate acid form of the ligand $X^-$; (d) the ligand-bound ternary complex of rAPX that is stabilised by the distal H-bond network, which includes His42 and Arg38. At neutral pH the key equilibrium is $K_{ad}$ but as solution pH decreases the other equilibria, which disfavour the formation of the ternary complex, result in diminished ligand-binding affinity.

Wild-type rAPX equilibrium dissociation constants obtained for fluoride, azide and cyanide are certainly an intractable combination of H-bond effects, ligand-field strength, and other forces that either influence the access of the anionic ligand to the haem-iron and/or are perturbed during the formation of the ligand-bound ternary complex. Therefore, the $K_d$-values obtained for wild-type rAPX act as standards that facilitate assessment of the extent of distal H-bonding network perturbation in variant enzymes.

The preferred physiological reducing substrate, L-ascorbic acid, was used to assay the specific activity of the isolated wild-type rAPX. Using the range of pH accessible with the 'mixed buffer', pH 5.0-9.5 $\mu$ = 0.950-0.115, the pH-dependency of the wild-type rAPX-catalysed oxidation of ascorbate by hydrogen peroxide was experimentally examined. The activity versus pH plot obtained for wild-type rAPX, Figure 2-7 (a), is broadly bell-shaped and is consistent with that previously reported for the native enzyme.[1] The maximum activity is found at about pH 7.0, with a decrease in activity at the extremes of pH studied.

Attempts to fit the experimental data to the Henderson-Hasselbach equation for a selection of multiple proton processes was restricted by the limited pH range of enzyme stability and the complexity of the mixture of species present at all pH's, discussed in Chapter 3. However, a reasonable fit to the data was obtained using a two-proton, two-$pK_a$ process, which yielded values for $pK_1$ and $pK_2$ of 8.2 ± 0.3 and 5.6 ± 0.2, respectively. These $pK_a$ values are conceivably the onset of base-induced denaturation and formation an inactivated acidic form (Chapter 3), although it is likely that there are more than two titratable residues underlying the steady-state activity pH-profile, particularly given the narrow pH-stability range.

The ascorbate concentration-dependence of wild-type rAPX steady-state activity, data shown in Figure 2-7 (b), is consistent with the reported literature.[1,29] Wild-type rAPX does not display Michaelis-Menten behaviour, and similar non-hyperbolic substrate concentration steady-state dependencies have been reported for APX enzymes isolated from other sources.[30] A cooperative process, which significantly affects enzymatic turnover rate, may result in a sigmoidal kinetic profile.[31] Although authentic wild-type pea cytosolic APX has been shown to exist as a homodimer,[1] it is unlikely that this dimeric interaction is the source of the reported deviations from Michaelis-Menten behaviour.[29] Evidence for cooperativity underlying the observed steady-state activity profile was ambiguous.

Comparison of the data obtained at a selection of different concentrations of enzyme support an alternative hypothesis: at low concentrations of ascorbate, the relatively high peroxide concentration (0.1 mM) used in the assays may inhibit the specific activity through the formation of the ferrous-oxy species (Compound III). The inherent instability of Compound I will facilitate generation of Compound III, described in further detail in Chapter 4, that is not a usual intermediate within the peroxidase catalytic cycle. Data obtained at several enzyme concentrations implied that the maximum specific activity is enzyme concentration-dependent, further evidence supporting the involvement of Compound III. Furthermore, initiation of the assays by the addition of peroxide, instead of rAPX, resulted in severely sigmoidal plots, consistent with $H_2O_2$-dependent inactivation of the enzyme.

An alternative interpretation of the steady-state data is the existence of two substrate-binding sites that interact during the binding of ascorbate, i.e. when ascorbate binds to either site the substrate-binding affinity at the vacant site is slightly raised. Independent studies, which have investigated wild-type rAPX binding of ascorbate, support the possibility of two redox active substrate-binding sites.[8,32] However, the existence of two slightly

cooperative substrate-binding sites would fail to account for the affect of enzyme concentration upon the maximum activity.

Detailed analysis of the steady-state oxidation of ascorbate by pea cytosolic ascorbate peroxidase is also complicated by a number of factors, including the potential generation of Compound III at low ascorbate concentrations, and ascorbate existing in an equilibrium of species. The transient-state kinetics, which underlie the observed steady-state behaviour, are the subject of further discussion in Chapter 4.

The broad high field proton resonances obtained in the spectrum at neutral pH* are consistent with a high-spin ferric haem iron-containing protopophyrin IX. Whilst a detailed investigation of the spectrum was not pursued, the neutral, acidic, and cyanide-bound paramagnetic $^1$H-NMR spectra are qualitatively discussed within Chapter 3.

Freezing-induced artifacts dominate the electron paramagnetic resonance spectrum obtained in the absence of glycerol and are consistent with those reported by Patterson et al.[22] Addition of glycerol, to act as a glassing-agent, greatly diminishes the low-spin signals within the EPR spectrum, although the rationale behind the action of glycerol is not wholly understood. It is plausible that the H-bonding network, which extends from the distal to the proximal domain, and which contains a significant number of internalised water molecules, is affected by freezing effects and may contribute to the observed anomalies. Similar observations have been reported when conducting spectroscopic studies using frozen samples of CcP.[33]

Cold-induced denaturation effects, which occur when the protein tertiary structure reorientates so as to minimise unfavourable interactions with the freezing solvent, might result in significant conformational changes that generate the observed spectral artifacts. Throughout this work, routine flash freezing of protein stocks prior to long-term storage and

their rapid defrosting within a cool water bath before use was essential to avoid freezing-induced spectral artifacts. Long-term storage in doubly deionised water was found to be far more favourable than storage in an aqueous buffered solution. The potentially dramatic changes induced by freezing of the buffered solution in both pH and ionic strength may be an underlying factor in this observation. Further study of the freezing-induced anomalies was not conducted but protein ageing will be discussed in Chapter 5.

Optically transparent thin-layer electrochemistry has not been reported for wild-type rAPX but the mid-point potential, -183 mV $vs$ SHE, is essentially the same as that reported for CcP, -194 mV $vs$ SHE.[23] The ferrous-ferric redox potential of wild-type rAPX has been successfully measured and the value obtained is consistent with a stabilisation of the higher oxidation states that are intermediates during enzymatic turnover.

Circular dichroism in the near UV region can be used to assess the α-helical content present within a protein structure. Using the molar elipticity at 222 nm, the change in the α-helical content was followed as a function of temperature; the first derivative of the data was used to calculate the mid-point 'melting temperature'. The reduced stability of the protein structure at mildly acidic pH is consistent with the observed decrease in specific activity. Thermal denaturation of wild-type rAPX has been measured using UV/visible electronic absorption spectroscopy, the stability assessment obtained from circular dichroism is consistent with that derived from temperature-dependent UV/visible data.[29]

The stabilising effect exhibited by cyanide upon the enzyme, particularly at mildly acidic pH, might suggest an underlying conformational change. However, the UV circular dichroism spectra of the cyanide-bound ternary complex and unligated ferric wild-type rAPX were essentially indistinguishable from one another. Therefore, any hypothesis behind the nature of the stabilisation solely reliant upon this data would be based upon conjecture and so the results should remain open to future interpretation.

## 2.10 Conclusions

Conclusions that can be drawn from the results presented in this chapter are as follows:

- Wild-type rAPX expresses as holoprotein without post-translational modification.

- The recombinant enzyme displays native enzyme UV/visible spectral properties and ligand-bound derivatives are consistent with those reported for other peroxidases.

- Equilibrium dissociation constants were obtained for fluoride, azide and cyanide binding.

- Steady-state measurements confirm the retention of native enzyme activity; under assay conditions Compound III may form resulting in non-Michaelis-Menten kinetics.

- The additional spectroscopic studies support a five-coordinate high-spin ferric haem-iron at neutral pH.

- Freezing artifacts were observed in the EPR spectrum but were alleviated by the addition of glycerol, raising implications regarding sample storage conditions.

- The ferric-ferrous mid-point potential of wild-type rAPX has been determined spectrophotometrically and reported for the first time.

- Thermal stability of the enzyme was established using circular dichroism and compares well with that measured by UV/visible spectroscopy.

## 2.11 References

1   Mittler, R. and Zilinskas, B. A. (1991) *Plant Physiol.*, **97**, 962-968

2   Patterson, W. R. and Poulos T. L. (1994) *J. Biol. Chem.*, **269**, 17020-17024

3   Patterson, W. R. and Poulos T. L. (1995) *Biochemistry*, **34**, 4331-4341

4   Marquez, L. A., Quitoriano, M., Ziliskas, B. A. and Dunford, H. B. (1996) *FEBS Letters*, **389**, 153-156

5   Cross, M. (2000) *NewScientist*, **2226**, Inside Science 128.

6   New England Biolabs Amylose resin protocol

7   World-wide web page concerning New England Biolabs protein fusion & purification (pMAL) system http://www.uk.neb.com/neb/faqs/faq_PFP.html#3.1

8   Hill, A. P., Modi, S., Sutcliffe, M. J., Turner, D. D., Gilfoyle, D. J., Smith, A. T., Tam, B. M. and Lloyd, E. (1997) *Eur. J. Biochem.*, **248**, 347-354

9   Dunford, H. B. (1991) in: *Peroxidases in chemistry and biology* (Everse, J., Everse, K. E. and Grisham, M. B. eds.), vol. 2, CRC Press, Boca Raton, [pp 1-24]

10  Schwartz, S. Berg, M. H., Bossenmaier, I. and Dinsmore, H. (1975) *Meth. Biochem. Analysis*, vol. III, 221-293

11  Pappa, H., Patterson, W. R. and Poulos, T. L. (1996) *J. Biol. Inorg. Chem.*, **1**, 61-66

12  Antonini, M. and Brunori E. (1971) in: *Hemoglobin and Myoglobin and their reactions with ligands* (Neuberger, A. and Tatum, E. L. eds.), North Holland Publishers, Amsterdam. [Pyridine haemochromagen method described pp 10-12]

13  Cheek, J., Mandelman, D., Poulos, T. L. and Dawson, J. H. (1999) *J. Biol. Inorg. Chem.*, **4**, 64-72

14  Brill, A. S. and Williams R. J. P. (1961) *Biochem. J.*, **78**, 246-253

15  Dunford, H. B. and Stillman, J. S. (1976) *Coord. Chem. Rev.*, **19**, 187-251

16  Nagano, S., Tanaka, M, Ishimori, K, Watanabe, Y. and Morishima, I. (1996) *Biochemistry*, **35**, 14251-1458

17  Vitello, L. B., Erman, J. E., Miller, M. A., Mauro, M. and Kraut, J. (1992) *Biochemistry*, **31**, 11524-11535

18  Dunford, H. B. (1999) in: *Heme Peroxidases*, Wiley-VCH, Chichester. [Ligand binding and the formation of compounds of HRP are described pp 58-66]

19 Bosshard, H. R., Anni, H. and Yonetani, T. (1991) in: *Peroxidases in Chemistry and Biology* (Everse, J., Everse, K. E. and Grisham, M. B. eds.), vol. 2, CRC Press, Boca Raton. [pp 51-85]

20 Teixeira, M., Campos, A. P., Aguiar, A. P., Costa, H. S., Santos, H., Turner, D. L. and Xavier, A. V. (1993) *FEBS Letters*, **317**, 233-236

21 Yonetani, T. and Anni, H. (1987) *J. Biol. Chem.*, **262**, 9547-9554

22 Patterson, W. R., Poulos, T. L. and Goodin, D. B. (1995) *Biochemistry*, **34**, 4342-4345

23 Conroy, C. W., Tyma, P., Daum, P. H. and Erman, J. E. (1978) *Biochim. Biophys. Acta.*, **537**, 62-69

24 Nie, G. and Aust, S. D. (1997) *Biochemistry*, **36**, 5113-5119

25 Dalton, D. A., Diaz del Castillo, L., Kahn, M. L., Joyner, S. L. and Chatfield, J. M. (1996) *Arch. Biochem. Biophys.*, **292**, 281-286

26 Dunford, H. B. and Stillman, J. S. (1976) *Coord. Chem. Rev.*, **19**, 187-251

27 Edwards, S. L. and Poulos, T. L. (1990) *J. Biol. Chem.*, **265**, 2588-2595

28 Erman, J. E. (1974) *Biochemistry*, **13**, 39-44

29 Mandelman, D., Schwartz, F. P., Li, H. and Poulos, T. L. (1998) *Prot. Sci.*, **7**, 2089-2098

30 Raven, E. L. (2000) *Subcellular Biochemistry*, **36**, 318-350

31 Shou, M., Mei, Q., Ettore Jr., M. W., Dai, R., Baille, T. A. and Rushmore, T. H. (1999) Biochem. J., **340**, 845-853

32 Mandelman, D., Jamal, J. and Poulos, T. L. (1998) *Biochemistry*, **37**, 17610-17617

33 Dunford, H. B. (1999) in: *Heme Peroxidases*, Wiley-VCH, Chichester. [An overview of the properties of cytochrome *c* peroxidase described pp 220-223]

# CHAPTER THREE

# HAEM-IRON

# COORDINATION

# GEOMETRY OF

# WILD-TYPE rAPX

# 3 Haem-Iron Coordination Geometry Of Wild-Type rAPX

The diverse physiological functions performed by haemoproteins were reviewed within Chapter 1, which also introduced principal peroxidase-conserved structure-function relationships. Behavioural properties of a recently characterised peroxidase, such as wild-type rAPX, may be semi-quantitatively assessed through comparisons with those of well-characterised enzymes, e.g. HRP or CcP. However, analogies made between structurally distinct polypeptides do not provide unambiguous evidence supporting the role, or indeed roles, of individual amino acid residues within the protein of interest. As discussed within Chapter 2, recombinant pea cytosolic ascorbate peroxidase retains the spectroscopic and steady-state properties reported previously for the native enzyme. The availability of a reliable recombinant expression system for the enzyme affords a more rigorous method of assessing protein structure-function relationships in wild-type rAPX.

Site-directed mutagenesis can be utilised to selectively alter specified genetic codons, and expression of variant proteins is observed where mutations lie within the target protein-encoding gene. Thus, the involvement of an individual protein residue in the functional properties of wild-type rAPX can be investigated in a systematic way, without recourse to tenuous functional analogies with structurally distinct polypeptides, by evaluating the properties of variant proteins with respect to those of the invariant wild-type enzyme. Variants of rAPX that incorporate single or multiple amino acid replacements have been reported previously.[1-3]

During routine spectrophotometric cyanide-binding titrations (Chapter 2), the ferric resting-state of wild-type rAPX was observed to display an unusual pH-dependent electronic absorption spectrum. At mildly acidic pH, six-coordinate low-spin absorption bands replace

the spectroscopic features observed at neutral pH, which are predominantly five-coordinate high-spin in character. Formation of a novel 'acidic form' of the enzyme was found to be independent of buffer composition and occurred in the absence of exogenous ligands, which suggests that an internal ligand binds as the pH decreases. The imidazole-like distal histidine residue (His42) was identified as a potential internal ligand.

Variant H42A rAPX was isolated, characterised and the effect upon the pH-dependent spectroscopic changes investigated. Consistent with replacement of the catalytic distal histidine residue with alanine, the variant H42A displays only nominal steady-state specific activity and yet retains essentially wild-type spectral properties. The effect of hydrogen ion concentration upon the spectroscopic properties of wild-type rAPX is discussed within this chapter, and the results presented highlight the need for great care in characterising a haemoprotein capable of interconverting between several haem-iron spin and coordination states.

## 3.1 Preparation and isolation of variant H42A

As discussed within Chapter 6, the protocol for isolating variant rAPX was essentially the same as that used to purify the recombinant wild-type enzyme (section 6.1). Site-directed mutagenesis was performed, according to the QuikChange™ protocol (Stratagene), using the wild-type APX-encoding pMAL-c2 vector and the H42A mutagenic oligonucleotides (Perkin Elmer, see Appendix A). Sequencing across the whole APX-coding gene confirmed the presence of the required codon and that the gene was free of any spurious mutations. No subsequent alterations to the wild-type enzyme protocol were required to successfully isolate variant H42A rAPX in moderate yields and of acceptably high purity ($R_Z \geq 1.85$). Throughout

the isolation and purification steps, the variant displayed no dramatic differences in stability or spectroscopic properties from that noted for the wild-type enzyme.

# Results

## 3.2 Characterisation of H42A

The wild-type rAPX characterisation experiments form the foundation upon which the variant studies are built; accordingly, the H42A variant protein was subjected to essentially the same series of experiments as that described in Chapter 2. This section summarises the spectroscopic data obtained for H42A.

### 3.2.1 Electrospray mass spectrometry

Mass spectrometric analysis of variant H42A rAPX gave an average mass of $27121.7 \pm 0.8$ Da, notably lower than the calculated apoprotein mass of 27126.74 Da. As any uncertainty in the actual peptide mass places a potential question mark over the authenticity of the H42A variant, particularly in compiling meaningful experimental results for comparison with wild-type rAPX, an alternative assessment of the integrity of the variant protein was sought.

Protease enzymes cause fragmentation of the polypeptide backbone of a protein through the hydrolysis of specific peptide bonds, e.g. the serine protease trypsin catalyses the hydrolysis of peptide and ester bonds involving the amino acids lysine and arginine. Therefore, an alternative approach to assessing the primary structure of an intact protein is through analysing the discrete peptide fragments that are produced following controlled peptide bond hydrolysis.

A sample of H42A variant rAPX was subjected to an overnight tryptic digest (12 hours at 35°C); the resulting peptide mixture was analysed using electro-spray mass spectrometry. Subsequently, discernible peaks within the 400-1600 m/z region of the electro-spray mass spectrum were compared with all 27 computationally predicted peptide fragments (as compiled within Table 3-1), and sequential combinations thereof. Discrete peptide fragments with masses <400 Da were not resolved; twenty-three peptide fragments were unambiguously identified and are highlighted within Table 3-1. The discernible fragments contained 247 of the 250 amino acid residues that comprise rAPX. Detection of singly and multiply charged forms of fragment 11, which comprises of rAPX residues 39-50, supports expression of H42A variant protein and is consistent with the H42A mutant gene sequence.

## 3.2.2 Pyridine haemochromagen assay

An absorption coefficient of $\varepsilon_{397} = 83 \pm 2$ mM$^{-1}$cm$^{-1}$ was obtained for H42A variant rAPX and was used to calculate the haem-based protein concentrations reported throughout this thesis. At neutral pH, the Soret band maximum of the H42A variant (397 nm) is blue-shifted by 6 nm relative to that observed for the wild-type enzyme (403 nm), which implies that a significant change in the geometry of the haem moiety has been induced by replacement of the distal histidine residue with alanine.

The spectroscopic features of the H42A variant are wholly consistent with retention of the predominantly five-coordinate high-spin haem exhibited by the wild-type rAPX: a broad Soret band located near 400 nm, indistinct $\alpha$ & $\beta$-bands (~540 nm), and an enhanced $\delta$-band (~375 nm). The electronic absorption bands of ferric wild-type and variant H42A rAPX are compiled within Table 3-2, and spectra of variant H42A and wild-type rAPX, normalised to the calculated absorption coefficient, are overlaid in Figure 3-1.

| Fragment | Residues | Sequence | Calculated MW | m/z | | | |
|---|---|---|---|---|---|---|---|
| | | | | M+H⁺ | M+2H⁺ | M+3H⁺ | M+4H⁺ |
| 1 | 1-3 | MGK | 334.17 | 335.18 | 168.09 | 112.40 | 84.55 |
| 1-2 | 1-14 | MGKSYPTVSPDYQK | 1617.77 | 1618.78 | 809.89 | 540.26 | 405.45 |
| 2 | 4-14 | SYPTVSPDYQK | 1283.60 | 1284.61 | 642.81 | 428.88 | 321.91 |
| 3 | 15-18 | AIEK | 459.27 | 460.28 | 230.64 | 154.10 | 115.83 |
| 3-4 | 15-20 | AIEKAK | 676.14 | 677.41 | 339.21 | 226.48 | 170.11 |
| 4 | 19-20 | AK | 217.14 | 218.15 | 109.58 | 73.39 | 55.29 |
| 5 | 21 | R | 174.11 | 175.12 | 88.06 | 59.05 | 44.54 |
| 6 | 22 | K | 146.11 | 147.11 | 74.06 | 49.71 | 37.53 |
| 7 | 23-24 | LR | 287.20 | 288.20 | 144.61 | 96.74 | 72.81 |
| 8 | 25-30 | GFIAEK | 663.36 | 664.37 | 332.69 | 222.13 | 166.85 |
| 8-10 | 25-38 | GFIAEKKCAPLILR | 1593.93 | 1594.94 | 797.97 | 532.32 | 399.74 |
| 9 | 31 | K | 146.11 | 147.11 | 74.06 | 49.71 | 37.53 |
| 9-10 | 31-38 | KCAPLILR | 930.57 | 931.58 | 466.29 | 311.20 | 233.65 |
| 10 | 32-38 | CAPLILR | 784.46 | 785.47 | 393.24 | 262.50 | 197.12 |
| 11 | 39-50 | **LAWASAGTFDSK** | **1252.61** | **1253.62** | **627.31** | **418.54** | **314.16** |
| 12 | 51-52 | TK | 247.15 | 248.16 | 124.58 | 83.39 | 62.80 |
| 13 | 53-61 | TGGPFGTIK | 876.47 | 877.48 | 439.24 | 239.16 | 220.13 |
| 14 | 62-79 | HQAELAHGANNGLDIAVR | 1884.96 | 1885.96 | 943.49 | 629.33 | 472.25 |
| 15 | 80-85 | LLEPIK | 711.45 | 712.46 | 356.73 | 238.16 | 178.87 |
| 16 | 86-119 | EQFPIVSYADFYQLAGVV AVEITGGPEVPFHPGR | 3688.86 | 3689.86 | 1845.44 | 1230.63 | 923.22 |
| 17 | 120-130 | EDKPEPPPEGR | 1249.59 | 1250.60 | 625.80 | 147.54 | 313.41 |
| 18 | 131-136 | LPDATK | 643.35 | 644.36 | 322.68 | 215.46 | 161.85 |
| 19 | 137-142 | GSDHLR | 683.35 | 684.34 | 342.68 | 228.79 | 171.84 |
| 20 | 143-147 | DVFGK | 564.29 | 565.30 | 283.15 | 189.10 | 142.08 |
| 21 | 148-170 | AMGLSDQDIVALSGGHT IGAAHK | 2248.13 | 2249.13 | 1125.07 | 750.38 | 563.04 |
| 22 | 171-172 | ER | 303.15 | 304.16 | 152.58 | 102.06 | 76.80 |
| 22-23 | 137-170 | ERSGFEGPWTSNPLIFD NSYFTELLTGEK | 3351.59 | 3352.60 | 1676.80 | 1118.20 | 838.91 |
| 23 | 173-199 | SGFEGPWTSNPLIFDNS YFTELLTGEK | 3048.44 | 3049.45 | 1525.23 | 1017.15 | 763.12 |
| 24 | 200-209 | DGLLQLPSDK | 1084.58 | 1085.58 | 543.30 | 362.53 | 272.15 |
| 25 | 210-223 | ALLTDSVFRPLVEK | 1586.90 | 1587.91 | 794.46 | 529.98 | 397.73 |
| 26 | 224-241 | YAADEDVFFADYAEAHLK | 2073.93 | 2074.94 | 1037.97 | 692.32 | 519.49 |
| 27 | 242-250 | LSELGFAEA | 935.46 | 936.47 | 468.74 | 312.83 | 234.87 |

**Table 3-1 Peptide fragments derived from the trypsin-catalysed hydrolysis of variant H42A rAPX.** The amino acid sequence and MW of all of the discrete peptides and identifiable combinations thereof are compiled within the table above. Electrospray ionisation results in singly and multiply charged ions; the m/z ratios of the protonated ions detected are highlighted using **bold** type. Fragment 11 is the peptide fragment that confirms expression of H42A variant rAPX, as this peptide cannot be derived from the wild-type enzyme.

| Derivative | $\delta$ | ($\gamma$) Soret | $CT_2$ | $\beta$ | $\alpha$ | $CT_1$ |
|---|---|---|---|---|---|---|
| Wild-Type Fe$^{III}$ | ~380$^{sh}$ | 403 (88) | 506 (11.3) | $\leftarrow$ ~540$^{sh}$ $\rightarrow$ | | 636 (3.4) |
| H42A Fe$^{III}$ | ~375$^{sh}$ | 397 (83) | 509 (10.9) | $\leftarrow$ ~540$^{sh}$ $\rightarrow$ | | 644 (3.0) |
| Wild-Type Fe$^{III}$-CN | ~363$^{sh}$ | 419 (104) | - | 540 (12.0) | 572$^{sh}$ | - |
| H42A Fe$^{III}$-CN | ~358$^{sh}$ | 420 (102) | - | 540 (11.7) | 574$^{sh}$ | - |

Table 3-2 The spectroscopic features of the ferric resting-state and cyanide-bound ternary complexes of H42A and wild-type rAPX. Millimolar absorption coefficients for resolved peaks are noted in parentheses, '$^{sh}$'denotes unresolved shoulder. Electronic absorption spectra of were recorded in sodium phosphate buffer at 25 °C (pH 7.0, $\mu$ = 0.1 M).

90
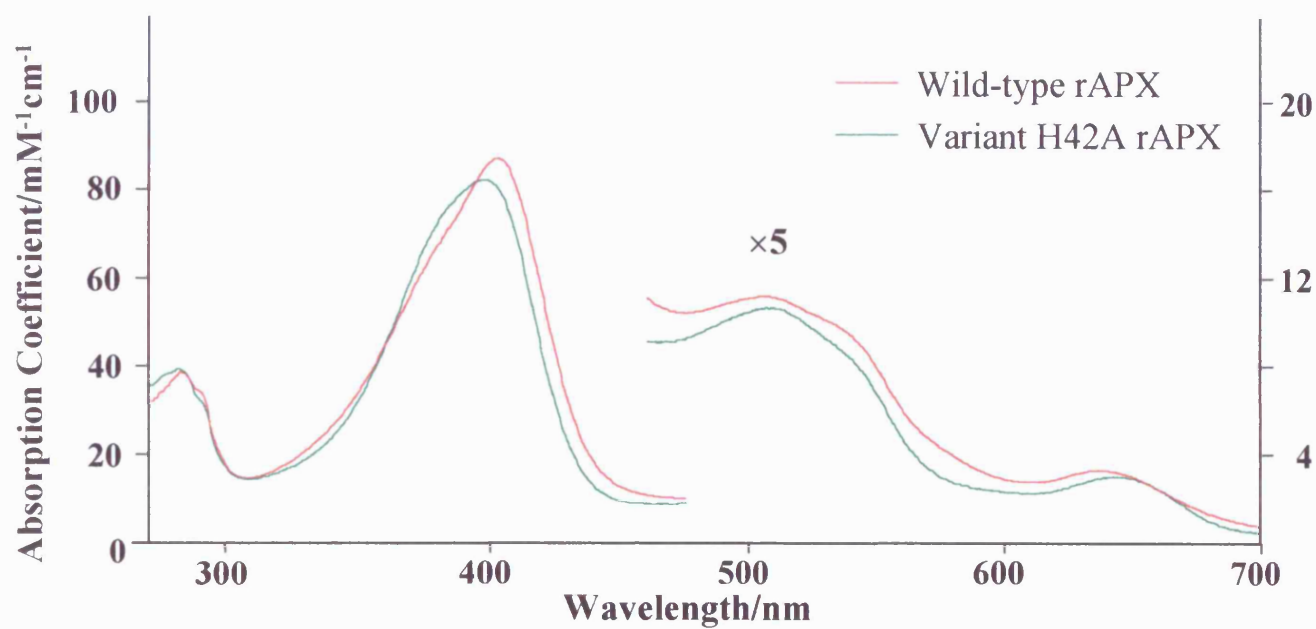
**Figure 3-1 Variant H42A rAPX UV/visible absorption spectra.** Normalisation has been made with respect to the calculated millimolar absorption coefficient; the region 450-700 nm has been multiplied by a factor of five. Sample conditions: 20 μM H42A, 25°C, NaPi pH 7.0, μ = 0.1 M.

### 3.2.3 Anionic ligand-binding equilibria

As discussed within Chapter 2, the conserved distal histidine residue is involved in maintaining electroneutrality in anionic ligand-binding equilibria, and accepts a proton from the uncharged conjugate acid form of the ligand, which preferentially diffuses into the protein matrix. Accordingly, the H42A variant is expected to display an anionic ligand-binding affinity lower than that of the wild-type.

Sub-molar concentrations of NaF and NaN$_3$ induced irreversible precipitation of variant H42A rAPX, which precluded spectrophotometric assessment of the equilibrium binding constants of either ligand. Conversely, cyanide-bound H42A rAPX displays UV/visible absorption bands that are essentially identical to the wild-type cyanide-bound derivative (Table 3-2). However, the cyanide-binding equilibrium dissociation constant calculated for H42A was 160 $\pm$ 40 $\mu$M, which is one hundred-fold less than that obtained for wild-type rAPX. Typical variant H42A cyanide-binding titration spectra are shown, along with the derived ligand-binding affinity plot, in Figure 3-2.

Since the worth of a detailed investigation was considered nominal, further analysis of the equilibrium cyanide-binding properties of variant H42A was not performed.

### 3.2.4 Specific activity measurements

Steady-state turnover of L-ascorbic acid by H42A was not observed under conditions identical to that used for the wild-type. However, the addition of imidazole (90 mM), which has been shown to partially restore the activity of variant H42A HRP,[4] and a ten-fold
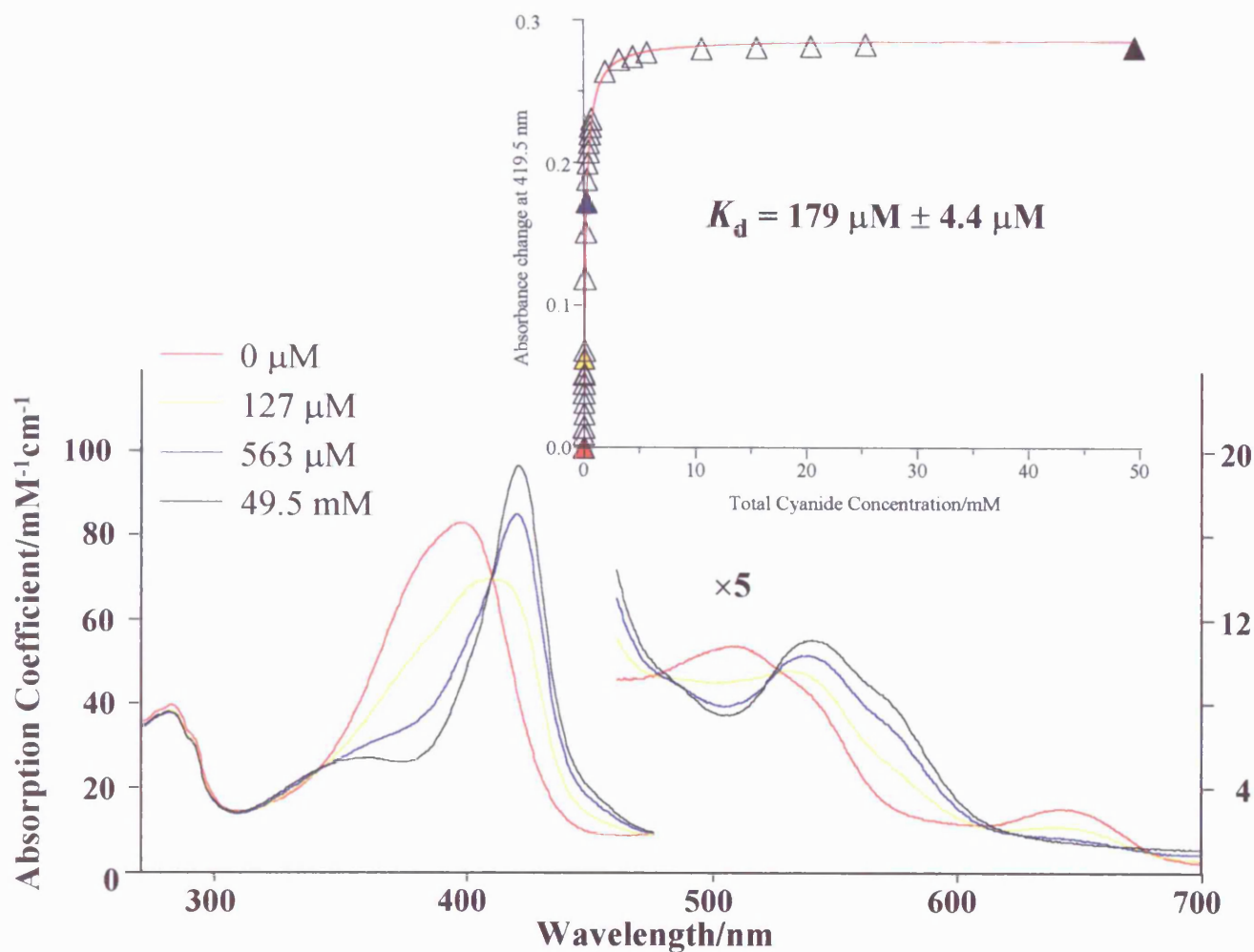
**Figure 3-2 Spectrophotometric cyanide-binding titration of H42A.** Normalisation has been made with respect to the calculated millimolar absorption coefficient; the region 450-700 nm has been multiplied by a factor of five. The calculated fit of the change in the experimentally measured absorbance at 419.5 nm ($\Delta A_{419.5}$) with the increase in total cyanide concentration is included as an inset. Total cyanide concentration for each spectrum is indicated by the coloured key, which is maintained in the inset as a fill colour for the data points included in the overlaid spectra. Sample conditions: 5 µM rAPX, 25°C, NaPi pH 7.0, µ = 0.1 M.

increase in the concentration of H42A (0.25 μM) yielded a measurable rate of ascorbate oxidation. Under such conditions, the specific activity of variant H42A rAPX was calculated to be $10^4$-fold lower than that measured for the wild-type. The pre-steady state kinetics of H42A and wild-type rAPX have also been investigated by Latesh Lad.[5]

## 3.3  pH-Dependent UV/visible spectra

Following the observation of a previously uncharacterised acidic species of rAPX, the spectroscopic properties of wild-type rAPX warranted further investigation. Initially, UV/visible electronic absorption spectra were studied, until the possibility of contamination had been excluded. A parallel experimental approach was adopted during the analysis of the variant, which means that whilst H42A was investigated independently from the wild-type enzyme, results for both variant H42A and wild-type rAPX are presented concurrently in this section.

### 3.3.1  Preliminary characterisation of the 'acidic form'

Initial observation of a low-spin acidic form of the enzyme was made during cyanide-binding studies. Thoroughly cleaned quartz cells were used for all ligand-binding experiments, and residual cyanide was quickly excluded as the origin of the spectra changes. However, a series of control experiments were conducted to confirm the authenticity of the observed pH-dependent spectra, and eliminate any remaining doubt that the unusual properties were due to a persistent experimental artifact.

The wild-type rAPX stocks that were used to prepare the samples for UV/visible spectroscopic analysis were identified as a potential cause of the observed behaviour.

However, contamination or deterioration of the stocks was ruled out, as freshly prepared enzyme samples were found to display pH-dependent spectra indistinguishable from those of spectra obtained using pre-existing stocks.

The 'acidic form' was still formed when samples were prepared using freshly-made buffers, which further excluded solution contamination as the source of the observed pH-dependent behaviour. Indeed, isosbestic points were observed when spectra obtained at pH 5.6 in phosphate and acetate buffers were overlaid with spectra of the neutral and acidic species. The spectra are wholly consistent with a pH-dependent equilibrium dominated by two species, specifically the neutral and acidic forms of the enzyme.

### 3.3.2 Spectrophotometric pH titration

A series of spectrophotometric pH titrations, aimed at demonstrating the reversible formation of the acidic species, were conducted on wild-type rAPX under the following conditions: unbuffered, 10 mM NaPi, and a mixture of sulphonic acid buffers made up to an ionic strength of ~0.1 M using NaCl. Under all the conditions used, a protein-derived buffer action was noted, which meant that cautious additions of base were required to avoid an excessive pH jump, particularly around pH 5.7, which coincides with the isoelectronic point reported for the native enzyme.[6]

Unfortunately, all such titrations were hampered by pH-induced precipitation of the enzyme. Indeed, a sample of wild-type rAPX prepared at pH 4.9 rapidly underwent irreversible protein denaturation, whereas above pH 8.5 the onset of alkaline denaturation was observed (data not shown). The most informative pH titrations were obtained with samples

prepared under mildly acid conditions (typically pH 5.1), which facilitated maximum formation of the acidic species. The sample pH was then titrated upwards, using small additions of sodium hydroxide solution.

A mixture of MES/MOPS/TAPS sulphonic acid buffers (Appendix A), which buffers well across the pH 5.0-9.0 range investigated, was used successfully and resulted in the cleanest titration spectra, an example of which is shown in Figure 3-3.

Isosbestic points ($\lambda$/nm = 400, 458, 551 & 585) indicate that two species predominate the pH-dependent equilibrium. At neutral pH the spectra contains a broad Soret band ($\lambda_{max}$ = 403 nm), but at mildly acidic pH the Soret band increases in intensity and narrows substantially. The spectrum of the acidic-form is comprised of predominantly six-coordinate low-spin features ($\lambda_{max}$ = 410 nm). Fluoride, azide and cyanide were all capable of displacing the weakly bound protein-derived ligand.

The absorbance changes at 413 nm between pH 8.0-5.1 were fitted to the Henderson-Hasselbach equation for a two-$pK_a$ two-proton process. However, the $pK_a$'s generated by the least-squares fit ($pK_1$ = 4.67 ± 0.17 & $pK_2$ = 8.76 ± 2.00) fall outside of the observed pH stability range; the large error in $pK_2$ is an unavoidable consequence of the narrow pH stability range of APX. As the low-spin species is ostensibly fully formed at pH 5.0, the value calculated for $pK_1$ is most probably too low. Attempts to extract a precise $pK_a$ from the spectroscopic titration data were unsuccessful.

Comparable spectrophotometric pH titrations were conducted using H42A, and the spectroscopic shifts observed were essentially the same as the wild-type enzyme, Figure 3-4. At neutral pH, the UV/visible spectrum contains a broad Soret band ($\lambda_{max}$ = 397 nm), but at mildly acidic pH six-coordinate low-spin features of the acidic-form predominate
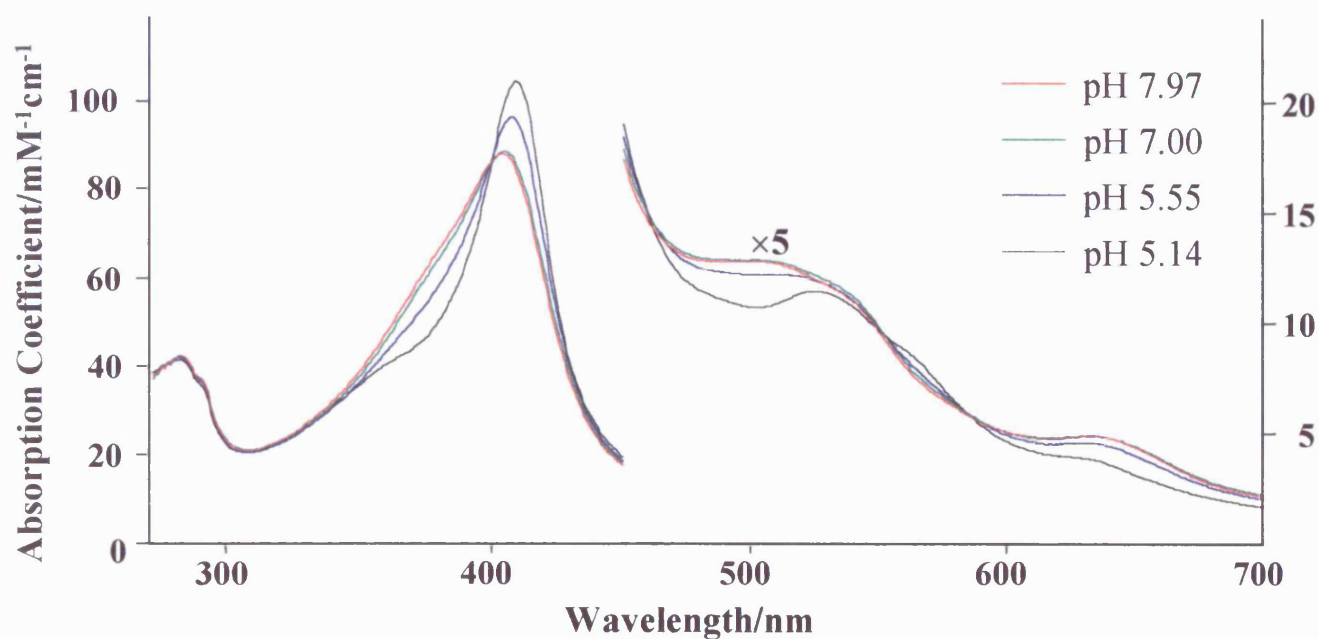
**Figure 3-3 Spectrophotometric pH titration of wild-type rAPX.** Normalisation has been made with respect to the calculated millimolar absorption coefficient; the region 450-700 nm has been multiplied by a factor of five. The solution pH is represented by the coloured key. Sample conditions: 5 μM wild-type rAPX, 25°C, mixed sulphonic acids buffer, μ = 0.950-0.115 M.
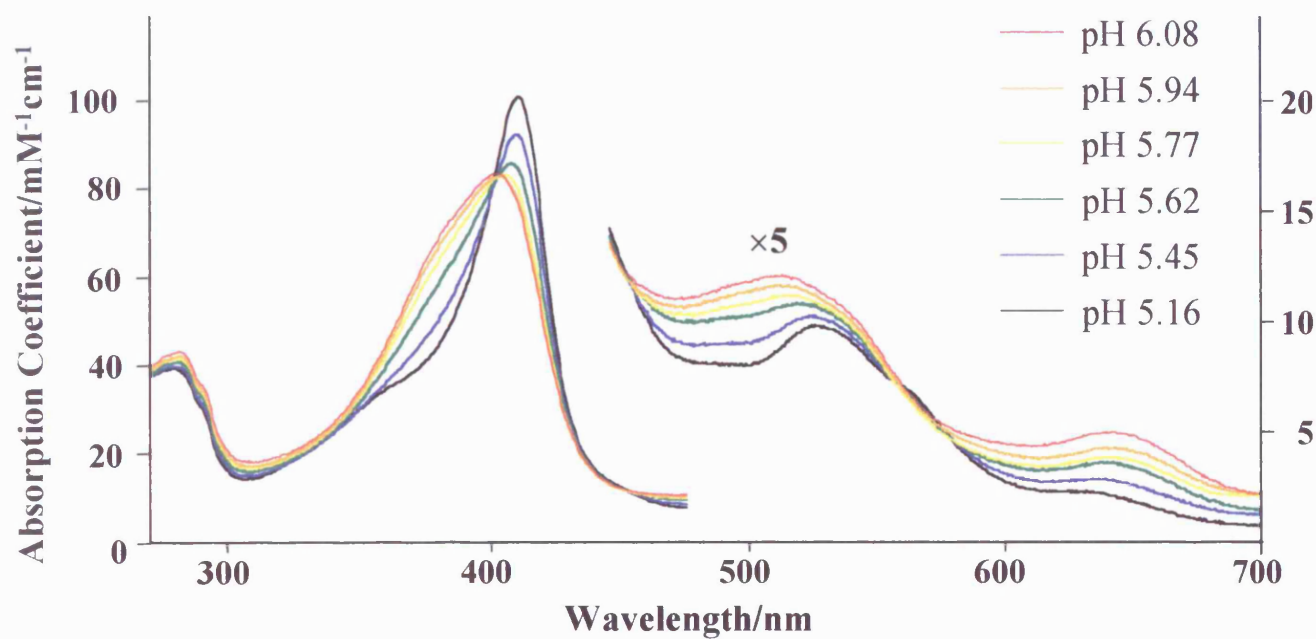
**Figure 3-4 Spectrophotometric pH titration of H42A.** Normalisation has been made with respect to the calculated millimolar absorption coefficient; the region 450-700 nm has been multiplied by a factor of five. The solution pH is represented by the coloured key. Sample conditions: 5 μM wild-type rAPX, 25°C, mixed sulphonic acids buffer, μ = 0.950-0.115 M.

($\lambda_{max}$ = 410 nm). Variant H42A rAPX displays a discernible acidic shift in the p$K_a$ of the pH-dependent transition relative to that of the wild-type enzyme: at pH 5.6, H42A is predominantly high-spin in character whereas wild-type rAPX clearly contains a significant proportion of low-spin haem. A slight shift in the transition p$K_a$ is consistent with the distal histidine weakly interacting with the ligand that binds at acidic pH.

## 3.4 Spectroscopic characterisation of the novel 'acidic-form'

Whilst wild-type rAPX and H42A display comparable electronic absorption properties, UV/visible spectroscopy is not particularly diagnostic of haem spin-state. More detailed elucidation of the haem environment necessitated the use of techniques of greater diagnostic capability, which would highlight subtle differences between the pH-dependent behaviour of the two recombinant proteins.

Accordingly, characterisation of the 'acidic-form', using a variety of spectroscopic techniques, was carried out with the aim of further investigating the nature of this novel low-spin form of rAPX.

### 3.4.1 Paramagnetic haem $^1$H-NMR spectroscopy

A paramagnetic haem dramatically influences the resonances that are derived from protons located within the porphyrin ring and those spatially close to the haem.[7] Paramagnetic haem $^1$H-NMR spectra of wild-type rAPX at neutral and acidic pH are shown in Figure 3-5. The porphyrin proton resonances observed in the $^1$H-NMR spectrum of ferric wild-type rAPX display high-field shifts, which are indicative of the presence of a high spin ferric iron.[7] In comparison, the spectrum of the wild-type rAPX cyanide-bound ternary complex is comprised of sharp features that lie within the 0-35 ppm region, which is consistent with a
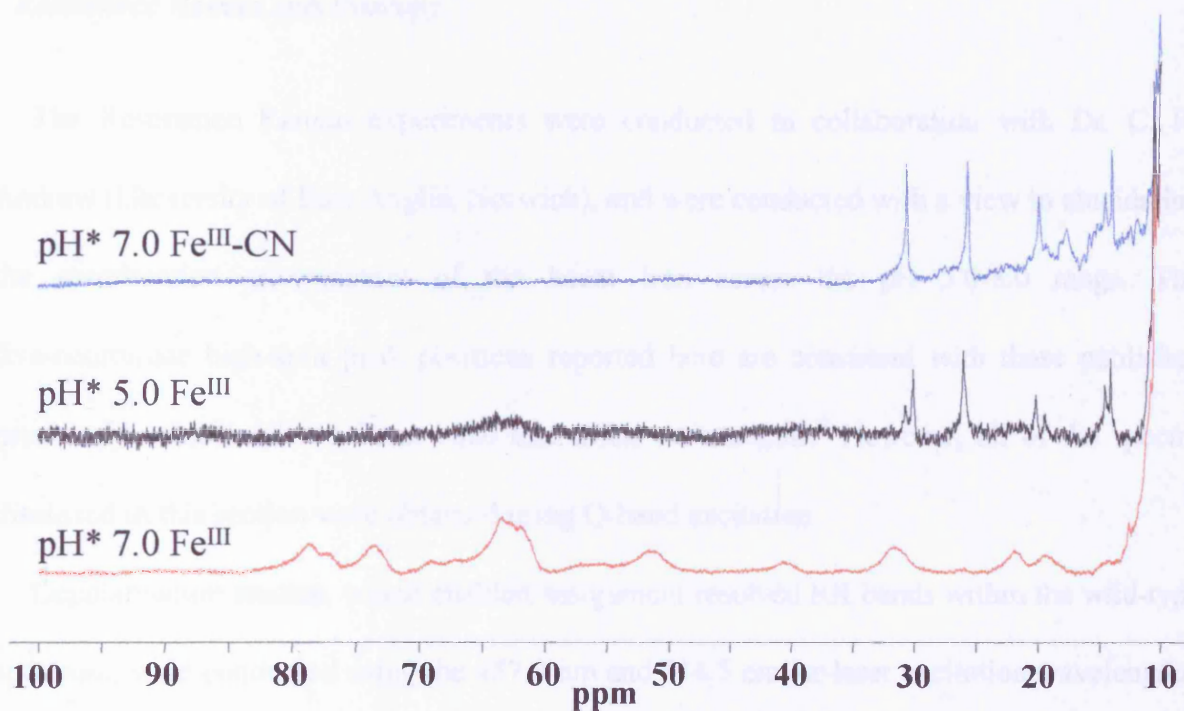
**Figure 3-5 Paramagnetic haem resonance ¹H-NMR spectra of wild-type rAPX.** Wild-type rAPX at neutral and acidic pH along with its cyanide-bound complex, spectra obtained using a solvent presaturation pulse sequence on a 400 MHz Bruker NMR machine. The cyanide-bound complex was prepared by adding a >10-fold excess of prebuffered 1 M KCN to the ferric sample (pH* 7.0). Conditions: 50 mM deuterated NaPi, 300 K.

six-coordinate low-spin haem.[7] At mildly acidic pH, the $^1$H-NMR spectrum of ferric wild-type rAPX is dominated by low-spin resonances, which further supports the tentative electronic absorption spin-state assignment.

## 3.4.2 Resonance Raman spectroscopy

The Resonance Raman experiments were conducted in collaboration with Dr. C. R. Andrew (University of East Anglia, Norwich), and were conducted with a view to elucidating the coordination environment of the haem iron across the pH 5.0-8.0 range. The five-coordinate high-spin peak positions reported here are consistent with those published previously, which utilised Soret band excitation wavelengths.[8] However, all of the spectra discussed in this section were obtained using Q-band excitation.

Depolarisation studies, which enabled assignment resolved RR bands within the wild-type spectrum, were conducted using the 457.9 nm and 514.5 nm Ar-laser excitation wavelengths, Figure 3-6. The superior resolution afforded by RR spectroscopy facilitates detection and assignment of spectral features that are distinctly associated with haem-iron coordination geometries.

A series of spectra were obtained at various pHs, using the perpendicular component of the 514.5 nm excitation wavelength, and are shown in Figure 3-7. Spectroscopic marker bands associated with the five-coordinate high-spin and six-coordinate low-spin species are clearly in equilibrium and the pH-dependence of the bands observed is wholly consistent with that of the UV/visible spectra. The Resonance Raman marker bands of wild-type rAPX are compiled within Table 3-3.

In contrast to the previously reported study,[8] laser-induced sample degradation was not observed when freshly prepared rAPX samples were irradiated for prolonged periods.
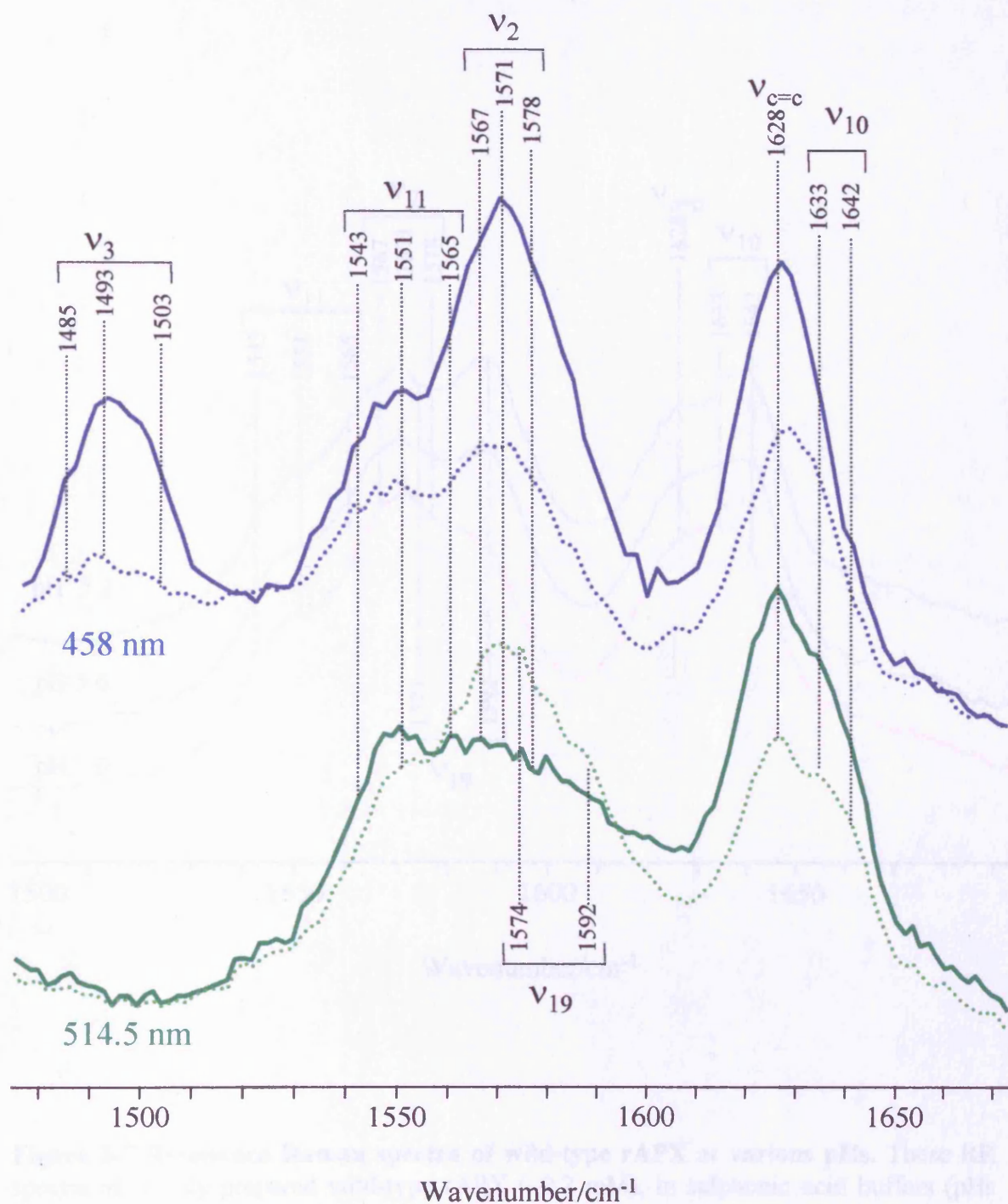
**Figure 3-6 Resonance Raman spectra of wild-type rAPX.** The RR spectra of freshly prepared wild-type rAPX (~0.2 mM), in sodium phosphate buffer (pH 7.0) were recorded at ambient room temperature (~20°C) using the parallel (solid line) or perpendicular (dotted line) component of 514.5 nm and 458 nm excitation wavelengths, laser power at sample ~35 mW.
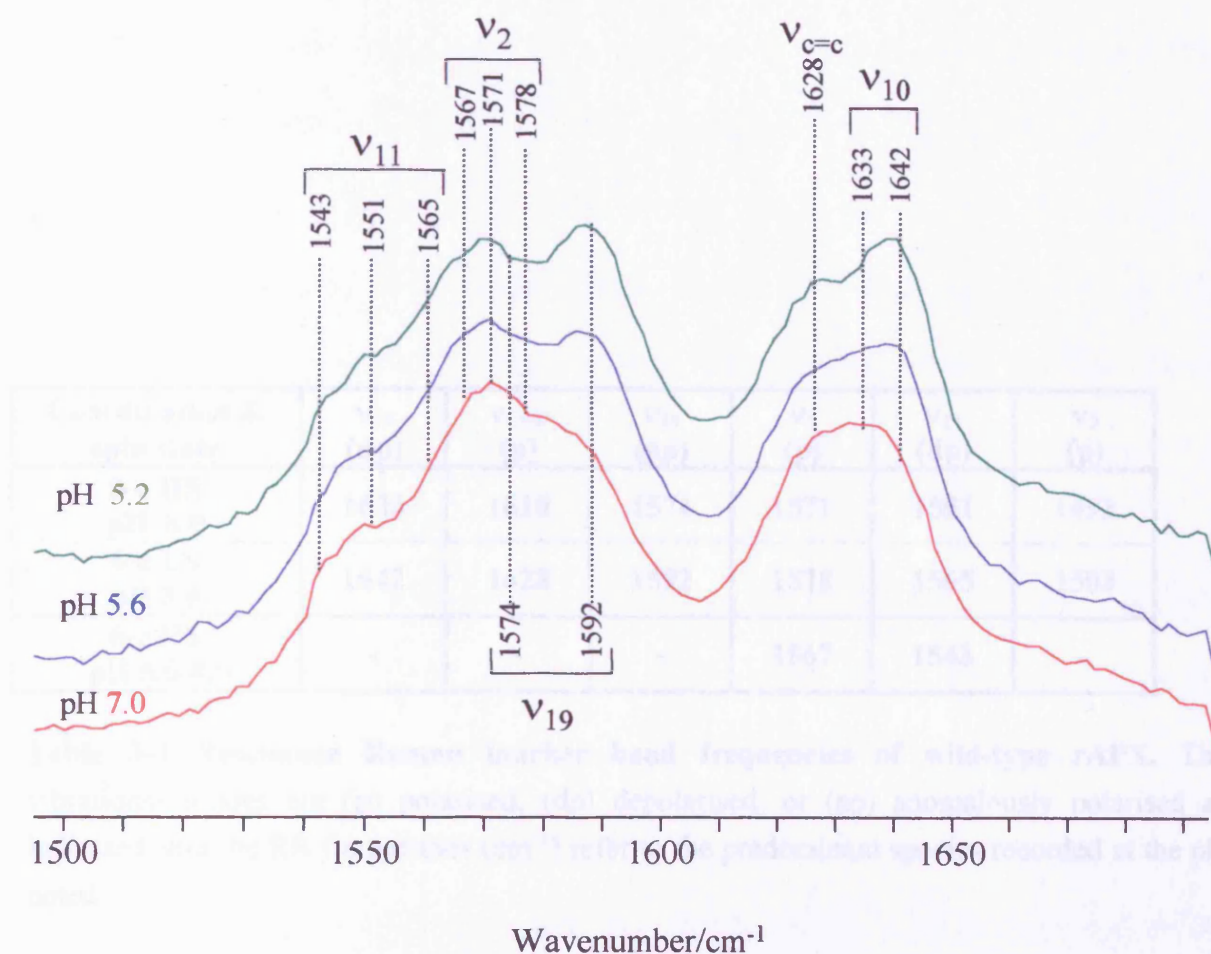
**Figure 3-7 Resonance Raman spectra of wild-type rAPX at various pHs.** These RR spectra of freshly prepared wild-type rAPX (~0.2 mM), in sulphonic acid buffers (pHs 7.0, 5.6 & 5.2), were recorded at ambient room temperature (~20 °C) using the perpendicular component of the 514.5 nm excitation wavelength, laser power ~35 mW.

| Coordination & spin state | $v_{10}$ (dp) | $v_{C=C}$ (p) | $v_{19}$ (ap) | $v_2$ (p) | $v_{11}$ (dp) | $v_3$ (p) |
|---|---|---|---|---|---|---|
| 5-c HS pH 8.0 | 1633 | 1628 | 1574 | 1571 | 1551 | 1493 |
| 6-c LS pH 5.0 | 1642 | 1628 | 1592 | 1578 | 1565 | 1503 |
| 6-c HS pH 5.0-8.0 | - | - | - | 1567 | 1543 | - |

Table 3-3 Resonance Raman marker band frequencies of wild-type rAPX. The vibrational modes are (p) polarised, (dp) depolarised, or (ap) anomalously polarised as indicated, and the RR frequencies ($cm^{-1}$) refer to the predominant species recorded at the pH noted.

However, samples exchanged into buffer using Centricon concentrators yielded anomalous six-coordinate high-spin marker bands that were consistent with partial denaturation of the haemoprotein. Similar spectroscopic artifacts were observed when studying samples of 'aged' H42A, which are considered later in this section. Freshly prepared samples were studied in order to reduce the amount of spectral artifacts originating from sample handling.

In comparison to wild-type rAPX, H42A displays a reduced proportion of low-spin RR features across the pH 5.0-8.0 range studied, Figure 3-8, which is consistent with the UV/visible spectrophotometric pH titration data. The Resonance Raman spectra of freshly prepared H42A are comprised of spectral marker bands that are identical to those of wild-type rAPX.

The low frequency region of ferrous haemoprotein RR spectra contain bands associated with the axial ligand-iron stretching vibrations. Dithionite-reduced wild-type and variant H42A rAPX displayed poor stability below pH 6.0, which precluded assessment of the six-coordinate low-spin ferrous spectral marker bands.

Variability in the resting-state electronic absorption spectrum of wild-type rAPX, purportedly due to the proportion of six-coordinate low-spin haem, has been noted in the literature.[9] Comparable spectroscopic variability was observed whilst studying 'aged' protein samples, which had either been frozen in the presence of a buffer or stored for a prolonged period, e.g. a week at 4°C. Resonance Raman spectra of 'aged' H42A samples consistently displayed an increase in the relative proportion of low-spin marker bands, Figure 3-9, and the result is a clearly anomalous representation of the combination of species present at each pH.
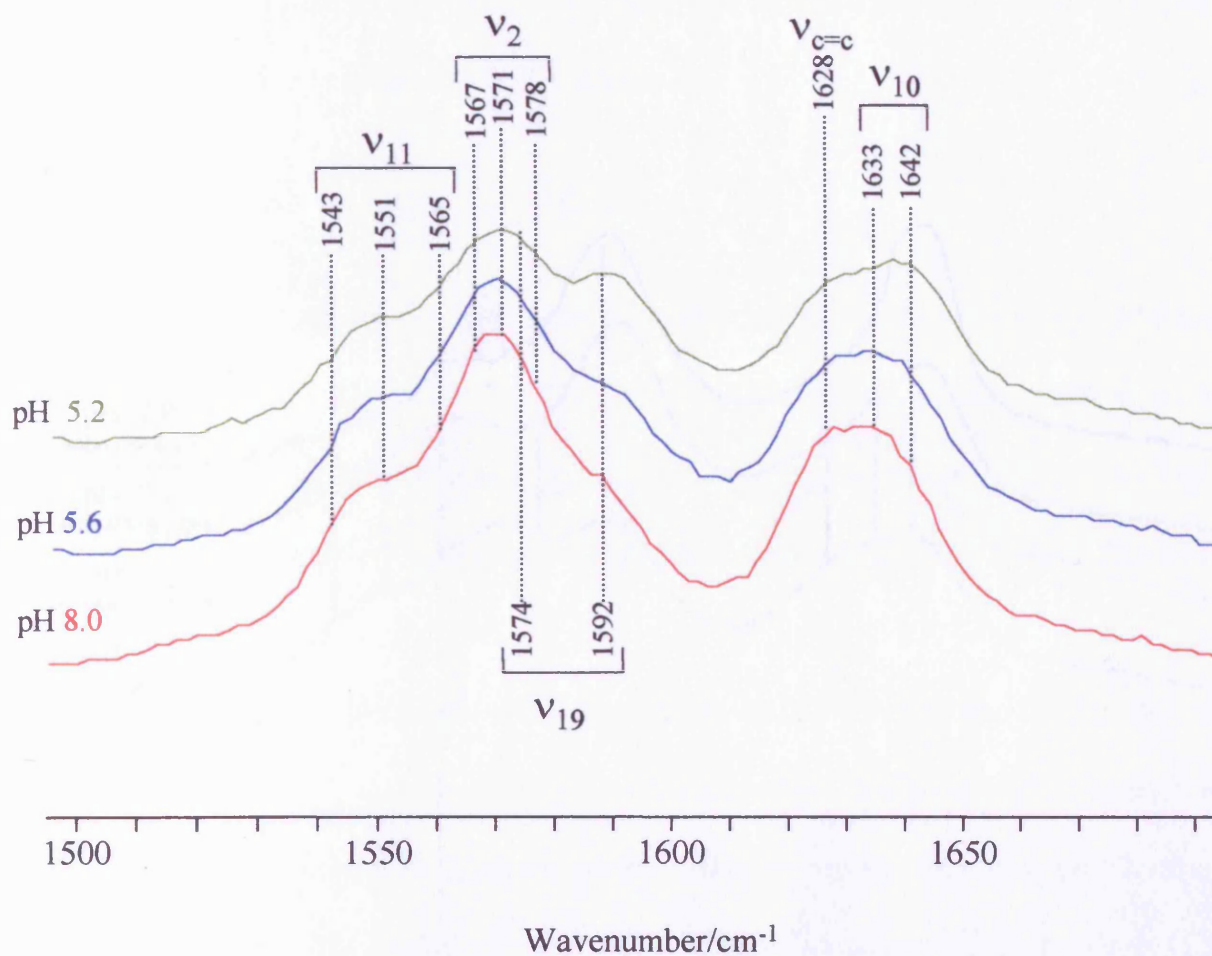
**Figure 3-8 pH-Dependent resonance Raman spectra of H42A.** The RR spectra of freshly prepared H42A (~0.2 mM), in mixed sulphonic acid buffers (pHs 8.0, 5.6 & 5.2), were recorded at ambient room temperature (~20 °C) using the perpendicular component of the 514.5 nm excitation wavelength, laser power ~35 mW.

$\nu_2$ $\quad$ $\nu_{C=C}$ 1628 $\quad$ $\nu_{10}$

1567 1571 1578 $\quad$ 1633 1642

$\nu_{11}$

1543 1551 1565

pH 7.0
H42A rAPX-CN

pH 5.2
MES/MOPS/TAPS

pH 5.6
MES/MOPS/TAPS

pH 7.0
NaPi

1574 1592

$\nu_{19}$

1500 $\qquad$ 1550 $\qquad$ 1600 $\qquad$ 1650

Wavenumber/cm$^{-1}$
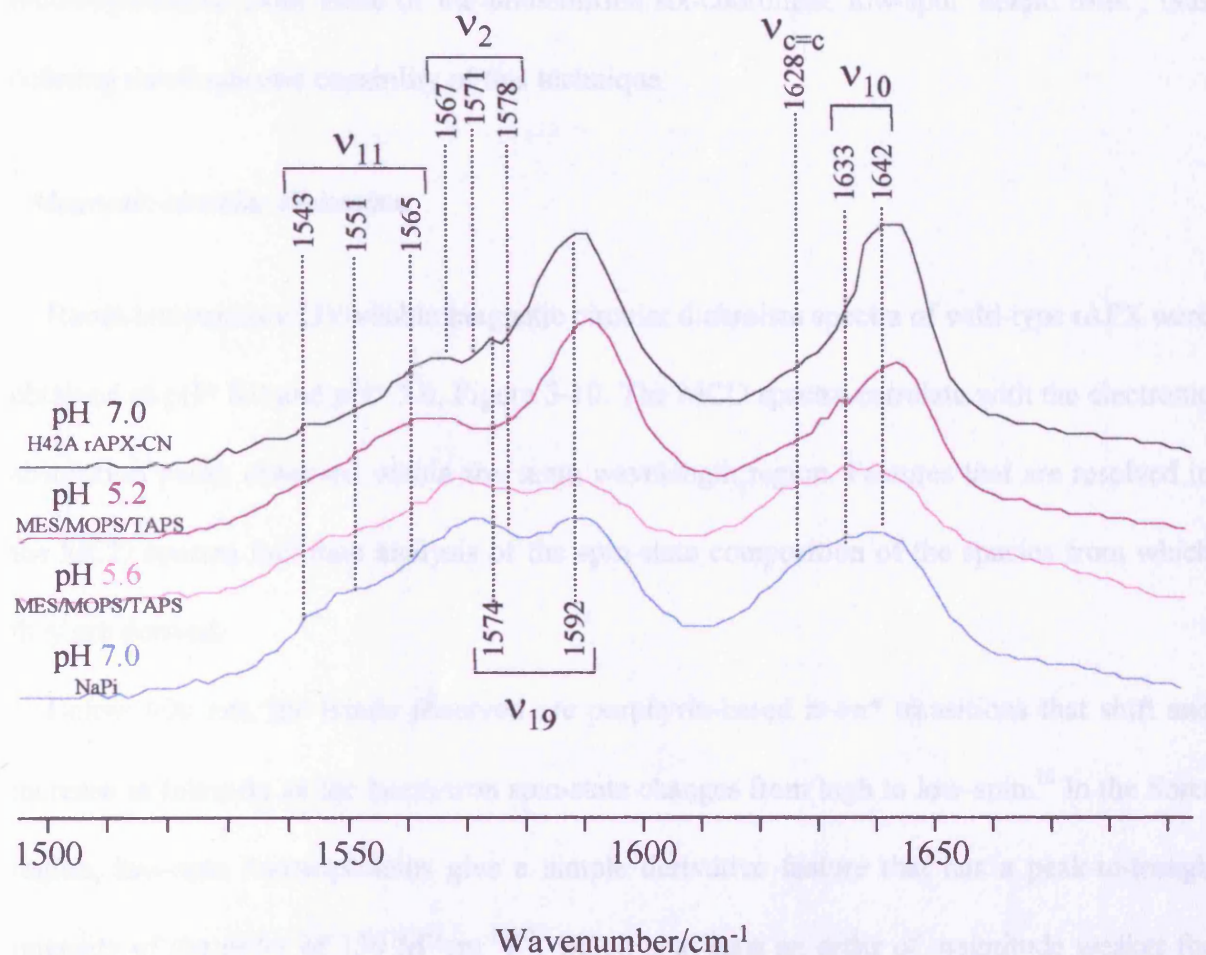
**Figure 3-9 Resonance Raman spectra of 'aged' H42A samples.** Room temperature RR spectra of H42A (~0.2 mM) were recorded using the perpendicular component of the 514.5 nm excitation wavelength, laser power ~35 mW. With the exception of the cyanide-bound ternary complex, which was freshly prepared in pH 7.0 NaPi, samples had been frozen and defrosted prior to analysis (pH and buffer are noted in figure).

Whilst an in-depth investigation of the processes involved in sample 'aging' was not conducted, the use of freshly prepared protein samples minimises any ambiguity in the marker band assignments of rAPX. Low-spin marker bands of cyanide-bound H42A are indistinguishable from those of the unidentified six-coordinate low-spin 'acidic form', thus defining the diagnostic capability of this technique.

### 3.4.3 Magnetic circular dichroism

Room temperature UV/visible magnetic circular dichroism spectra of wild-type rAPX were obtained at pH* 8.0 and pH* 5.6, Figure 3-10. The MCD spectra correlate with the electronic absorption peaks observed within the same wavelength region. Features that are resolved in the MCD spectra facilitate analysis of the spin-state composition of the species from which they are derived.

Below 600 nm, the bands observed are porphyrin-based $\pi \rightarrow \pi^*$ transitions that shift and increase in intensity as the haem-iron spin-state changes from high to low-spin.[10] In the Soret region, low-spin haemoproteins give a simple derivative feature that has a peak-to-trough intensity of the order of 150 $M^{-1}cm^{-1}T^{-1}$, which is at least an order of magnitude weaker for five and six-coordinate high-spin haemoproteins.[10] Clearly, the Soret region peak-to-trough intensity of the wild-type rAPX UV/visible MCD spectra is pH-dependent, and thus consistent with the high-to-low-spin transition hypothesis.

At wavelengths longer than 600 nm, the energies of porphyrin$\rightarrow Fe^{III}$ charge-transfer (CT) bands give additional information on the nature of the haem axial ligands: high-spin haem gives two CT bands and low-spin haem gives one.[11,12] The higher energy high-spin CT band (known as the "630-band" and diagnostic of this spin state) gives rise to a derivative-shaped feature, the low-energy trough of which can be used as a marker for specific ligand sets.[13]
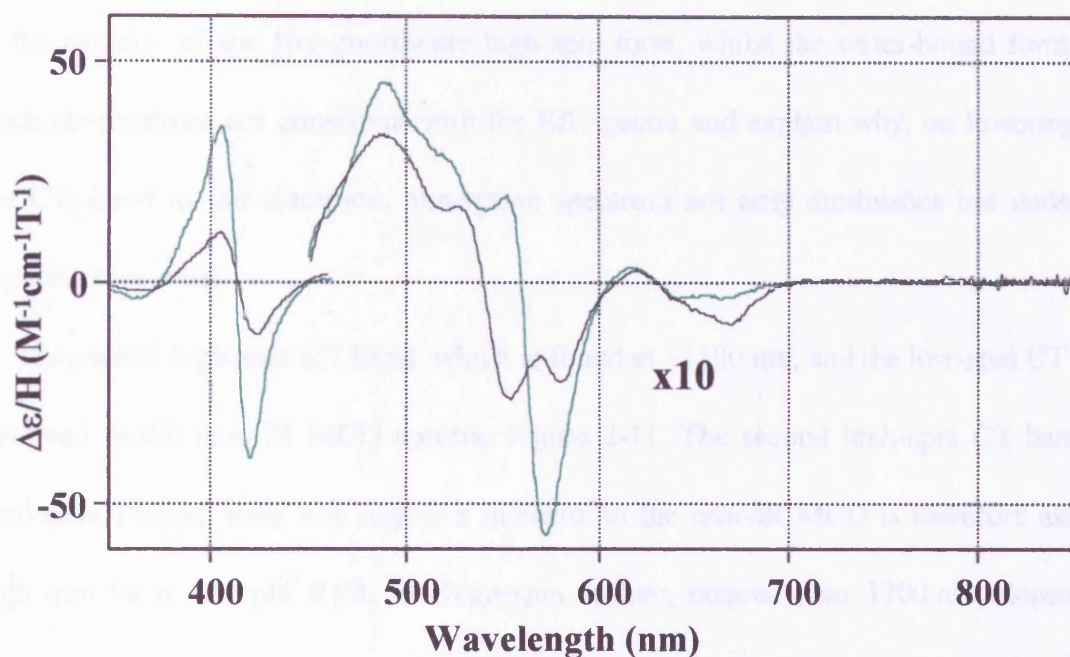
**Figure 3-10 Room temperature UV/visible MCD spectra of wild-type rAPX.** Samples in deuterated 50 mM NaPi pH* 5.62 (288 µM) and pH* 8.0 (313 µM), pH* uncorrected for the deuterium isotope effect, magnetic field of 6 T.

CT-derived troughs near 642 nm and 668 nm indicate that there are two high-spin forms of wild-type rAPX. The 668 nm feature is typical for a five-coordinate high-spin haem iron with histidine as the fifth ligand, as found for HRP or cytochrome c'.[14-16] The 642 nm band is characteristic of histidine-water ligation and is found for a range of met-myoglobins.[17] Furthermore, when the pH* is lowered the wild-type enzyme becomes low-spin it is primarily at the expense of the five-coordinate high-spin form, whilst the water-bound form persists. Such observations are consistent with the RR spectra and explain why, on lowering the pH, the $CT_1$-band in the electronic absorption spectrum not only diminishes but undergoes an apparent blue-shift.

The second high-spin CT band, which is found at ~1100 nm, and the low-spin CT band are observed in the near-IR MCD spectra, Figure 3-11. The second high-spin CT band is also derivative shaped; thus, any negative intensity in the near-IR MCD is therefore assigned to high-spin haem. At pH* 8.00, the high-spin feature, centred near 1200 nm, dominates the MCD spectrum and its wavelength confirms that the majority high-spin species, at this pH, is five-coordinate. The low-spin CT feature comprises a positive peak with a weaker vibrational sideband to higher energy and, at pH* 5.62, is observed at 1590 nm, a wavelength characteristic of coordination by two nitrogenous ligands.[10] The intensity of this band suggests that it is due to 50-60% of one haem, consistent with the UV-visible MCD spectra.

The pH-dependent UV/visible MCD spectra of variant H42A rAPX were obtained at room temperature, and the spectral features observed are essentially indistinguishable from those of the wild-type, Figure 3-12. Near-IR MCD spectra of variant H42A, at pH* 5.27, is characterised by the same 1590 nm band that was observed for wild-type rAPX and the signal intensity of the peak suggests that ~25% of the sample is low-spin at this pH, Figure 3-13. As
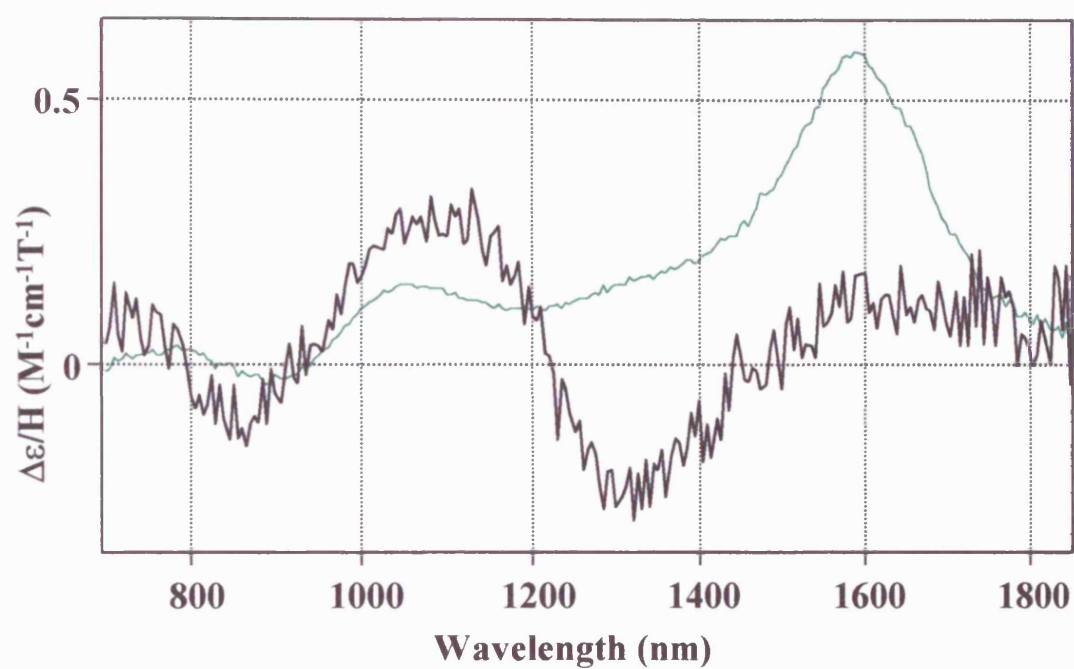
**Figure 3-11 Room temperature near-IR MCD spectra of wild-type rAPX.** Samples in deuterated 50 mM NaPi pH* 5.62 and pH* 8.0 (pH* uncorrected for the deuterium isotope effect), magnetic field of 6 T.
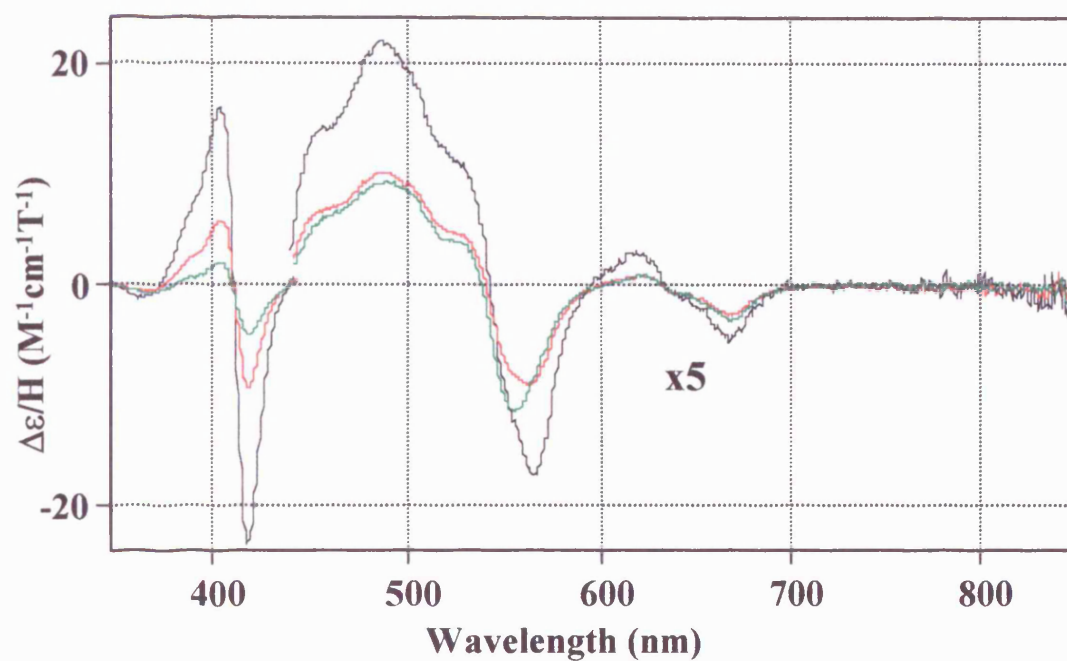
**Figure 3-12 Room temperature UV/visible MCD spectra of H42A.** Samples in deuterated 50 mM NaPi pH* 5.27, 5.68 & 8.0 (pH* uncorrected for the deuterium isotope effect).
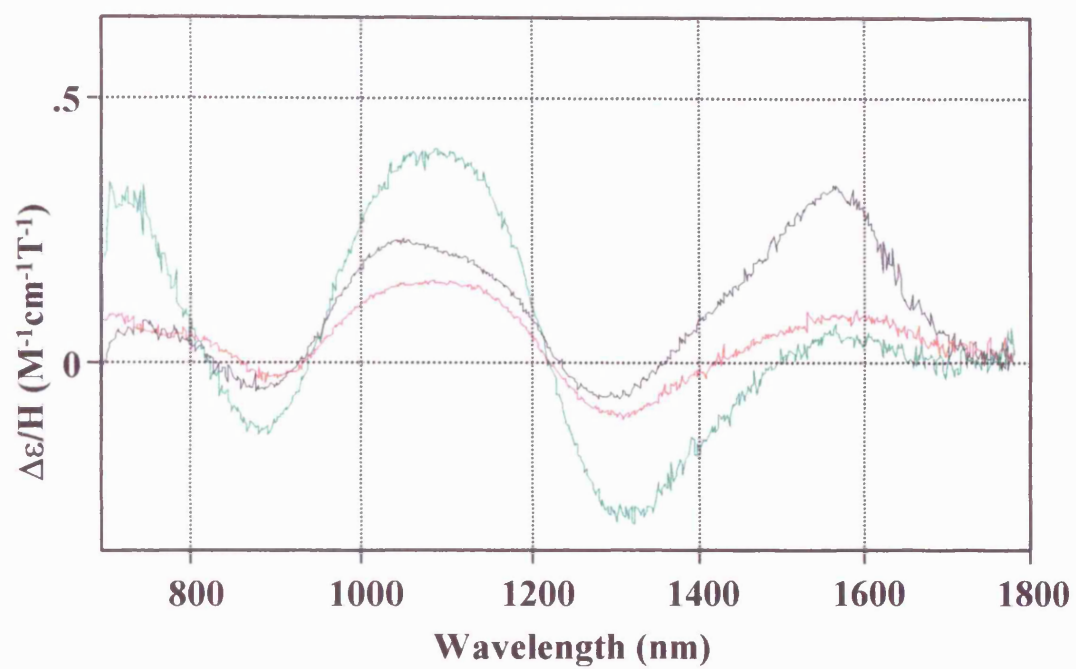
**Figure 3-13 Room temperature near-IR MCD spectra of H42A.** Samples in deuterated 50 mM NaPi pH* 5.27, 5.68 & 8.0 (pH* uncorrected for the deuterium isotope effect).

hitherto observed with all the spectroscopic methods employed, the $pK_a$ for the high to low-spin transition is lower for variant H42A than wild-type rAPX.

Comparison of the MCD spectra of variant H42A and wild-type rAPX supports the hypothesis that the high- to low-spin transition of both haemoproteins results in the same 'acidic form'. The 'acidic form' observed is consistent with a haem coordinated by two nitrogenous ligands, and assuming that the proximal histidine-iron bond remains intact, the sixth ligand is most probably a distal protein residue. Mutagenic replacement of the distal histidine has not precluded the formation of the 'acidic form', which suggests that this residue is not the nitrogenous donor ligand that coordinates to the haem-iron.

### 3.4.4 Electron paramagnetic resonance spectroscopy

Low temperature electron paramagnetic resonance spectra of wild-type rAPX were obtained at neutral and acidic pH in the presence and absence of glycerol, which was added to act as a glassing-agent, Figure 3-14. At pH* 8.00, in the absence of glycerol, the EPR spectrum is dominated by a rhombic trio with g-values of 2.65, 2.19 & 1.77; whilst a minority high-spin species gives rise to features near g = 6, the principal features are characteristic of a low-spin ferric haem with His/hydroxide coordination, Figure 3-14(A).[18] At pH* 5.62, simple axial EPR features are observed at g = 6.00 and g = 1.99 that are consistent with a six-coordinate high-spin haem that is coordinated by histidine and water, Figure 3-14(C). The low temperature EPR spectra indicate that wild-type rAPX undergoes dramatic changes in haem coordination and spin-state upon freezing in the absence of a glassing-agent, which is wholly consistent with the observations previously described by Patterson et al.[19]

In the presence of 50% glycerol, Figure 3-14(B&D), the freezing-induced changes are significantly reduced. At neutral pH, the majority species observed in the EPR spectrum is a
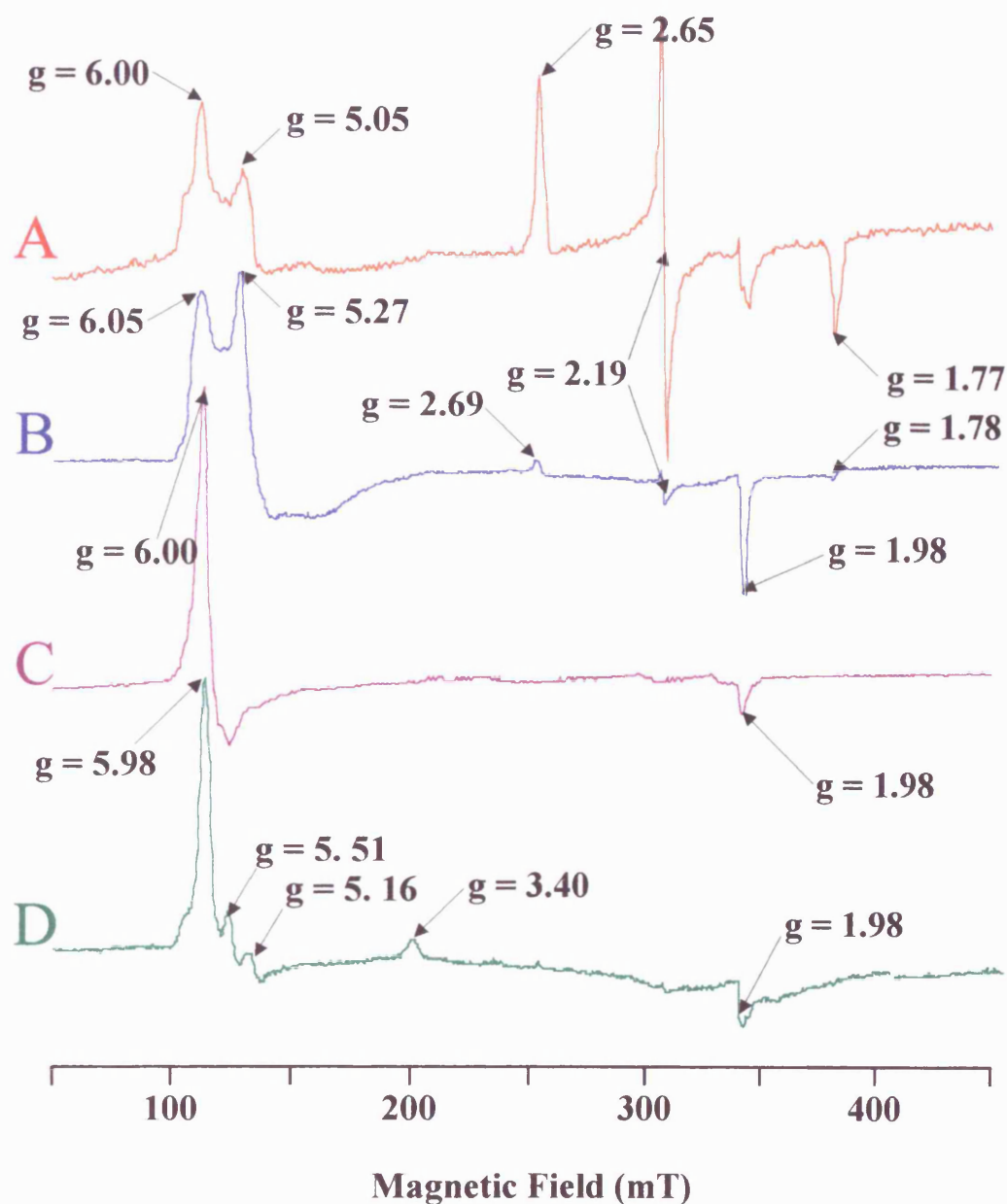
**Figure 3-14 Low temperature electron paramagnetic spectra of ferric wild-type rAPX in the presence and absence of glycerol.** Sample conditions: (A) pH* 8.0 without glycerol; (B) pH 7.0 in the presence of 50% glycerol; (C) pH* 5.2 without glycerol; and (D) pH 5.0 in the presence of 50% glycerol (full experimental conditions may be found in section 6.9).

rhombic high-spin haem with split features ($g = 6.05$, $5.27$), which is characteristic of the five-coordinate high-spin form that is observed at room temperature. In accordance with the interpretation of the MCD spectra, a minority amount of hydroxy-bound haem persists in the spectrum ($g = 2.69$, $2.21$ & $1.79$), Figure 3-14(B). At mildly acidic pH, the EPR spectra of wild-type rAPX, obtained in the presence of 50% glycerol, displays predominantly high-spin features that include a substantial rhombic component ($g = 5.98$, $5.51$ & $5.16$), Figure 3-14(D). Moreover, addition of a glassing-agent resolves a feature at $g = 3.40$, which is likely to correspond to the $g_z$-value of the room-temperature low-spin 'acidic form'.

## 3.5 Discussion

Within this section, the spectral similarities and differences displayed by wild-type rAPX and H42A will be discussed. The pH-dependent spectroscopic properties of both recombinant proteins have been investigated thoroughly using several independent spectroscopic techniques. Data collected at room-temperature supports the formation of a novel 'acidic' species at mildly acidic pH. The 'acidic form' is predominantly six-coordinate low-spin and yet still binds exogenous anionic ligands, albeit with considerably reduced binding-affinities (Table 2-2).

Semi-quantitative assessment of the nature of the endogenous ligand was sought using the diagnostic pairing of MCD and EPR. Identification of haemoprotein axial ligands using the combined application of magnetic circular dichroism and electron paramagnetic spectroscopies is facilitated by the fingerprint library that has been based upon analysis of haemoproteins of known ligation properties.[13] However, freezing-induced artifacts, which dominated the low-temperature EPR spectra of wild-type rAPX, rendered this approach ineffective at distinguishing the nature of the 'acidic form'. A novel near-IR MCD band is

reported and the limited diagnostic ability of this approach is discussed when low temperature

EPR proves anomalous. The consensus of the pH-dependent data supports ligation of the

ferric resting-state haem by either an anomalous hydroxide or the distal arginine residue

(Arg38) at low pH.

The mutagenic replacement of the distal histidine with alanine resulted in a recombinant

protein that was essentially inactive, which is consistent with the loss of the

peroxidase-conserved protein residue. Such a heavily diminished specific activity is

consistent with previously published work conducted by Erman *et al.* and Newmyer and Ortiz

de Montellano on distal histidine variants of CcP and HRP respectively.[4,20]

Exogenous imidazoles are capable of mimicking the action of the distal histidine residue,

and partial recovery of the peroxidase activity of HRP variant H42A was observed upon the

addition of imidazole.[20] However, imidazole-induced recovery of the peroxidase activity of

HRP variant H42A is competitively inhibited by formation of the inactive imidazole-bound

ternary complex at higher ligand concentrations. Alkylated derivatives of imidazole, which

readily diffuse into the distal haem pocket without binding to the haem-iron, were found to be

more effective distal histidine analogues than imidazole *per se.* H42A was partially

reactivated upon addition of exogenous imidazole. Consistent with previously reported work

conducted on the identical variant of recombinant HRP,[20] certain imidazole-derivatives were

found to be more effective mimics of the distal histidine than imidazole *per se* (Latesh Lad,

University of Leicester, unpublished data).

The electronic absorption spectrum of H42A is consistent with a five-coordinate high-spin

haem. Notwithstanding the increased equilibrium dissociation constant, the cyanide-bound

ternary complex of variant H42A is spectroscopically the same as that of wild-type rAPX.

The UV/visible spectra of the fluoride and azide-bound derivatives could not be obtained due

to irreversible protein precipitation. Therefore, whilst the enzymatic properties of the resting-state of the enzyme are significantly affected by the replacement of the distal histidine, the structure of the distal haem pocket appears to have remained largely unaltered.

Reversible formation of an 'acidic form' of rAPX was examined by conducting spectrophotometric pH titrations in a mixture of sulphonic acid buffers. The UV/visible spectral features of the 'acidic form' of wild-type rAPX ($\lambda_{max}$ = 410 nm, 525.5 nm, ~563[sh] nm & ~622[sh] nm) are comparable to those observed for the ferric enzyme in the presence of a non-saturating concentration of imidazole ($\lambda_{max}$ = 409 nm, 525 nm, ~566[sh] nm & ~635nm). The low-spin 'acidic form' was formed rapidly and reversibly in a variety of buffer solutions.

Replacement of the distal histidine residue did not prevent the pH-dependent formation of a six-coordinate low-spin species. The 'acidic form' of variant H42A was spectroscopically indistinguishable from that of wild-type rAPX. However, a slightly more acidic pH was required to fully form the low-spin species of H42A, which suggests that the distal histidine of wild-type rAPX interacts to some extent with the protein residue(s) associated with the pH-dependent changes.

Resonance Raman spectroscopy facilitated quantitative analysis of the pH-dependent properties of both wild-type rAPX and H42A. The room temperature RR spectra of wild type rAPX comprise of features derived from three different coordination and spin-state combinations that co-exist throughout the pH range 5-8: the five-coordinate high-spin species which predominates at pH 8, a small amount of six-coordinate high-spin haem persistent at all pHs examined, and the six-coordinate low-spin species that predominates at pH 5. The spectra obtained of wild-type rAPX at pH 8.0 are similar to that reported by Nissum *et al* for the same enzyme at pH 7.0.[8] Comparison of the marker bands assigned to the five-coordinate high-spin species yields an agreement of ± 1 cm$^{-1}$, with the exception of $\nu_{10}$ which is assigned to a value

4 cm$^{-1}$ higher than that published previously. The RR spectra obtained at low pH were comprised of mainly six-coordinate low-spin features that are consistent with low-spin marker bands reported previously, which were attributed to a small proportion of six-coordinate low-spin haem.[8]

Interestingly, close examination of RR spectra of different samples of wild type rAPX revealed that the amount of six-coordinate high-spin haem was rather variable and likely associated with prolonged storage and/or non-specific freezing effects. Similar artifacts associated with protein preparation and storage have been highlighted for CcP using RR spectroscopy.[18] In the case of rAPX, the corresponding spectral shifts observed in the UV/visible absorption spectra of 'aged' samples are probably due to an increase in the proportion of six-coordinate low-spin marker bands. Six-coordinate high-spin artifacts have also been reported following laser-induced sample degradation,[8] and were comparable to the features observed when studying 'aged' CcP.[18] Within isolated batches of wild-type rAPX, the presence of a variable amount of six-coordinate high-spin haem probably accounts for the subtle differences in the UV/visible spectra of the ferric resting-state that have been noted within the literature.[9] These effects were not studied in detail.

In agreement with the spectrophotometric pH titration data, variant H42A rAPX consistently displayed a greater proportion of five-coordinate high-spin marker bands than the wild-type enzyme at the same pH. Variant H42A rAPX retains the wild-type enzyme RR

marker bands across the pH range examined, which further supports the hypothesis that both wild-type and H42A generate the same six-coordinate low-spin species at low pH.

Unfortunately, electron paramagnetic resonance spectra for wild type rAPX were not consistent with the room temperature data. In fact, EPR diagnosis of haemoproteins in general, and peroxidases in particular, are complicated by freezing-induced artifacts and cryogenic data does not necessarily correlate with room temperature data obtained from other spectroscopic sources.[21-23] The freezing-induced spin-state changes observed at pH* 8.00 observed in this work are entirely consistent with those reported previously for wild-type rAPX.[19] In the absence of glycerol, hydroxide-bound haem is the dominant form of wild-type rAPX at neutral pH and cryogenic temperature, and this form has been similarly observed in RR spectra obtained at low temperature.[8] Evidence of hydroxide-bound haem is not observed at room-temperature using other forms of spectroscopy, which suggests that freezing-induced conformational distortions result in conditions favouring the formation and subsequent binding of hydroxide.[27] The haem contained within rAPX is sandwiched between the proximal and distal protein domains;[25] consequently, any freezing-induced conformational changes in the surrounding protein milieu may significantly perturb the encapsulated haem. Moreover, as discussed within Chapter 2, relocation of internal water molecules is likely to occur as the extensive hydrogen-bonding network relays the changing properties of the surrounding bulk solvent.

The EPR spectrum of the 'acidic form', which has not previously been published, clearly shows that this six-coordinate low-spin species is just as susceptible to freezing-induced artifacts as the five-coordinate high-spin resting-state.

Addition of glycerol alleviated but did not quench the freezing-induced artifacts within the EPR spectrum. At low pH, a diminutive low-spin feature at g = 3.40 appears to be all that persists of the authentic 'acidic form' EPR signal. Accordingly, whatever mechanism results in the formation of the hydroxide-bound haem (above), the low-spin EPR features of this hydroxide species do not correspond to those of the room temperature 'acidic form', although formation of hydroxide-bound haem appears to be partially prevented at low pH.

Analysis of MCD data provided more detailed insight into the nature of the pH-dependent equilibrium. Throughout the 450-600 nm region both high- and low-spin species contribute to the spectrum, with bands derived from the low-spin form being at least twice the intensity of the high-spin bands. Spectra obtained at neutral and mildly acidic pH differed solely in the relative proportions of the five-coordinate high-spin and six-coordinate low-spin components, with an increased proportion of the latter at low pH. The invariant amount of six-coordinate high-spin haem detected in the MCD spectra probably corresponds to an essentially unreactive proportion of 'aged' enzyme (also above), similar to that identified in a recent mechanism-based inactivation study.[26]

Variant H42A rAPX displays low-spin MCD spectroscopic features at low pH that are identical to the wild-type enzyme. Accordingly, bis-imidazole ligation involving the distal histidine is precluded as the origin of the 'acidic form' in H42A and, by implication, the wild-type enzyme. However, the low-spin 1590 nm band that was observed for both wild-type and variant H42A rAPX suggests that pH-dependent spectral changes, whilst not deriving from ligation of the distal histidine, are likely to be due to the coordination of another nitrogenous protein residue.[13] An alternative interpretation of the MCD data is that an anomalous hydroxide provides the sixth ligand,[27,28] although this would be counterintuitive at low pH. Examination of the distal pocket of rAPX indicates that Arg38 is the only residue

121

able to coordinate to the haem under these conditions and that this residue is likely to undergo a considerable pH-dependent conformational change associated with the drop in pH. Clearly, unambiguous confirmation of the structural changes and haem coordination alterations associated with formation of the acidic species requires crystallographic information, which is not available at this time as a result of the poor stability of the enzyme at low pH. Attempts to probe these changes in an alternative way, by site-specific replacement of Arg38, failed to generate samples of recombinant holoenzyme under any conditions and were, therefore, not pursued in this work.

The 'acidic form' of wild-type rAPX displays UV/visible and MCD features essentially identical to those of a $K^+$-binding site variant prepared and studied by Cheek et al.[3] Replacement of the amino acids that ligate to the potassium cation (Asp187, Thr164, Thr180, Asn182) resulted in a significant conformational change, which was characterised by the formation of a low-spin form of the enzyme with electronic and MCD properties similar to those observed for bis-histidine ligated haemoproteins (e.g. cytochrome $b_5$).[3] Unfortunately, near-IR MCD spectra were not reported by Cheek et al, which precludes further comparative assessment of the $K^+$-binding site variant with the acidic form of rAPX reported in this work. However, in the absence of an unambiguous assignment of the axial ligands in the $K^+$-binding site variant, these authors propose ligation of the distal histidine residue in the low spin form. However, in view of the essentially identical spectroscopic properties of the $K^+$-binding site variant[3] and the acidic forms of both wild type rAPX and H42A, we propose that ligation by histidine is unlikely and that the mechanism of formation of the low-spin species in all cases involves disruption of the hydrogen bonding network in the vicinity of the potassium binding site – by either removal of the metal ligands (for the $K^+$-binding site variant) or titration of the metal ligands (at low pH for rAPX and H42A) – followed by an associated conformational

122

change that results in coordination of an alternative nitrogenous donor, likely Arg38, to the haem.

It is clear, therefore, that the potassium cation plays an important role in maintaining both the native protein structure and the resting-state haem coordination environment of rAPX. Structural calcium ions are also important for both lignin and manganese peroxidases: thermal deactivation of lignin and manganese peroxidase involves release of calcium and formation of six-coordinate low-spin species that are spectroscopically similar to the 'acidic form' of rAPX.[29,30] A number of other peroxidases display pH-dependent changes in the haem-iron ligation state. Barley peroxidase is inactive above pH 5.0,[31] cytochrome $c$ peroxidase displays an 'alkaline form' at high pH,[32] and horseradish peroxidase similarly displays a well-defined alkaline transition.[33] However, the transition observed for both wild-type rAPX and H42A is not akin to any reported previously for a haem-containing enzyme.

## 3.6 Conclusions

Conclusions that can be drawn from the results presented in this chapter are as follows:

- A novel 'acidic form' of wild-type rAPX was observed and characterised using a variety of complementary spectroscopic techniques.

- Six-coordinate low-spin features associated with the 'acidic form' were consistent with those reported previously for comparable species.

- Mutagenic replacement of the distal histidine with alanine results in an essentially inactivated variant (H42A), which is spectroscopically similar to wild-type rAPX.

- Comparison of wild-type rAPX and H42A data confirms that the pH-dependent high-to-low-spin transition is only slightly perturbed by mutagenic replacement of the distal histidine residue.

- Analysis of the room temperature spectroscopic data of wild-type rAPX and H42A supports the formation of a bis-nitrogenous ligated low-spin haem at low pH.

- Freezing-induced artifacts that are only partially alleviated by the presence of a glassing-agent complicate low temperature EPR spectra.

- The wild-type rAPX and H42A 'acidic form' near-IR MCD spectra contain a low-spin feature at 1590 nm that we tentatively assign to coordination by the proximal histidine and the distal arginine at low pH.

- Comparison of the 'acidic form' of wild-type rAPX and H42A data with that previously published on the $K^+$-binding site variant (Cheek *et al*) substantiates the hypothesis: at low pH, the hydrogen bonding network in the vicinity of the potassium binding site is disrupted and causes an associated conformational change that results in coordination of a nitrogenous donor, likely Arg38, to the haem-iron.

## 3.7 References

1 Mandelman, D., Schwartz, F. P., Li, H. and Poulos, T. L. (1998) *Protein Science*, 7, 2089-2098

2 Mandelman, D., Jamal, J. and Poulos, T. L. (1998) *Biochemistry*, 37, 17610-17617

3 Cheek, J., Mandelman, D., Poulos, T. L. and Dawson, J. H. (1999) *J. Biol. Inorg. Chem.*, 4, 64-72

4 Newmyer, S. L. and Ortiz de Montellano, P. R. (1996) *J. Biol. Chem.*, 271, 14891-14896

5 Lad, L. and Raven, E. L. Unpublished data.

6 Mittler, R. and Zilinskas, B. A. (1991) *Plant. Physiol.*, 97, 962-968

7 Morishima, I., Ogawam, S., Inubushi, T., Yonezawa, T and Iizuka, T. (1977) *Biochemistry*, 16, 5109-5115

8 Nissum, M., Neri, F., Mandelman, D, Poulos, T. L. and Smulevich, G. (1998) *Biochemistry*, 37, 8080-8087

9 Hiner, A. N. P., Martínez, J. I., Arnao, M. B., Acosta, M., Turner, D. D., Raven, E. and Rodríguez-López, J. N. (submitted for publication)

10 Cheesman, M.R., Greenwood, C. and Thomson, A.J. (1991) *Adv. Inorg. Chem.*, 36, 201-255

11 Braterman, P.S., Davies, R.C. and Williams, R.J.P. (1964) *Adv. Chem. Phys.*, 7, 359-407

12 Cheng, J.C., Osborne, G.A., Stephens, P.J. and Eaton, W.A. (1973) *Nature*, 241, 193-194

13 Cheesman, M.R., Watmough, N.J., Gennis, R.B., Greenwood, C., and Thomson, A.J. (1994) *Eur. J. Biochem.*, 219, 595-602

14 Nozawa, T., Kobayashi, N. and Hatano, M. (1976) *Biochim. Biophys. Acta*, 427, 652-662

15 Kobayashi, N., Nozawa, T. and Hatano, M. (1977) *Biochim. Biophys. Acta*, 493, 340-351

16 Bracete, A.M., Sono, M. and Dawson, J.H. (1991) *Biochim. Biophys. Acta*, 1080, 264-270

17 Matsuoka, A., Kobayashi, N. and Shikama, K. (1992) *Eur. J. Biochem.*, 210, 337-34

18 Yonetani, T. and Anni, H. (1987) *J. Biol. Chem.*, 262, 9547-9554

19 Patterson, W. R., Poulos, T. L. and Goodin, D. B. (1995) *Biochemistry*, 34, 4342-4345

20 Erman, J. E., Vitello, L. B., Miller, M. A., Shaw, A., Brown, K. A. and Kraut, J. (1993) *Biochemistry*, 32, 9798-9806

21 Ferrer, J. C., Turano, P., Banci, L., Bertini, I., Morris, I. K., Smith, K. M., Smith, M. and Mauk, A. G. (1994) *Biochemistry*, 33, 7819-7829

22 Turano, P., Ferrer, J. C., Cheesman, M. R., Thomson, A. J., Banci, L., Bertini, I. and Mauk, A. G. (1995) *Biochemistry*, **34**, 13895-13905

23 Bujons, J., Dikiy, A., Ferrer, J. C., Banci, L. and Mauk, A. G. (1997) *Eur. J. Biochem.*, **243**, 72-84

24 Smulevich, G., Mantini, A. R., English, A. M. and Mauro, J. (1989) *Biochemistry*, **28**, 5058-5064

25 Patterson, W. R. and Poulos, T. L. (1995) *Biochemistry*, **34**, 4331-4341

26 Hiner, A. N. P., Rodríguez-López, J. N., Arnao, M. A., Lloyd Raven, E., García-Cánovas, F. and Acosta, M. (2000) *Biochem. J.*, **348**, 321-328

27 Cheesman, M. R. Personal communication

28 Gadsby, P.M.A. and Thomson, A.J. (1990) *J. Am. Chem. Soc.*, **112**, 5003-5011

29 Nie, G. and Aust, S. D. (1997) *Biochemistry*, **36**, 5113-5119

30 Sutherland, G. R. J., Zapanta, L. S., Tien, M. and Aust, S. D. (1997) **36**, 3654-3662

31 Ramussen, C. B., Bakovic, M., Welinder, K. G. and Dunford, H. B. (1993) *FEBS Letters*, **321**, 102-105

32 Dunford, H. B. (1999) *Heme Peroxidases*, Wiley-VCH, New York, Chichester, Weinheim, Brisbane, Singapore, Toronto. [pp220-223]

33 Feis, A., Marzocchi, M. P., Paoli, M. and Smulevich, G. (1994) *Biochemistry*, **33**, 4577-4583

# CHAPTER FOUR

# SUBSTRATE BINDING IN APX: THE ROLE OF ALA134

# 4 Substrate Binding In APX: The Role Of Ala134

As discussed within Chapter 1, enzymes that comprise the plant peroxidase superfamily display considerably diverse catalytic and substrate binding properties, which essentially reflect the different roles that these ubiquitous enzymes fulfil within nature. Probing the role of substrate binding and interaction sites in overcoming thermodynamic barriers to catalytic reactions is an important area in present peroxidase research, and considerable effort has been directed towards determining the structural basis of interactions between peroxidases and small molecules. Until recently, however, the only crystallographic data for substrate-bound peroxidase complexes was limited to CcP-cytochrome $c$ and MnP-Mn$^{2+}$,[1,2] which were considered too atypical to be utilised as general structural models for other peroxidase-substrate interactions.

New insights into substrate binding and catalysis in haem peroxidases have been obtained through site-directed mutagenesis, a technique that is crucial in furthering our appreciation of the diversity of substrate-binding sites associated with peroxidases from different sources. A recently published review paper summarised some of the advances that have been made in elucidating the underlying structural factors that control peroxidase-catalysed reactions.[3] Complementary investigations have been concerned with engineering novel properties into peroxidases.[4-10] Ultimately, this approach aims to result in 'designer peroxidases' that are tailored for particular applications.

The ascorbate-binding site of recombinant pea cytosolic ascorbate peroxidase has been probed using conventional spectroscopic and chemical modification methods.[11] Derived from $^1$H-NMR paramagnetic relaxation times, substrate proton to haem iron distance constraints were applied to a molecular model that revealed two spatially distinct binding sites, one close

to the 6-propionate group of the haem (γ-meso position) and one close to the C20 carbon

(δ-meso position) of the haem, as shown in Figure 4-1. From the consensus of two

computer-based enzyme active site searches, and consistent with

phenylhydrazine-modification experiments, the ascorbate-binding site in the vicinity of the

haem C20 carbon was preferred. In particular, an alanine residue at position 134 in wild-type

rAPX was highlighted, as shown in Figure 4-2, since the corresponding residue in MnP, LiP,

ARP and PnP is proline. This was suggestive of a possible functional role for this residue in

the general control of peroxidase function, and specifically in the control of ascorbate

oxidation and haem accessibility in rAPX.[11]

Whilst the role of Ala134 was being investigated in our laboratory, additional information

on the nature of the ascorbate-binding site of rAPX was reported independently by

Mandelman et al.[12] Site-specific replacement, by serine, or chemical modification of Cys32

was found to decrease the activity of rAPX against ascorbate by ≈3-fold and ≈1000-fold,

respectively, indicative of an ascorbate interaction in the vicinity of the haem propionates near

to this residue, i.e. analogous to the γ-meso binding site identified by Hill et al. Furthermore,

Mandelman et al reported that oxidation of guaiacol, a classical aromatic substrate, was found

to be unaffected by either replacement or modification of Cys32. Accordingly, the authors

proposed that aromatic substrates probably interact with rAPX at an alternative location,

distinct from that identified for ascorbate, possibly situated close to the exposed δ-meso haem

edge, as implicated by the phenylhydrazine modification experiments (conducted by Hill et

al) that revealed that δ-meso-modified haem is the dominant product.

Hence, the aim of the work presented in this chapter was the assessment of the effect of

replacing Ala134 in wild-type rAPX with proline on the binding and catalytic oxidation of
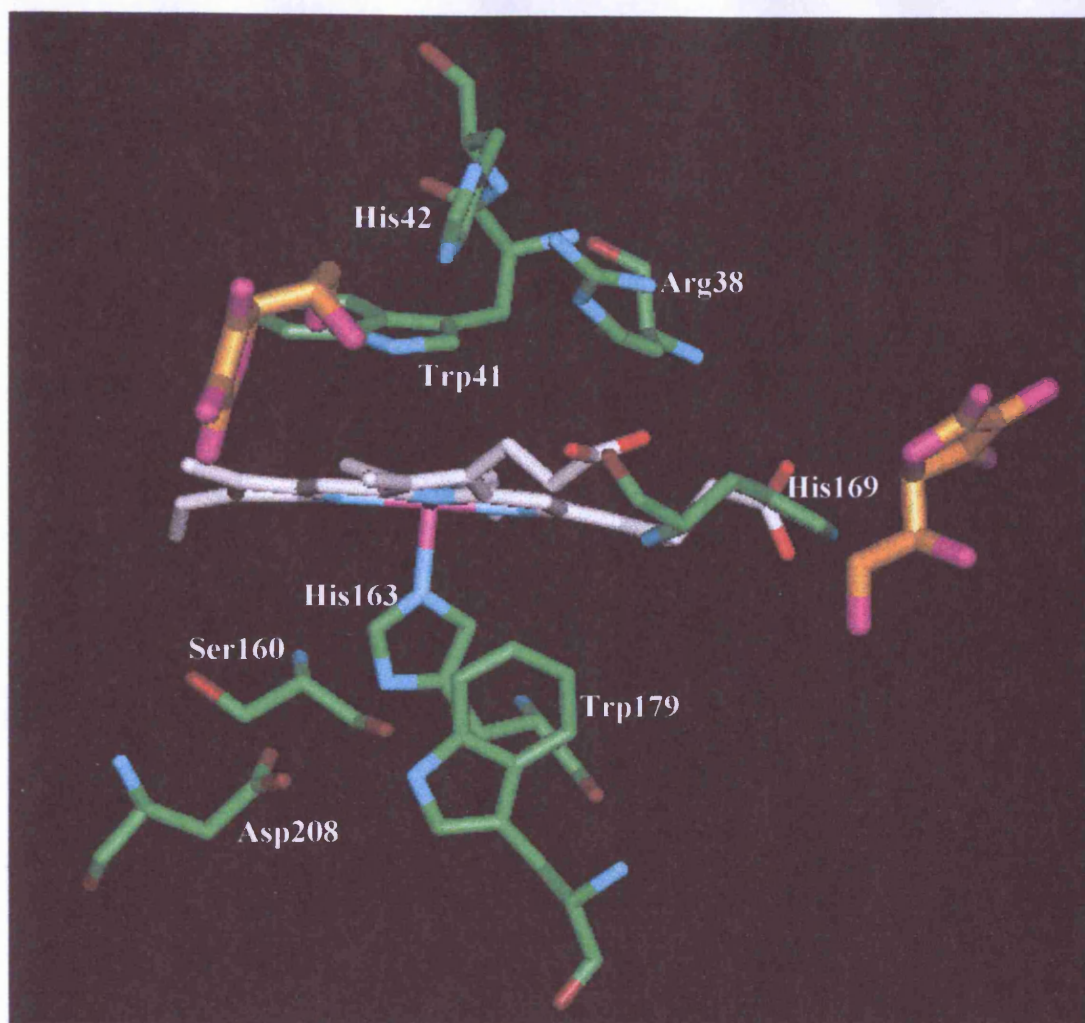
**Figure 4-1 Location of the two proposed ascorbate-binding sites on wild-type rAPX.** Computer-based molecular modelling has identified two potential ascorbate-binding sites, based upon NMR-derived ascorbate-iron distance constraints and the published protein crystal structure coordinates [Patterson, W. R. and Poulos, T. L. (1995) *Biochemistry*, **34**, 4331-4341]. The ascorbate molecules in the proposed binding locations are shown in orange, the haem in silver and the proximal and distal amino acid residues in green. [Reproduced with permission from Hill, A. P., Modi, S., Sutcliffe, M. J., Turner, D. D., Gilfoyle, D. J., Smith, A. T., Tam, B. M. and Lloyd, E. (1997) *Eur. J. Biochem.*, **248**, 347-354.]

δ–meso
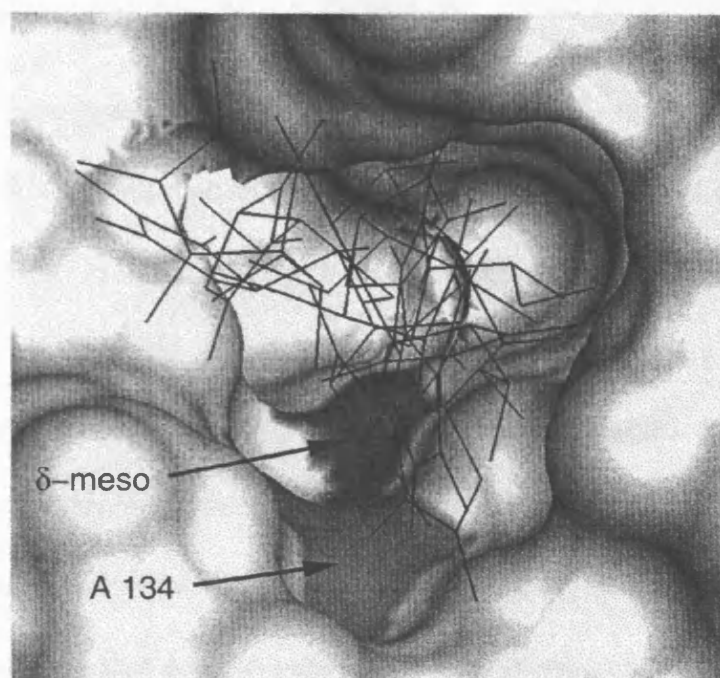
A 134

**Figure 4-2 Proposed ascorbate-binding site in ascorbate peroxidase.** The protein surface around the ascorbate-binding site: the positions of the ascorbate molecules from the 11 final models are denoted by lines, and the positions of Ala134 and the C20 of the haem are shown in light and dark grey, respectively. [Reproduced with permission from Hill, A. P., Modi, S., Sutcliffe, M. J., Turner, D. D., Gilfoyle, D. J., Smith, A. T., Tam, B. M. and Lloyd, E. (1997) *Eur. J. Biochem.*, **248**, 347-354.]

ascorbate and guaiacol. The altered peroxidase activity of A134P is discussed with reference to haem edge accessibility and the potential role of the residue in position 134 in aromatic substrate recognition.

## 4.1 Preparation and isolation of variant A134P

Site-directed mutagenesis was performed, according to the QuikChange™ protocol (Stratagene), using the wild-type APX-encoding pMAL-c2 vector and the A134P mutagenic oligonucleotides (Perkin Elmer, see Appendix A). Sequencing across the whole APX-coding gene confirmed the presence of the required codon and that the gene was free of any deleterious mutations. No subsequent alterations to the wild-type enzyme protocol were required to successfully isolate A134P in moderate yields and of acceptably high purity $(R_Z \geq 1.7)$. As discussed within Chapter 6, the protocol for isolating variants of rAPX was essentially the same as that used to purify the wild-type recombinant enzyme (section 6.1). Throughout the isolation and purification steps, A134P displayed no dramatic differences in stability or spectroscopic properties from those noted for the wild-type enzyme.

## Results

## 4.2 Characterisation of A134P

The integrity of the isolated A134P was investigated through a series of UV/Visible spectroscopic experiments, which were conducted in an identical manner to those used to characterise wild-type rAPX. This section summarises the electronic absorption spectra and chemical modification data that were obtained for A134P.

## 4.2.1   Pyridine haemochromagen assay

An absorption coefficient of $\varepsilon_{404} = 92 \pm 3$ mM$^{-1}$cm$^{-1}$ was obtained for A134P and was used to calculate the haem-based protein concentrations reported throughout this thesis. Electronic absorption spectra of wild-type rAPX, and the H42A and A134P variants are overlaid in Figure 4-3. At neutral pH, the Soret band maximum of A134P (404 nm) is perceptibly red-shifted by 1 nm relative to that observed for the wild-type enzyme (403 nm), and suggests that replacement of the proline residue with alanine has influenced the coordination geometry of the haem moiety. Comparison of the near-UV region of the electronic absorption spectra of the recombinant proteins provides evidence supporting the premise that isolated A134P probably contains a significant but indeterminate proportion of apo-protein.

## 4.2.2   Anionic ligand-binding equilibria

As discussed within Chapter 3, spectroscopic investigation of ligand-binding equilibria of rAPX variants provides an expedient method of semi-quantitatively assessing active-site integrity of the recombinant haemoprotein. Spectrophotometric ligand-binding titrations reveal that replacement of Ala134 with proline does not affect the equilibrium dissociation constants calculated for cyanide, fluoride or azide; the $K_d$s obtained for these anionic ligands with A134P are compiled within Table 4-1. Moreover, the UV/visible absorption spectra of the resulting ligand-bound ternary complexes of A134P, overlaid in Figure 4-4, are analogous to the equivalent wild-type rAPX species ($\lambda_{max}$ are compared in Table 4-2), which is wholly
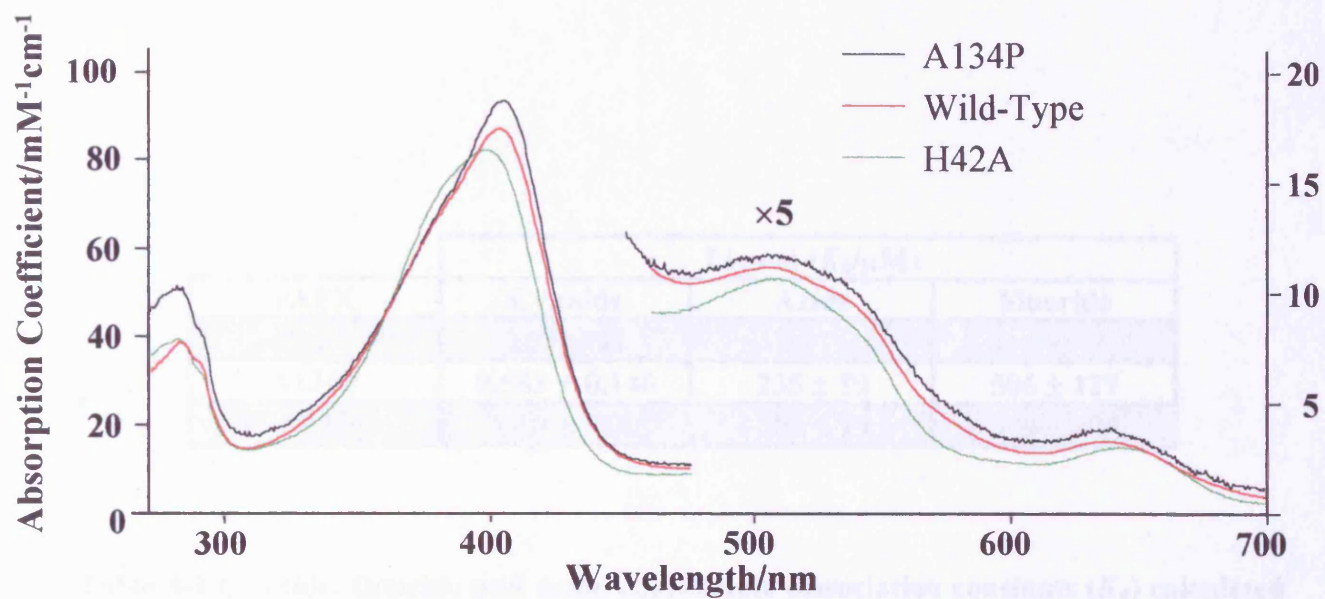
**Figure 4-3 Comparison of the UV-visible absorption spectra of wild-type rAPX, H42A and A134P ferric resting-states.** Normalisation has been made with respect to the calculated millimolar absorption coefficient; the region 450-700 nm has been multiplied by a factor of five. Sample conditions: ~1 µM rAPX, 25°C, NaPi pH 7.0, µ = 0.1 M.

| rAPX | Ligand ($K_d/\mu M$) | | |
|------|---------|-------|----------|
|      | Cyanide | Azide | Fluoride |
| H42A | 160 ± 40 | - | - |
| A134P | 0.583 ± 0.146 | 235 ± 59 | 506 ± 127 |
| Wild-Type | 1.18 ± 0.30 | 300 ± 75 | 800 ± 200 |

Table 4-1 Cyanide, fluoride and azide equilibrium dissociation constants ($K_d$) calculated for wild-type rAPX, H42A and A134P. Spectrophotometric titrations were conducted at 25.0°C in sodium phosphate buffer (pH 7.0, $\mu$ = 0.1 M). The estimated error of these determinations is ± 25 %.

135
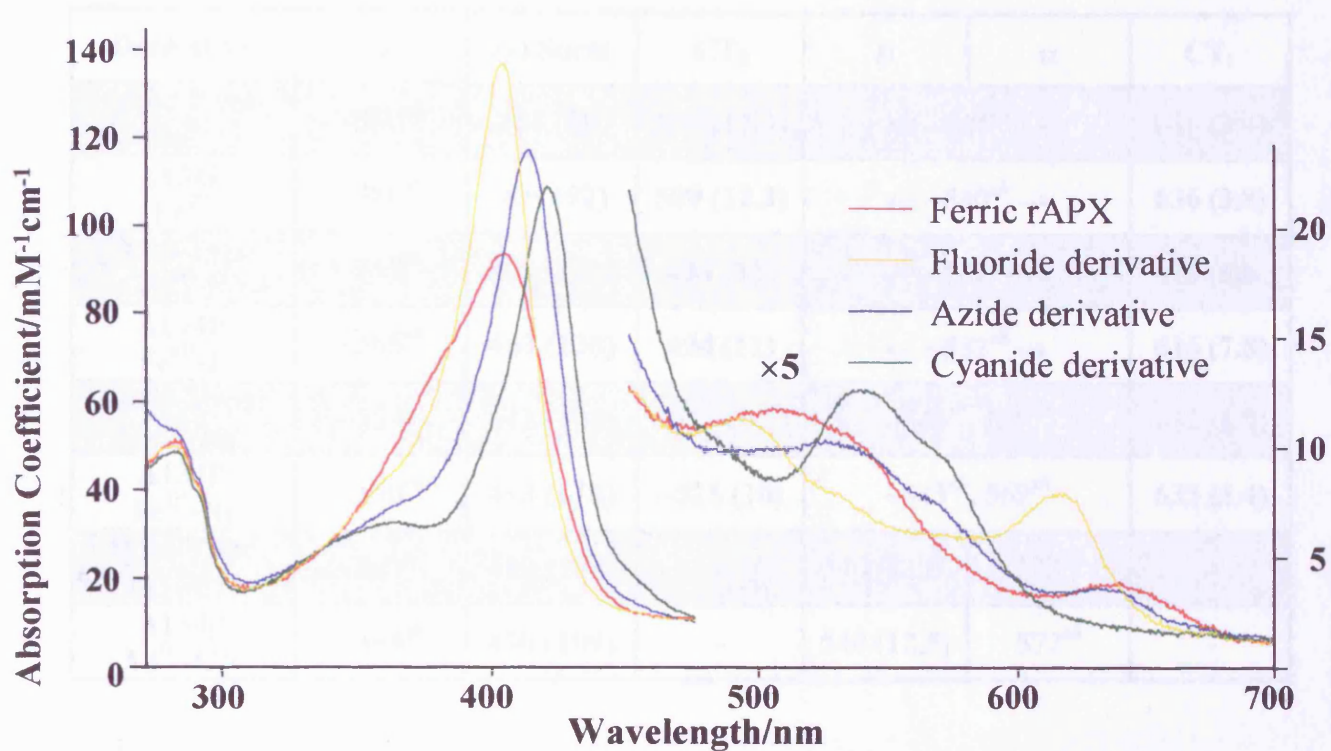
**Figure 4-4 Ferric A134P ligand-bound derivative spectra.** Normalisation has been made with respect to the calculated millimolar absorption coefficient; the region 450-700 nm has been multiplied by a factor of five. Sample conditions: ~1.3 µM A134P, 25°C, NaPi pH 7.0, µ = 0.1 M.

136

| Derivative | δ | (γ) Soret | CT$_2$ | β | α | CT$_1$ |
|---|---|---|---|---|---|---|
| Wild-Type Fe$^{III}$ | ~380$^{sh}$ | 403 (88) | 506 (11.3) | ← ~540$^{sh}$ → | | 636 (3.4) |
| A134P Fe$^{III}$ | ~380$^{sh}$ | 404 (92) | 500 (12.3) | ← ~540$^{sh}$ → | | 636 (3.8) |
| Wild-Type Fe$^{III}$-F | ~365$^{sh}$ | 403 (111) | 494 (10) | ← ~532$^{sh}$ → | | 616 (5.8) |
| A134P Fe$^{III}$-F | ~365$^{sh}$ | 403 (138) | 494 (11) | ← ~532$^{sh}$ → | | 616 (7.8) |
| Wild-Type Fe$^{III}$-N$_3$ | ~360$^{sh}$ | 412 (106) | ~525 (9.7) | ~543$^{sh}$, 569$^{sh}$ | | 633 (2.9) |
| A134P Fe$^{III}$-N$_3$ | ~360$^{sh}$ | 413 (118) | ~525 (10) | ~543$^{sh}$, 569$^{sh}$ | | 633 (3.4) |
| Wild-Type Fe$^{III}$-CN | ~363$^{sh}$ | 419 (104) | - | 540 (12.0) | 572$^{sh}$ | - |
| A134P Fe$^{III}$-CN | ~363$^{sh}$ | 420 (109) | - | 540 (12.5) | 572$^{sh}$ | - |

Table 4-2 The spectroscopic features of the ferric resting-states and ligand-bound ternary complexes of A134P and wild-type rAPX. Millimolar absorption coefficients for resolved peaks are noted in parentheses, "$^{sh}$"denotes unresolved shoulder. All spectra were obtained at 25.0°C, pH 7.0 NaPi μ= 0.10 M.

consistent with the replacement of a residue that is spatially separated from the haem-iron, and that is not directly involved in ligand-binding.

### 4.2.3 Phenylhydrazine modification

Phenylhydrazine modification of wild-type rAPX results in a larger proportion of C20-phenyl haem than control incubations of HRP (see Figure 4-5 for the structure and nomenclature of ferriprotoporphyrin IX used in this chapter).[11] This data was consistent with greater access and/or retention of the phenyl radical in the vicinity of the δ-meso haem edge of wild-type rAPX than that afforded by HRP. As the replacement of Ala134 with proline was conducted in an attempt to occlude the exposed haem edge, verification of the extent of haem access retained by the variant was sought using chemical modification.

Haem-derived components isolated from phenylhydrazine-modified A134P, HRP and wild-type rAPX were analysed, under the supervision of Mr G. A. Lord, in collaboration with Dr J. L. Luo and Dr C. K. Lim (Centre for Mechanisms in Human Toxicity, Leicester University). The enzymes (25 μM, 250 μl) were turned over in the presence of the suicide substrate (0.6 mM), and the three separate mixtures of haem derivatives were extracted, isolated and analysed by reverse-phase HPLC.

Preliminary experiments revealed no significant differences between the product distributions isolated from modified A134P and wild-type rAPX (data not shown). However, observation that the sequence of colour changes – indicative of conversion of the enzyme from the ferric resting-state to Compound II and back again – occurred more rapidly for A134P than wild-type rAPX suggested that, whilst the extent of haem modification may be essentially unchanged, the rate of chemical modification was moderately enhanced for the
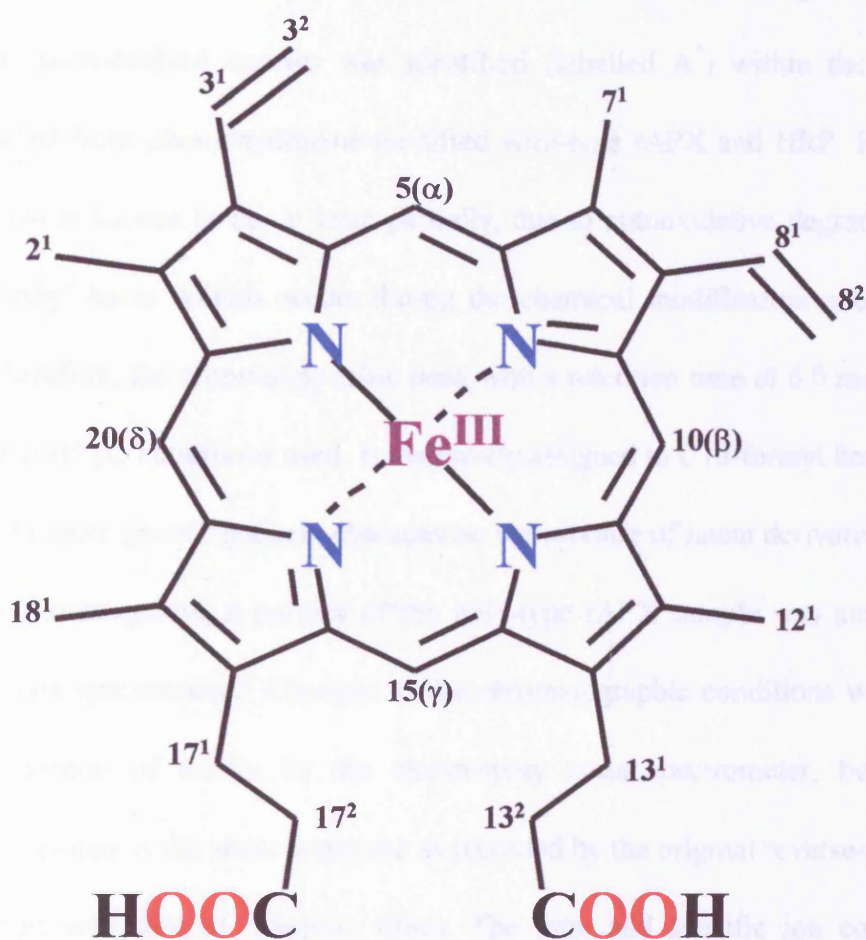
**Figure 4-5 Structure and nomenclature of ferriprotoporphyrin IX.** Proton-bearing carbon atoms are numbered according to the IUB/IUPAC system with Fischer notation in parentheses.

variant. Overlaid in Figure 4-6 are the HPLC traces of the haem-derived components extracted from samples treated for just 1½ minutes.

As well as the C18-hydroxymethyl and C20-phenyl haem derivatives (Figure 4-6, peaks A & C), another haem-derived species was identified (labelled A*) within the mixture of products extracted from phenylhydrazine-modified wild-type rAPX and HRP. Formation of C18-formyl haem is known to be, at least partially, due to autooxidative degradation of the C18-hydroxymethyl haem, which occurs during the chemical modification and/or isolation procedure.[13] Therefore, the chromatographic peak with a retention time of 6.0 minutes, under the reverse-phase HPLC conditions used, is tentatively assigned to C18-formyl haem.

In an effort to more unambiguously characterise the mixture of haem derivatives observed in the HPLC chromatograms, a portion of the wild-type rAPX sample was analysed using HPLC-linked mass spectrometry. Changes to the chromatographic conditions were required for optimal detection of hemin by the electrospray mass spectrometer, but the haem derivatives were eluted in the same sequence as recorded by the original reverse-phase HPLC conditions, albeit with altered retention times. The total and specific ion concentrations detected throughout the elution profile are shown in Figure 4-7.

## 4.3    Transient and steady-state kinetic analysis of A134P

Spectroscopic and kinetic properties of native pea cytosolic ascorbate peroxidase, isolated from young pea shoots,[14] have been investigated in detail using the physiological substrates: hydrogen peroxide and ascorbate.[15] The availability of preliminary transient and steady-state kinetic data for the native enzyme facilitates direct assessment of the catalytic integrity of wild-type rAPX and A134P.
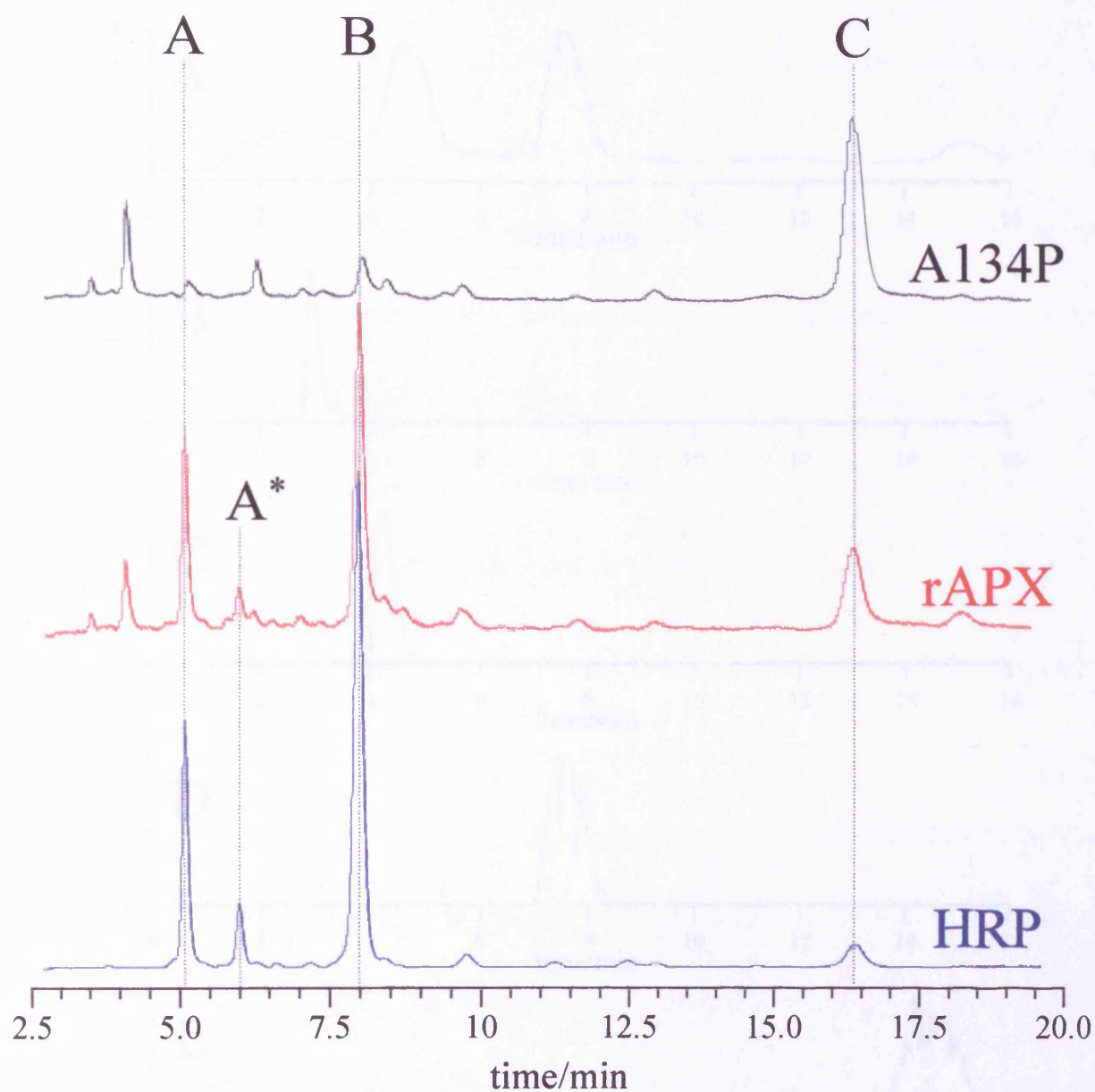
**Figure 4-6 Reverse-phase HPLC traces of haem-derived products.** Separation of the mixture of metalloporphyrins extracted from phenylhydrazine-modified HRP, A134P and wild-type rAPX was conducted as described in Chapter 6, section 6.13. The haem adducts were detected by monitoring the absorbance at 400 nm, and the major products identified through comparison with that known for HRP: (A) C18-hydroxymethyl, (A*)C18-formyl, (B) unmodified haem and (C) C20-phenyl.
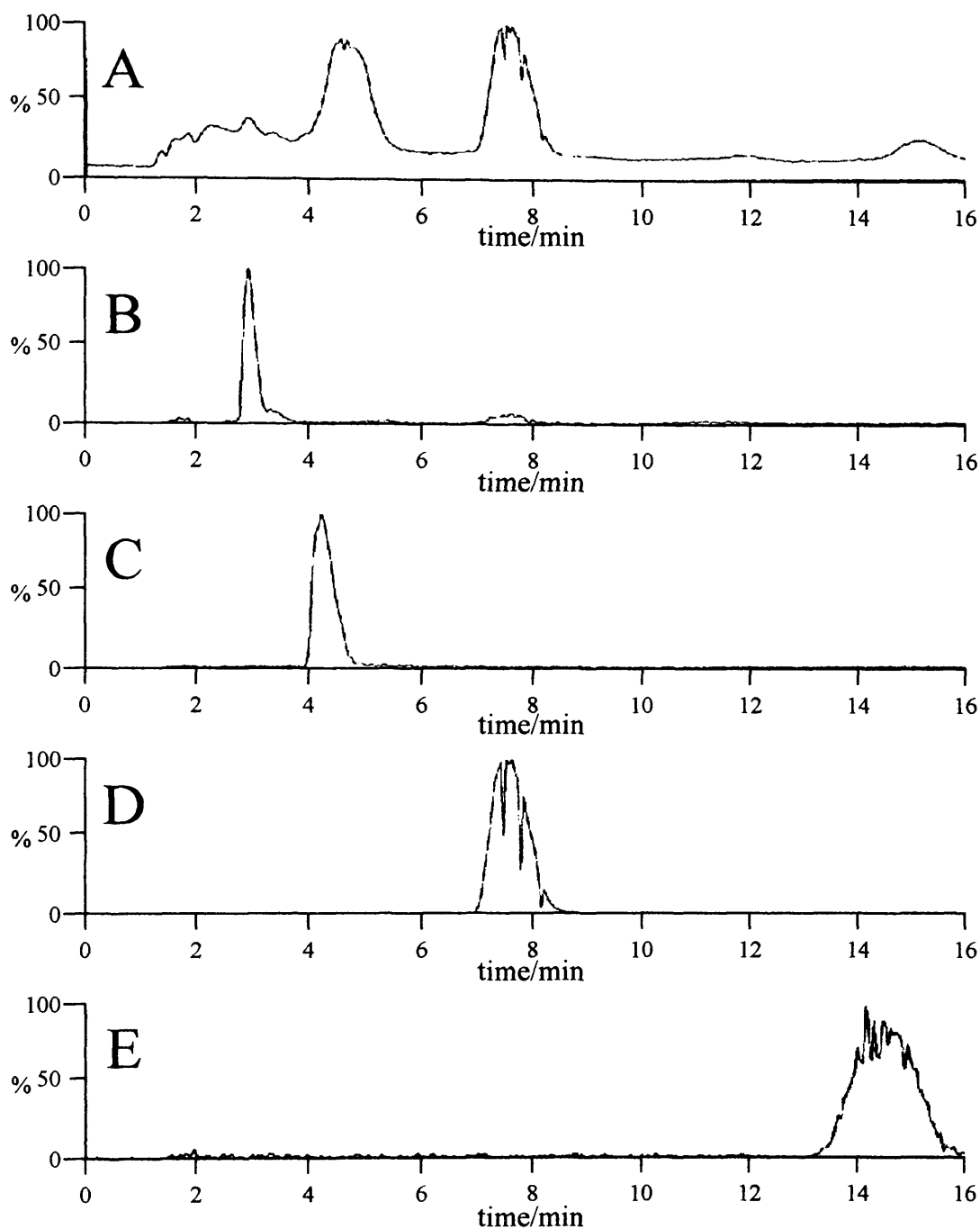
**Figure 4-7 HPLC-linked electrospray mass spectrometry.** Haem adducts extracted from a sample of phenylhydrazine-modified A134P were applied to a C-18 reverse-phase HPLC column, and the elution front was analysed by electrospray mass spectrometry. Chromatograms represent the total and specific ion concentrations detected: (A) total ion concentration; (B) C18-hydroxymethyl; (C) unmodified haem; (D) C20-phenyl; and (E) protoporphyrin IX, *i.e.* iron-free haem.

142

## 4.3.1 Transient-state kinetics

Acquisition of wild-type rAPX and A134P transient-state kinetic data was conducted, in collaboration with Mr Latesh Lad (Department of Chemistry, Leicester University), using a SX.18 MV microvolume stopped-flow spectrofluorimeter (Applied Photophysics), section 6.12. Single wavelength transients were obtained at or near an appropriate isosbestic point previously identified in photodiode array spectra, Figure 4-8: for example Compound II formation was monitored at 407 nm, an isosbestic point between ferric and Compound II. All transient-state kinetic measurements were conducted in pH 7 NaPi at 5°C.

Using the single-mixing mode, the second-order rate constants for Compound I formation, $k_1$, for wild-type rAPX and A134P were obtained from plots of the observed pseudo-first-order rate constants, $k_{1,obs}$, against hydrogen peroxide concentration, $[H_2O_2]$, (Figure 4-9). The rates calculated for wild-type rAPX and A134P, $(6.36 \pm 0.19) \times 10^7 \ M^{-1}s^{-1}$ and $(5.10 \pm 0.28) \times 10^7 \ M^{-1}s^{-1}$, respectively, are comparable to that reported for the native enzyme, $8.0 \times 10^7 \ M^{-1}s^{-1}$ (pH 7.8 NaPi at 20°C).[15] Nominal intercepts of $17.0 \pm 16.1 \ s^{-1}$ and $31.4 \pm 18.8 \ s^{-1}$ were calculated from the linear least-squares fit of the $k_1$ plots of A134P and wild-type rAPX, respectively.

An equally fast rate second-order constant has been measured for the reaction between Compound I of the native enzyme and L-ascorbate, $8.0 \times 10^7 \ M^{-1}s^{-1}$.[15] Sequential-mixing mode was employed to study the reaction between Compound I and ascorbate, which leads to

143
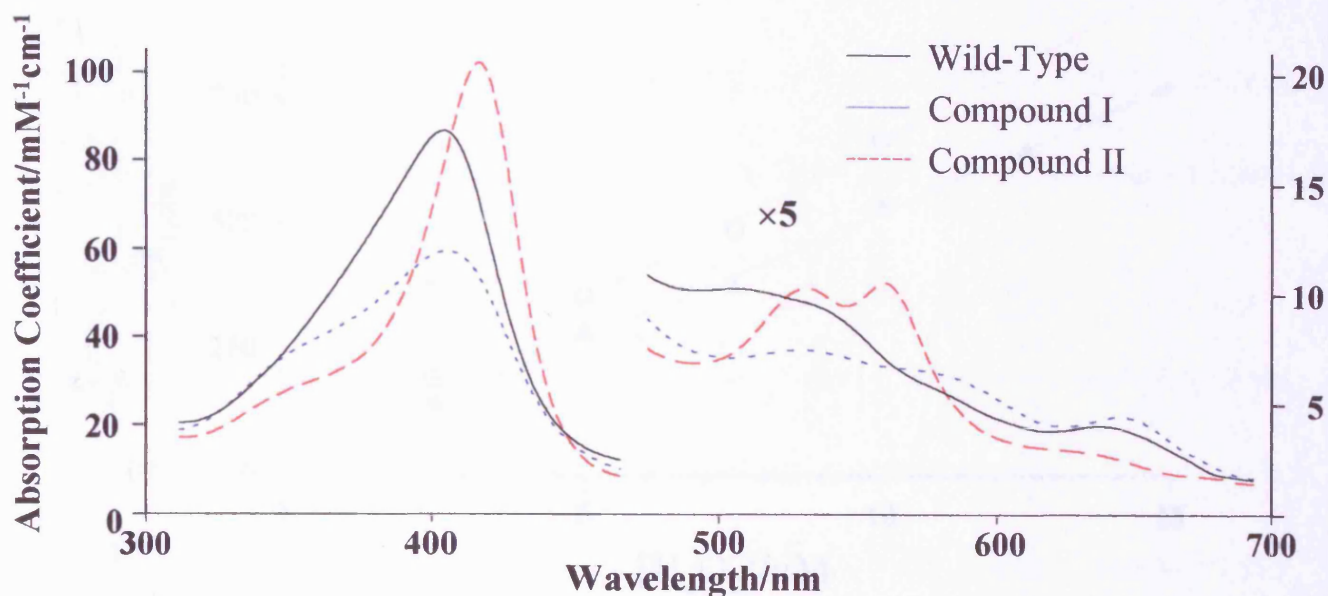
**Figure 4-8 Transient-state photodiode array UV/visible spectra.** Electronic absorption spectra of Compound I and Compound II, which were formed by the addition of a 1:1 and 10:1 ratio of hydrogen peroxide to wild-type rAPX respectively. Normalisation has been made with respect to the calculated millimolar absorption coefficient; the region 475-700 nm has been multiplied by a factor of five. Sample conditions: ~2 μM rAPX, 5°C, NaPi pH 7.0, μ = 0.1 M.

144
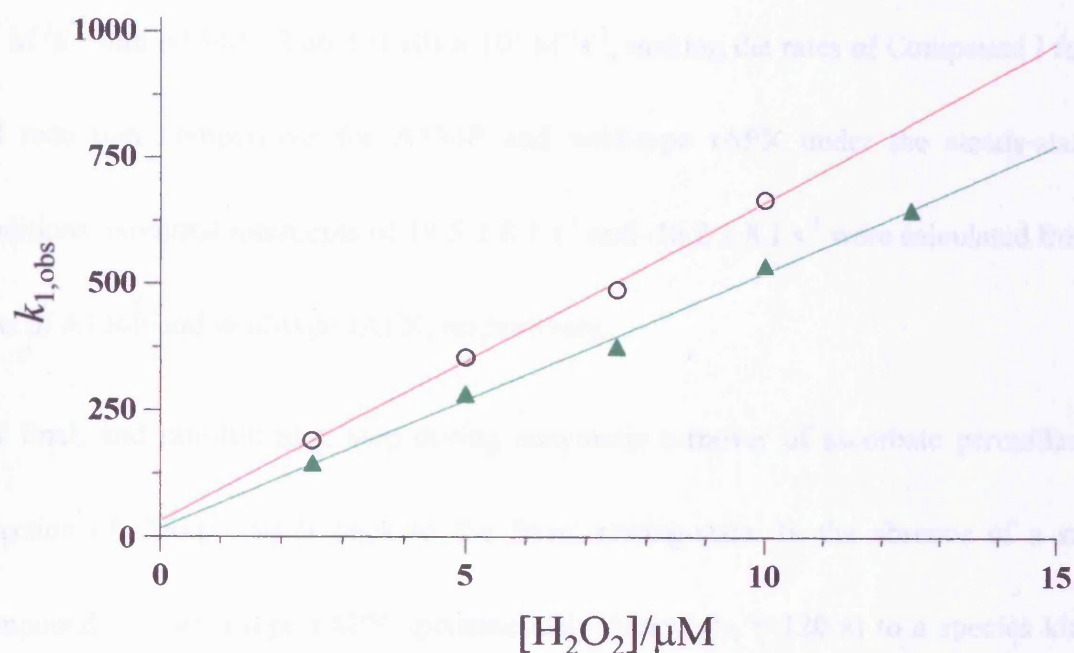
**Figure 4-9 Stopped-flow determination of $k_1$ for wild-type rAPX and A134P.** Plots of pseudo-first-order rate constant, $k_{1,obs}$, versus hydrogen peroxide concentration, [$H_2O_2$], for wild-type rAPX (◯) and A134P (▲). The second-order rate constants for formation of Compound I, $(6.36 \pm 0.19) \times 10^7$ $M^{-1}s^{-1}$ and $(5.10 \pm 0.28) \times 10^7$ $M^{-1}s^{-1}$ for wild-type rAPX and A134P, respectively, were obtained from the slopes of the plots. Measurements were obtained at 398 nm, an isobestic point between Compound I and Compound II. Single-mixing mode conditions: 0.5 µM rAPX, 5°C, NaPi pH 7.0, µ = 0.1 M.

the formation of Compound II; at 5°C, using ten molar equivalents of peroxide, a minimum of

250 ms delay was required to allow complete formation of Compound I. Plots of $k_{2,obs}$ versus

[L-ascorbic acid], Figure 4-10, were used to calculate the second-order rate constant, $k_2$ for

both recombinant enzymes. The rate constants calculated for wild-type rAPX, $(2.96 \pm 0.10) \times$

$10^7$ $M^{-1}s^{-1}$, and A134P, $(2.86 \pm 0.10) \times 10^7$ $M^{-1}s^{-1}$, making the rates of Compound I formation

and reduction competitive for A134P and wild-type rAPX under the steady-state assay

conditions. Nominal intercepts of $19.5 \pm 8.1$ $s^{-1}$ and $-16.2 \pm 8.1$ $s^{-1}$ were calculated from the $k_2$

plots of A134P and wild-type rAPX, respectively.

The final, and rate-limiting, step during enzymatic turnover of ascorbate peroxidase is the

reduction of Compound II back to the ferric resting-state. In the absence of a substrate,

Compound I of wild-type rAPX spontaneously decays ($t_{\frac{1}{2}} = 120$ s) to a species kinetically

similar to authentic Compound II.[15,16] The stopped-flow measurements of $k_3$ were conducted

using the single-mixing mode and Compound II formed from aged Compound I, as previously

described by Çelik et al.[17] As shown in Figure 4-11, the plots of the experimentally measured

$k_{3,obs}$ against [L-ascorbic acid] for both wild-type rAPX and A134P clearly reveal saturation

kinetics, indicative of a substrate-binding equilibrium. Kinetic behaviour of this kind is

consistent with the following mechanism, Equation 4-1,

$$\text{Cmpd II} + \text{S}_{red} \underset{}{\overset{K_a}{\rightleftharpoons}} [\text{Cmpd II S}_{red}] \overset{k_{lim}}{\rightarrow} \text{rAPX} + \text{S}_{ox} \qquad [4\text{-}1]$$
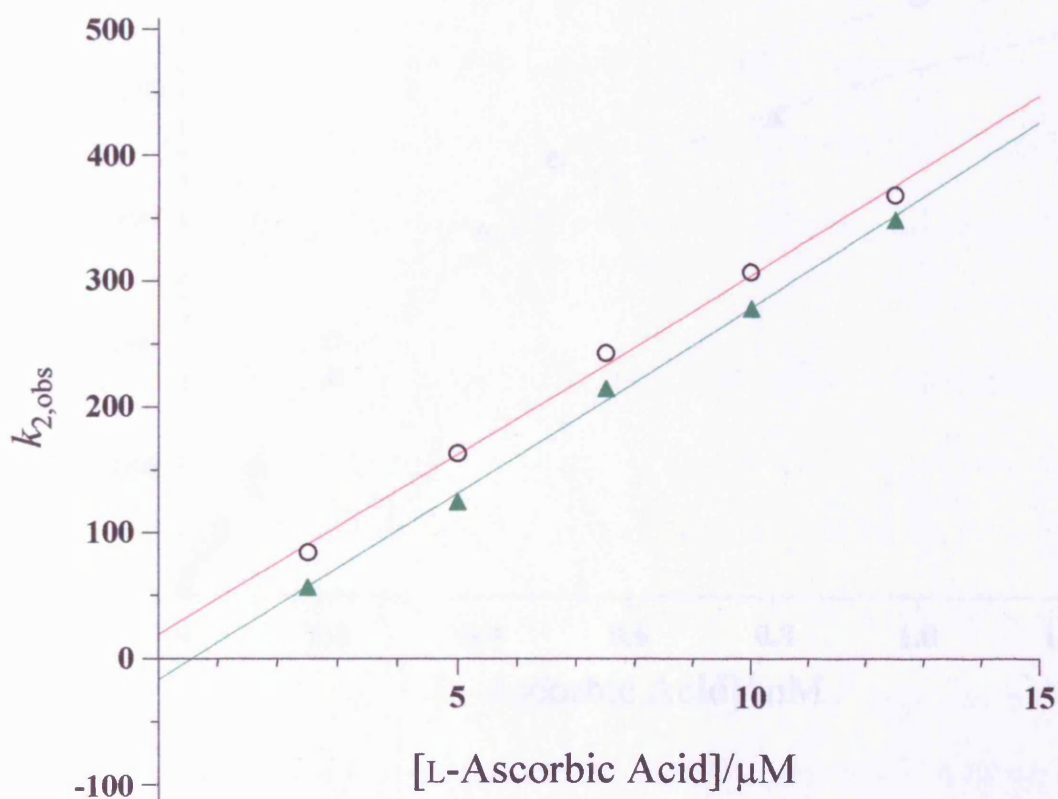
**Figure 4-10 Rate of Compound I reduction by L-ascorbic acid.** Pseudo-first-order rate constant, $k_{2,obs}$, plotted against L-ascorbic acid concentration, [L-ascorbic acid] for wild-type rAPX ($\bigcirc$) and A134P ($\blacktriangle$). The second-order rate constants for the reaction of Compound I with ascorbate, $(2.96 \pm 0.10) \times 10^7$ M$^{-1}$s$^{-1}$ and $(2.86 \pm 0.10) \times 10^7$ M$^{-1}$s$^{-1}$ for wild-type rAPX and A134P respectively, were obtained from the slopes of the plots. Measurements were obtained at 407 nm, an isobestic point between the ferric enzyme and Compound II. At 5°C, using ten molar equivalents of peroxide, a minimum of 250 ms delay was required to allow complete formation of Compound I. Sequential-mixing mode conditions: 0.5 μM rAPX, 5°C, NaPi pH 7.0, μ = 0.1 M.

**Figure 4-11 Rate of Compound II reduction by L-ascorbic acid.** The pseudo-first-order rate constant, $k_{3,obs}$, plotted against concentration of L-ascorbic acid, [L-ascorbic acid] for wild-type rAPX (○) and A134P (▲). The limiting rate constant, $k_{lim}$, for the reaction of Compound II with L-ascorbic acid, $74.5 \pm 3.6$ s$^{-1}$ and $65.9 \pm 4.5$ s$^{-1}$ for wild-type rAPX and A134P respectively, were obtained from fitting the data to Equation 4-2. Measurements were obtained at 420 nm, an isobestic point between the Compound I and Compound II. The data were collected using the single-mixing mode of the stopped-flow apparatus, and Compound II was preformed in the syringe from aged Compound I. Single-mixing mode conditions: 0.5 µM rAPX, 5°C, NaPi pH 7.0, $\mu = 0.10$ M.

from which an expression for $k_{3,obs}$ can be derived, Equation 4-2,

$$k_{3,obs} = \frac{k_{lim}}{1+K_d/[S_{red}]} \quad [4\text{-}2]$$

were $[S_{red}]$ is the concentration of ascorbate and $K_d$ the equilibrium dissociation constant for

the substrate-bound complex $(K_d = 1/K_a)$. Therefore, according to Equation 4-2, non-linear

least-squares fit of the plots of $k_{3,obs}$ against [L-ascorbic acid] allowed $K_d$s of 562 ± 55 μM and

561 ± 71 μM to be calculated for wild-type rAPX and A134P, respectively, which suggests

that replacement of Ala134 with proline has not altered the binding of ascorbate to the

enzyme. The limiting rate constant for Compound II reduction, $k_{lim}$, by enzyme-bound

ascorbate is only slightly lower for A134P (65.9 ± 4.5 s$^{-1}$) than wild-type rAPX

(74.5 ± 3.6 s$^{-1}$), consistent with minimal perturbation of the electron-transfer pathway between

ascorbate and the ferryl haem-iron.

The transient-state kinetics of rAPX-catalysed guaiacol oxidation were also investigated

for both A134P and the wild-type enzyme. Unlike the $k_2$ measurements conducted with

ascorbate, saturation kinetics are indicated by the plots of $k_{2,obs}$ against [guaiacol],

Figure 4-12, for the reaction of Compound I with the non-physiological substrate. Formation

of an enzyme-substrate complex is implicated and, as above for reduction of Compound II by

ascorbate, is consistent with the following mechanism, Equation 4-3,

$$\overset{K_a}{\underset{}{}} \qquad \overset{k_{lim}}{\underset{}{}}$$
$$Cmpd\ I + S_{red} \rightleftharpoons [Cmpd\ I\ S_{red}] \rightarrow Cmpd\ II + S_{ox} \quad [4\text{-}3]$$

from which an expression for $k_{2,obs}$ can be derived, Equation 4-4,

$$k_{2,obs} = \frac{k_{lim}}{1+K_d/[S_{red}]} \quad [4\text{-}4]$$

The limiting rate constant, $k_{lim}$, for conversion of Compound I to Compound II by guaiacol is

marginally smaller for wild-type rAPX (239 ± 11.6 s$^{-1}$) than A134P (350 ± 14.1 s$^{-1}$); the

short-lived substrate-enzyme complex, which gives rise to the observed kinetic saturation, has
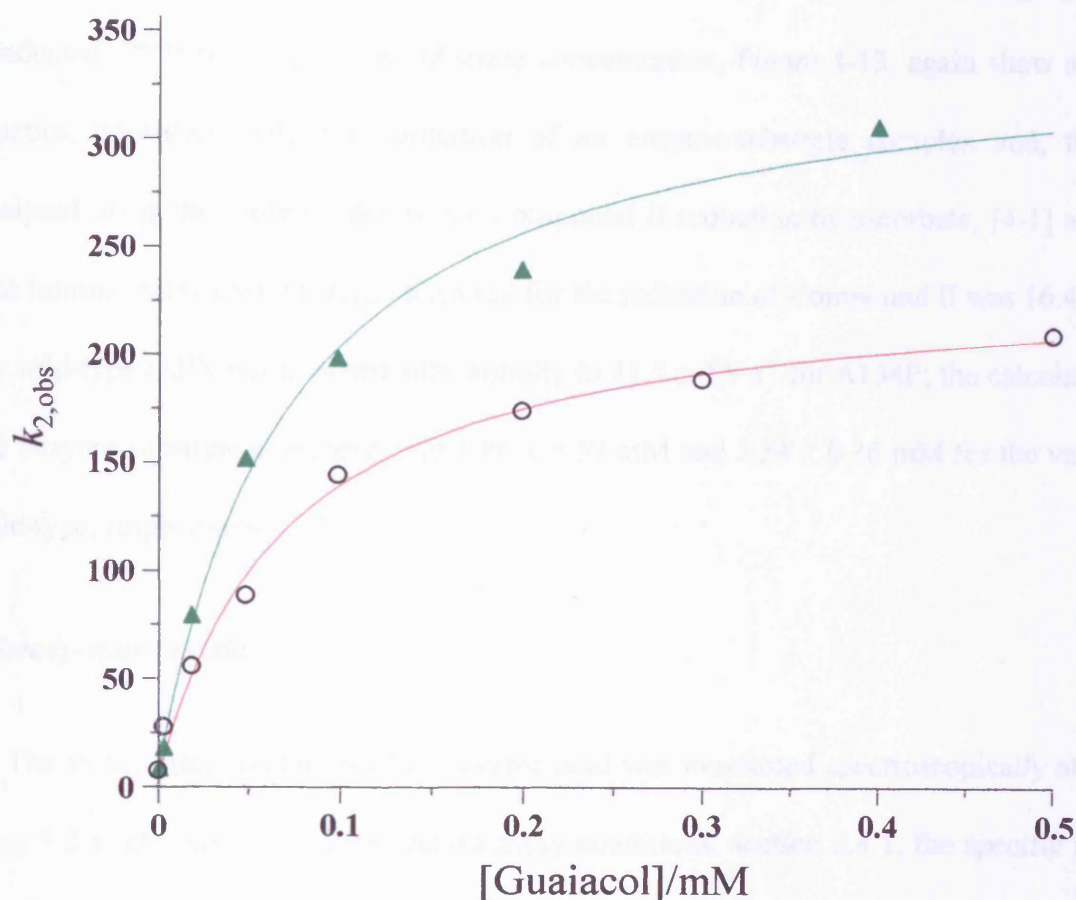
**Figure 4-12 Rate of Compound I reduction by guaiacol.** Pseudo-first-order rate constant, $k_{2,obs}$, plotted against guaiacol concentration, [guaiacol] for wild-type rAPX ($\bigcirc$) and A134P ($\blacktriangle$). The limiting rate constant, $k_{lim}$, for the reaction of Compound I with guaiacol, $239 \pm 11$ s$^{-1}$ and $350 \pm 14$ s$^{-1}$ for wild-type rAPX and A134P respectively, were obtained from fitting the data to Equation 4.4. Measurements were obtained at 407 nm, an isobestic point between the ferric enzyme and Compound II. At 5°C, using ten molar equivalents of peroxide, a minimum of 250 ms delay was required to allow complete formation of Compound I. Sequential-mixing mode conditions: 0.5 μM rAPX, 5°C, NaPi pH 7.0, μ = 0.10 M.

a calculated $K_d$ of 71.2 ± 11.3 μM and 72.2 ± 8.7 μM for wild-type rAPX and A134P, respectively.

Similarly, kinetic analysis of the reaction between Compound II and guaiacol was conducted. Plots of $k_{3,obs}$ versus substrate concentration, Figure 4-13, again show saturation kinetics, consistent with the formation of an enzyme-substrate complex and, thus, was analysed using the same model as for Compound II reduction by ascorbate, [4-1] and [4-2]. The limiting rate constant, $k_{lim}$, measured for the reduction of Compound II was 16.4 ± 2.7 s$^{-1}$ for wild-type rAPX but is raised substantially to 41.5 ± 1.9 s$^{-1}$ for A134P; the calculated $K_d$ of the enzyme-substrate complexes are 1.86 ± 0.59 mM and 3.34 ± 0.36 mM for the variant and wild-type, respectively.

## 4.3.2 Steady-state kinetics

The steady-state oxidation of L-ascorbic acid was monitored spectroscopically at 290 nm ($\varepsilon_{290}$ = 2.8 mM$^{-1}$cm$^{-1}$). Under standard assay conditions, section 2.4.1, the specific activities measured for wild-type rAPX and A134P were 363 ± 22 and 293 ± 17 units per mg APX, respectively. In accordance with the literature,[14] plots of wild-type rAPX and A134P specific activity against ascorbate concentration are non-Michaelis-Menton, Figure 4-14, and possibly indicate a "loose" complex between the substrate and enzyme.[12] The differences in the steady-state activity profiles of A134P and wild-type rAPX are nominal and are consistent with only a small decrease in the turnover capacity of the variant.

It has been reported[12] that wild-type rAPX displays an ionic strength dependent specific activity for L-ascorbic acid, at least in the presence of KCl. However, activity measurements across the 0.05-0.5 M ionic strength range, conducted in the absence of exogenous chloride and at least two different fixed concentrations of ascorbate, revealed no dramatic changes in

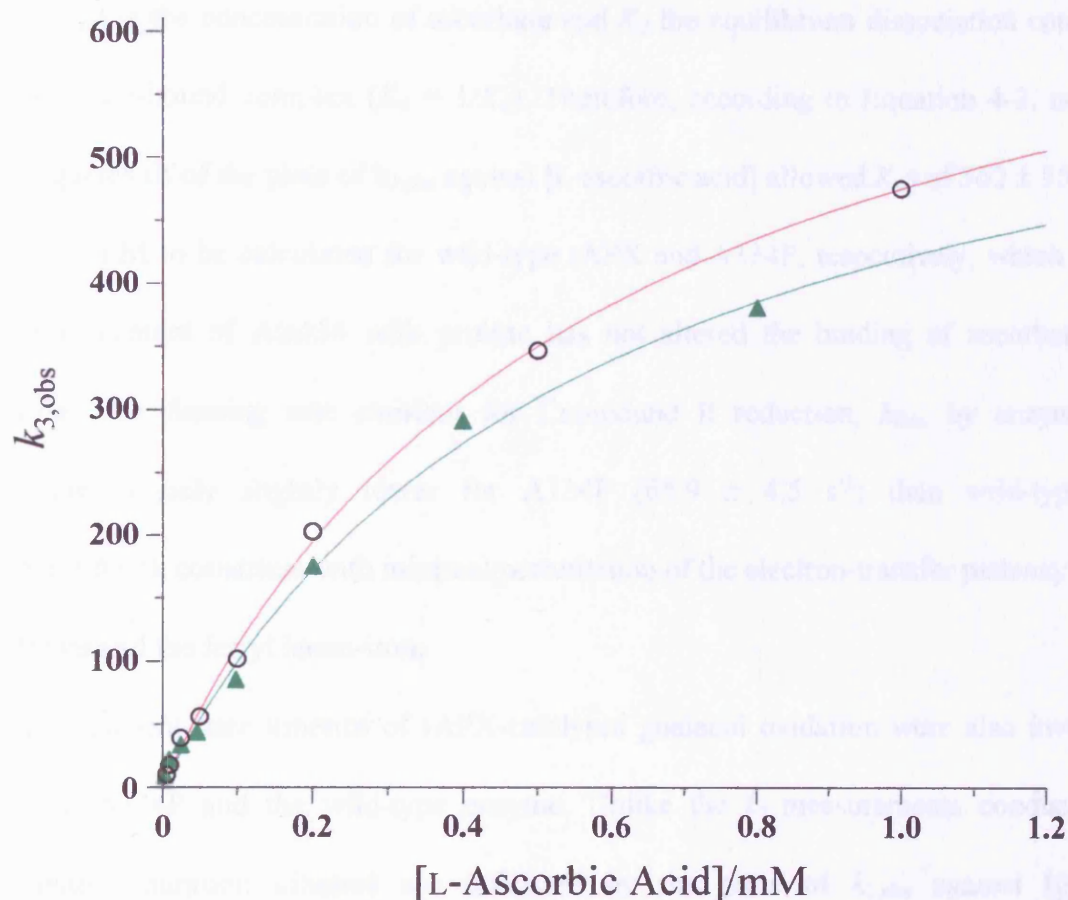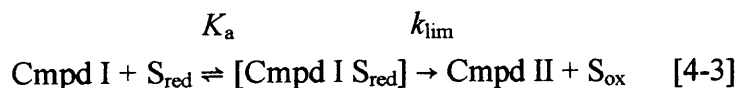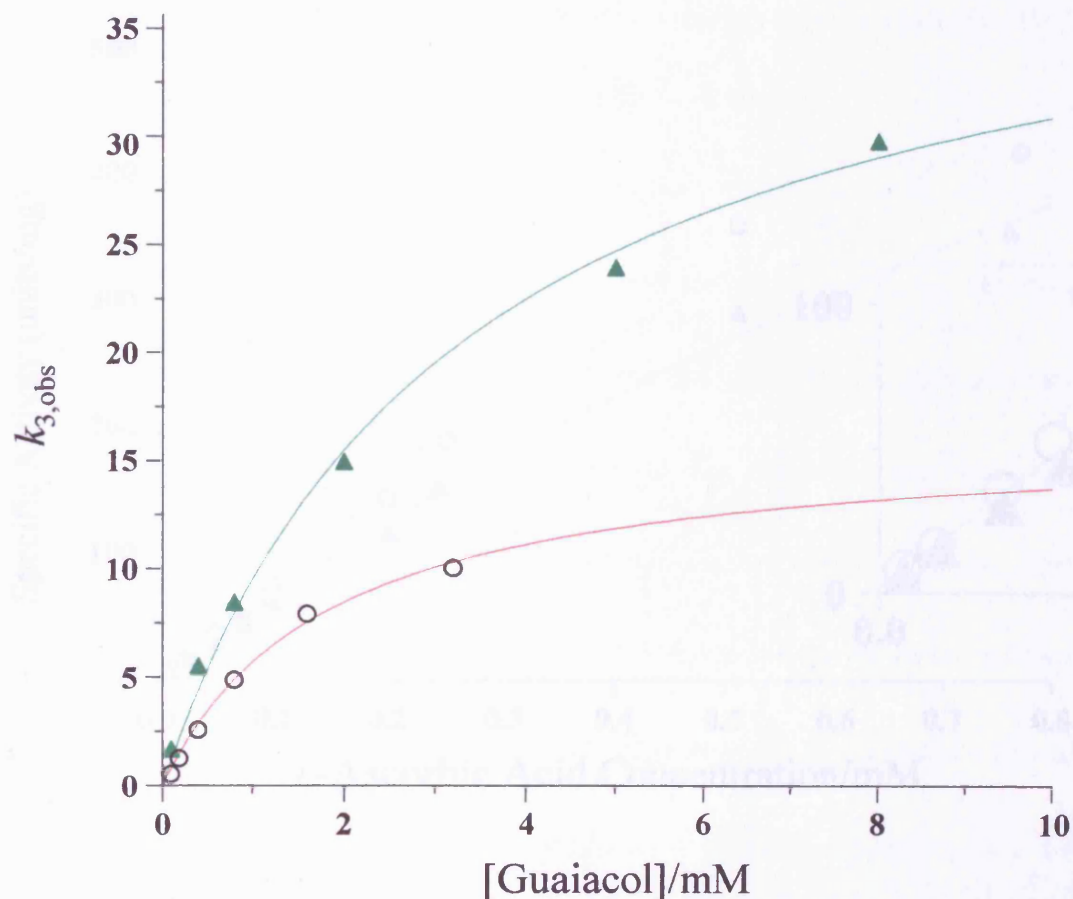**Figure 4-13 Rate of Compound II reduction by guaiacol.** The Pseudo-first-order rate constant, $k_{3,obs}$, plotted against guaiacol concentration, [guaiacol] for wild-type rAPX (○) and A134P (▲). The limiting rate constant, $k_{lim}$, for the reaction of Compound II with guaiacol, $16.4 \pm 2.63$ s$^{-1}$ and $41.5 \pm 1.90$ s$^{-1}$ for wild-type rAPX and A134P respectively, were obtained from fitting the data to Equation 4.2. Measurements were obtained at 420 nm, an isobestic point between the Compound I and Compound II. The data was collected using the single-mixing mode of the stopped-flow apparatus, and Compound II was preformed in the syringe from aged Compound I. Single-mixing mode conditions: 0.5 μM rAPX, 5°C, NaPi pH 7.0, μ = 0.1 M.
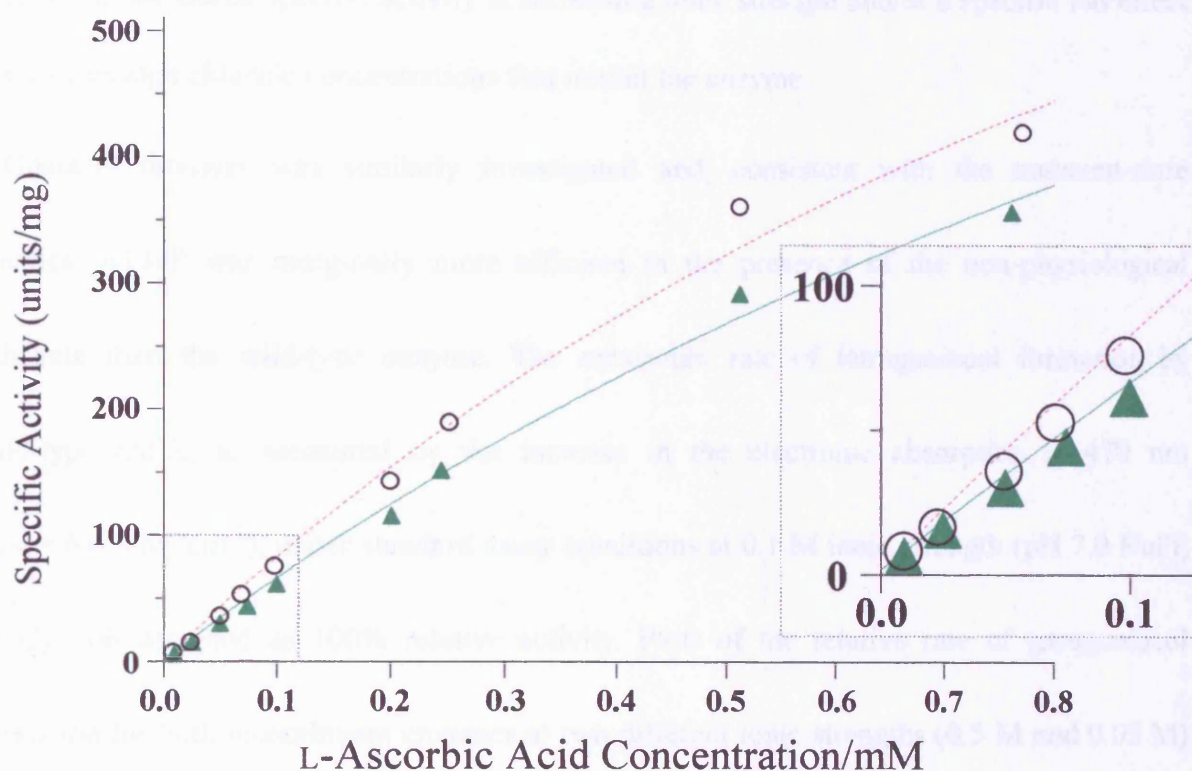
**Figure 4-14 Steady-state L-ascorbic acid oxidation by A134P.** Plots of specific activity of wild-type rAPX (○) and A134P (▲) versus L-ascorbic acid concentration. Attempts to fit the steady state data to the Michaelis-Menten equation are denoted by the dashed red and green lines for wild-type rAPX and A134P, the inset highlights the sigmoidal deviation from the simple kinetic model. Assay conditions: 25 nM rAPX & 0.1 mM $H_2O_2$ at 25°C, pH 7.0 NaPi $\mu$ = 0.10 M.

153

the specific activity of either recombinant enzyme (data not shown), A134P displaying ≈85% of the wild-type rAPX activity throughout the range investigated. A detailed investigation was not conducted in this work, but the preliminary data were indicative of either a marginal decrease in measured specific activity at increasing ionic strength and/or a specific ion effect that causes high chloride concentrations that inhibit the enzyme.

Guaiacol turnover was similarly investigated and, consistent with the transient-state kinetics, A134P was marginally more efficient in the presence of the non-physiological substrate than the wild-type enzyme. The maximum rate of tetraguaiacol formation by wild-type rAPX, as measured by the increase in the electronic absorption at 470 nm ($\varepsilon_{470}$ = 6.6 mM$^{-1}$cm$^{-1}$), under standard assay conditions at 0.1 M ionic strength (pH 7.0 NaPi, 25°C), was assigned as 100% relative activity. Plots of the relative rate of tetraguaiacol formation for both recombinant enzymes at two different ionic strengths (0.5 M and 0.05 M) are shown in Figure 4-15. At low concentrations (<10 mM) of guaiacol the steady-state activity profile is hyperbolic and consistent with substrate saturation, but the coloured product stability detrimentally affects the steady-state measurements at higher substrate concentrations (>10 mM). Whilst the data supports activation of the guaiacol oxidation activity of rAPX by replacement of Ala134 with proline, detailed analysis of the variant and wild-type enzyme guaiacol oxidation is precluded by the interference that is produced by non-enzyme-dependent reactions. Assessing the kinetic stabilities of the coloured products of guaiacol oxidation is outside the scope of this work, and has long been acknowledged as the
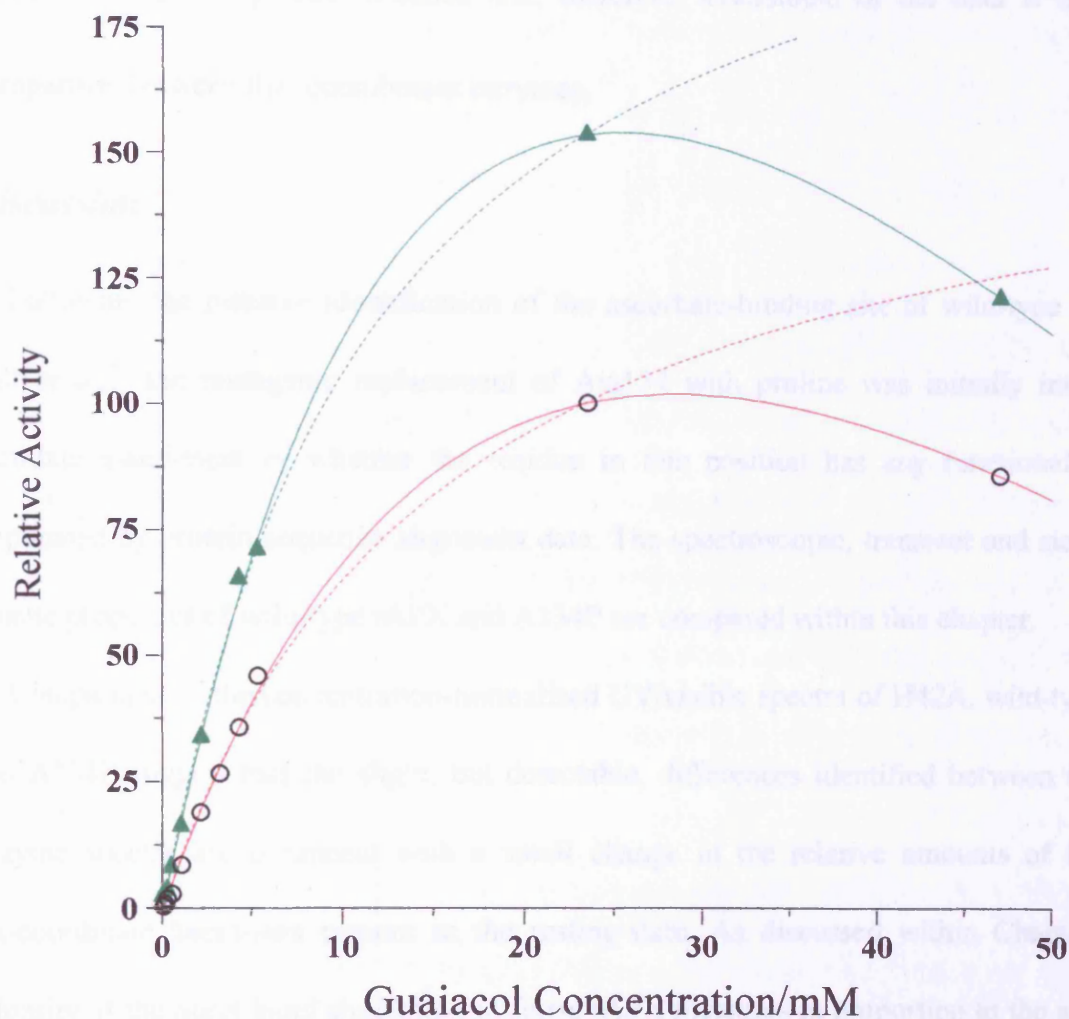
**Figure 4-15 Steady-state guaiacol oxidation by A134P.** Plots of relative activity of wild-type rAPX (○) and A134P (▲) versus L-ascorbic acid concentration. Attempts to fit the steady state data (<30 mM guaiacol) to the Michaelis-Menten equation are denoted by the dashed red and green lines for wild-type rAPX and A134P; the solid lines represent a fit to the data (all concentrations) using a biphasic model that takes into account further oxidation of tetraguaiacol by the enzyme. Assay conditions: 10 nM rAPX & 0.1 mM $H_2O_2$ at 25°C, pH 7.0 NaPi μ = 0.10 M.

main source of error associated with this particular peroxidase assay.[18] Calculation of the steady-state parameters for $k_{cat}$ and $K_m$ was not considered an appropriate model for the steady-state activity profile obtained and, therefore, assessment of the data is limited to comparison between the recombinant enzymes.

## 4.4 Discussion

Following the putative identification of the ascorbate-binding site of wild-type rAPX by Hill et al,[11] the mutagenic replacement of Ala134 with proline was initially intended to facilitate assessment of whether the residue in this position has any functional role, as implicated by protein sequence alignment data. The spectroscopic, transient and steady-state kinetic properties of wild-type rAPX and A134P are compared within this chapter.

Comparison of the concentration-normalised UV/visible spectra of H42A, wild-type rAPX and A134P suggest that the slight, but detectable, differences identified between the ferric enzyme spectra are consistent with a small change in the relative amounts of five- and six-coordinate haem-iron present in the resting-state. As discussed within Chapter 3, the intensity of the Soret band absorption of ferric rAPX increases in proportion to the amount of six-coordinate high- and low-spin haem present in the enzyme. At pH 7.0, the Soret band millimolar absorption coefficients of H42A ($\varepsilon_{397}$ = 83 ± 2 mM$^{-1}$cm$^{-1}$), wild-type rAPX ($\varepsilon_{403}$ = 88 ± 2 mM$^{-1}$cm$^{-1}$) and A134P ($\varepsilon_{404}$ = 92 ± 3 mM$^{-1}$cm$^{-1}$) suggest that A134P is probably comprised of a larger proportion of six-coordinate haem than either wild-type rAPX or H42A. Alternatively, the complex steric constraints imposed by each of the closely related, but structurally different, protein matrices on the haem might account for the distinct spectroscopic properties observed for the three recombinant haemoproteins. The protein

matrices of wild-type rAPX and cytochrome $c$ peroxidase constrain the vinyl groups of their respective haem chromophores in markedly different orientations and, despite the 33% amino acid sequence identity shared by the class I peroxidases, the spectroscopic properties of the two enzymes are appreciably modulated by the degree of conjugation of the vinyl groups with the haem.[19] However, in the absence of crystallographic data for H42A and A134P, the specific structural factors that control the haem electronic absorption spectrum of the rAPX variants cannot be substantiated.

Ligand-bound ternary complexes of A134P are spectroscopically similar to that of wild-type rAPX and, furthermore, the calculated $K_d$s of the cyanide, azide and fluoride derivatives of A134P are of the same order of magnitude as that of the corresponding wild-type compound. The close correlations between the anionic ligand-binding properties of A134P and wild-type rAPX are consistent with the replacement of a protein residue that is not located in the vicinity of the haem-iron. Thus, unlike H42A, the distal haem pocket of A134P retains wild-type architecture.

Mechanism-based chemical modification of peroxidases by suicide substrates, including but not limited to alkyl- and arylhydrazines, has revealed the extent to which prosthetic haem reactivity is controlled by protein encapsulation.[13,20-22] The regiospecific haem-derived products extracted from phenylhydrazine-modified HRP were identified as comprising of a mixture of C18-hydroxymethyl haem, unmodified and C20-phenyl haem.[13] Therefore, unlike other haemoproteins (e.g. myoglobin and P450s), the suicide substrate does not have direct access to the haem-iron, and instead interacts with the periphery of the haem moeity.[23] Substantial C20-haem alkylation accompanied the treatment of both HRP and MnP by a variety of alkylhydrazines and, consequently, the inactivation of both peroxidases was

157

ascribed, in part, to disruption of the substrate-binding sites, putatively located in the vicinity of the exposed haem edge.[20,21]

Until recently, the most complete source of information concerning the substrate recognition properties of wild-type rAPX was published by Hill *et al.*[11] Utilising NMR-derived ascorbate-iron distance constraints, in combination with the protein crystal structure coordinates,[24] two potential ascorbate-binding sites were revealed by computer-based molecular modelling programs, one close to the 6-propionate group of the haem, Figure 4-1, and one close to the C20 ($\delta$-meso) position. Comparison of phenylhydrazine-treated samples of HRP and wild-type rAPX revealed that the latter is substantially more susceptible to covalent modification, and resulted in a greater proportion of C20-phenyl haem.[11] Hence, of the two sites, the ascorbate-binding site located near to the exposed haem C20-carbon of wild-type rAPX was identified as being wholly consistent with the widely held view that the haem edge is involved in substrate recognition and/or oxidation.

Exposure of wild-type rAPX and A134P samples to the phenylhydrazine incubation mixture for a prolonged period (>3 minutes) resulted in HPLC chromatograms identical to that reported by Hill *et al* for fully inactivated wild-type rAPX.[11] Similar treatment of HRP resulted in no significant alterations to the product distribution detected after turnover of the enzyme in the presence of phenylhydrazine for only two minutes. Following restricted turn over (1½ minutes) of the three haemoproteins in the presence of phenylhydrazine, the proportion of C20-phenyl haem detected in the products extracted from A134P was substantially greater than that extracted from either wild-type rAPX or HRP. The consensus drawn from the chemical modification experiments suggests that replacement of Ala134 with proline has resulted in a variant that has the same haem exposure as the wild-type enzyme, but is modified by phenylhydrazine moderately more rapidly.

A detailed examination of the HPLC-linked mass spectra, confirmed that most of minor products resolved by the UV/visible detector were ascribable to demetallated or solvated haem derivatives, and a number of aggregate compounds. Such species were detected in all of the phenylhydrazine-modified samples analysed by HPLC.

Consistent with the catalytic mechanism, discussed in detail within Chapter 1, the presence of ascorbate, or guaiacol, did not noticeably affect the values obtained for $k_1$ (Latesh Lad, unpublished data). The second-order rate constants measured for wild-type rAPX $(6.4 \times 10^7 \, M^{-1}s^{-1})$ and A134P $(5.1 \times 10^7 \, M^{-1}s^{-1})$ Compound I formation were comparable to that reported for the native enzyme at 20°C, pH 7.8 NaPi $(8.0 \times 10^7 \, M^{-1}s^{-1})$. Formation of Compound I is fractionally slower for A134P than wild-type rAPX and, as suggested by the resting-state electronic absorption spectra, confirms that only minor perturbations have been introduced to the active-site and haem of the variant. Detailed characterisation of the porphyrin $\pi$ cation species, generated by the reaction between A134P and hydrogen peroxide, has not been pursued; yet, stopped-flow photodiode array spectroscopy revealed no significant differences between the transient-state spectra of A134P and wild-type rAPX (Latesh Lad, unpublished data).

The second-order rate constants measured for the formation of Compound II in the presence of L-ascorbic acid were the same order of magnitude as Compound I formation. Consequently, at equimolar concentrations of peroxide and ascorbate, the $k_1$ and $k_2$ processes are kinetically competitive for both A134P and wild-type rAPX. For both recombinant enzymes, reduction of Compound I by guaiacol was considerably slower ($\approx 10^5$-fold) than the reaction with the physiological substrate and, consistent with the formation of a substrate-bound enzyme complex, resulted in saturation kinetics. The limiting rate constant measured for the reaction between guaiacol and A134P $(350 \, s^{-1})$ is 1½ times that of wild-type

rAPX (239 s$^{-1}$), the $K_d$s calculated for the transient guaiacol-bound complexes of A134P (65.9 ± 4.5 s$^{-1}$) and wild-type rAPX (74.5 ± 3.6 s$^{-1}$) are essentially the same.

Reduction of Compound II by ascorbate results in saturation kinetics, and the equilibrium dissociation constants of the ascorbate-bound complex of wild-type rAPX and A134P are 562 ± 55 μM and 561 ± 71 μM, respectively. Rate-limiting reduction of Compound II of A134P (65.9 s$^{-1}$) and wild-type rAPX (74.5 s$^{-1}$) predict that, under typical steady-state assay conditions, the variant should display ≈88% of the wild-type enzyme specific activity. Indeed, across the range of ascorbate concentrations investigated (0-0.8 mM), the rate of steady-state ascorbate oxidation by A134P is only slightly lower (≈82%) than that measured for wild-type rAPX. The nominal activity loss suggests that the replacement of Ala134 with proline does not detrimentally affect the ascorbate-binding site *per se*, but rather the variant is comprised of an intractable mixture of active, inactive and unreactive enzyme. Accordingly, the consensus drawn from the kinetic data is that, in terms of the ability of the variant to perform its physiological role, A134P displays essentially wild-type rAPX behaviour.

Stopped-flow analysis of the reaction between Compound II and guaiacol revealed that A134P (41.5 s$^{-1}$) is not reduced very more rapidly than wild-type rAPX (16.4 s$^{-1}$) in the presence of the non-physiological substrate. The equilibrium dissociation constant calculated for the guaiacol-bound complex of A134P (3.34 ± 0.36 mM) is essentially the same as that of wild-type enzyme (1.86 ± 0.59 mM). The $K_d$ and limiting rate constant, $k_{lim}$, measured for the reaction between guaiacol and wild-type rAPX compare favourably with those reported for

*p*-cresol ($k_{lim}$ = 18.5 s$^{-1}$, $K_d$ = 1.54 mM),[17] and suggests that the phenolic substrates are oxidised at the same non-specific substrate binding-site.

During the course of this work, site-directed mutagenesis and chemical modification experiments on rAPX provided evidence in support of the existence of two functionally, and spatially, distinct substrate-binding sites.[12] Site-specific replacement, by serine, or chemical modification of Cys32 was found to decrease the activity of rAPX against ascorbate by ≈3-fold and ≈1000-fold, respectively, indicative of an ascorbate interaction at the haem edge in the region of this residue, possibly involving Arg172, *i.e.* analogous to the γ-meso binding site identified by Hill *et al.*[11] Accordingly, the nominal effect that replacing Ala134 with proline has on the physiologically relevant properties of rAPX is, in view of this recently published data, wholly consistent with the residue being spatially remote from the vicinity of the catalytically relevant ascorbate-binding site. The hypothesis that aromatic substrates interact with rAPX at an alternative location to that implicated for ascorbate oxidation was substantiated by the observation that replacement or modification of Cys32 did not affect the rAPX-catalysed oxidation of guaiacol.[12] The results of wild-type phenylhydrazine modification experiments[11] showed that the C20 position of the haem is accessible to the products of suicide substrate oxidation, and suggested that the exposed δ-meso haem edge is, probably, involved in the oxidation of aromatic substrates by rAPX. Subsequently, mutagenic assessment of the role of Arg172, implicated by the Cys32 data, has provided further evidence that supports the existence of two substrate-binding sites in ascorbate peroxidase.[25] The existence of a second non-specific binding site is not unprecedented since discrete substrate-binding sites have been identified in lignin peroxidase.[26]

At low substrate concentrations (<10 mM), steady-state measurements of guaiacol oxidation by A134P and wild-type rAPX are consistent with Michaelis-Menten kinetics but,

at moderately high concentrations (>10 mM), the reactions deviate considerably from this simple kinetic model. Sigmoidal substrate concentration-dependencies have been reported for the steady-state oxidations of ascorbate and $p$-cresol by wild-type rAPX and, whilst the origin of the observed behaviour is not wholly understood, guaiacol oxidation is not noticeably sigmoidal. The stability of tetraguaiacol, the coloured product used to monitor the reaction progress, was noticeably influenced by the concentration of guaiacol and, to a lesser extent, the solution ionic strength; thus, calculation of $V_{max}$ (or $k_{cat}$) and $K_m$ for A134P and wild-type rAPX has not been attempted. However, an increase in the rate of conversion of phenylhydrazine, via phenyldiazene, to the phenyldiazenyl radical would generate a higher steady-state concentration of phenyl radicals during the modification treatment, and consequently result in more rapid C20-haem arylation. Therefore, faster oxidation of aromatic substrates by A134P might explain why the variant is slightly more susceptible to phenylhydrazine modification than the wild-type enzyme.

The haem edge of C$c$P has been implicated in the catalytic oxidation of guaiacol by the enzyme.[27,28] Cytochrome $c$ peroxidase contains an alanine residue (Ala147) that corresponds to Ala134 in rAPX, and the replacement of Ala147 with methionine and tyrosine resulted in a decrease in the steady-state guaiacol activity of the enzyme to 86% and 16% that of wild-type enzyme, respectively.[29] The steady state and pre-steady state data for A134P do not show significant deviations from the behaviour of the wild type rAPX (although the variant is marginally more reactive, which is also reflected in the modification profiles observed by HPLC). Unfortunately, the A134F variant was not isolatable from $E.\ coli$ in the form of holo-protein, and reconstitution protocols with exogenous haem did not generate catalytically active enzyme, which prevented the replacement of Ala134 with a very bulky residue ($e.g.$ phenylalanine) that might have resulted in a more substantial effect on guaiacol oxidation.

Thus, the consensus of the available rAPX data is that replacement of Ala134 by a proline residue has not altered the accessibility of the δ-meso haem and, accordingly, the associated catalytic reactivity towards aromatic substrates is essentially unchanged. Therefore, provided that the aromatic substrate-binding site of rAPX is in the vicinity of exposed haem edge, the substituted proline must be in a conformation that essentially mimics that of Ala134 in the wild-type, otherwise, the absence of any substantial differences in the oxidation of guaiacol for the A134P variant is difficult to reconcile. However, given the lack of crystallographic data for A134P, the extent to which the residue in position 134 modulates the exposure of the δ-meso haem edge cannot be substantiated.

Recent publication of crystallographic data for a substrate-bound peroxidase complex,[30] between ferulic acid and the cyanide-bound ternary complex of HRP, has suggested that the peptide-bond carbonyl of Pro139 (the residue analogous to Ala134 of rAPX) is involved in an extensive H-bonding network that contributes to stabilisation of the substrate-bound complex. Amongst class III peroxidases that oxidise small aromatic substrate molecules (e.g. ArP, LiP, PnP and HRP) the proline residue in the vicinity of the exposed haem edge is highly conserved, but for CcP and rAPX (class I peroxidases) alanine is located in the analogous position. The A134P data is wholly consistent with the peptide-bond carbonyl of the residue in this position, rather than its side-chain, being involved in the binding, and subsequent oxidation, of aromatic substrates in the vicinity of the exposed haem edge. Thus, particularly in the context of enzyme-catalysed reactions, the exact structural features that define the substrate binding and recognition properties of peroxidases remain to be resolved, and further experimental work is required before these effects can be wholly understood. Detailed understanding of the roles that residues in the vicinity of the δ-meso haem edge have in

peroxidase structure-function is required before the catalytic properties of these enzymes can

be manipulated in a predictive way.

## 4.5 Conclusions

Conclusions that can be drawn from the results presented in this chapter are as follows:

- Mutagenic replacement of Ala134 in wild-type rAPX with proline results in a recombinant enzyme, A134P, that has been isolated and characterised in order to assess the effect that the residue in this position has on the binding and catalytic oxidation of ascorbate and guaiacol.

- Electronic absorption spectra and equilibrium dissociation constants for various ligand-bound derivatives indicate that A134P retains essentially the same active-site architecture as the wild-type protein.

- The proportion of C20-phenyl haem detected in the mixture of haem-derived adducts extracted from phenylhydrazine-modified A134P suggests that the accessibility of the δ-meso haem edge of the variant is comparable to that of wild-type rAPX.

- Steady- and transient-state kinetic data indicate that the binding and oxidation of ascorbate by A134P is unaffected by the amino acid replacement, and is consistent with published data that suggests the physiological substrate binds to rAPX near to Cys32 and Arg172.[12,25]

- The consensus of all the A134P data is that substituting a proline residue in position 134 for alanine does not significantly alter haem accessibility or the catalytic activity of rAPX; thus, further evidence is needed to support a functional role for this residue.

## 4.6 References

1 Pelletier, H. and Kraut, J. (1992) *Science*, 258, 1748-1755

2 Sundaramoorthy, M., Kishi, K., Gold, M. H. and Poulos, T. L. (1994) *J. Biol. Chem.*, 269, 32759-32767

3 Smith, A. T. and Veitch, N. C. (1998) *Curr. Opin. Struct. Biol.*, 2, 269-278

4 Fitzgerald, M. M., Churchill, M. J., McRee, D. E. and Goodin, D. B. (1994) *Biochemistry*, 33, 3807-3818

5 Timofeevski, S. L., Nie, G., Reading, N. S. and Aust, S. D. (1999) *Biochem. Biophys. Res. Comm.*, 256, 500-504

6 Bonagura, C. A., Sundaramoorthy, M., Bhaskar, B. and Poulos, T. L. (1999) *Biochemistry*, 38, 5538-5545

7 Sigman, J. A., Kwok, B. C., Gengenbach, A. and Lu, Y. (1999) *J. Am. Chem. Soc.*, 121, 8949-8950

8 Wang, X. and Lu, Y. (1999) *Biochemistry*, 38, 9146-9157

9 Sigman, J. A., Pond, A. E., Dawson, J. H. and Lu, Y. (1999) *Biochemistry*, 38, 11122-11129

10 Bonagura, C. A., Bhaskar, B., Sundaramoorthy, M. and Poulos, T. L. (1999) *J. Biol. Chem.*, 274, 37827-37833

11 Hill, A. P., Modi, S., Sutcliffe, M. J., Turner, D. D., Gilfoyle, D. J., Smith, A. T., Tam, B. M. and Lloyd, E. (1997) *Eur. J. Biochem.*, 248, 347-354

12 Mandelman, D., Jamal, J. and Poulos, T. L. (1998) *Biochemistry*, 37, 17610-17617

13 Ator, M. A. and Ortiz de Montellano, P. R. (1987) *J. Biol. Chem.*, 262, 1542-1551

14 Mittler, R. and Zilinskas, B. A. (1991) *Plant. Physiol.*, 97, 962-968.

15 Marquez, L. A., Quitoriano, M., Zilinskas, B. A. and Dunford, H. B. (1996) *FEBS Lett.*, 389, 153-156

16 Patterson, W. R., Poulos, T. L. and Goodin, D. B. (1995) *Biochemistry*, 34, 4342-4345

17 Çelik, A., Cullis, P. M. and Lloyd Raven. E. (2000) *Arch. Biochem. Biophys.*, 373, 175-181

18 Chance, B. and Maehly, A. C. unpublished data

19 Nissum, M., Neri, F., Mandelman, D., Poulos, T. L. and Smulevich, G. (1998) *Biochemistry*, 37, 8080-8087

20 Ator, M. A., David, S. K. and Ortiz de Montellano, P. R. (1987) *J. Biol. Chem.*, 262, 14954-14960

21  Harris, R. Z., Wariishi, H., Gold, M. H. and Ortiz de Montellano, P. R. (1991) *J. Biol. Chem.*, 266, 8751-8758

22  Mazumdar, A., Adak, S., Chatterjee, R. and Banerjee, R. K. (1997) *Biochem. J.*, 324, 713-719

23  Ortiz de Montellano, P. R. (1987) *Acc. Chem. Res.*, 207, 289-294

24  Patterson, W. R. and Poulos, T. L. (1995) *Biochemistry*, 34, 4331-4341

25  Bursey, E. H. and Poulos, T. L. (2000) *Biochemistry*, 39, 7374-7379

26  Doyle, W. A., Blodig, W., Veitch, N. C., Piontek, K., and Smith, A. T. (1998) *Biochemistry* 37, 15097-15105

27  DePillis, G. D., Sishta, B. P., Mauk, A. G., and Ortiz de Montellano, P. R. (1991) *J. Biol. Chem.*, 266, 19334- 19341

28  Ortiz de Montellano, P. R. (1992) *Ann. Rev. Pharmacol. Toxicol.*, 32, 89-107

29  Wilcox, S. K., Jensen, G. M., Fitzgerald, M. M., McRee, D. E., and Goodin, D. B. (1996) *Biochemistry*, 35, 4858-4866

30  Henriksen, A., Smith, A. T. and Gajhede, M. (1999) *J. Biol. Chem.*, 49, 35005-3501

# CHAPTER FIVE

# DETECTION OF A

# TRYPTOPHAN RADICAL

# IN THE REACTION OF

# ASCORBATE

# PEROXIDASE WITH

# HYDROGEN PEROXIDE

# 5 Detection Of A Tryptophan Radical In The Reaction Of Ascorbate Peroxidase With Hydrogen Peroxide

As discussed within Chapter 1, the ability of haem peroxidases to react with hydrogen peroxide and form a stable oxidised intermediate, known as Compound I, distinguishes them from other haemoproteins. Peroxidase catalytic turnover (Equations 5-1–5-3) proceeds through two detectable intermediates,[1] known as Compound I and Compound II:
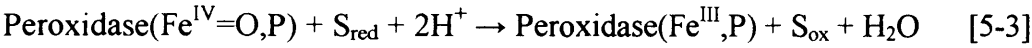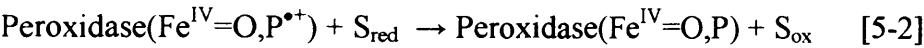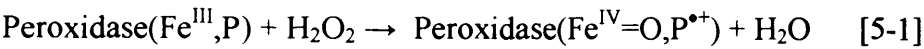
$$\text{Peroxidase}(\text{Fe}^{III},\text{P}) + \text{H}_2\text{O}_2 \rightarrow \text{Peroxidase}(\text{Fe}^{IV}=\text{O},\text{P}^{\bullet+}) + \text{H}_2\text{O} \qquad [5\text{-}1]$$

$$\text{Peroxidase}(\text{Fe}^{IV}=\text{O},\text{P}^{\bullet+}) + \text{S}_{red} \rightarrow \text{Peroxidase}(\text{Fe}^{IV}=\text{O},\text{P}) + \text{S}_{ox} \qquad [5\text{-}2]$$

$$\text{Peroxidase}(\text{Fe}^{IV}=\text{O},\text{P}) + \text{S}_{red} + 2\text{H}^+ \rightarrow \text{Peroxidase}(\text{Fe}^{III},\text{P}) + \text{S}_{ox} + \text{H}_2\text{O} \qquad [5\text{-}3]$$

where $\text{S}_{red}$ & $\text{S}_{ox}$ are the reduced and oxidised forms of the substrate, S; $\text{Fe}^{III},\text{P}$ corresponds to the peroxidase resting-state; $\text{Fe}^{IV}=\text{O},\text{P}^{\bullet+}$ & $\text{Fe}^{IV}=\text{O},\text{P}$ are the intermediates Compound I and Compound II respectively. Both intermediates are oxyferryl species, $\text{Fe}^{IV}=\text{O}$, with Compound I storing the second oxidising equivalent in the form of either a protein-based radical or a porphyrin π-cation radical, $\text{P}^{\bullet+}$.[1] The electronic structure of Compound I and in particular the identity and location of the radical, $\text{P}^{\bullet+}$, has been the subject of considerable study for many years.[2-5]

The presence of a stable protein-based radical in Compound I (traditionally known as Compound ES) of CcP was first suggested more than thirty years ago,[6] but two decades elapsed before a tryptophan residue (Trp191) was unambiguously identified as the site of the radical species.[7] It is now widely accepted that protein-based radicals play a crucial role in all kinds of metalloenzyme catalysis,[8] yet, despite considerable efforts, the factors affecting radical formation and stability have yet to be defined in a rational and predictable way. In the

case of CcP, the early availability of crystallographic information[9] and an expression system[10] for site-directed mutagenesis meant that the spectroscopic properties of the Trp191 radical and the functional influence of amino acid substitutions at this position could be probed in a systematic way.[11,12] In this sense, CcP has become a paradigm not only for haem peroxidases in general, but also for other haem enzymes.[13-17]

Most other peroxidases, notably HRP, are known to form porphyrin $\pi$-cation radicals during their catalytic cycle.[18] As such, the electronic absorption spectrum of HRP Compound I is quite different from that of CcP,[2] and the absence of a readily oxidisable amino acid in HRP at the position corresponding to Trp191 (HRP contains a phenylalanine residue, Phe221, at this position) has provided a satisfactory rationalisation of these data. The most obvious and striking difference between the Compound I electronic spectra of HRP and CcP is in the Soret band. In HRP, an approximate 50% loss of intensity and a slight blue shift (from 403 to 400 nm) accompany formation of Compound I. In contrast, the electronic spectrum of Compound I of CcP has an absorption coefficient for the Soret band of similar intensity to the ferric enzyme and a red shift (from 408 nm to 420 nm) is observed. In fact, the electronic absorption spectrum of CcP Compound I is remarkably similar, particularly in the Soret region, to that of HRP Compound II ($\lambda_{max}$ = 420 nm) in which no radical is present, although these species can easily be distinguished using EPR.[2]

Recently, pea cytosolic APX, another class I peroxidase that shares 33% sequence homology with CcP[19] and catalyses the $H_2O_2$-dependent oxidation of ascorbate in plants,[20,21] has been found to contain the same active site tryptophan residue (Trp179, Figure 5-1) homologous to the site of the Trp191 radical in CcP. Hence, with both high-resolution crystallographic information[22] and an expression system[23] available, APX provided a new opportunity to re-examine previous working hypotheses and to establish more specifically
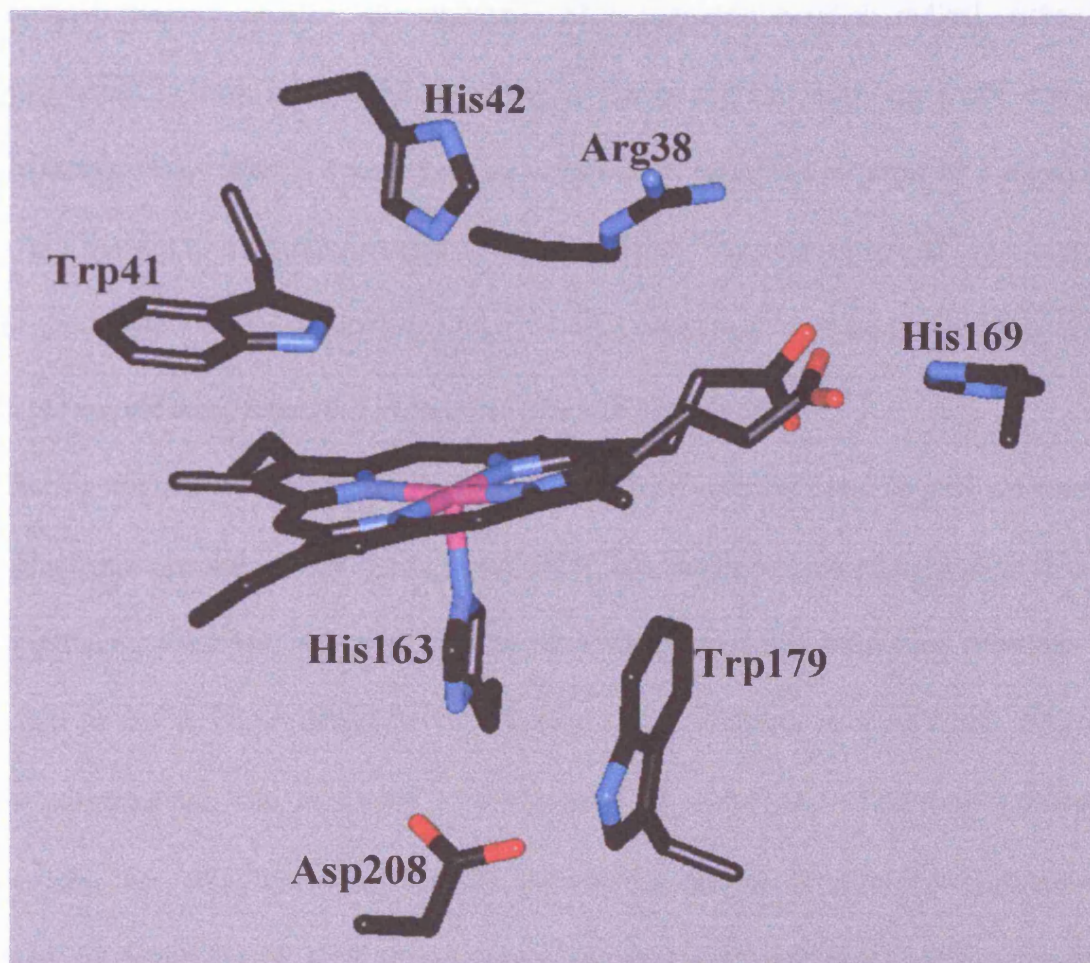
**Figure 5-1 The active site of wild-type rAPX.** Computer-based molecular model of wild-type rAPX based upon the published protein crystal structure coordinates [Patterson, W. R. and Poulos, T. L. (1995) *Biochemistry*, **34**, 4331-4341].

whether protein radical formation in C$c$P represented, in a general sense, the mechanistic chemistry of all class I peroxidases. In view of the high sequence homology and the known catalytic behaviour of C$c$P, the existence of a porphyrin $\pi$-cation radical, rather than a protein-based radical, in the EPR spectrum of Compound I of wild-type rAPX was a rather unexpected observation.[24] These data were partially reconciled in terms of a metal-binding site, not present in C$c$P, located only 8 Å from Trp179[22] that was proposed to prevent protein radical formation on electrostatic grounds[24] and various theoretical arguments have since been able to provide data in support of the experimental observations.[25-28]

During the course of this work on rAPX, small but persistent perturbations were noticed in the electronic spectra of ferric samples of rAPX that had been exposed to $H_2O_2$ in the absence of a reducing substrate, which did not occur in the presence of a reducing substrate. Hence, the aim of the work presented in this chapter was to establish in more detail the nature of these perturbations. The reactivity of wild-type rAPX with $H_2O_2$ has been re-examined using UV/visible and EPR spectroscopies. Detection of a previously unresolved, protein-derived radical in quick-freeze EPR experiments suggests that wild-type rAPX is capable of supporting a protein radical. The implications of these data are discussed with reference to haem peroxidase Compound I stability and the possible role of a tryptophan-based radical in the physiological function of ascorbate peroxidase.

Throughout this chapter reference will be made to the reaction scheme illustrated in Figure 5-2, which indicates the various reaction pathways that have been identified during the course of this work.

rAPX(Fe$^{III}$,P,Trp)

Ferric resting-state

$+ 1\ eq\ H_2O_2$
$k_1 = (6.36 \pm 0.19) \times 10^7\ M^{-1}s^{-1}$

rAPX(Fe=O,P$^{\bullet+}$,Trp)

Compound I

$+ 1\ eq$ L-ascorbic acid
$k_2 = (2.96 \pm 0.10) \times 10^7\ M^{-1}s^{-1}$

XS H$_2$O$_2$

rAPX(Fe=O,P,Trp$^{\bullet+}$)

Compound I*

rAPX(Fe=O,P,Trp)

Compound II

rAPX(Fe$^{II}$-O$_2$,P,Trp)

Compound III

$k_{decay}' = (2.7 \pm 0.3) \times 10^{-4}\ s^{-1}$

$k_{decay} = (1.1 \pm 0.2) \times 10^{-3}\ s^{-1}$

rAPX(Fe$^{III}$,P,TrpOH)

Ferric-like

rAPX(Fe$^{III}$,P,Trp)

Ferric resting-state
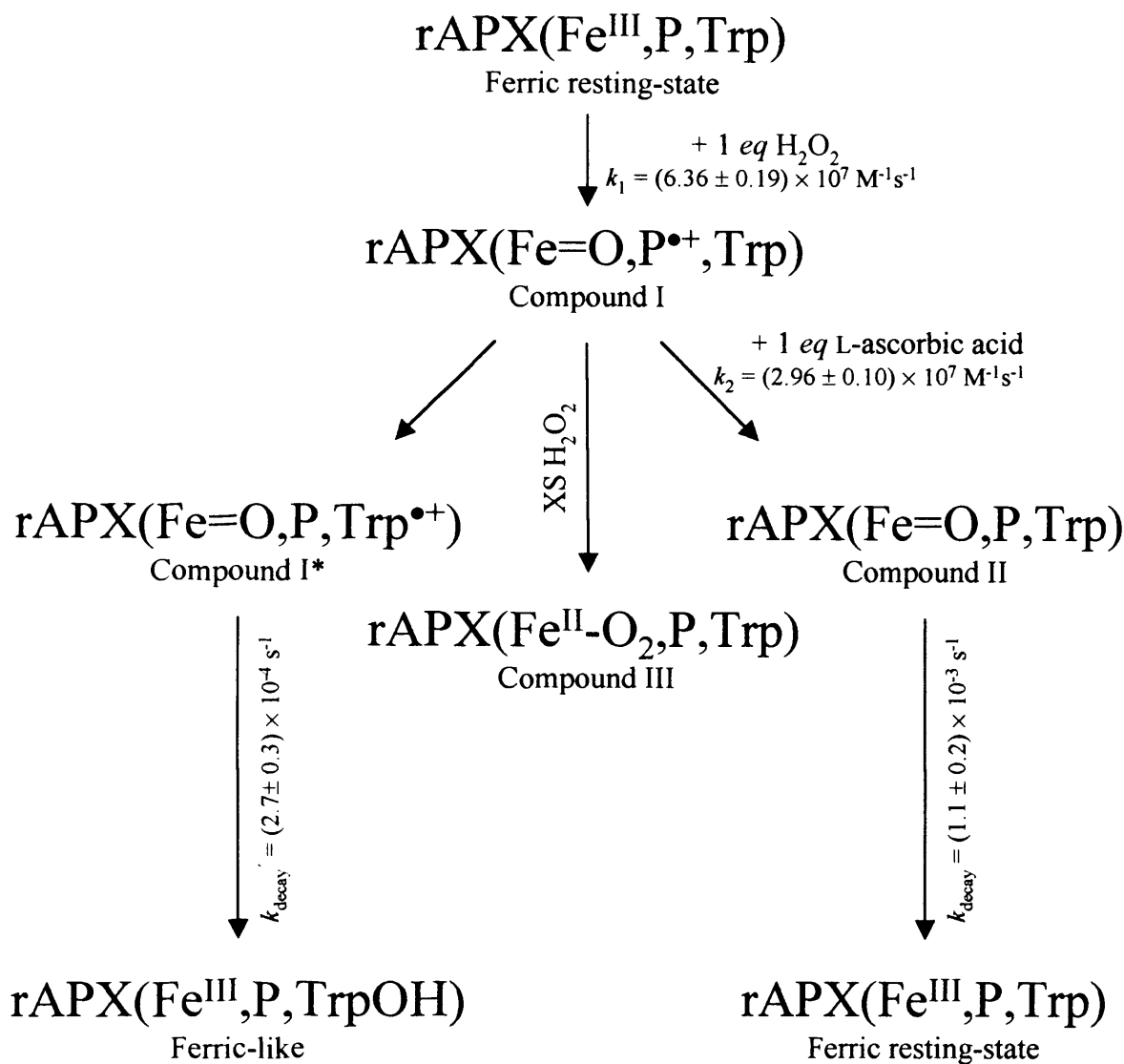
**Figure 5-2 Proposed kinetic scheme for the reaction of APX with H$_2$O$_2$ in the absence and presence of ascorbate.** Second-order rate constants $k_1$ and $k_2$ are taken from Chapter 4 (pH 7.0, 5°C). Scheme modified from [Hiner, A. N. P., Martínez, J. I., Arnao, M. B., Acosta, M., Turner, D. D., Raven, E. and RodríguezLópez, J. N. (submitted for publication)].

173

# Results

## 5.1 Electronic absorption spectroscopy

This section summarises the UV/visible electronic absorption spectra obtained for the various rAPX species observed in the course of re-examining the reaction between wild-type rAPX and stoichiometric amounts of hydrogen peroxide, in the presence and absence of ascorbate. The spectroscopic properties of several discrete oxidised species of wild-type rAPX are compared.

### 5.1.1 Spectrophotometric peroxide titration

Addition of an equimolar amount of $H_2O_2$ to ferric wild-type rAPX, Figure 5-3, resulted in rapid formation of Compound I – too transient to be detected by traditional UV/visible electronic absorption spectroscopy – followed by immediate (within several minutes) conversion to a species designated hereafter as Compound I*. The spectroscopic features of the final species ($\lambda$/nm = 414, 528, 559 & $350^{sh}$) were reminiscent of HRP Compound II[2] and CcP Compound I,[12] which supports the retention of the oxyferryl haem-iron centre, $Fe^{IV}{=}O$, in Compound I*. Although, the spectroscopic features of this oxidised species of wild-type rAPX[29] ($\lambda$/nm = 413, 532, 560 nm using 1:1 rAPX:$H_2O_2$) and native enzyme[30] ($\lambda$/nm = 413, 528 & 558 using 1:10 APX:$H_2O_2$) have been reported previously, the spectra have not been examined in detail; hitherto, the stable decay product that forms following the spontaneous decay of Compound I has been ascribed as Compound II and not recognised as a separate species.
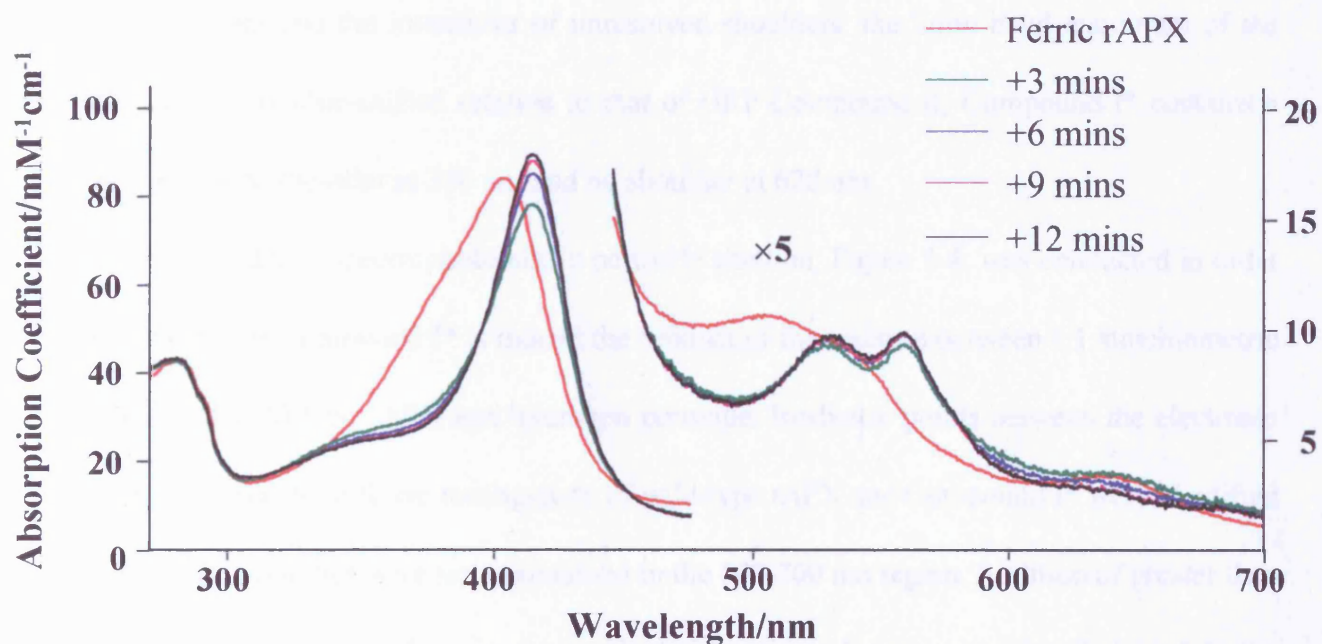
**Figure 5-3 UV/visible spectra of Compound I\* formation.** Rapid-scanning electronic absorption spectra (480 nm/min) of wild-type rAPX after the addition of an equimolar amount of hydrogen peroxide. The time that the sample has been exposed to peroxide is indicated in the legend. Normalisation has been made with respect to the calculated millimolar absorption coefficient; the region 450-700 nm has been multiplied by a factor of five. Sample conditions: ~1 μM wild-type rAPX, 5°C, pH 7.0 NaPi μ = 0.1 M.

For comparison, a sample of HRP Compound II was prepared with slightly less than an equimolar amount of $H_2O_2$ in the presence of a slight excess of ascorbic acid. The spectroscopic features of HRP Compound II ($\lambda$/nm = 418, 527, 554, $350^{sh}$ & $628^{sh}$) were found to be consistent with previous literature.[2] Careful examination of the UV/visible spectra of HRP Compound II and APX Compound I* revealed small but significant differences in the peak positions and the intensities of unresolved shoulders: the Soret band maximum of the APX species is blue-shifted relative to that of HRP Compound II; Compound I* contains a less prominent shoulder at 350 nm and no shoulder at 628 nm.

Subsequently, a spectrophotometric peroxide titration, Figure 5-4, was conducted in order to confirm that Compound I* is indeed the product of the reaction between 1:1 stoichiometric amounts of wild-type rAPX and hydrogen peroxide. Isosbestic points between the electronic absorption spectra of ferric resting-state of wild-type rAPX and Compound I* were identified at 407 & 451 nm, but were not maintained in the 500-700 nm region. Addition of greater than 1 molar equivalent resulted in the gradual formation of a new species, Figure 5-5, the spectroscopic features of which ($\lambda$/nm = 414, 539, 574 & $350^{sh}$) were consistent with those of an oxyperoxidase complex, i.e. Compound III.[31] Accordingly, in the absence of a reducing substrate, the predominant oxidised species present in samples of wild-type rAPX incubated with an equimolar amount of $H_2O_2$ is Compound I*.

Consistent with previously published data,[23] wild-type rAPX Compound I* was relatively stable and persisted for several hours – the first order rate constant of this decay ($k_{decay}'$ in Figure 5-2), has been measured (by Dr N. Rodríguez-López) as (2.7 ± 0.3) × $10^{-4}$ $s^{-1}$.[32] However, in apparent disagreement with the published data, careful monitoring of Compound I* decay revealed that the resulting enzyme species was spectroscopically different from that of authentic ferric rAPX. Subsequently, 'stop-start' turnover experiments – involving the
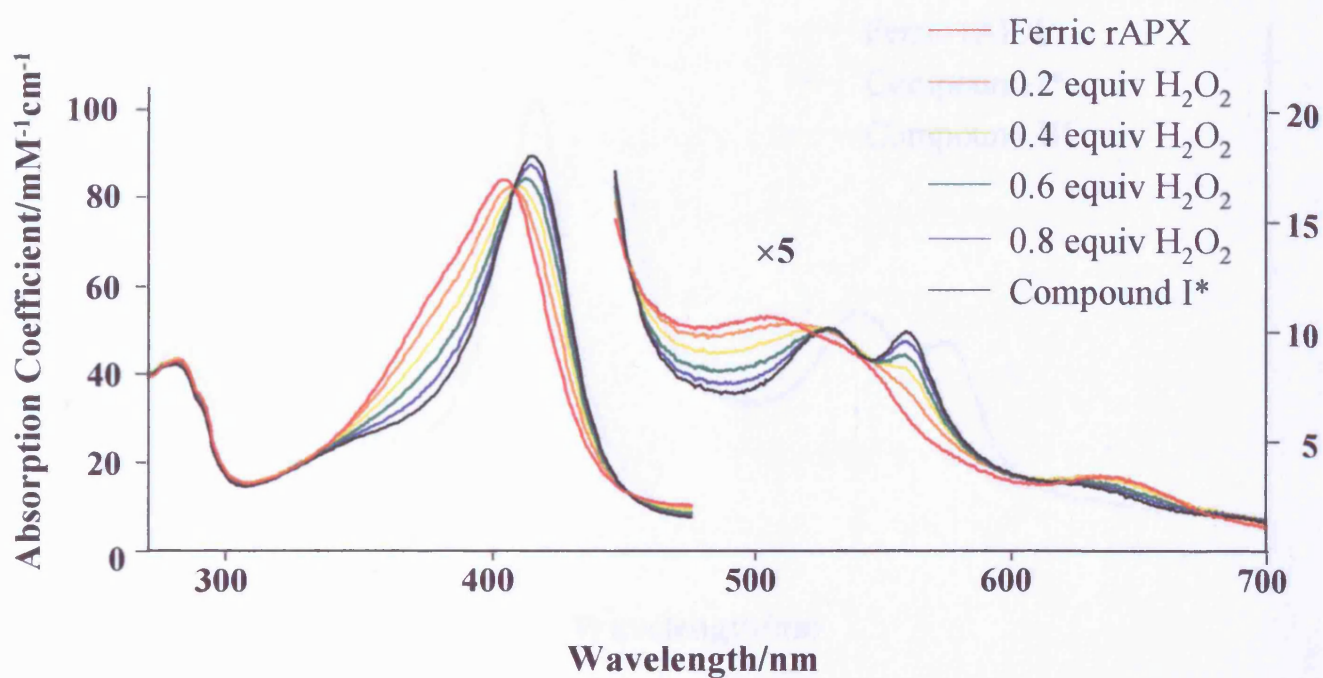
**Figure 5-4 Spectrophotometric peroxide titration.** Normalisation has been made with respect to the calculated millimolar absorption coefficient; the region 450-700 nm has been multiplied by a factor of five. Selection of overlaid UV/visible spectra obtained throughout a titration of ferric wild-type rAPX with hydrogen peroxide. Sample conditions: ~1 μM wild-type rAPX, 25°C, pH 7.0 NaPi μ = 0.1 M.
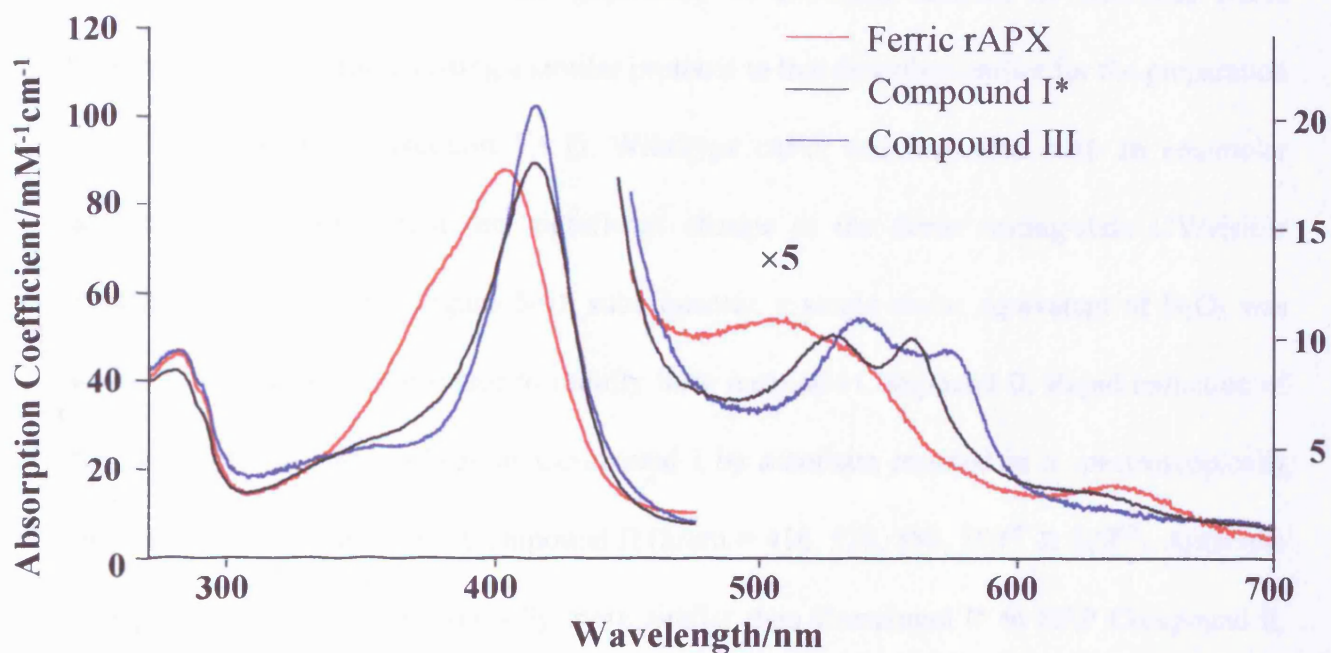
**Figure 5-5 Formation of Compound III.** Normalisation has been made with respect to the calculated millimolar absorption coefficient; the region 450-700 nm has been multiplied by a factor of five. Compound I* was formed from the addition of an equimolar amount of hydrogen peroxide to wild-type rAPX, and Compound III was formed by addition of a 20-fold excess of peroxide. Sample conditions: ~1 μM wild-type rAPX, 25°C, pH 7.0 NaPi μ = 0.1 M.

stepwise addition of stoichiometric quantities of hydrogen peroxide and ascorbate to samples of wild-type rAPX – have resolved this apparent discrepancy (section 5.1.3).

## 5.1.2 Authentic Compound II

An alternative method for the generation of authentic samples of wild-type rAPX Compound II was adopted using a similar protocol to that described earlier for the preparation of HRP Compound II (section 5.1.1). Wild-type rAPX was incubated with an equimolar amount of L-ascorbic acid, no significant change to the ferric resting-state UV/visible spectrum was observed (Figure 5-6); subsequently, a single molar equivalent of $H_2O_2$ was added to the incubation mixture to rapidly form authentic Compound II. Rapid reduction of the porphyrin π-cation radical of Compound I by ascorbate resulted in a spectroscopically distinct species (Figure 5-6), Compound II ($\lambda$/nm = 416, 528, 559, $350^{sh}$ & $628^{sh}$). Authentic Compound II was spectroscopically more similar than Compound I* to HRP Compound II, Table 5-1. More importantly, the isosbestic points observed between the ferric resting-state and Compound I* ($\lambda$/nm = 407 & 451 nm), and the ferric resting-state and Compound II ($\lambda$/nm = 407.5, 449, 521, 598 nm) were noticeably different. Simultaneous addition of an equimolar amount of ascorbate and peroxide to wild-type rAPX resulted in incomplete formation of Compound II (Figure 5-6).

Authentic Compound II was also not as stable as Compound I* – the first order rate constant of this decay ($k_{decay}$ in Figure 5-2), has been measured (by Dr N. Rodríguez-López) as $(1.1 \pm 0.2) \times 10^{-3}$ s$^{-1}$.[32] At pH 7.0, time-dependent UV/visible spectra revealed that Compound II gradually converts to another species that is spectroscopically indistinguishable
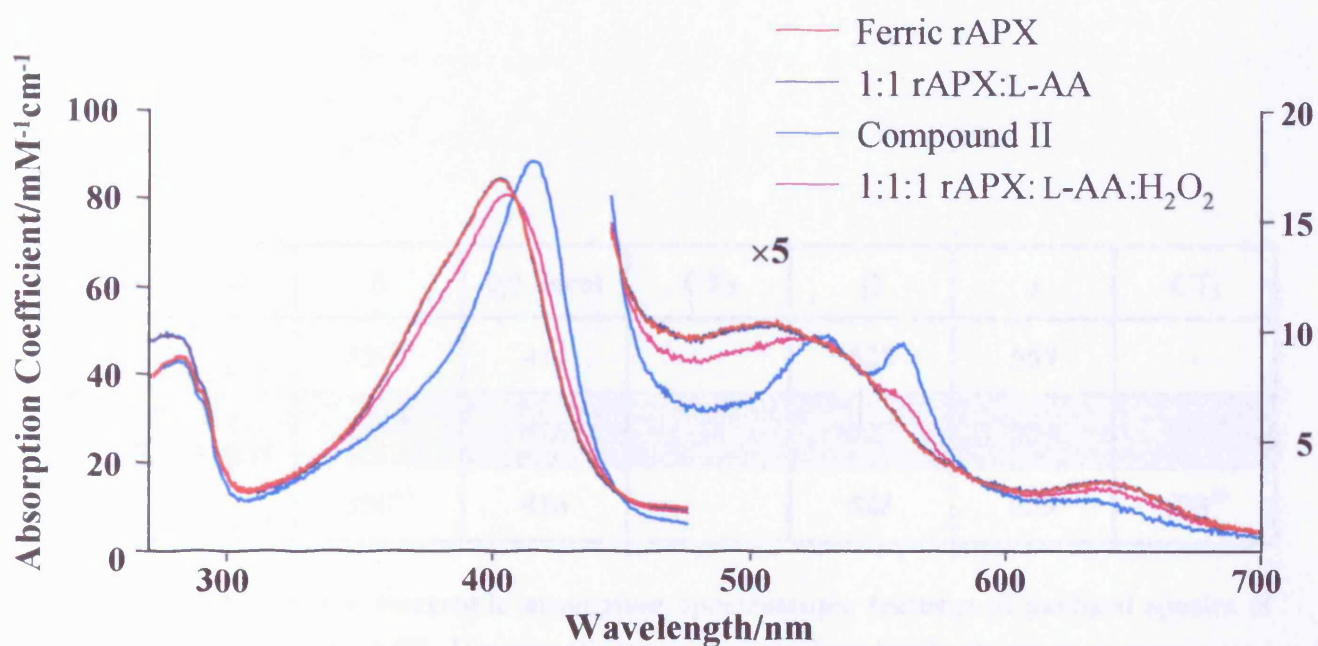
**Figure 5-6 UV/visible electronic absorption spectrum of Compound II.** Normalisation has been made with respect to the calculated millimolar absorption coefficient; the region 450-700 nm has been multiplied by a factor of five. Compound II was formed from the addition of an equimolar amount of hydrogen peroxide to wild-type rAPX incubated in the presence of an equimolar amount of L-ascorbic acid. Simultaneous addition of equimolar amounts of both hydrogen peroxide and L-ascorbic acid resulted in <20% Compound II formation. Sample conditions: ~1 μM wild-type rAPX, 25°C, pH 7.0 NaPi μ = 0.1 M.

| Derivative | δ | (γ) Soret | CT$_2$ | β | α | CT$_1$ |
|---|---|---|---|---|---|---|
| rAPX Compound I* | 350$^{sh}$ | 414 | - | 528 | 559 | - |
| HRP Compound II | 350$^{sh}$ | 418 | - | 527 | 554 | 628$^{sh}$ |
| rAPX Compound II | 350$^{sh}$ | 416 | - | 528 | 559 | 628$^{sh}$ |

Table 5-1 UV/visible electronic absorption spectroscopic features of oxidised species of HRP and wild-type rAPX. Wavelength maxima of resolved bands are given in nanometers, "$^{sh}$"denotes unresolved shoulder. All spectra were obtained at 25.0°C, pH 7.0 NaPi μ= 0.10 M.

from the ferric resting-state. Subsequently, 'stop-start' turnover experiments confirm that unmodified wild-type rAPX is regenerated by reduction of authentic Compound II (section 5.1.3).

## 5.1.3 'Stop-start' turnover experiments

As mentioned above, spontaneous decay of Compound II and Compound I* proceeds at measurably different rates and results in the formation of distinct species (Figure 5-2).[32] Single and multiple 'stop-start' turnover experiments were designed to confirm whether only one or both of these species was relevant to the normal peroxidase activity of wild-type rAPX.

As outlined previously, Compound I* is readily prepared by reacting wild-type rAPX with a single mole equivalent of hydrogen peroxide and allowing the resulting Compound I to decay spontaneously. Complete formation of Compound I*, was confirmed spectrophotometrically through the absorbance at its Soret band absorption maximum, i.e. $A_{414}$; a stoichiometric excess of L-ascorbic acid was then added in an attempt to regenerate the ferric resting-state. However, the rapid reaction resulted in formation of a new 'ferric-like' species that is characterised by a 406 nm Soret band absorption maxima, Figure 5-7. This ferric-like species is spectroscopically similar, but not identical to, authentic ferric wild-type rAPX. Analogous 'stop-start' turnover experiments were performed using Compound II, which was prepared by incubating the enzyme with an equimolar amount of L-ascorbic acid followed by addition of a single molar equivalent of hydrogen peroxide. In contrast to the reaction between Compound I* and ascorbate, the addition of a stoichiometric excess of L-ascorbic acid to Compound II rapidly returned the oxidised-species of the enzyme to its original ferric resting-state, Figure 5-8.
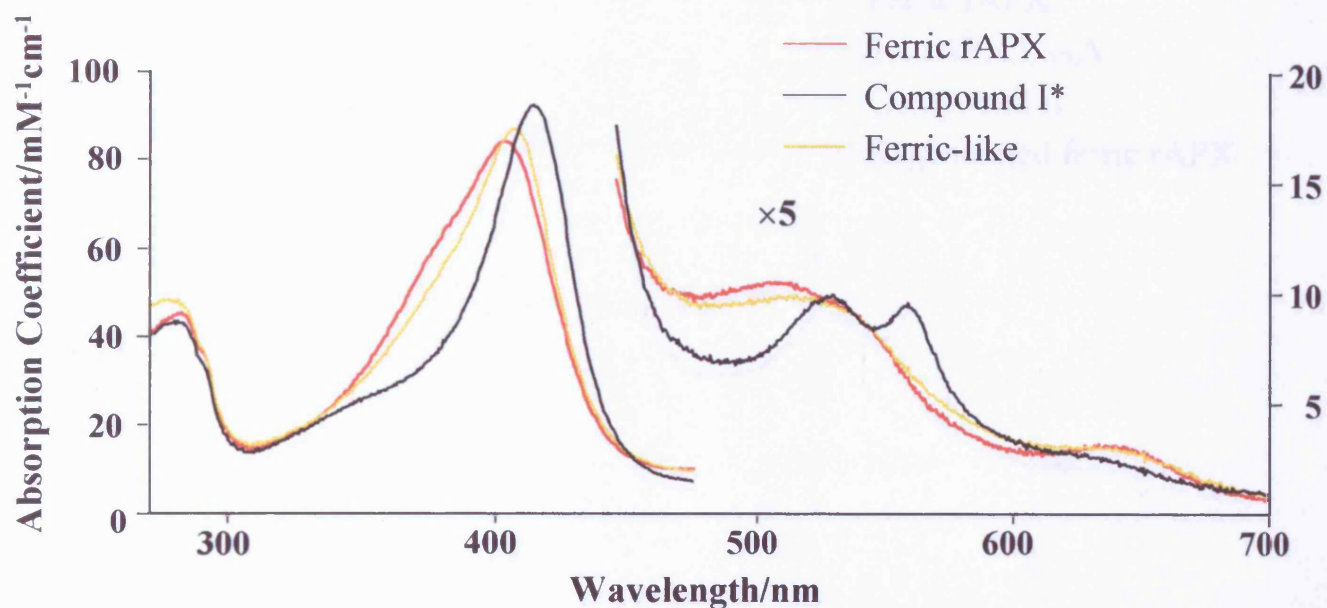
**Figure 5-7 UV/visible electronic absorption of ferric-like wild-type rAPX.** Normalisation has been made with respect to the calculated millimolar absorption coefficient; the region 450-700 nm has been multiplied by a factor of five. Addition of a slight molar excess of L-ascorbic acid to Compound I* resulted in formation of ferric-like rAPX. Sample conditions: ~1 µM wild-type rAPX, 25°C, pH 7.0 NaPi µ = 0.1 M.
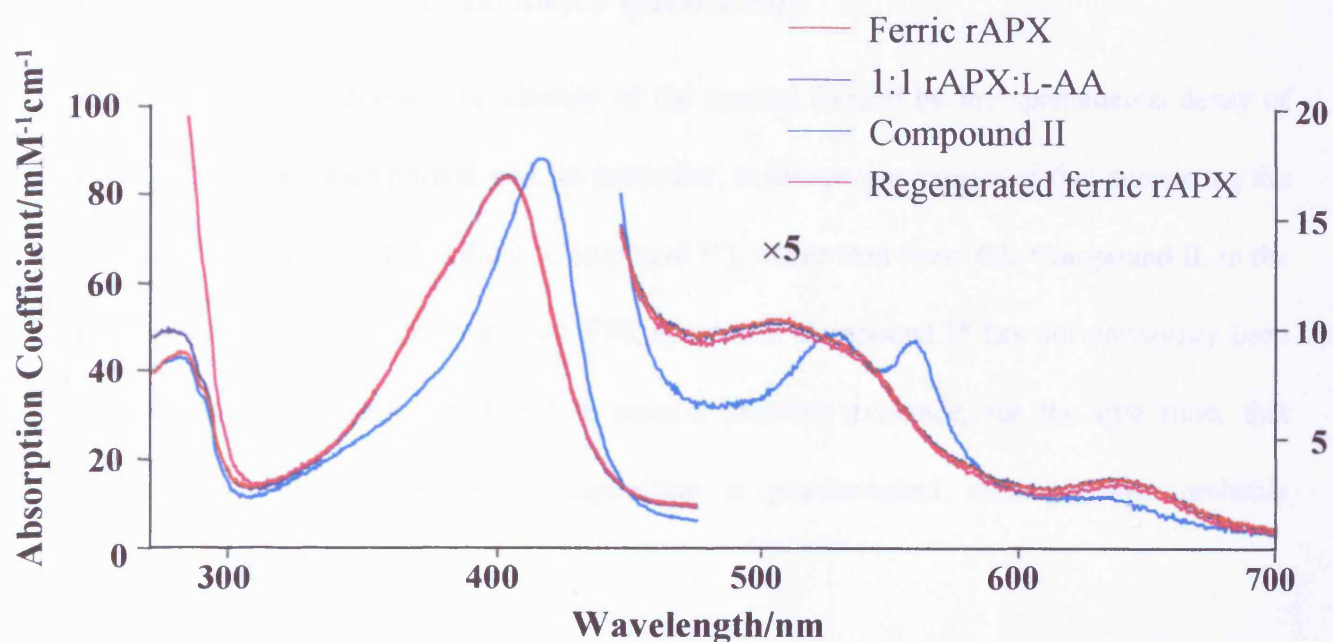
**Figure 5-8 'Stop-start' turnover of wild-type rAPX.** Normalisation has been made with respect to the calculated millimolar absorption coefficient; the region 450-700 nm has been multiplied by a factor of five. Addition of a slight molar excess of L-ascorbic acid to Compound II regenerated the original ferric resting-state spectrum. Sample conditions: ~1 μM wild-type rAPX, 25°C, pH 7.0 NaPi μ = 0.1 M.

Successive 'stop-start' turnover (>10 times) of wild-type rAPX, repeatedly cycling through Compound II, did not significantly affect the resulting ferric resting-state UV/visible absorption spectrum, and were equivalent to incubating the enzyme in an excess of L-ascorbic acid and performing successive stepwise additions of peroxide (as shown in Figure 5-9).

## 5.2 Electron paramagnetic resonance spectroscopy

In the previous section, the identity of the species formed by the spontaneous decay of Compound I was re-examined and, in particular, evidence was presented that supporting the formation of a novel intermediate (Compound I*), rather than *bona fide* Compound II, in the absence of a reducing-substrate. The EPR spectra of Compound I* has not previously been examined and the data introduced in section provides evidence, for the first time, that wild-type rAPX is capable of supporting a protein-based radical (most probably tryptophan-based).

### 5.2.1 Detection of a protein-based radical

Samples of wild-type rAPX were provided to Dr. J. N. Rodríguez-López (Departmento de Bioquímica y Biología Molecular-A, Universidad de Murcia, Spain) and Dr. M. Acosta (Departamento de Biología Vegetal (Fisiología Vegetal), Facultad de Biología, Universidad de Murcia, Spain) for EPR analysis using a Bruker ESP380E spectrometer. A manually operated rapid mixing device was used to prepare samples of Compound I at room temperature, by reacting wild-type rAPX with 0.97 mole equivalents of $H_2O_2$; aliquots 100 μL of the Compound I solution were injected into EPR tubes and flash-frozen at 77K at different reaction times.[32]
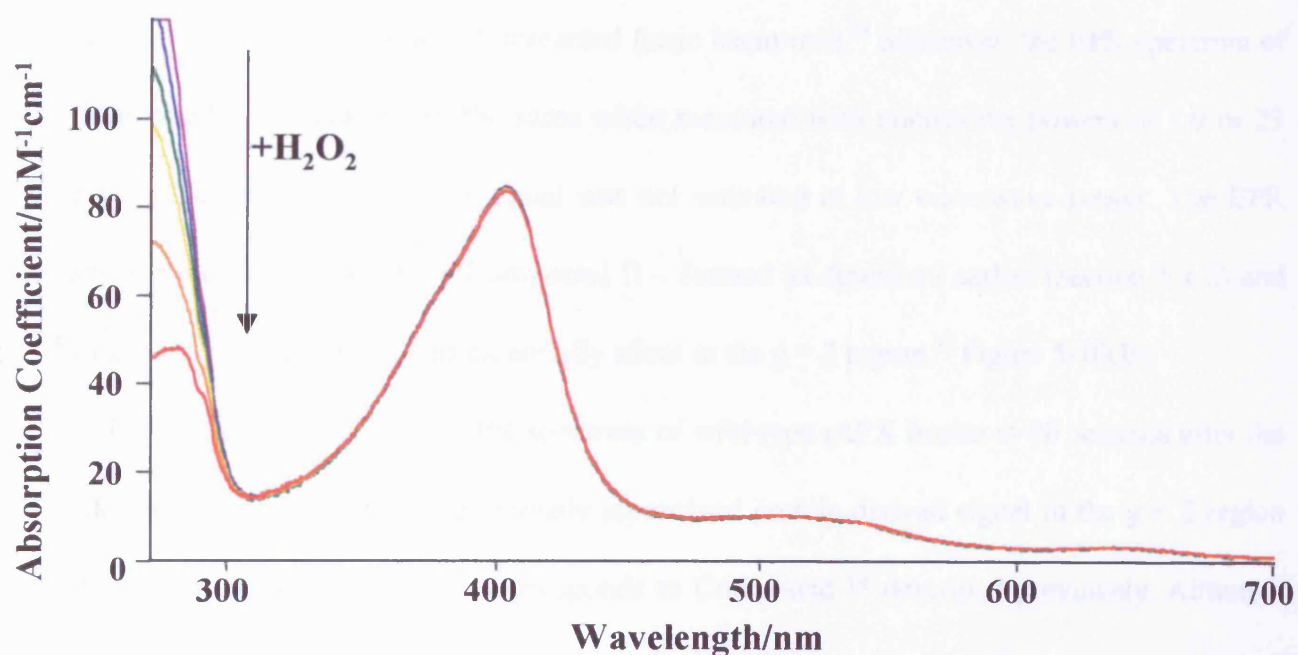
**Figure 5-9 Stepwise turnover of wild-type rAPX.** Normalisation has been made with respect to the calculated millimolar absorption coefficient; the region 450-700 nm has been multiplied by a factor of five. Incubation of wild-type rAPX in a 20-fold molar excess of L-ascorbic acid followed by successive additions of 1 molar equivalent of hydrogen peroxide. [The absorbance decrease <300 nm corresponds to the oxidation of ascorbate.] Sample conditions: ~1 μM wild-type rAPX, 25°C, pH 7.0 NaPi μ = 0.1 M.

186

A quick-freeze experiment was performed in which the product of the reaction of wild-type rAPX with 0.97 equivalent of $H_2O_2$ was frozen at 77K within 5 seconds. The EPR spectrum obtained, Figure 5-10(A), was comprised of two clearly resolved signals at $g = 3.3$ and $g = 1.99$,[32] and was consistent to that previously reported for wild-type rAPX Compound I.[24] The presence of an additional feature, at $g = 6.00$, was observed and has been assigned as arising from a small amount of unreacted ferric haem-iron.[24] Moreover, the EPR spectrum of Compound I was essentially the same when measured with microwave powers of 1.0 or 23 mW, which indicates that the signal was not saturated at low microwave power. The EPR spectrum of wild-type rAPX Compound II – formed as described earlier (section 5.1.2) and frozen after 10 seconds – was essentially silent in the $g = 2$ region,[32] Figure 5-10(B).

Close examination of the EPR spectrum of wild-type rAPX frozen at 90 seconds after the addition of $H_2O_2$ revealed a previously unresolved protein-derived signal in the $g = 2$ region (Figure 5-11), which probably corresponds to Compound I* described previously. Although the "parallel" part of this new axial signal ($g_{\parallel} = 2.038$) is well resolved, the "perpendicular" part of this signal ($g_{\perp} = 2.005$) is superimposed onto the high field part of the remaining porphyrin $\pi$-cation radical signal ($g = 1.99$). At 10K, the Compound I* signal showed saturation even at very low microwave power and resolution was considerably worse at 0.9 mW than 4.6 $\mu$W (Figure 5-11 A & B respectively). The EPR spectrum of Compound I* was also obtained at 70K using a microwave powers of 1.0 mW and 0.1 mW (Figure 5-11 C & D), and saturation effects were evident even with the lower microwave power. The temperature-dependent behaviour and shape of the Compound I* signal are similar to those described for the tryptophan radical detected in F221W variant HRP,[33] but differ from those observed for the radical in CcP.[34,35]
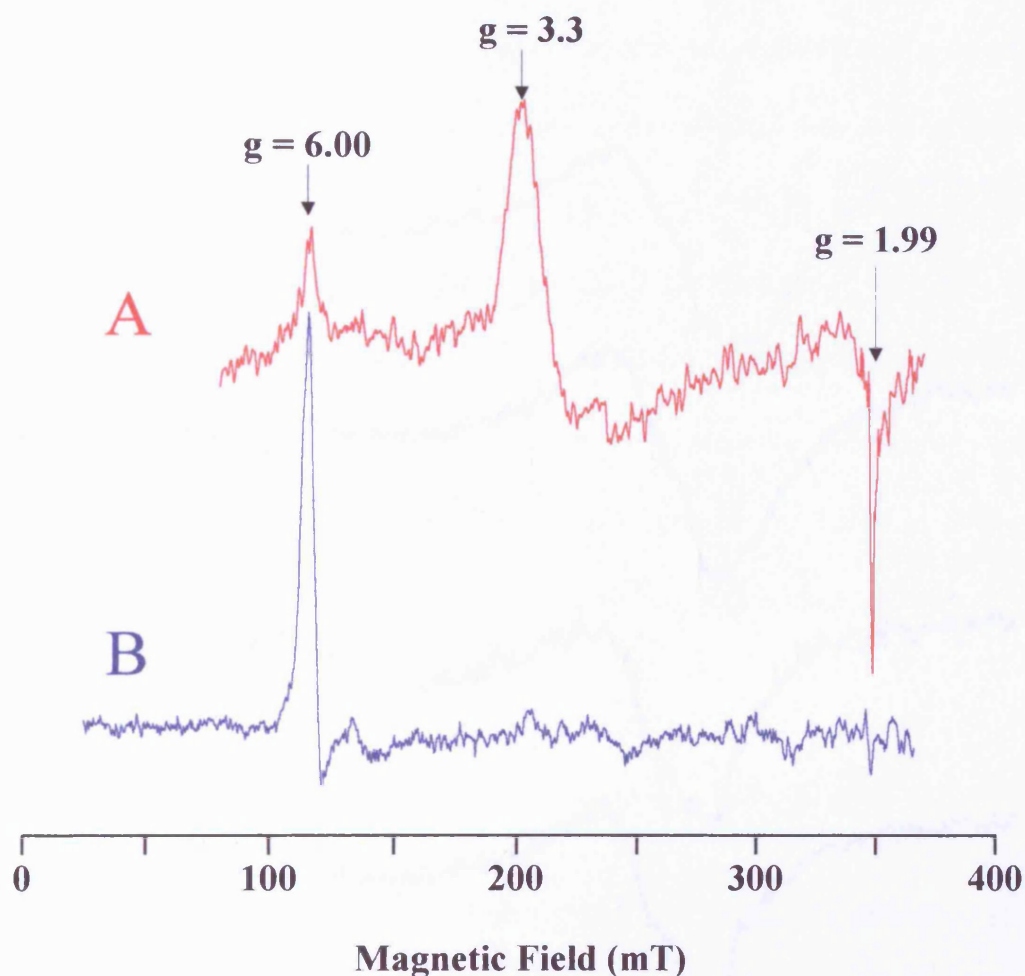
**Figure 5-10 Quick-freeze electron paramagnetic resonance spectra of wild-type rAPX Compound I and Compound II.** Sample conditions: A: EPR spectrum of Compound I (10 K, microwave power 23 mW) recorded 5 s after the reaction of wild-type rAPX (70 $\mu$M) with 68 $\mu$M of $H_2O_2$. B: EPR spectrum of Compound II (10 K, microwave power 0.9 mW) recorded 5 s after the reaction of wild-type rAPX (70 $\mu$M) with 68 $\mu$M of $H_2O_2$ in the presence of 68 $\mu$M ascorbic acid. The microwave frequency was 9.706 GHz for both spectra.
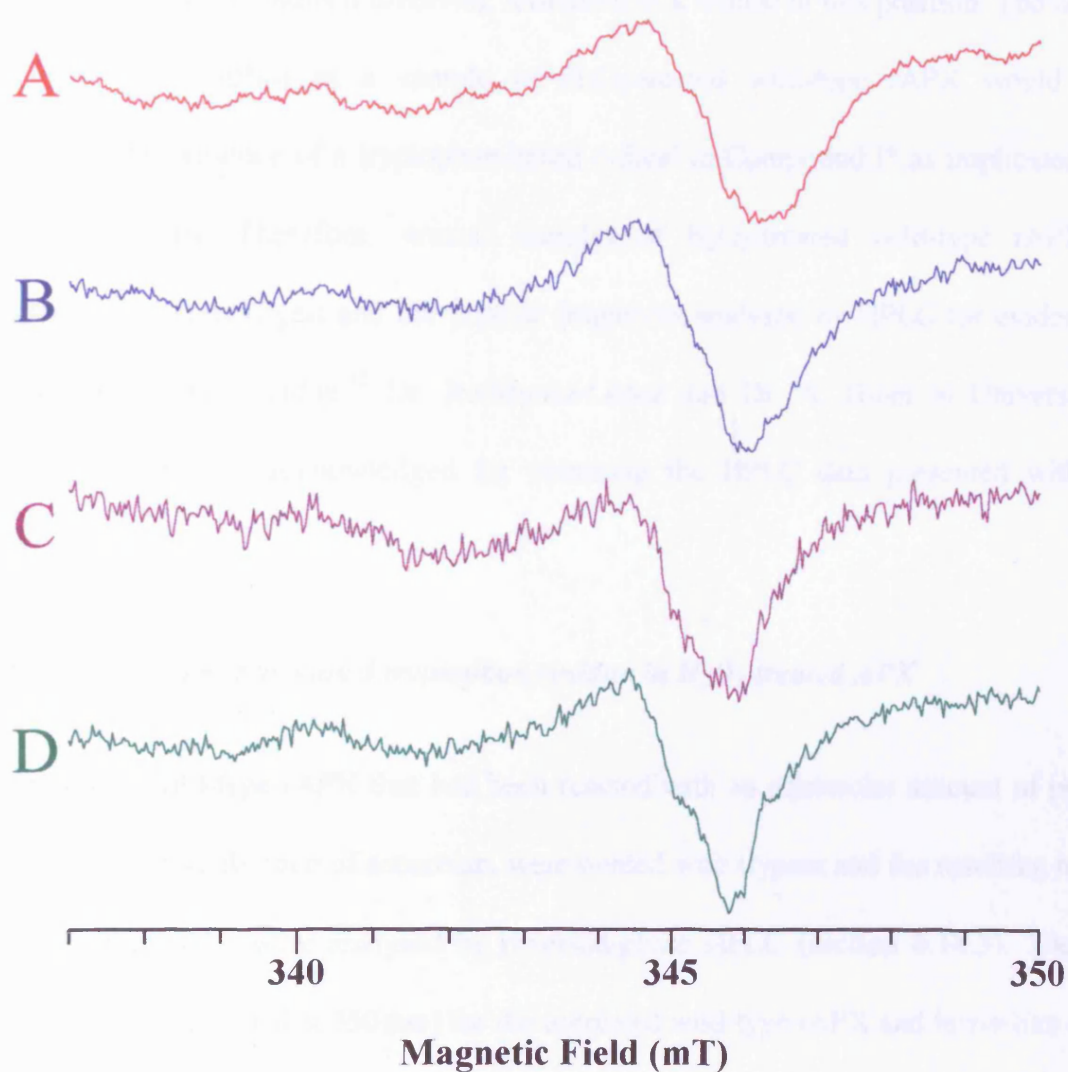
**Figure 5-11 Electron paramagnetic resonance spectra of Compound I\*.** Resolution of of a protein-based radical signal at different temperatures and microwave powers: A – 10 K, 0.9 mW; B – 10 K, 4.6 µW; C – 70 K, 1 mW; and D – 70 K, 0.1 mW (microwave frequency and the modulation amplitude were 9.706 GHz and 5.1 G, respectively, for all spectra). All samples were frozen 90 s after the start of the reaction of wild-type rAPX (70 µM) with 68 µM of $H_2O_2$.

## 5.3 Reverse-phase HPLC protein chromatography

Treatment of lignin peroxidase (LiP) with hydrogen peroxide results in the formation of a hydroxylated tryptophan residue,[36] which has been identified as being due to modification of LiP at Trp171 by a mechanism involving formation of a radical at this position. The detection of β-hydroxy-tryptophan in a sample of $H_2O_2$-treated wild-type rAPX would further substantiate the presence of a tryptophan-based radical in Compound I* as implicated by the EPR spectroscopy. Therefore, several samples of $H_2O_2$-treated wild-type rAPX were subjected to a tryptic digest and the peptide fragments analysed by HPLC for evidence of a modified tryptophan residue.[32] Dr. Rodríguez-López and Dr. A. Hiner at Universidad de Murcia are gratefully acknowledged for obtaining the HPLC data presented within this section.

### 5.3.1 Detection of a β-hydroxylated tryptophan residue in $H_2O_2$-treated APX

Samples of wild-type rAPX that had been reacted with an equimolar amount of peroxide, in the presence and absence of ascorbate, were treated with trypsin and the resulting mixtures of peptide fragments were analysed by reversed-phase HPLC (section 6.14.3). The HPLC chromatograms (recorded at 330 nm) for the untreated wild-type rAPX and ferric-like enzyme samples are shown in Figure 5-12.

In the HPLC chromatogram of the ferric-like sample, a peak with a retention time of 22 minutes is detected that is not present in the chromatogram of untreated wild-type rAPX. The electronic absorption spectrum of the peak (Figure 5-13) was similar to that of β-hydroxy-tryptophan detected in LiP[36] after treatment with $H_2O_2$. Furthermore, the identified modification of the tryptophan requires a mechanism involving formation of a radical at this
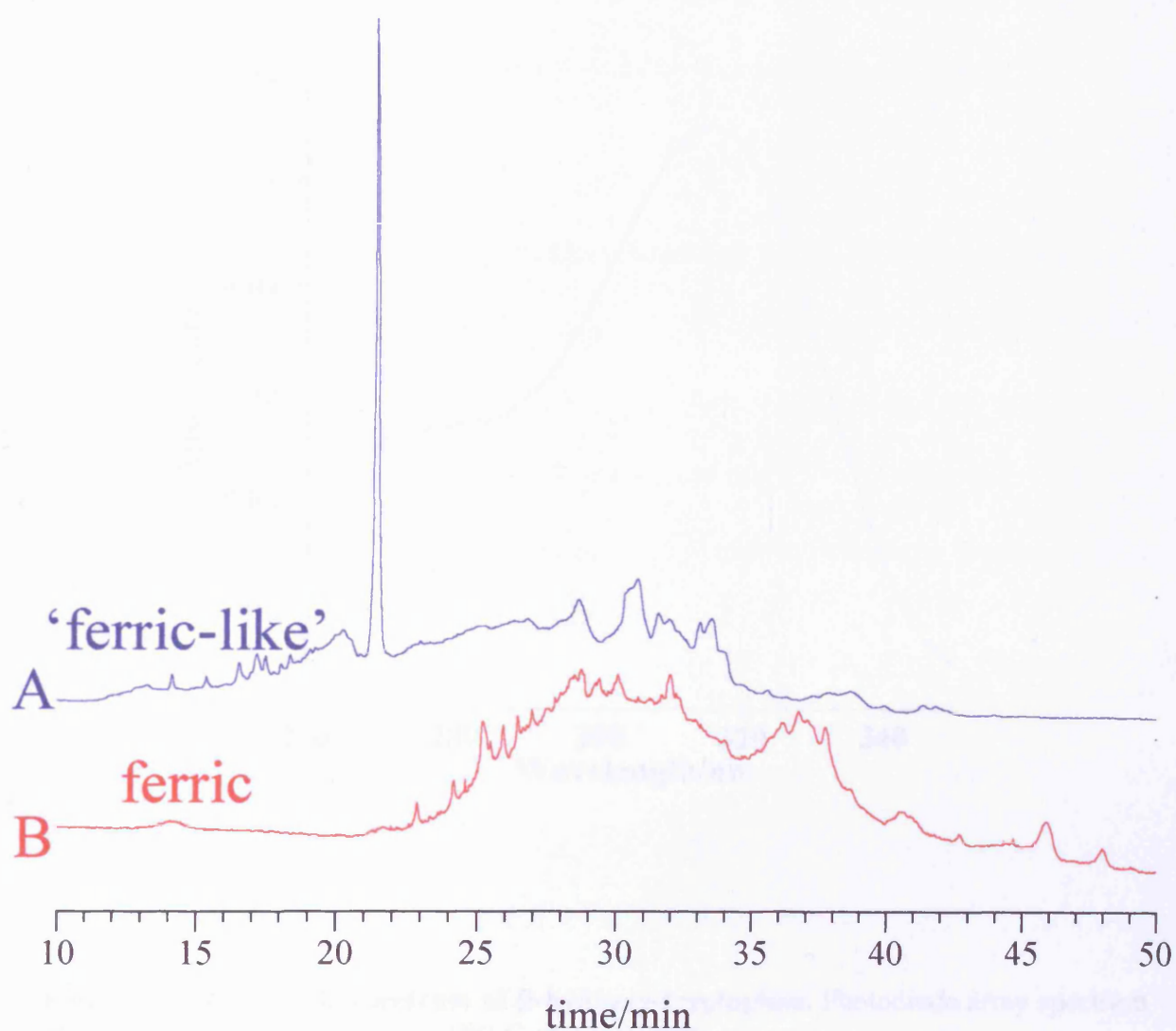
**Figure 5-12 HPLC traces of tryptic fragments of ferric and 'ferric-like' wild-type rAPX.** Samples were applied to a C-18 reversed phase HPLC column after digestion with trypsin (see text). Chromatograms were recorded at 330 nm. (A) Untreated ferric wild-type rAPX. (B) Ferric-like APX made by 3 hour incubation of the enzyme with 1 eq. of $H_2O_2$. (Inset) Absorption spectrum of the 22 min peak in trace B.
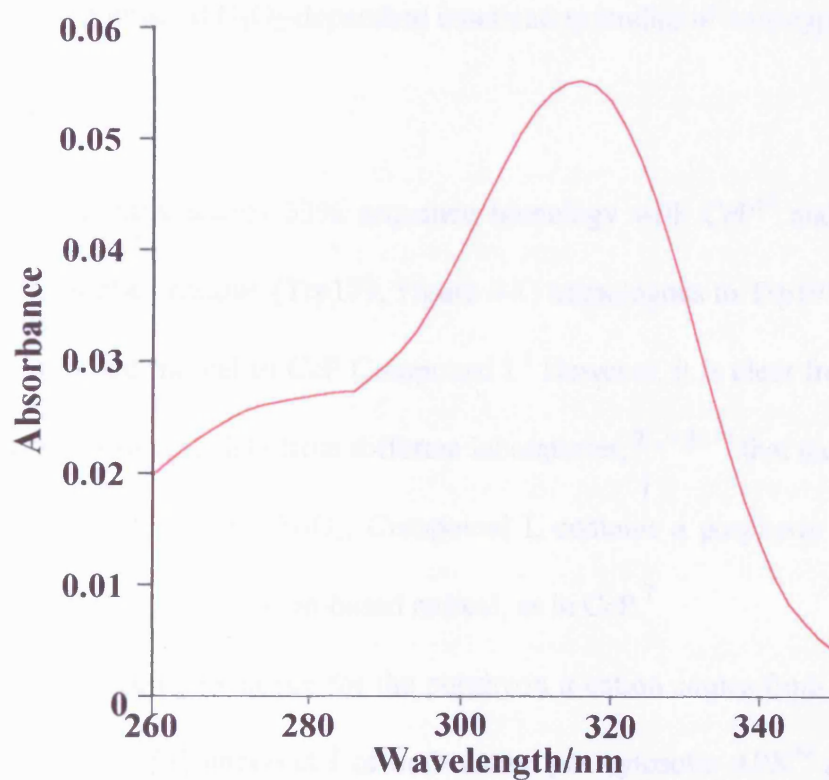
**Figure 5-13 UV/visible spectrum of β-hydroxy-tryptophan.** Photodiode array spectrum of the 22 min peak in ferric-like HPLC chromatogram.

position: as wild-type rAPX incubated with ascorbate prior to the addition of $H_2O_2$ did not undergo any changes compared to untreated APX. Therefore, ascorbate acts as a protective agent to irreversible chemical modification of wild-type rAPX by peroxide, an observation consistent with published $H_2O_2$-dependent inactivation studies of wild-type rAPX.[37]

## 5.4 Discussion

Pea cytosolic APX shares 33% sequence homology with CcP[19] and contains the same active site tryptophan residue (Trp179, Figure 5-1) homologous to Trp191,[22] which is the site of the protein-based radical in CcP Compound I.[7] However, it is clear from the consensus of kinetic and spectroscopic data from different laboratories,[23,24,30,32] that the initial intermediate in the reaction of APX with $H_2O_2$, Compound I, contains a porphyrin $\pi$-cation radical, as found in HRP,[18] and not a protein-based radical, as in CcP.[7]

The most convincing evidence for the porphyrin $\pi$-cation comes from the similarity of the UV/visible spectra of Compound I of both native pea cytosolic APX[30] and wild-type rAPX (Raven, E. L. & Lad, L., unpublished data), and for tea APX[38,39] to those previously published for HRP,[3] and also from EPR data for wild-type rAPX.[24] Thus, in terms of the electronic structure of its oxidised intermediates, the catalytic mechanism of wild-type rAPX is more like a class III peroxidase, i.e. classical plant peroxidase enzyme, than CcP. Indeed, various theoretical arguments[25-38] have been proposed that ostensibly rationalise the formation of the experimentally observed porphyrin $\pi$-cation instead of a CcP-like Compound I, with a protein-based radical located on Trp179. Specifically, the potassium-binding site present in wild-type rAPX, which is located in the vicinity of Trp179, is proposed to preclude radical formation at Trp179 on electrostatic grounds.[24] Indeed, the mutagenic incorporation of a

metal binding site, analogous to that found in APX, into CcP has been shown to destabilise radical formation at Trp191.[40,41]

Hence, although detection of a porphyrin π-cation radical was unexpected, the nature of wild-type rAPX Compound I has been rationalised in terms of the electrostatic environment in the vicinity of Trp179. However, whilst wild-type rAPX Compound I has been investigated spectroscopically, the inherent instability of the porphyrin π-cation intermediate has not been reconciled, or indeed examined in any depth whatsoever.

It has been previously established, in studies conducted using both recombinant wild-type[23,24] and native[30] enzymes, that the ferric resting-state of pea cytosolic APX reacts rapidly with a stoichiometric amount of $H_2O_2$ to form Compound I, a transient green species, with a UV/visible spectrum similar to that of HRP Compound I.[18] In the absence of ascorbate (or an alternative peroxidase substrate), Compound I rapidly evolves to a brown species that is spectroscopically similar to HRP Compound II,[18] and has previously been assigned to Compound II.[29,30,42] Wild-type rAPX Compound II prepared from aged Compound I, i.e. enzyme that has been reacted with peroxide and allowed to evolve in the absence of a reducing substrate, has been reported[23] as being: "...quite stable and 'relaxes' back to the ferric resting-state spectrum over a period of hours." (sic). However, spectroscopic data for authentic Compound II, i.e. Compound I that has been reduced by ascorbate (or an alternative peroxidase substrate), has not been published.

Recently, it has been observed that after incubation with a single mole equivalent of $H_2O_2$ the steady-state activity of wild-type rAPX with various reducing substrates was only approximately 80% that of enzyme not previously exposed to peroxide. Whilst, no difference was measured in steady-state activity for wild-type rAPX incubated with a single mole equivalent of $H_2O_2$ in the presence of ascorbate, i.e. under conditions that would allow the

194

enzyme to turnover normally. In contrast to the steady-state data, and as described in Chapter 4 (section 4.3.1), transient-state kinetics of Compound II reduction have been routinely conducted using pre-prepared Compound II.[29,43] No significant differences were measured in the observed rate constant, $k_{3,obs}$, obtained from sequential-mixing experiments, which generated authentic Compound II (Latesh Lad, unpublished data).

In the course of this work, small but persistent perturbations were noted in the UV/visible electronic absorption spectra of samples of ferric wild-type enzyme that had been exposed to $H_2O_2$ in the absence of reducing substrate, which did not occur in the presence of a reducing substrate. Indeed, spectrophotometric peroxide titration data have now shown that Compound I*, formed spontaneously from Compound I by reaction of 1 equivalent of $H_2O_2$ with ferric rAPX, possesses an electronic absorption spectrum that is different from compound I of rAPX itself and similar, but not identical, to both HRP Compound II and CcP Compound I.[3] Careful comparison of the electronic absorption spectra of Compound I* with a sample of authentic rAPX Compound II, formed by reaction of wild-type rAPX with $H_2O_2$ in the presence of ascorbate, also reveal small but significant differences, suggesting that Compound I* is quite distinct from Compound II.

The consensus drawn from the 'stop-start' turnover experiments – in which the enzyme was sequentially reacted with stoichiometric amounts of either hydrogen peroxide or ascorbate – is that Compound I formed in the absence of a suitable reducing substrate (e.g. ascorbate) does not evolve to *bona fide* Compound II. Indeed, consistent with the retention of both peroxide-derived oxidising equivalents, the porphyrin $\pi$-cation of Compound I is most probably reduced by an intramolecular electron-transfer reaction that results in permanent chemical modification of the polypeptide, however, the oxyferryl haem-iron is retained in Compound I*. The presence of an equimolar concentration of ascorbate was sufficient to

prevent irreversible changes to the haem chromophore, and resulted in rapid formation of authentic Compound II. Whilst wild-type Compound II could be readily reacted with ascorbate to regenerate the original ferric resting-state spectrum, the analogous reaction with Compound I* generated a new 'ferric-like' species that was characterised by a red-shift ($\lambda_{max}$ = 406 nm) and narrowing in the Soret band absorption peak. The 'ferric-like' species was perceptibly slower at reacting with a second equimolar amount of peroxide, which is consistent with published $H_2O_2$-inactivation data.[37]

EPR spectra obtained at low microwave power support this conclusion and seemingly indicate that formation of a protein-base radical accompanies conversion of Compound I to Compound I*. Hence, the shape and g-values for the EPR signal of rAPX Compound I* were almost identical to those found for CcP Compound I[34,35] and for the intermediate formed in the reaction of variant F221W of HRP with $H_2O_2$,[33] both of which are known to contain tryptophan-based radicals. Subsequently, this assignment was further substantiated by reverse-phase HPLC analysis of the tryptic fragments of untreated and 'ferric-like' samples of wild-type rAPX, where the detection of a new peak at 330 nm – which for LiP has been assigned[36] as arising from formation of a hydroxylated tryptophan residue through a mechanism involving radical formation at this position – provided clear evidence that the 'ferric-like' form of wild-type rAPX contains a β-hydroxy-tryptophan residue.

These data are consistent with the original observations that the decay product of Compound I formation, in the absence of substrate, is not spectroscopically identical to the ferric resting-state (even on addition of ascorbate to facilitate recovery of ferric enzyme) and is not the same as the decay product from an authentic sample of Compound II. Clearly, the formation and decay of the protein radical in rAPX leads to permanent changes in

spectroscopic properties and must also – by virtue of the diminished activity for the 'ferric-like' product[37] – have an effect on the functional ability of the enzyme.

A characteristic feature of the protein radical in wild-type rAPX Compound I* was its stability: Compound I* evolved to the 'ferric-like' species with a half-life of approximately 40 minutes, which is approximately 10-fold more slowly than the decay of Compound II. Therefore, the half-life of the protein-derived radical signal in Compound I* was longer than that of the tryptophan-based radical detected in CcP Compound I, which survives for more than 5 minutes in the absence of cytochrome c, and very much higher than the analogous intermediate identified in variant F221W of HRP, which completely disappears within 60 seconds.[33]

Whilst the exact location of the protein radical in rAPX is still not certain, by analogy with CcP the most likely candidate is Trp179. Although the physiological implications of radical formation in APX are currently not defined,[32] it is worth noting that LiP Compound I – a porphyrin π-cation radical – is similarly unstable in the absence of reducing substrate and an electron-transfer conduit between the haem and Trp171, leading to the formation of a radical at this position, has also been identified.[44,45]

The reaction of wild-type rAPX with hydrogen peroxide raises interesting questions as to the dynamics of radical formation and stability in haem peroxidases in general, particularly since various theoretical arguments have been put forward to account for the apparent inability of wild-type rAPX to support a CcP-like protein-based radical.[24-28] Hitherto, the potassium-binding site located ≈8 Å from Trp179[22] has been proposed to destabilise protein radical formation at this residue in wild-type rAPX, and the incorporation of a metal binding site, analogous to that found in wild-type rAPX, into CcP has been shown to destabilise radical formation at Trp191.[44,45] However, the quick-freeze EPR spectra obtained at low

microwave power suggest that wild-type rAPX can support a tryptophan-based radical. Whilst the location of this radical has yet to be assigned, it is clear that the factors affecting radical formation and stability are complex and, even for very closely related enzymes, are, at this stage, difficult to predict.

Formation of Compound I* is likely to have been a complicating factor in previous pre-steady state kinetics analyses of Compound II reduction, in which authentic samples of Compound II were assumed to have been formed by incubation of ferric wild-type rAPX with $H_2O_2$.[29,42] The similarity between the UV/visible electronic absorption spectra of Compound I* and authentic Compound II necessitates that care be taken in future to avoid erroneously describing the behaviour of wild-type rAPX.

## 5.5  Conclusions

Conclusions that can be drawn from the results presented in this chapter are as follows:

- Wild-type rAPX reacts rapidly with hydrogen peroxide to form Compound I, which contains a porphyrin $\pi$-cation radical; in the absence of an electron-donor substrate, Compound I spontaneously evolves to a novel species that has been designated Compound I*.

- Spectrophotometric peroxide titrations and 'stop-start' turnover experiments reveal that authentic Compound II, and not Compound I*, is formed in the reaction between wild-type rAPX and $H_2O_2$ in the presence of ascorbate.

- The EPR spectrum of Compound I* has been obtained and, at low microwave powers, signals attributable to a tryptophan-based radical ($g_{\parallel} = 2.038$ & $g_{\perp} = 2.005$) are resolved.

- Reaction of Compound I* with ascorbate does not regenerate the original ferric resting-state, and instead results in the formation of a 'ferric-like' species.

- Detection of $\beta$-hydroxy-tryptophan in the HPLC chromatogram of tryptic-digest fragments of 'ferric-like' wild-type rAPX supports formation of a tryptophan-based radical in Compound I*.

- The location of the tryptophan-based radical is the focus of ongoing research.

## 5.6 References

1 Dunford, H. B. (1991) in *Peroxidases in Chemistry and Biology.* (Everse, J., Everse, K. E. & Grisham, M. B., eds) pp. 1-24, CRC Press, Boca Raton FL

2 Dunford, H. B. and Stillman, J. S. (1976) *Coord. Chem. Rev.*, **19**, 187-251

3 Dunford, H. B. (1999) *Heme Peroxidases*, Wiley-VCH, New York, Chichester, Weinheim, Brisbane, Singapore, Toronto.

4 Erman, J. E., Vitello, L. B., Mauro, J. M. and Kraut, J. (1989) *Biochemistry*, **28**, 7992-7995

5 Erman, J. E. (1998) *J. Biochem. Mol. Biol.*, **31**, 307-327

6 Yonetani, T., Schleyer, H. and Ehrenberg, A. (1966) *J. Biol. Chem.*, **241**, 3240-3243

7 Sivaraja, M., Goodin, D. B., Smith, M. and Hoffman, B. M. (1989) *Science*, **245**, 738-740

8 Stubbe, J. and van der Donk, W. A. (1998) *Chem. Rev.*, **98**, 705-762

9 Finzel, B. C. and Poulos, T. L. (1984) *J. Biol. Chem.*, **259**, 13027-13036

10 Fishel, L. A., Villafranca, J. E., Mauro, J. M. and Kraut, J. (1987) *Biochemistry*, **26**, 351-360

11 English, A. M. and Tsaprailis, G. (1995) *Adv. Inorg. Chem.*, **43**, 79-125

12 Bosshard, H. R., Anni, H. and Yonetani, T. (1991) in *Peroxidases in Chemistry and Biology* (Everse, J., Everse, K. E. & Grisham, M. B., eds) pp. 51-85, CRC Press, Boca Raton FL

13 Ortiz de Montellano, P. R. (1987) *Acc. Chem. Res.*, **20**, 289-294

14 Dawson, J. H. (1988) *Science*, **240**, 433-439

15 Ortiz de Montellano, P. R. (1992) *Ann. Rev. Pharma. Toxicol.*, **32**, 89-107

16 Poulos, T. L. (1993) *Curr. Opin. Biotechnol.*, **4**, 484-489

17 Poulos, T. L. and Fenna, R. E. (1994) in *Metal Ions in Biological Systems* (Sigel, H. & Sigel, A., eds) pp. 25-75, Dekker, New York

18 Dolphin, D., Forman, A., Borg, D. C., Fajer, J. and Felton, R. H. (1971) *Rec. Res. Dev. Agr. Food Chem.*, **68**, 614-618

19 Mittler, R. and Zilinskas, B. A. (1991) *FEBS Lett.*, **289**, 257-259

20 Asada, K. (1992) *Physiol. Plant.*, **85**, 235-241

21 Miyake, C. and Asada, K. (1996) *Plant Cell Physiol.*, **37**, 423-430

22 Patterson, W. R. and Poulos, T. L. (1995) *Biochemistry*, **34**, 4331-4341

23 Patterson, W. R. and Poulos, T. L. (1994) *J. Biol. Chem.*, **269**, 17020-17024

24 Patterson, W. R., Poulos, T. L. and Goodin, D. B. (1995) *Biochemistry*, **34**, 4342-4345

25 Poulos, T. L., Patterson, W. R. and Sundaramoorthy, M. (1995) *Biochem. Soc. Trans.*, **23**, 228-232

26 Pappa, H., Patterson, W. R. and Poulos, T. L. (1996) *J. Biol. Inorg. Chem.*, **1**, 61-66

27 Náray-Szabó, G. (1997) *J. Biol. Inorg. Chem.*, **2**, 135-138

28 Jense, G. M., Buunte, S. W., Warshel, A. and Goodin, D. B. (1998) *J. Phys. Chem.*, **102**, 8221-8228

29 Mandelman, D., Jamal, J. and Poulos, T. L. (1998) *Biochemistry*, **37**, 17610-17617

30 Marquez, L. A., Quitoriano, M., Zilinskas, B. A. and Dunford, H. B. (1996) *FEBS Lett.*, **389**, 153-156

31 Nakajima, R. and Yamazaki, I. (1987) *J. Biol. Chem.*, **262**, 2576-2581

32 Hiner, A. N. P., Martínez, J. I., Arnao, M. B., Acosta, M., Turner, D. D., Raven, E. and Rodríguez-López, J. N. (submitted for publication)

33 Morimoto, A., Tanaka, M., Takahashi, S., Ishimori, K., Hori, H. and Morishima, I. (1998) *J. Biol. Chem.*, **273**, 14753-14760

34 Hori, H. and Yonetani, T. (1985) *J. Biol. Chem.*, **260**, 349-355

35 Hoffman, B. M., Roberts, J. E., Kang, C. H. and Margoliash, E. (1981) *J. Biol. Chem.*, **273**, 14753-14760

36 Blodig, W., Doyle, W. A., Smith, A. T., Winterhalter, K., Choinowski, T. and Piontek, K. (1998) *Biochemistry*, **37**, 8832-8838

37 Hiner, A. N. P., Rodríguez-López, J. N., Arnao, M. B., Lloyd Raven, E., García-Cánovas, F. and Acosta, M. (2000) *Biochem. J.*, **348**, 321-328

38 Kvaratskhelia, M., Winkel, C. and Thorneley, R. N. F. (1997) *Plant Physiol.*, **114**, 1237-1245

39 Kvaratskhelia, M., Winkel, C., Naldrett, M. T. and Thorneley, R. N. F. (1999) *J. Plant Physiol.*, **154**, 273-282

40 Bonagura, C. A., Sundaramoorthy, M., Pappa, H. S., Patterson, W. R. and Poulos, T. L. (1996) *Biochemistry*, **35**, 6107-6115

41 Bonagura, C. A., Sundaramoorthy, M., Bhaskar, B. and Poulos, T. L. (1999) *Biochemistry*, **38**, 5538-5545

42 Bursey, E. H. and Poulos, T. L. (2000) *Biochemistry*, **39**, 7374-7379

# CHAPTER SIX

# EXPERIMENTAL

# 6 Experimental

This chapter will focus upon the materials and methods used in the preparation, isolation and characterisation of wild-type and variant recombinant APX. Pea cytosolic APX cDNA, from *Pisum Sativum L.*, was a generous gift from Dr. Barbara Zilinskas (Rutgers University, New Jersey, USA).[1] The cDNA was sub-cloned by Dr Emma Raven (University of Leicester) and Miss Beatrice Tam (University of British Colombia) into the *Xmn*I and *Bam*HI restriction sites of the pMAL-c2 expression vector (New England Biolabs).

Detailed COSSH assessments were prepared, and submitted for inclusion on the departmental COSSH database, for all chemicals that were used during the course of these experiments. Handling procedures and protocols for handling hazardous materials were strictly followed. Further details of some of the materials used, *e.g.* oligonucleotide sequences and constituents of media, can be found in Appendix A.

## 6.1 Preparation of wild-type and variant recombinant APX

Competent *E. Coli* TOPP2 cells (Stratagene) were transformed, in accordance with the associated Stratagene transformation protocol, with the required variant or wild-type rAPX-encoding pMALc-2 expression vector (New England Biolabs). Subsequent bacterial expression of rAPX occurs as a MBP-fusion product; the consequent protein purification follow a protocol adapted from the procedures published by Patterson and Poulos in 1994.[2]

203

### 6.1.1 Preparation of sterile media and plates

All media were sterilised using a 20 minute cycle, with a slow pressure release, in a laboratory steriliser (Dent & Hellyer). Any dry glassware, eppendorfs and/or pipette tips that were required were sterilised similarly but utilised the faster pressure release setting. Filter sterilisation of solutions, including ampicillin and IPTG, was conducted using 0.2 μm syringe-top filters (Acrodisc) prior to use.

### 6.1.2 Expression of MBP-fusion product

Uninduced *E. Coli* TOPP3 cells, transformed with the ampicillin-resistant pMAL-c2 vector, taken from a frozen (-20°C) glycerol stock (Appendix A), were streaked onto LB-ampicillin agar plates (Appendix A). Once streaked, the plates were incubated at a constant temperature of 37°C for ~8 hours. Using a sterilised wooden toothpick, a single colony was picked and transferred into a conical flask (250 ml) containing 100 ml rich LB-medium (Appendix A); the cells within the flask form the basis of an overnight culture. The cell culture was allowed to grow for 10-12 hours in a shaker incubator at a constant 37°C and with good aeration (~250 rpm).

Typically, eight 2 l shaker flasks, each containing 0.7 l of rich medium, were inoculated with 10 ml of an overnight culture; subsequently the flasks were placed into the shaker incubator and the cells allowed to grow under conditions identical to that previously described for the overnight culture. At periodic intervals, about an hour apart, 1 ml aliquots were removed from the culture contained within a specific shaker flask and the cell growth was assessed spectroscopically using the absorbance at 600 nm ($A_{600}$). About $2\frac{1}{2}$ hours after

inoculation, when $A_{600} \approx 0.5$, such that a cell density of ~2 × $10^8$ cells/ml had been reached, expression was induced using filter sterilised IPTG, added to a final concentration of 0.3 mM.

Six hours after induction, the cells were collected by centrifugation (10,000 × g for 15 minutes at 4°C) and the supernatant medium was discarded. Pelleted cells were resuspended in 3 ml lysis buffer (Appendix A) per gram of *E. Coli* cells, wet weight, before being frozen (at -20°C).

### 6.1.3   SDS-polyacrylamide gel electrophoresis analysis

Pelleted cells, obtained by bench-top centrifugation (2 minutes at 13,000 rpm) of aliquots (1 ml) of the medium, were checked for over-expression of the MBP-fusion product. Pellets were resuspended in SDS-containing sample buffer and then analysed by SDS-PAGE, a 15% polyacrylamide gel was used for the resolving portion of gels used throughout this work, including subsequent purity assessment of the isolated APX.

### 6.1.4   Isolation of APX-MBP fusion product

Frozen cells were defrosted overnight in a refrigerator at ~4°C; phenylmethylsulfonyl fluoride and dithiothreitol were added to the suspension to a final concentration of 1 mM. Cell lysis was accomplished enzymatically using 100 mg of hen egg white lysozyme (Sigma); the cells were placed in an ice bath situated upon a gently oscillating (~50 rpm) orbital shaker for about $2\frac{1}{2}$ hours and then refrozen (-20°C). After 24 hours, the lysed cells were defrosted and ~5 mg DNase (Sigma) and 1 ml of 1 M $MgCl_2$ were added to the viscous

suspension. The suspension was then shaken on ice for about 2 hours until it became free flowing.

The cell-free extract was obtained after pelleting the remains of the lysed cells by centrifugation (10,000 × g for 30 minutes at 4°C); the supernatant was maintained at 4°C prior to further purification. All subsequent column chromatography and dialysis were performed in a cold-room, ambient temperature of ~4°C; protein samples were collected after each purification step and analysed by SDS-PAGE.

The first stage of purification was to isolate the MBP-fusion product from the numerous solubilised proteins present in the cell-free extract. A 2.5 × 20 cm column of amylose affinity resin (New England Biolabs) was pre-equilibrated using >5 column volumes of AC buffer (Appendix A). Typically, the cell-free extract from three successive grow-ups were pooled and diluted five-fold with AC buffer before being loaded onto the equilibrated amylose column at a flow rate of about 1 ml/min.

The colouration of wild-type rAPX enabled the loading of the MBP-fusion product to be visually monitored; upon completion, the amylose affinity column was washed thoroughly with AC buffer until the flow-through protein absorbance at 280 nm ($A_{280}$) approached the base-line level. Where expression of a recombinant variant yielded predominantly apo-protein, reconstitution was not attempted until after further purification, care was taken as to ensure that the almost colourless fusion product remained bound to the resin.

Elution of the bound fusion protein was accomplished using AC buffer containing ~10 mM maltose, typically 100 ml, at a flow rate of about 1 ml/min; all red-coloured fractions

were pooled. The MBP-fusion protein solution was concentrated to a volume of ~20 ml using either a stirred ultrafiltration cell (Amicon, model 8050) or a Centriprep-10 (Amicon) fitted with the Amicon YM10 membrane, cut-off 10 kDa MW. The maltose was removed through exhaustive exchanges into AC buffer.

## 6.1.5 Cleavage of MBP-fusion product and separation of rАPX

Cleavage of the coloured fusion product was achieved using trypsin (Bovine Pancreas Type III, Sigma), rather than factor Xa, at 1:100 trypsin to MBP-fusion product w/w.[2] Under these conditions, after digestion for an hour no fragmentation of the recombinant holo-protein was observed. Spectroscopic determination of the concentration of the MBP-fusion product was achieved using the absorbance at the Soret maximum and the absorption coefficient of the rАPX at this wavelength. Typically, cleavage was complete after 60 minutes incubation at ambient room temperature (~20°C), as confirmed by SDS-PAGE; further digestion was inhibited by the addition of a corresponding amount of trypsin inhibitor (soybean, Sigma).

The trypsin-digested solution was diluted with cold AC buffer, such that the total protein concentration was <2.5 mg/ml, before being loaded onto a freshly equilibrated amylose column at a flow rate of about 1 ml/min. Maltose-binding protein remaining bound to the amylose resin whilst coloured rАPX fractions were eluted from the column. **N.B.** The variable capacity of amylose resin for the initial MBP-fusion product can be attributed to the effect of the target protein, in this case АPX, upon the maltose-binding site.[3] Equally significant, maltose-binding protein can become 'damaged', i.e. either partially or wholly

207

denatured, through the initial isolation stages. 'Damaged' MBP consequently displays diminished binding affinity for amylose resin.[3] At the separation stage, the result is co-elution of MBP with the rAPX. Whilst 'damage' cannot be controlled *per se*, it may be limited by rapidly isolating the fusion protein from the cell-free extract.

### 6.1.6 Purification of rAPX by anion exchange chromatography

Pooled rAPX-containing fractions (~100 ml), eluted from the 2nd amylose affinity column, were either dialysed or exchanged into FFQ column buffer (Appendix A). Dialysis was conducted twice (5 hours duration) against 10 l of high-quality deionised water (drawn from an Elgastat Option 2 water purifier, which is fed with deionised water) and finally against 10 l of FFQ column buffer. Alternatively, ultrafiltration was used to concentrate and exchange the fractions into the low ionic strength potassium phosphate buffer.

Typically, a 2.5 × 10 cm column of FFQ-Sepharose anion exchange resin was prepared and equilibrated with >5 column volumes of FFQ column buffer. The rAPX, in FFQ column buffer, was applied to the anion exchange column at a flow rate of about 1 ml/min; a dark band was observed as the enzyme bound at the top of the packed resin.

Once the rAPX solution had loaded, the column was washed thoroughly with >5 column volumes of FFQ column buffer; elution of the enzyme was achieved using a linear KCl gradient 0-150 mM. The predominant choice of cation was potassium, but NaCl was used on several occasions to determine whether the purported structural cation was substitutable: in

208

this case, the FFQ buffer was changed to sodium phosphate, thereby minimising the potassium content of the column buffer.

## 6.1.7 Spectroscopic analysis of rAPX

Coloured fractions were analysed spectroscopically, measuring the absorbencies at the Soret maximum and 280 nm ($A_{Soret}$ & $A_{280}$); those fractions for which the calculated $R_z$-purity number ($A_{Soret}/A_{280}$) >1.9 were pooled. The reinheitzahl, $R_z$, value is dependent upon the coordination state of the haem iron and the Soret maxima position and shape can provide information about the active site environment; the limits of this method as a purity gauge are clear, especially where a mixture of spins is present.

It was duly noted that a small amount of MBP mixed with a larger amount of high holo-containing rAPX could appear to be of poorer spectroscopic purity than a sample of mostly apo-protein. Therefore, evidence supporting the qualitative spectroscopically determined enzyme purity was obtained by conducting SDS-PAGE analysis of pooled fractions. The highest level of rAPX purity would be substantiated by a single protein band at ~28 kDa MW. However, the staining compound, Coumassie blue (Sigma), used to visibly mark the protein bands present within the SDS-PAGE was noted to stain MBP significantly more efficiently than rAPX. Given that isolations afforded an inconsistent proportion of apo and holo-protein, it appears that no single form of purity assessment was entirely suitable for purity quantification.

### 6.1.8  Preparation for long-term storage

The recombinant proteins where exhaustively exchanged into doubly distilled deionised water (Elgastat) and concentrated to a minimum volume (~3 ml) using ultrafiltration, which was conducted using either the stirred cell, fitted with the aforementioned Amicon YM10 membranes, or a Centriprep-10. The darkly coloured enzyme solution, typically ~8 mg/ml, was divided into ~50 µl aliquots and transferred into cryogenic storage vials which were flash frozen and stored in liquid nitrogen.

## 6.2  Variant rAPX – modifications to wild-type preparation protocol

Site-directed mutagenesis was performed, according to the QuikChange™ protocol (Stratagene), using the wild-type APX-containing pMAL-c2 vector and the appropriate purified mutagenic oligonucleotides (Perkin Elmer), see Appendix A. Plasmid DNA sequencing, performed using New England Biolabs pUC and *malE* sequencing primers, was conducted in the protein and nucleic acid laboratory (Centre for Mechanisms in Human Toxicity, Leicester University). Individual mutations were confirmed by sequencing across the whole APX-coding gene and were free of any additional mutations.

### 6.2.1  Reconstitution of apo rAPX variants

Supported by the observation of slight variations in the spectroscopically determined $R_z$-purity number, the $A_{Soret}/A_{280}$ ratio, apo-protein was probably present as an intractable component of all the MBP-fusion product over-expressions. However, where the amount of

holo-protein was exceedingly low, reconstitution was attempted, according to the following protocol.

An aliquot (2-5 µl) of the eluted and exchanged MBP-fusion product was accurately diluted into a total volume of 1ml of AC buffer. Then the room temperature sample was spectrophotometrically titrated with small additions (0.5-2 ul) of hemin chloride (Sigma) dissolved in 0.1 M NaOH, care was taken to ensure that equilibrium was reached after each new addition. The quantification of the amount of haem required for full reconstitution was achieved by examining difference spectra, obtained by arithmetic manipulation within the Grams software program (Galactic Software Limited) of the titration spectra, the concentration at which a broad protoporphyrin absorbance maxima (~350 nm) persisted was duly noted. Accordingly, the reconstitution was scaled up, using a slight molar excess of haem. The completed equilibrium of haem incorporation into the apo-protein was confirmed spectrophotometrically, after over-night incubation at 4°C in a refrigerator, centrifugation was used to remove any aggregates from solution.

Reconstitution by this method avoided the need to use gel filtration to separate excess haem from the holo-protein. The decision to reconstitute at an early stage, prior to the tryptic digest, was made both to improve the stability of recombinant protein and facilitate spectroscopic quantification of the haem-containing fusion protein.

### 6.2.2 Over-fragmentation of trypsin sensitive apo-protein

Variants that expressed predominantly as apo-protein were quantified spectrophotometrically, following small-scale hemin reconstitution, by the formation of the

211

cyanide ternary complex. Apo-protein expressed variants were qualitatively found to be more rapidly digested, under identical cleavage conditions, than the wild-type holo-enzyme. Hence reconstitution of predominantly apo-protein was favoured prior to trypsin cleavage. However, only a nominal increase in the trypsin-induced fragmentation resistance, of the rAPX protein, was afforded by reconstitution of the variant apo-proteins prior to cleavage. These complications have been reported independently, within a study of a variant replacing the purported $K^+$-binding site with a CcP-like H-bonding network.[4] Cheek *et al* utilised an N-terminal histidine-tagged rAPX expression vector, an alternative method of preparing the recombinant protein, which yielded stable apo-protein that, once purified, readily reconstituted with hemin.

### 6.2.3 Anion exchange elution profiles

Under identical chromatographic conditions to that used for wild-type rAPX, variants were observed to bind to the FFQ Sepharose resin in varying degrees and thus displayed different elution profiles. Hence, variant A134P variant rAPX bound comparatively weakly, eluting with <30 mM KCl and requiring the use of 5 mM potassium phosphate, whilst wild-type enzyme eluted between 50-95 mM chloride. Co-elution of MBP repeatedly occurred but the chloride gradient was changed so as to maximise separation of the rAPX from MBP; the isoelectronic point of the variant rAPX was assumed to be the key-determining factor.

## 6.3 Electrospray ionisation mass spectrometry

Removal of the trace salt content from a sample of pure rAPX was achieved using a Centricon-10 concentrator (Amicon) and successive centrifugation and dilution with highly

purified water (Elgastat). Samples of ~2 mg/ml rAPX (20 μl) were then diluted ten-fold with a solution of 50:50 acetonitrile to water v/v containing 1% trifluoroacetic acid.

Samples of rAPX were provided to Dr. G. Sweetman, in the laboratory of Dr. P. Farmer (Centre for Mechanisms of Human Toxicity, Leicester University), for mass spectral analysis using a Micromass Quattro BQ (Tandem Quadrupole) electrospray mass spectrometer. Horse heart myoglobin (Sigma) was prepared as described for rAPX, and used to calibrate the spectrophotometer in the range 600-1400 m/z. The prepared protein samples were introduced into the instrument at a 5 μl/min flow rate; several scans were obtained from the rAPX sample provided for analysis.

### 6.3.1 Tryptic digest analysis

Samples of wild-type and H42A variant rAPX (10 μl, 0.1 mM) were prepared in 10 mM ammonium bicarbonate (pH 8) and treated with the required ratio of trypsin w/w (12 hours at 35°C). The samples were then analysed using the same protocol outlined for the undigested rAPX samples (section 6.3). Comparisons of the digestion products mass spectra were then made with theoretical values for the expected trypsin cleavage products.

### 6.4 UV/visible spectroscopy

Predominantly, spectra were obtained using a variable slit Perkin Elmer Lambda14 UV/visible spectrometer, linked to an Exacta 466D computer and an Epson LQ-1060 printer. Temperature control (± 0.1 °C) was achieved using a thermally-jacketed cell holder that was connected to a circulating water bath (Julabo U3) and a water cooler (MK Refrigeration Limited) which were operated in tandem. The pathlength for both the 3 ml and

1 ml quartz cells that were used was 10 mm. A typical 270-700 nm scan was obtained using a scan speed of 120 nm/min, acquiring at 0.5 nm intervals and with a 1 nm slit width.

### 6.4.1 Buffers and solution preparation

Sodium phosphate buffer (NaPi) was used in the pH range 5.5-8.0 and sodium acetate (NaOAc) in the range 4.8-5.8, buffer ionic strength was 0.1 M throughout. For the pH-dependent studies, a mixed MES/MOPS/TAPS sulphonic acid buffer was prepared, Appendix A; the use of this 'mixed buffer' enabled the pH range 5-8 to be covered with a single buffer. Prior to use the 'mixed buffer' was titrated to the necessary pH and allowed to equilibrate, the ionic strength of this buffer system ranges between 95 and 110 mM depending upon the solution pH. Measurements of aqueous solution pH were taken using a Russell pH-electrode attached to a digital pH-meter (Radiometer Copenhagen, model PHM93). Calibrations were made daily using two standardised solutions, and an accuracy of typically ± 0.001 pH unit at 20°C was maintained.

Unless otherwise indicated, dilutions were calculated by mass and were performed directly within the quartz cells used. The solution temperature in the cell was a constant 25.0 ± 0.1°C; baseline correction was made with respect to the buffer/solvent used.

### 6.4.2 rAPX absorption coefficient determination

The pyridine-haemochromagen method was used to calculate the molar absorption coefficients of wild-type and variant rAPX.[5] A 400 µl sample of rAPX, of known absorbance (~50 µM), was diluted four-fold using 1200 µl of a basic pyridine solution

(Appendix A). About half (~800 μl) of oxidised pyridine-haemochromagen formed was left for a few minutes before being assayed spectroscopically; the second aliquot was left for several hours to ensure that complete extraction of haem had occurred. Assay of the haem concentration of the solution was conducted spectroscopically by measuring the absorbance at 557 nm ($A_{557}$) of the reduced pyridine-haemochromagen that was formed immediately after the addition of solid sodium dithionite (<1 mg). The 557nm absorption coefficient, $\varepsilon_{557}$ = 32.0 mM$^{-1}$cm$^{-1}$, used in the determination corresponds to that of the proto-haem reduced pyridine-haemochromagen.[5]

Iron atomic absorption spectroscopy was initially used to confirm the wild-type rAPX absorption coefficient; agreement between the values obtained using both methods, aided the assessment of the standard error associated with the pyridine-haemochromagen determination (± 5 %).

### 6.4.3 Ligand-bound derivative spectra

Reagent grade potassium cyanide, sodium fluoride and sodium azide (Sigma) were used without further purification. Ferric ligand-bound derivatives were obtained by making small additions of excess ligand (pre-buffered 1-2 M NaF, KCN or NaN$_3$ stock solutions) to a solution of rAPX (~20 μM), equilibrated at pH 7.0 (NaPi). The spectra of the wild-type and H42A variant rAPX-imidazole ternary complexes were prepared by addition of excess solid imidazole (Sigma) to a solution of ferric enzyme (10-20 μM); to ensure that basic denaturation was not a factor, due to the action of imidazole, deviation from the initial pH was measured.

215

The ferrous enzyme was prepared by the addition of dithionite to a solution of $N_2$-degassed ferric rAPX (~10 $\mu$M); having obtaining the spectrum of the ferrous derivative, CO gas was slowly bubbled through the ferrous rAPX in order to form the ferrous-CO ternary complex. Ferrous-CN rAPX was prepared by the addition of solid dithionite (~1 mg) to a solution of ferric-CN rAPX (~10 $\mu$M).

Normalised spectra were converted from relative absorbance into millimolar absorptivity using Grams (Galactic Software Limited).

## 6.4.4 Ligand-binding studies

Buffered KCN solutions (5-200 mM) were prepared immediately prior to use and kept sealed, with a minimum air-gap, to minimise loss through the equilibrium formation of HCN.[6] Due to a variation in the rAPX spectrum with pH (Chapter 3) all concentrations of rAPX were calculated based upon the known enzyme stock absorbance and the dilution factor of each sample in relation to that stock.

Titrations were preceded by a 'dummy titration', in order to preserve clean isosbestic points, an artifact seemingly associated with the use of stoppered cells. A 'dummy titration' consisted of the removal and replacement of the stopper from the cell and remixing the sample by inversion. There is no simple explanation for the necessity to re-equilibrate the sample prior to the addition of the titrating ligand.

Titrations were conducted using small additions (0.5-10.0 $\mu$l) of the ligand solutions to a thermally equilibrated enzyme sample (1 ml, typically 10 $\mu$M rAPX). The titrations were monitored spectroscopically by following the absorbance at a fixed wavelength at the

absorbance maxima of either rAPX or rAPX-ligand spectrum. The equilibrium dissociation

constant from each titration was calculated, using Scientist, by linear least-squares fit of

titration absorbance changes to Equation 6-1,

$$\Delta A = \frac{\Delta A_\infty}{2[APX]} \times ([APX]+[X]+K_d\ (([APX]+[X]+K_d)^2(4[APX][X]))^{\frac{1}{2}}) \quad [6\text{-}1]$$

where [APX] and [X] represent the calculated concentrations of total enzyme and total

ligand, after each addition, $\Delta A$ and $\Delta A_\infty$ are the absorbance changes corresponding to the

intermediate and saturating ligand concentrations, and $K_d$ is the equilibrium dissociation

constant. During fitting the values of $\Delta A_\infty$ & $K_d$ were calculated based upon the

experimental values of $\Delta A$, [APX] and [X].[a] Especially where comparatively large volumes

of the titrating ligand solution were required to approach saturation, comparison of the

calculated $\Delta A_\infty$ with that experimentally observed assisted evaluation of the goodness-of-fit.

### 6.4.5 Spectrophotometric pH titration

A series of pH titrations of wild-type and variant rAPX in both unbuffered or weakly

buffered solutions were attempted, although these often resulted in precipitation. The rAPX

enzymes all exhibit a strong buffering effect around their isoelectronic point (pH 5.6-5.8)

---

[a] Each addition of ligand raises the amount of X and concomitantly increases the total solution volume. Accordingly, the values of [X] and [APX] for each addition were calculated, using the added volume and initial volume to adjust for dilution, from the cumulative amount of dissolved ligand and initial enzyme concentration, respectively. Similarly, the relationship between [APX] and $\Delta A_\infty$ was incorporated into the fitting process.

and were much less tolerant to the addition of acid than base. The 'mixed buffer', capable of buffering across the pH 5.0-8.0 range (section 6.4.1), was used with a degree of success.

Using the mixed buffers (previously adjusted with 0.1M NaOH to pH 5.0), solutions of rAPX (~10 μM) were prepared in 3 ml quartz cells containing a tiny magnetic stirrer bar, and the initial pH of the mixture was recorded. Adjustment of the pH was conducted, with continuous mixing in order to reduce the possibility of precipitation, by small additions (2-10 μl) of NaOH (0.1 M or 1 M) to raise the pH. The pH was measured before and after obtaining each equilibrated spectrum, an average of the two values was recorded; only small deviations (± 0.01) were observed between any pair of readings. Attempts to obtain a reverse titration by making small additions of dilute HCl (1 M) resulted in excessive precipitation and solution turbidity prevented quantitative assessment of the UV/visible spectra.

## 6.4.6 Low temperature spectra

This work was conducted by Dr. E. Raven (Department of Chemistry, Leicester University) in the laboratory supervised by Prof. A. G. Mauk (Department of Biochemistry and Molecular Biology, University of British Columbia, Vancouver, Canada). Electronic absorption spectrum of wild-type rAPX were recorded at 77K with an SLM-Aminco Model DW-2C dual wavelength spectrophotometer fitted with sample holders with 2 mm pathlengths; spectra were collected with the corresponding buffer in the reference beam at the same temperature as the sample.

## 6.5 Steady-state activity measurements

Activity measurements were conducted using the Perkin-Elmer spectrophotometer in a fixed wavelength scan mode, acquiring at 0.1 second intervals, monitoring at a wavelength that is dominated by either the reducing substrate or oxidised product. Enzyme concentrations (10-25 nM) were calculated from the dilution made to a stock of known absorbance (typically 0.5 μM).

### 6.5.1 L-Ascorbic acid activity

The method that was used to assay rAPX specific activity is essentially identical to that reported in the literature.[7] The oxidation of ascorbate into dehydroascorbate, the stable monodehydroascorbate radical disproportionation product, was monitored spectroscopically, in the near-UV region, at 290 nm ($A_{290}$). The calculated absorption coefficient for ascorbate at 290 nm ($\varepsilon_{290}$ = 2.8 mM$^{-1}$cm$^{-1}$) was used throughout.[8] This value was confirmed by the plotting absorbance at 290 nm against ascorbate concentration and linear regression analysis, analytical grade L-ascorbic acid (Sigma) was used for all specific activity assays. The absorbance maximum of ascorbate in the 235-300 nm region is at 265 nm but the greater molar absorptivity of the substrate at this wavelength prohibits UV spectroscopic analysis. Neither dehydroascorbate nor the monodehydroascobate radical absorb significantly at 290 nm.[8]

The reaction was initiated by the addition of ~20 nM APX, which was found to be the most efficient method of initiating turnover, thereby minimising any non-hydrogen peroxide

dependent enzymatic oxidation[b]. Specific enzyme activities were calculated from the initial slope, measured from the linear decay section of the time-dependent data obtained, derived using a linear least squares fit program (Scientist, Micromath or Excel, Microsoft). All ascorbate assay data were adjusted, by a factor of two, to account for the disproportionation of the monodehydroascorbate radical; the reported specific activities are in moles of ascorbate oxidised to monodehydroascorbate radicals per min per mg APX (units per mg APX). The steady-state concentration of monodehydroascorbate ($\varepsilon_{360} = 3.3$ mM$^{-1}$cm$^{-1}$), present under assay conditions, was confirmed spectroscopically by monitoring at 360 nm.[9]

### 6.5.2 Other reducing substrates

For the other substrates investigated, oxidations were monitored at the appropriate wavelength and calculations used the reported absorption coefficient as taken from the cited literature, e.g. the 407nm wavelength was used for guaiacol oxidations at which tetraguaiacol formation is observed ($\varepsilon_{407} = 22.6$ mM$^{-1}$cm$^{-1}$).[10] The concentrations of the reducing substrates were noted, as a range of concentrations was required to obtain optimal substrate oxidation. Specific enzyme activities were calculated from the initial slope, from the linear decay section of the time-dependent data obtained, derived using a linear least squares fit program (Scientist, Micromath or Excel, Microsoft).

---

[b] Hydrogen peroxide and L-ascorbic acid were not observed to react significantly across the pH 5-10 range in the absence of the enzyme. However, ferric rAPX promoted oxidation of ascorbate in the absence of an exogenous oxidant such as peroxide.

### 6.5.3 pH-dependence of rAPX specific activity

Within a 1 ml quartz cuvette: 0.5 mM L-ascorbic acid and 0.1 mM hydrogen peroxide (~2.5 μl, ~30 mM$^c$), were preincubated (25 °C) for several minutes in the mixed sulphonic acid buffer (identical to that described in section 6.4.1) titrated to the appropriate pH (μ = 0.95-0.110). Reactions were initiated by the addition of rAPX (20-30 nM) and monitored at 290 nm using the same fixed wavelength mode described above, section 6.5.1.

## 6.6 $^1$H-NMR spectroscopy

Paramagnetic haem-resonance $^1$H-NMR spectra were recorded at 300K with a 400 MHz Bruker NMR machine using a solvent presaturation pulse sequence. Exhaustive exchange of rAPX into >99.5 % D$_2$O was conducted using either Centricon-10 or Centriprep-10 concentrator. To avoid excessive aggregation, observed at near millimolar APX concentrations, buffering was achieved by sample dilution into deuterated phosphoric acid, previously adjusted with NaOD to the appropriate pH$^*$ (uncorrected for the deuterium-isotope effect), final concentration of 50 mM.

Adjustment of the sample pH$^*$ was achieved by successive Centricon exchanges into deuterated NaPi buffer (50 mM) of the required pH$^*$. The flowthrough pH$^*$ was measured to confirm equilibration of the sample, and spectra were taken at intermediate values as required.

---

$^c$ Measured spectrophotometrically using $\varepsilon_{240} = 39.4$ mM$^{-1}$ cm$^{-1}$.

## 6.7 Resonance Raman spectroscopy

Resonance Raman experiments were conducted in collaboration with Dr. C. R. Andrew (University of East Anglia, Norwich), a diagram of the apparatus used is depicted in Figure 6-1. All experiments were conducted in a darkened room in order to minimise ambient light levels; a notch filter was used to attenuate Raleigh scattered radiation from entering the spectrophotometer. The optical rotator ensured that the argon laser radiation (15-40 mW at sample) was optimally polarised before being focused onto the edge of a glass capillary tube containing an APX sample. Scattered light was collected at 90° to the incident beam and the radiation that was focused by the second lens passed through a notch filter (Kaiser) before entering the spectrophotometer (SPEX).

With the entrance slit (120 μm) open, a vertical diffraction pattern image was formed on the surface of the CCD; each column of pixels corresponding to a defineable Raman shift. The slit was held open for 30 second periods, each referred to as a shot; the signal-to-noise ratio was increased by obtaining accumulation-averaged images. Prior to each set of scans, a diffraction image obtained from Raman scattering of solid aspirin and/or indene was saved as a calibration. Subsequently, the horizontal pixel coordinates were converted into Raman shifts, based upon the coordinates of assigned Raman bands of the calibration spectrum, and are accurate to $\pm$ 1 cm$^{-1}$ for intense isolated bands. The resonance Raman spectra of APX samples were obtained by converting the image data according to the relevant calibration and after manual baseline interpolation (Grams, Galactic Software Limited).
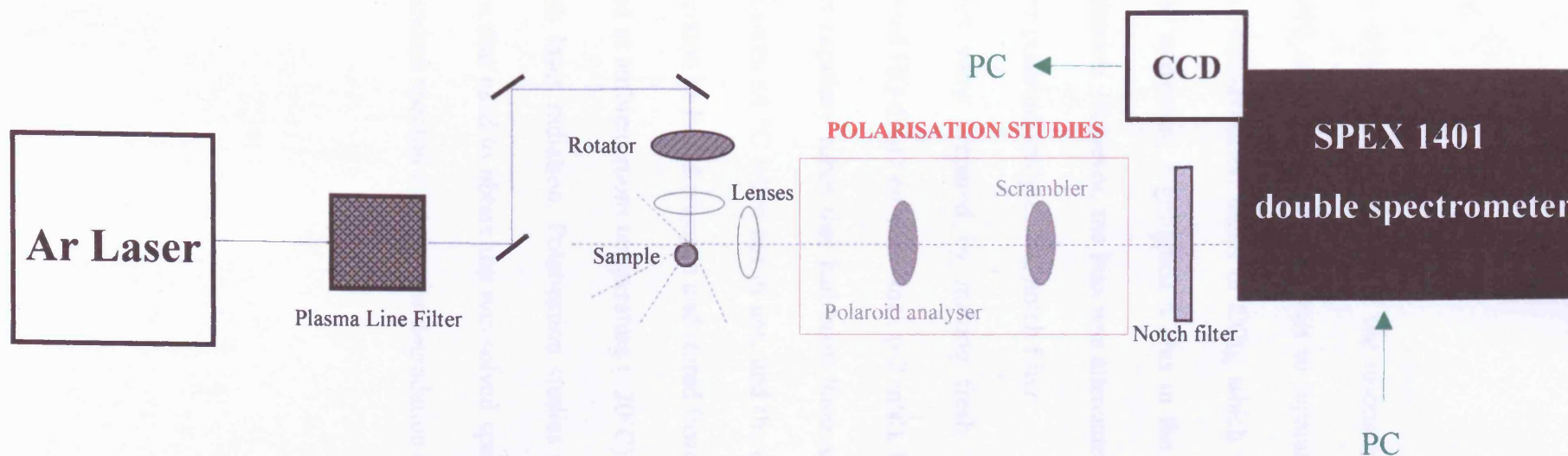
**Figure 6-1 A diagrammatic representation of the RR apparatus.** Solid blue lines indicate the path of the laser beam, and the blue dashed lines indicate the scattered radiation. The section contained within the red dashed line represents the additional optics that were required during the polarisation studies (section 6.7.1).

## 6.7.1 Polarisation studies

To enable a more definitive assignment of the resonance Raman spectra, polarisation studies were conducted using a polaroid analyser to separate parallel and perpendicularly polarised bands. The depolarisation ratios of $CCl_4$, which were used for the polarisation calibration of the RR apparatus, highlighted a bias in the subsequent CCD detection of parallel-polarised radiation. However, the bias was attenuated through the introduction of a scrambler between the polaroid analyser and notch filter.

All rAPX samples were prepared by making fresh 10-fold buffer dilutions of a concentrated unbuffered $HQ-dH_2O$ enzyme stock (~2 mM). Enzyme samples (~25 µl) were transferred into glass capillary tubes that had been flame-sealed at one end. All samples were kept at temperatures ≤4 °C when not in use, and the unbuffered protein stocks were flash frozen by immersion in liquid nitrogen and stored frozen at -70°C. Resonance Raman spectra were obtained at ambient room temperature (~20°C) using either the 457.9 nm and 514.5 nm wavelength laser radiation. Polarisation studies required a higher laser power setting (40 mW) than that used to obtain the unresolved spectra (20 mW), but the samples showed no time-dependent spectral evidence for degradation during acquisition.

## 6.8  Magnetic circular dichroism

Magnetic circular dichroism experiments were conducted in collaboration with Dr. M. R. Cheesman in the laboratory of Prof. A. J. Thomson (University of East Anglia, Norwich). MCD spectra were recorded using JASCO J500D (280-1000 nm) or JASCO J730 (800-2000 nm) circular dichrographs, with an Oxford Instruments superconducting solenoid capable of generating magnetic fields up to 6 Tesla. All spectra were recorded at room temperature, and due to their linear dependence upon magnetic field, are expressed per unit of magnetic field $(H^{-1}cm^{-1}T^{-1})$.

Samples of rAPX were prepared in buffered $D_2O$ by dilution, resulting in 50 mM NaPi at the indicated pH*; UV/visible spectra were taken of all rAPX samples (30-300 $\mu$M). The UV/Vis MCD haemoprotein samples were also studied in the near IR region, which required either dilution or a doubling-up of the sample volume to obtain the optimum IR MCD signal strengths. The use of highly deuterated solutions of protein ensured that neither the proton nor deuteron-derived vibrational absorbtion bands prohibitively absorbed near IR radiation, which would otherwise obscure important haemoprotein-derived MCD signals.

## 6.9  Electron paramagnetic resonance spectroscopy

EPR spectroscopic studies were conducted initially obtained in the presence of 50% glycerol in collaboration with Dr. F. Rosell, in the laboratory supervised by Prof. A. G. Mauk (University of British Columbia, Vancouver, Canada). X-band EPR spectra were obtained at 7K using a Bruker ESP Model 300E spectrometer (modulation frequency 100 kHz, modulation amplitude 12.8 G, microwave frequency 9.46 GHz, microwave power

0.5-1.0 mW) equipped with an HP5352B microwave frequency counter and an Oxford

Instruments ESR900 continuous flow cryostat. A mixture of 1:1 glycerol to NaPi v/v (pH

7.0, $\mu$ = 0.1 M) was used to prepare an EPR sample of wild-type rAPX (~1 mM). After

recording the 7K EPR spectrum of rAPX at pH 7.0, the sample was defrosted and adjusted

to pH 5.0; another spectrum was recorded at low pH.

Subsequently, a second EPR study was conducted in collaboration with Dr. M. R.

Cheesman, in the laboratory supervised by Prof. A. J. Thomson (University of East Anglia).

Spectra were recorded in the absence of glycerol using an X-band ER-200D spectrometer

(Bruker Electrospin) interfaced to an ESP1600 computer and fitted with an Oxford

Instruments ESR-9 liquid helium flow cryostat. Unless stated otherwise, the samples used

were those prepared for the MCD spectra.

## 6.10 Spectroelectrochemistry

Spectroelectrochemistry experiments were conducted by Dr. E. Raven (Department of

Chemistry, University of Leicester) using apparatus in the laboratory supervised by Prof. A.

G. Mauk (University of British Columbia Vancouver, Canada).

A sample of wild-type rAPX (~0.3 mM) was prepared in degassed sodium phosphate (pH

6.99, $\mu$ = 0.1 M). Phenosafranine (~0.35 mol/mol, $E^0$ = -249 mV vs SHE), anthraquinone-2-

sulfonate (~0.35 mol/mol, $E^0$ = -225 mV vs SHE), and 2-hydroxy-1,4-napthoquinone (~0.35

mol/mol, $E^0$ = -139 mV vs SHE) were used as mediators. A trace amount of Rhus

vernicifera laccase and catalase (Sigma type C-100) were added to an optically transparent

thin-layer electrode (OTTLE)[11] in order to remove dissolved oxygen from the solution and

avoid undesired oxidative side reactions.

An OTTLE (optical pathlength $\approx$ 0.2 mm), fitted with a Pt wire counter electrode and a saturated calomel reference electrode (calibrated at +244.4 mV vs SHE), was located in the water-jacketed cell holder of a Carey Model 219 spectrophotometer, linked to a microcomputer (OLIS). The applied potential was controlled using a Princeton Applied Research Model 173 potentiostat, and the cell temperature was maintained by a circulating-water bath. Midpoint potentials ($E^0$) were obtained by a Nernst plot of applied voltage (mV vs. SHE) against $\log_{10}\frac{A_{Red}-A_i}{A_i-A_{Ox}}$, where $A_{Red}$ and $A_{Ox}$ are the absorbance values, at $\Delta A_{Max}$, of the fully reduced and fully oxidised forms, respectively; $A_i$ is the absorbance for an intermediate potential (i mV).

Spectra were recorded at a temperature of 25.0 $\pm$ 0.1 °C, and at intervals of ~50 mV from about -450 mV upto +150 mV vs SHE; ~60 minutes was required to achieve equilibration at each potential. The average Nernst slope of two wild-type rAPX mid-point potential determinations was 73 $\pm$ 2 mV.

## 6.11 Circular dichroism

Thermal stability studies were conducted by Dr. E. Raven (Department of Chemistry, Leicester University) using apparatus in the laboratory supervised by Prof. A. G. Mauk (University of British Columbia Vancouver, Canada). Samples taken from protein stocks (~10 $\mu$M) were prepared in the appropriate buffer at the required pH and placed in a water-jacketed quartz cell (pathlength 0.1 cm). Cyanide bound derivatives, were prepared by addition of a suitable volume of 1 M KCN to the ferric sample.

Temperature dependent spectra were recorded using a computer-controlled Jasco model J-720 spectropolarimeter, calibrated using ammonium D-camphor-10-sulphonate, fitted with

a Neslab model RTE-110 circulating water bath and a Neslab model RS-2 remote sensor. The ellipticity at 222 nm was recorded between 25-75°C under an applied heating rate of 50°C per hour; the midpoint melting temperature ($T_m$) of each sample was determined from the first derivative of the plot of ellipticity *vs* temperature.

## *6.12 Transient-state kinetics*

Transient-state kinetic measurements were obtained using a SX.18 MV microvolume stopped-flow spectrofluorimeter (Applied Photophysics), with an arc lamp source and pbp SpectraKinetic Monochromator (Applied Photophysics), controlled by an Archimides 410-1 microcomputer running SpectraKinetic software (Applied Photophysics). A photomultiplier detector was used for the single wavelength studies whereas a photodiode array facility allowed multiple wavelength stopped-flow kinetics, using the X-scan software. A circulating water bath (Neslab, model RTE-200) ensured that the injection chamber and syringes were maintained at the required temperature (typically 5.0°C). Mr Latesh Lad (Department of Chemistry, Leicester University) assisted with the acquisition of transient-state kinetic data, and the discussions that were connnected with this work proved invaluable during the interpretation of experimental results.

Non-linear regression analysis of single wavelength kinetics was conducted using Applied Photophysics software, fitting to the appropriate model. Spectral deconvolution, based upon global analysis and integration, of the multiple wavelength transients was performed using the PROKIN software. Further data manipulation and plots were obtained using the Grafit software package (Version 2.0, Erithacus Software Ltd.).

Single wavelength transients were obtained at or near an appropriate isosbestic point, *i.e.*

Compound II formation was monitored at the isosbestic point between ferric and Compound

I, taken from photodiode array spectra. In either the single-mixing or sequential-mixing

modes, the typical final enzyme concentration in the cell was 0.5 $\mu$M. Concentrations of

rAPX and peroxide were confirmed spectrophotometrically and freshly prepared reducing

substrates were prepared volumetrically, from concentrated stocks of known molarity.

## 6.13 HPLC analysis of phenylhydrazine modified haems

Phenylhydrazine modification of horseradish peroxidase, wild-type and A134P variant

rAPX was conducted by turning over the enzyme in the presence of the suicide substrate

(0.6 mM phenylhydrazine; 0.2 mM $H_2O_2$ and ~20$\mu$M enzyme, total volume 250 $\mu$l). The

buffered protein samples (pH 7.0 NaPi, $\mu$ = 0.1 M) were denatured using 6 M Guandine/HCl

and 200 mM Lysine (pH 2, 250 $\mu$l). The released haem was extracted into butan-2-one (500

$\mu$l). The volatile solvent was removed and the haem isolated *in vacuo*.

### 6.13.1 HPLC identification of modified haems

High performance liquid chromatographic analysis was conducted in collaboration with

Dr J. L. Luo and Dr C. K. Lim (Centre for Mechanisms in Human Toxicity, University of

Leicester). A 5 $\mu$m Hypercil BDS C-18 column (4.6 mm × 250 mm, Thermoquest) was

inserted into a computer-controlled HPLC chromatographic apparatus (Variant). An

isocratic acetonitrile/water/trifluoroacetic acid elution buffer (50:50:0.1 by volume) was

prepared and the column equilibrated at the 1 ml/min flow rate. The haem residue was

redissolved in a minimal volume (<100 μl) of the buffer and samples injected using a 20 μl

sample loop. Eluting haem adducts were detected by the absorbance at 400 nm.

### 6.13.2 HPLC-linked mass spectrometry

The HPLC separated haem adducts, which had been detected by UV/visible, were

characterised using electrospray mass spectrometric analysis. Samples were analysed under

the supervision of Mr G. A. Lord (Centre for Mechanisms in Human Toxicity, Leicester

University). Detection of haem-derived ions was optimised using a sample of hemin (Sigma)

dissolved in the isocratic HPLC elution buffer. Adjustments to the chromatographic

conditions were required in order to produce a detectable haem ion concentration (>100

μM). Maintaining the isocratic reversed-phase HPLC elution conditions, signal-to-noise was

further enhanced by using a 3 μm Luna C18 ODS column (1 mm × 100 mm, Phenomenex),

and 10 μl sample injections. The flow rate was reduced to 50 μl/min, which permitted direct

attachment of the HPLC elution outlet to the Micromass Quattro BQ (Tandem Quadrupole)

electrospray mass spectrometer.

## 6.14 Reaction of wild-type rAPX with hydrogen peroxide

The reaction between wild-type rAPX and peroxide was investigated in collaboration

with Dr. J. N. Rodríguez-López (Departmento de Bioquímica y Biología Molecular-A,

Universidad de Murcia, Spain) and Dr. M. Acosta (Departamento de Biología Vegetal

(Fisiología Vegetal), Facultad de Biología, Universidad de Murcia, Spain.[12]

### 6.14.1 UV-visible spectroscopy and 'stop-start' turnover experiments

As described in section 6.4, UV/visible spectra were obtained using a variable slit Perkin Elmer Lambda14 UV/visible spectrometer. Wild-type rAPX was reacted with an equimolar amount of $H_2O_2$ and allowed to evolve, for several minutes to a few hours, Compound I* spectra were obtained at various times after the start of the reaction. For the formation of Compound II of rAPX, the ferric enzyme was incubated in the presence of an equimolar amount of L-ascorbic acid and the reaction initiated by addition of 1 equivalent of $H_2O_2$. Performing accurate additions of stoichiometric quantities of either peroxide or ascorbate to a sample of wild-type rAPX allowed 'stop-start' turnover experiments to be conducted, i.e. the stepwise reaction of the enzyme through its catalytic cycle according to its discrete kinetic steps.

### 6.14.2 EPR spectroscopy

Samples of wild-type rAPX were provided to Drs. J. N. Rodríguez-López and M. Acosta (Universidad de Murcia, Spain) for EPR analysis. EPR spectra were recorded on a Bruker ESP380E spectrometer operating in X-band (9-10 GHz) with an Oxford CF935 liquid helium cryostat. EPR experiments for the reaction of rAPX with 0.97 equivalent of $H_2O_2$ at room temperature were carried out using a manually operated rapid mixing device. A 100 μL aliquot of each solution was injected into the EPR tube and then frozen at 77K at different reaction times.

## 6.14.3 Tryptic digestion and HPLC analysis

Samples of wild-type rAPX were provided to Drs. J. N. Rodríguez-López and M. Acosta (Universidad de Murcia, Spain) for HPLC analysis. Haem was extracted from wild-type rAPX ($\approx$100 µg) – either prior to exposure to $H_2O_2$ or after incubation for 6 hours with 1 equivalent of $H_2O_2$ or 1 equivalent of L-ascorbic acid plus 1 equivalent of $H_2O_2$ in buffer – into 400 µL acidified (HCl) butanone on ice. The aqueous phase containing polypeptide was spun (15 minutes, 8000 g) in a microcentrifuge filter unit (10000 NMWL, Ultrafree-MC, Millipore) to remove low molecular weight contaminants. The retained fraction was re-suspended in a mixture of 8 M urea, 0.4 M ammonium chloride and 10 mM dithiothreitol. After incubation at 50°C for 10 minutes, the samples were diluted 3-fold with water and digested with L-1-tosylamide-2-phenylethyl-chloromethyl-ketone-treated trypsin (Sigma) for 16 hours at 37°C. After filtration (0.2 µm nylon) the samples were injected on a Waters Delta-Pak C18, 5 µm, 300 Å reversed phase HPLC column. A Beckman System Gold programmable HPLC system was used running a linear gradient of acetonitrile in 0.1 % aqueous trifluoroacetic acid (0 to 50 %, 20 minutes followed by 20 minutes at 50 % at a flow rate of 0.7 ml min$^{-1}$). Chromatograms were recorded at 330 nm. Spectra of the main peaks were recorded using a diode-array detector attached to the HPLC.

## 6.15 References

1  Mittler, R. and Zilinskas, B. A. (1991) *FEBS*, **289**, 257-259

2  Patterson, W. R. and Poulos T. L. (1994) *J. Biol. Chem.*, **269**, 17020-17024

3  World-wide web page concerning New England Biolabs protein fusion & purification (pMAL) system http://www.uk.neb.com/neb/faqs/faq_PFP.html#3.1

4  Cheek, J., Mandelman, D., Poulos, T. L. and Dawson, J. H. (1999) *J. Biol. Inorg. Chem.*, **4**, 64-72

5  Antonini, M. and Brunori, E. (1971) in: *Hemoglobin and Myoglobin and their reactions with ligands* (Neuberger, A. and Tatum, E. L. eds.), North Holland Publishers, Amsterdam. [Pyridine haemochromagen method described pp 10-12]

6  Erman, J. E. (1974) *Biochemistry*, **13**, 39-44

7  Mittler, R. and Zilinskas, B. A. (1991) *Plant. Physiol.*, **97**, 962-968

8  Jung, C. H. and Wells, W. W. (1998) *Arch. Biochem. Biophys.*, **355**, 9-14

9  Yu, S. W., Kim, Y. R. and Kang, S. O. (1998) *Biochem. J.*, **341**, 755-763

10  Yoshimura, K., Ishikawa, T., Nakamura, Y., Tamoi, M., Takeda, T., Tada, T., Nishimura, K. and Shigeoka, S. (1998) *Arch. Biochem. Biophys.*, **353**, 55-63

11  Heineman, W. R., Norris, B. J. and Goelz, J. F. (1975) *Anal. Chem.*, **47**, 79-84

12  Hiner, A. N. P., Martínez, J. I., Arnao, M. B., Acosta, M., Turner, D. D., Raven, E. and Rodríguez-López, J. N. (submitted for publication)

# APPENDIX A

# Appendix A

## 1000×Ampicillin

100 mg ampicillin per ml of HQ-dH₂O, filter sterilised.

## LB-Ampicillin plates

Per litre: 10 g NaCl, 10 g tryptone, 5 g yeast extract, 20 g agar and HQ-dH₂O to 1 litre; autoclave, allow to cool ≤55 °C, and add 0.5 ml 1000× ampicillin, and pour ~50 ml into each petri dish, allow to set.

## Glycerol Stock

300 μl glycerol (50%) and 700 μl of an overnight culture; stored frozen at -20°C.

## Rich medium

Per litre: 10 g tryptone, 5 g yeast extract, 5 g NaCl, 2 g glucose and dH₂O to 1 litre; autoclave, allow to cool ≤55 °C, and add 0.7 ml 1000× ampicillin.

## Lysis buffer

50 mM tris(hydroxymethyl)aminomethane-HCl, pH 8.0, 10 mM diaminoethanetetra-acetic acid.

## AC buffer

20 mM tris(hydroxymethyl)aminomethane-HCl pH 7.5, 200 mM NaCl.

## FFQ column buffer

10 mM KPi pH 7.0.

## Basic pyridine solution

1 ml pyridine, 0.3 ml 1 M NaOH and 3 ml dH₂O.

## Oligonucleotides

```
R38AF    5'(GCGCTCCTCTAATTCTCGCTTTGGCATGGC)3'
R38AR    3'(CGCGAGGAGATTAAGAGCGAAACCGTACCG)5'


R38CF    5'(GCGCTCCTCTAATTCTCTGCTTGGCATGGC)3'
R38CR    3'(CGCGAGGAGATTAAGAGACGAACCGTACCG)5'


R38MF    5'(GCGCTCCTCTAATTCTCATGTTGGCATGGC)3'
R38MR    3'(CGCGAGGAGATTAAGAGTACAACCGTACCG)5'


H42AF    5'(CGTTTGGCATGGGCTTCTGCTGGTAC)3'
H42AR    3'(GCAAACCGTACCCGAAGACGACCATG)5'


A134FF   5'(CGCTTGCCTGATTTCACTAAGGGTTCTG)3'
A134FR   3'(GCGAACGGACTAAAGTGATTCCCAAGAC)5'


A134PF   5'(CGCTTGCCTGATCCGACTAAGGGTTCTG)3'
A134PR   3'(GCGAACGGACTAGGCTGATTCCCAAGAC)5'


H169AF   5'(CATTGGAGCTGCAGCTAAGGAGCGTTCTG)3'
H169AR   3'(GTAACCTCGACGTCGATTCCTCGCAAGAC)5'


malE     5'(GGTCGTCAGACTGTCGATGAAGCC)3'  Forward sequencing primer


M13/pUC  5'(CGCCAGGGTTTTCCCAGTCACGAC)3'  Reverse sequencing primer
```

236